# UNIVERSITY OF SOUTHAMPTON


## FACULTY OF MEDICINE, HEALTH AND LIFE SCIENCES

## DIVISION OF NEUROSCIENCE


# AN INVESTIGATION INTO THE MODE OF ACTION OF THE ANTHELMINTIC EMODEPSIDE ; A MOLECULAR, PHARMACOLOGICAL AND ELECTROPHYSIOLOGICAL CHARACTERISATION


**By**

**Marcus Guest**


**Thesis for the degree of Doctor of Philosophy**

**September 2008**

**UNIVERSITY OF SOUTHAMPTON**
**FACULTY OF MEDICINE, HEALTH AND LIFE SCIENCES**
**DIVISION OF NEUROSCIENCE**

**Doctor of Philosophy**

# AN INVESTIGATION INTO THE MODE OF ACTION OF THE ANTHELMINTIC EMODEPSIDE; A MOLECULAR, PHARMACOLOGICAL AND ELECTROPHYSIOLOGICAL CHARACTERISATION

**Marcus James Guest**

Resistance to anthelmintics is increasingly becoming a problem for the agricultural industry. Emodepside is a novel anthelmintic that is effective against a variety of parasitic nematodes in which resistance to other anthelmintics has developed (Harder and Samson-Himmelstjerna, 2002). This suggests that emodepside has a novel mode of action. The aim of this study was to further investigate the mechanism of action of emodepside using the model organism *Caenorhabditis elegans*.

The latrophilin receptors have previously been implicated in the mechanism of action of emodepside. The natural compound from which emodepside is derived (PF1022A) has been shown to bind the *Haemonchus contortus* receptor latrophilin receptor HC110R (Saeger *et al* 2001). *Caenorhabditis elegans* have latrophilin homologues, *lat-1* and *lat-2*. Targeting of *lat-1* by RNA interference reduces the sensitivity of the *C. elegans* pharynx to emodepside (Willson *et al* 2004). Targeting of either *lat-1* or *lat-2* by RNA interference reduced the sensitivity of *C. elegans* to emodepside's effects on locomotion. Simultaneous targeting of *lat-1* and *lat-2* by RNA interference reduced the sensitivity of *C. elegans* to emodepside's effects on locomotion to a similar extent (Amliwala 2005). RNA interference of latrophilin receptors does not abolish emodepside's effect, indicating either an incomplete knock down by RNA interference or the presence of an additional mechanism of action. To further investigate role of the latrophilin receptors, the sensitivity of *C. elegans* mutants carrying deletions in *lat-1*(*ok1465*) and *lat-2*(*tm463*) were tested. Neither of these putative null mutants displayed any difference in sensitivity to emodepside's effects on locomotion compared with the *N2* wild type strain. In order to investigate the possibility of a redundancy between *lat-1* and *lat-2* a *lat-2*(*tm463*) *lat-1*(*ok1465*) double mutant was constructed. The *lat-2*(*tm463*) *lat-1*(*ok1465*) double mutant did not display any difference in sensitivity to emodepside's effects on locomotion compared to *N2*. However, both *lat-1*(*ok1465*) and *lat-2*(*tm463*) *lat-1*(*ok1465*) have reduced sensitivity to emodepside's effects on the pharynx (Bull 2007). This suggests that *lat-1* has a role in mediating emodepside's effects in the pharynx but not in the motor nervous system. Therefore, an alternative mechanism by which emodepside acts in the motor nervous system must exist.

The voltage gated calcium sensitive potassium channel *slo-1* was previously identified through a mutagenesis screen as a mediator of emodepside's effect in *C. elegans* (Amliwala 2005). In this study, further emodepside resistant mutants were isolated. Through the use of genetic complementation tests it was demonstrated that all emodepside resistant mutants are alleles of *slo-1*. The *slo-1*(*js379*) loss of function mutants is highly resistant (insensitive to 10 μM emodepside) to the effects of emodepside, suggesting emodepside activates SLO-1. Sequencing of *slo-1* in mutants isolated for the mutagenesis screens revealed the presence of mutations in regions of SLO-1 involved in the regulation of potassium conductance, supporting the idea that emodepside affects SLO-1 channel activity. *slo-1* loss of function mutants are reported to have an increased reversal frequency and an increased sensitivity to the acetylcholine esterase inhibitor aldicarb (Wang *et al* 2001). Using these phenotypes as a read out of SLO-1 function, the relationship between emodepside sensitivity and SLO-1 function was characterised.

In order to confirm a role for *slo-1* in the action of emodepside, *slo-1*(+) was expressed in a *slo-1*(*js379*) mutant background. This resulted in restoration of emodepside sensitivity, confirming that SLO-1 mediates emodepside's effects on locomotion. Expression in either body wall muscle or neurons restored emodepside sensitivity. The effect of emodepside on the rate of aldicarb induced paralysis was investigated. In general, aldicarb hypersensitive worms have increased ACh release and aldicarb resistant worms have reduced ACh release (Mahoney *et al* 2006). Emodepside reduced the sensitivity of *N2* worms to aldicarb, indicating that it causes a reduction in ACh release. These results indicate that emodepside acts on SLO-1 in both muscle and neurons to inhibit locomotion. A direct activation of SLO-1 by emodepside was hypothesised. This was pursued using HEK293 exogenous expression system and patch clamp analysis. The identification of SLO-1 as a target for emodepside provides potential for the development of further anthelmintics as well as the possibility of identifying novel applications for emodepside.

# Publications

**Guest M**, Bull K, Walker RJ, Amliwala K, O'Connor V, Harder A, Holden-Dye L, Hopper NA. (2007). The calcium-activated potassium channel, SLO-1, is required for the action of the novel cyclo-octadepsipeptide anthelmintic, emodepside, in *Caenorhabditis elegans*. *International Journal for Parasitology*. **37**,1577-1588.

Holden-Dye L, O'Connor V, Hopper NA, Walker RJ, Harder A, Bull K, **Guest M**. (2007). SLO, SLO, quick, quick, slow: Calcium-activated potassium channels as regulators of *Caenorhabditis elegans* behaviour and targets for anthelmintics. *Invertebrate Neuroscience*. **7**,199-208.

**Guest M**, Bull K, Amliwala K, Willson J, Hopper NA, Harder A, Walker RJ, O'Connor V, Holden-Dye L. (2005). The Paralytic Action of the Anthelmintic Emodepside Requires Latrophilin, a Receptor Involved in Neurotransmitter Release. Biochemical society. Molecular Determinants of Synaptic Function: Molecules and Models. Abstract **P-015**.

**Guest M**, Bull K, Amliwala K, Willson J, Walker RJ, Hopper NA, Holden-Dye L. (2006). Investigations into the mode of action of the novel anthelmintic emodepside. *European worm meeting.* Abstract **P-063**.

**Guest M**, Bull K, Harder A, Walker R, Hopper NA, Holden-Dye L. (2007). The mode of action of the novel anthelmintic emodepside. BSP spring and Malaria meeting.

# Contents

## Chapter 1: Introduction

## Page 1



## Chapter 2: Methods

## Page 45

# Figures

## Tables

# Declaration of Authorship

# Acknowledgements

I would like to thank my supervisors Professor Lindy Holden-Dye and Professor Robert Walker for their continued support throughout the course of my PhD candidature.

I would like to thank my colleagues in wormland, especially Dr Neil Hopper, Dr Neline Kriek and Dr Alan Cook whose expertise and assistance have enabled me to conduct this research. I would also like to thank Barbara York who assisted with the mapping and sequencing of the *slo-1* alleles. Thanks also to Achim Harder and Georg von Samson–Himmelstjerna for their hospitality in Germany.

I am grateful to the BBSRC and Bayer AG, Germany for financially supporting this research.

Finally I would like to thank Solenne Wells and my family for their support and encouragement during my PhD.

## Abbreviations

| | |
|---|---|
| AADs | Amino-acetonitrile derivatives |
| ACE | Acetylcholine esterase |
| Ach | Acetylcholine |
| ADH | Alcohol dehydrogenase |
| AMPA | alpha-amino-3-hydroxy-5-methyl-4-isoxazolepropionic acid |
| 4-AP | 4-aminopyridine |
| *A. suum* | *Ascaris suum* |
| ATP | Adenosine-5'-triphosphate |
| | |
| BLAST | Basic local alignment search tool |
| *C. elegans* | *Caenorhabditis elegans* |
| CGC | *C. elegans* genomics centre |
| CICR | Calcium induced calcium release channel |
| cM | Centimorgan |
| *C. oncophora* | *Cooperia oncophora* |
| $ddH_2O$ | Double distilled water |
| DAG | Diacylglycerol |
| DEPC | Diethylpyrocarbonate |
| DMEM | Dulbecco modified Eagle's medium |
| DMS | Dorsal muscle strip |
| DNA | Deoxyribonucleic acid |
| EDTA | Ethylenediaminetetraacetic acid |
| EJC | Excitatory junctional current |
| EJP | Excitatory junctional potential |
| EPSC | Excitatory post synaptic current |
| EPSP | Excitatory post synaptic potential |
| EMS | Ethyl-methane sulphonate |
| EPG | Electropharyngeogram |
| ER | Emodepside resistant |
| FLP | FMRFamide like peptide |
| GABA | Gamma-aminobutyric acid |

| | |
|---|---|
| GFP | Green fluorescent protein |
| *G. pallida* | *Globodera pallida* |
| GPCR | G-protein coupled receptor |
| *G. rostochiensis* | *Globodera rostochiensis* |
| *H. contortus* | *Haemonchus contortus* |
| HEK293 | Human embryonic kidney cell 293 |
| 5-HT | 5-Hydroxy tryptamine |
| IBTX | Iberiotoxin |
| $IC_{50}$ | 50 % Inhibitory concentration |
| $IP_3$ | Inositol trisphosphate |
| kDa | Kilodalton |
| KLH | Keyhole limpet haemocyanin |
| LTX | Latrotoxin |
| LB | Luria-Bertani Media |
| MCS | Multiple cloning site |
| mEPSC | Mini excitatory post synaptic current |
| mV | Millivolt |
| nA | Nanoamp |
| nACHR | Nicotinic acetylcholine receptor |
| NAD | Nicotinamide adenine dinucleotide |
| NBRP | National bioresource project |
| NEB | New England Biolabs |
| NGM | Nematode growth medium |
| NGO | Non-governmental organisation |
| NLP | Neuropeptide like protein |
| NMDA | N-methyl-D-aspartic acid |
| NMJ | Neuromuscular junction |
| pA | Picoamp |
| PBS | Phosphate buffered solution |
| PC | Personal computer |
| PCR | Polymerase chain reaction |
| PF2 | *Panagrellus* FMRFamide-like peptide two |
| $PIP_2$ | Phosphatidylinositol bisphosphate |
| PLC-β | Phospholipase C β |

| | |
|---|---|
| PPC | Partners for parasitic control |
| RCF | Relative centripetal force |
| RCK | Regulation of potassium conductance |
| RFLP | Restriction fragment length polymorphism |
| RNA | Ribonucleic acid |
| RNAi | Ribonucleic acid interference |
| RT-PCR | Reverse transcriptase polymerase chain reaction |
| SAP | Shrimp alkaline phosphatase |
| SNP | Single nucleotide polymorphism |
| TBE | Tris/Borate/EDTA |
| *T. canis* | *Toxicara canis* |
| TEA | Tetraethylammonium |
| *T. leonine* | *Toxicara leonine* |
| WHO | World health organisation |
| WT | Wild type |

| | |
|---|---|
| A | Alanine |
| G | Glycine |
| Q | Glutamine |
| R | Arginine |
| V | Valine |
| W | Tryptophan |

| | |
|---|---|
| C | Cytosine |
| G | Guanine |
| A | Adenine |
| T | Thymine |

# Chapter 1

# Introduction

## 1.01 Nematodes

Nematodes may be defined as "Of or belonging to the large phylum Nematoda (or Nemata), comprising worms with slender, tapering, unsegmented bodies that are round in cross-section, which may be free-living or parasites of animals or plants" (Oxford English Dictionary). The nematode phylum may be categorised into five clades based on small subunit ribosomal sequence (Blaxter *et al* 1998). Each of these five clades contain both free living and parasitic nematodes, suggesting independent emergence of parasitism within clades. Table 1.01 shows the nematode phylogeny (Blaxter *et al* 1998).

| | | |
|---|---|---|
| V | Strongylida | ● |
| | Rhabditida (including *C. elegans*) | ● ● ● |
| | Diplogasterida | ● ● |
| IV | Rhabditida | ● |
| | Rhabditida | ● |
| | Rhabditida | ● |
| | Rhabditida | ● |
| | Aphelenchida | ● ● ● |
| | Tylenchida | ● ● ● |
| III | Oxyurida | ● |
| | Spirurida | ● |
| | Rhigonematida | ● |
| | Ascaridida | ● |
| | Plectidae | ● |
| | Chromadorida | ● ● |
| | Monhysterida | ● |
| II | Enoplida | ● ● |
| | Triplonchida | ● |
| I | Trichocephalida | ● |
| | Dorylaimida | ● ● |
| | Mermithida | ● |
| | Mononchida | ● ● |

| | |
|---|---|
| Bacteriovore | ● |
| algivore-omnivore-predator | ● |
| fungivore | ● |
| plant parasite | ● |
| entomopathogen | ● |
| invertebrate parasite | ● |
| vertebrate parasitic | ● |

**Table 1.01 Nematode phylogeny.** Nematode phylogeny as defined by small subunit ribosome sequence (Adapted from Blaxter *et al* 1998).

Research of nematodes and the treatment of nematode infections is important. They have a high financial cost on agriculture as well as a high human cost in the developing world. The free living nematodes *Caenorhabditis elegans* (*C. elegans*) is widely used as a model system for research in a variety areas of biological science and is particularly useful as it is genetically tractable (Brenner 1974).

## 1.02 *C. elegans*

*C. elegans* is a small free living soil nematode. There are two sexes, a hermaphrodite and a male, each about 1 mm long when adult. The life cycle takes about 3 days and the life span is about 17 days (Figure 1.01). The hermaphrodite produces both sperm and oocytes and can therefore either self-fertilize or be fertilized by a male. A self-fertilized hermaphrodite can lay approximately 300 eggs over the course of 3 days, and then live for a further 10 to 15 days.

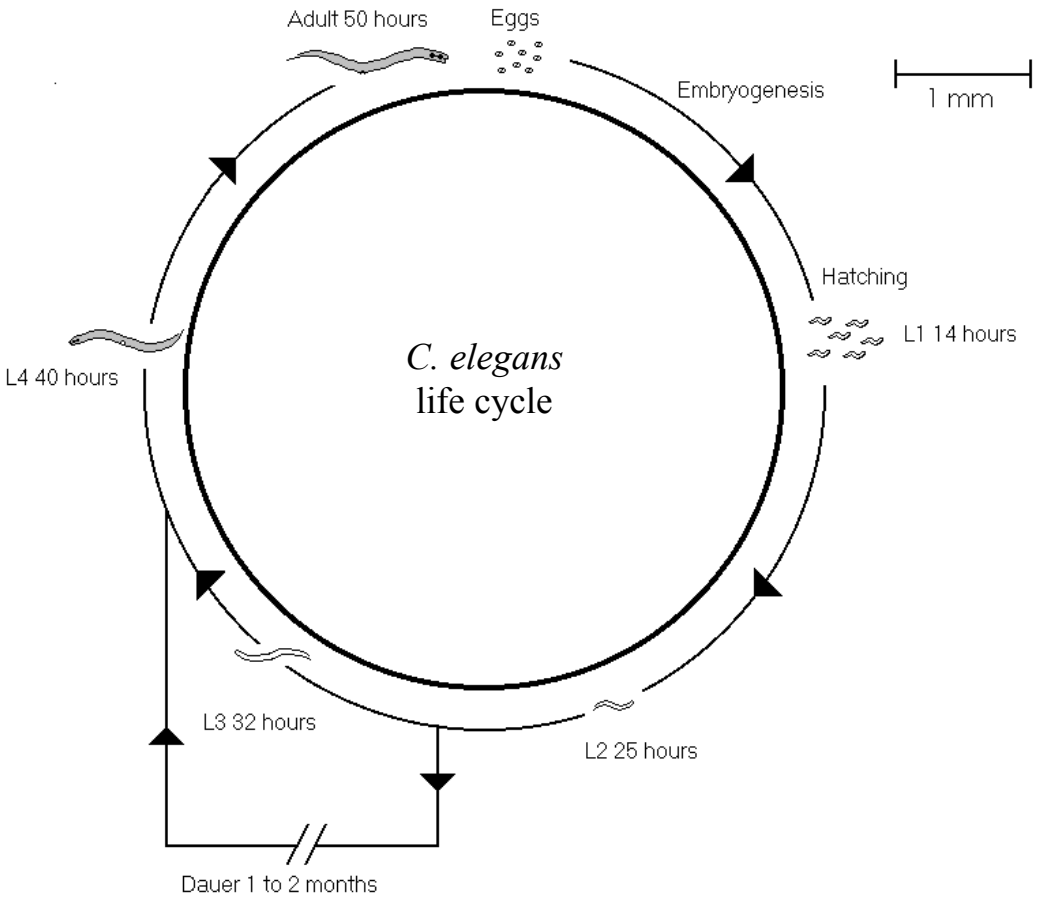


**Figure 1.01. Life cycle of *C. elegans* showing the different stages of growth, L1, L2, L3, L4 and adult.** At L4 stage the forming vulva is visible. If worms are deprived of food in larval stages they will enter a growth stage known as dauer, in which development is arrested. When food becomes available development will continue. (After Wood *et al* 1980).

If food is limited at an early stage of development (L2), the worm may form dauers. In this state the worm does not feed and will not desiccate. It can remain in this phase for 3 months or more, until food becomes available and normal development can resume. The hermaphrodite and male worms consist of 959 and 1031 somatic cells respectively. The haploid genome size is $9.7 \times 10^7$ base pairs, and contains about 20,000 genes. The genome consists of five pairs of autosomal chromosomes and a pair of sex chromosomes: XX in the hermaphrodite and XO in the male (Wood 1988). Males arise infrequently in *C. elegans* populations, about 0.1%. This can be increased through heat shock of L4 hermaphrodites. Once males have been obtained, a population containing up to 50% males can be maintained through mating. *C. elegans* can be easily maintained in the laboratory on agar plates. It is also very amenable to genetic manipulation, through mutagenesis, transgene expression and RNA interference.

## 1.03 *C. elegans* as a parasite model

*C. elegans* provides a useful model for the investigation of the mode of action of anthelmintics. The usefulness of this model is dependent on the similarity between *C. elegans* and the parasite for which the anthelmintic is intended. *C. elegans* belongs to clade V group of nematodes. Clade V also includes the ruminant parasitic nematodes, the strongylida (including *H. contortus*). Ascaridia, another important group of nematodes, are in clade III. It would be expected that the value of *C. elegans* as a model will reduce as the phylogenetic distance between the species to be compared increases. *C. elegans* have many similarities with regard to anatomy, neurobiology and genetics when compared with nematodes across the clades.

## 1.04 *C. elegans* physiology

*C. elegans* are cylindrical in shape. They essentially consist of an inner and outer tube separated by the pseudocoelomic space. The inner tube contains the gonad, pharynx and intestine and the outer tube contains neurons, muscle, excretory system, hypodermis and cuticle. Figure 1.02 shows a photograph and diagram of a gravid adult *C. elegans* with the pharynx, nerve ring (brain), intestine and the reproductive system highlighted.

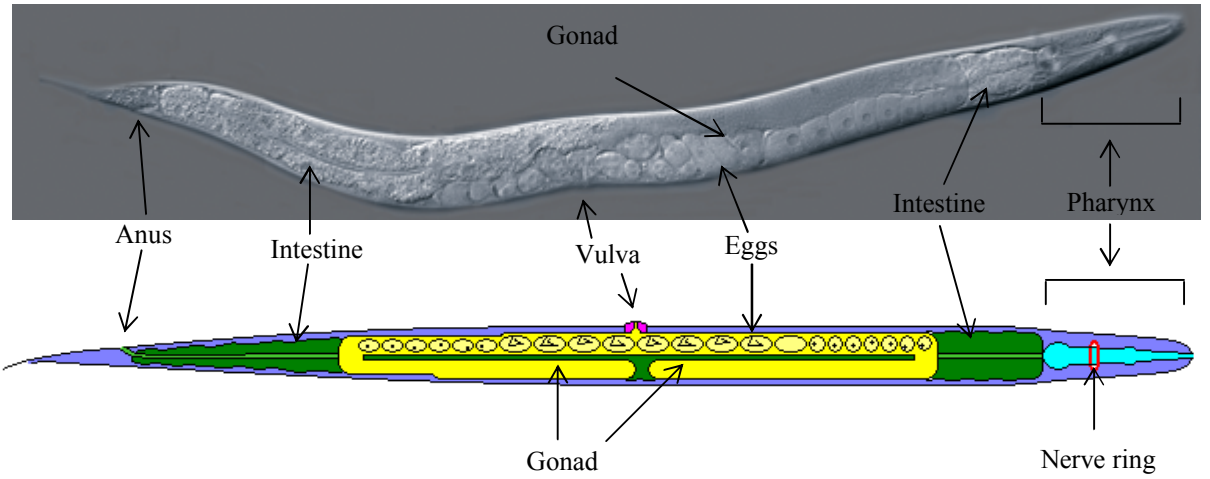


**Figure 1.02. Anatomical features of an adult *C. elegans*.** Key features of *C. elegans* anatomy are highlighted. The pharynx (pale blue), intestine (green), gonad (yellow), vulva (pink) and nerve ring (red). (After White 1988) (Photograph courtesy of Neil Hopper).

**Pharynx:** The *C. elegans* pharynx is required for the ingestion and mechanical digestion of food. The pharynx consists of 34 muscle cells, 9 marginal cells, 9 epithelial cells, 5 gland cells and 20 neurons (Albertson and Thomson, 1976). There is a basement membrane isolating the pharynx from the rest of the animal, making it an almost completely self contained system. The structure of the pharynx consists of four regions, the procorpus, metacorpus, isthmus and terminal bulb (Figure 1.03 A). The procorpus and metacorpus acts as a sieve, trapping food whilst allowing fluid to be regurgitated. The terminal bulb acts to grind up the food before it is passed into the intestine through the pharyngeal-intestinal valve. The pharyngeal nervous system coordinates the pharyngeal muscle cells allowing food to be sucked in, broken down and passed into the intestine. This process is referred to as pharyngeal pumping. The pharyngeal pumping of *C. elegans* can either be counted manually or electro-physiologically. The method of recording pumping electro-physiologically is referred to as

the electro-pharyngeogram or EPG (Raizen and Avery 1994, Cook *et al* 2006). This is an extra-cellular recording that can be performed on intact worms or on isolated pharynxes. As well as producing a read-out of pump rate, this technique can also be used to provide information on neuronal activity of the pharynx. The EPG trace has excitatory and inhibitory components that can be attributed to the function of specific pharyngeal neurons (Figure 1.03 B).

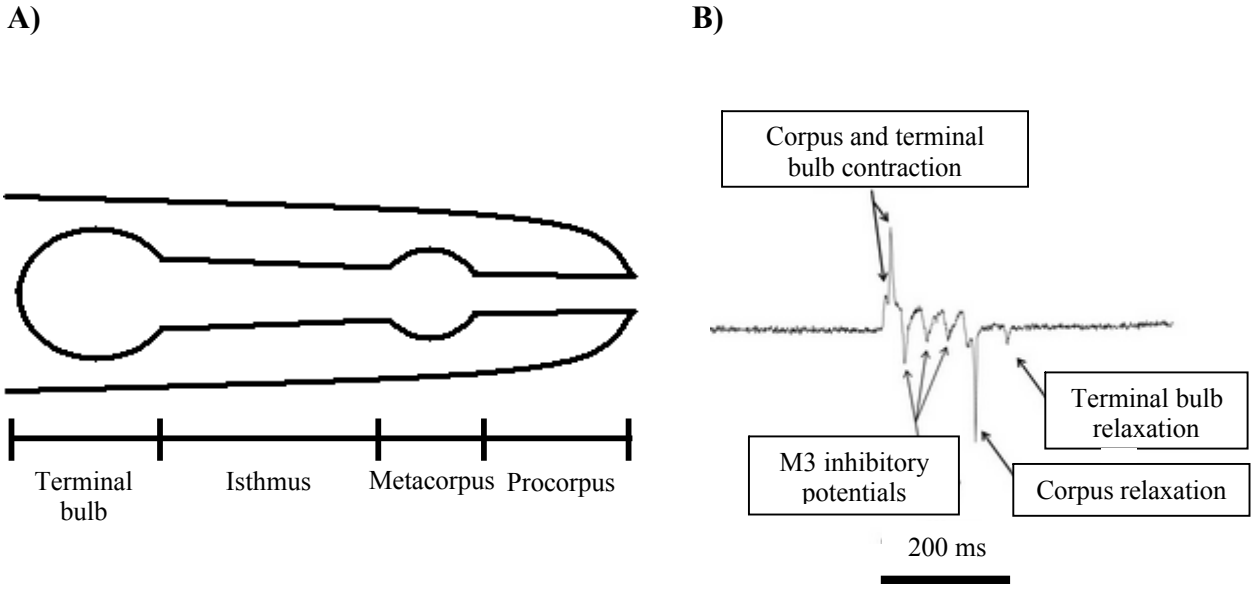


**Figure 1.03. *C. elegans* pharynx and EPG**. **A)** The pharynx consists of the procorpus, metacorpus, isthmus and terminal bulb. **B)** The EPG consists of initial excitatory spikes, followed by a series of small inhibitory spikes that are attributed to glutamate release from the M3 neuron. This is followed by relaxation of the corpus and terminal bulb. (From Cook *et al* 2006)

**Reproductive system:** The reproductive system of the hermaphrodite *C. elegans* consists of the gonadal sheath, the spermatheca, the spermatheca-uterine valve, the uterus and the vulva. Distal gonadal sheath cells form a covering for the germ line component of each gonad arm, and are important for the promotion of germ line proliferation. Proximal gonad sheath cells are required for oocytes maturation and have contractile properties and are required for transfer of oocytes into the spermatheca. The spermatheca contains sperm and is the site of oocytes fertilisation. Once fertilised, the newly formed embryo passes through the spermatheca-uterine valve into the uterus. The uterine and vulval muscles are then used to force the eggs out through the vulva (Kimble and Hirsh 1979). The stage of gonad development can be used to determine the larval stage of a worm. For example, when the gonad development is at the four cell stage the worm is at L1. At later developmental stages,

the appearance of the vulva can be used to determine the larval stage of a worm (Hirsh *et al* 1976).

**Nervous system and motor control:** The nervous system consists of 302 neurons. The majority of neurons are located in the head and make up the nerve ring. It also contains a variety of sensory neurons. The nerve ring is a region of high neuronal density that encircles the pharynx. *C. elegans* has two nerve cords, dorsal and ventral, that project from the nerve ring and run the length of its body. Neurons and muscles are either electrically coupled, via gap junctions, or chemically coupled. Chemical synapses occur *en passant* in *C. elegans*.

*C. elegans* moves in a sinusoidal pattern on solid media. The pattern of movement is achieved through the alternate contraction of dorsal and ventral sets of muscles. It is able to move in this way due to the organisation of its nervous system and musculature. An adult worm has 95 body muscle cells. These are arranged in quadrants running the length of the body. The left ventral quadrant contains 23 muscle cells and the other three quadrants contain 24 muscle cells each (Sulston & Horvitz 1977). Figure 1.04, which is taken from White *et al* (1986), shows a cross section of a worm with the muscle and nerve cords marked. The body muscle cells can be divided into three groups on the basis of synaptic input. Those that receive motor input from the nerve ring (the anterior four muscles in each quadrant), those that receive motor input from the nerve ring and ventral cord (the next four muscles in each quadrant) and those that receive input from the ventral cord alone (the remainder of the cells). The muscle cells in each row are coupled by gap junctions. Motor neuron cell bodies are situated in the ventral cord. These motor neurons either innervate ventral or dorsal muscle cells. Motor neurons that innervate dorsal muscle cells pass processes from the ventral cord and must then pass over to the dorsal cord. These processes are known as commissures. Muscle cells and motor neurons synapse along the ventral and dorsal nerve cords. The muscle cells of nematodes are unusual in that they have processes that extend from the main body of the muscle cells to the nerve cord. These processes are known as muscle arms. Muscle arms have multiple digits that synapse with the dorsal and ventral nerve cords (White *et al* 1986).

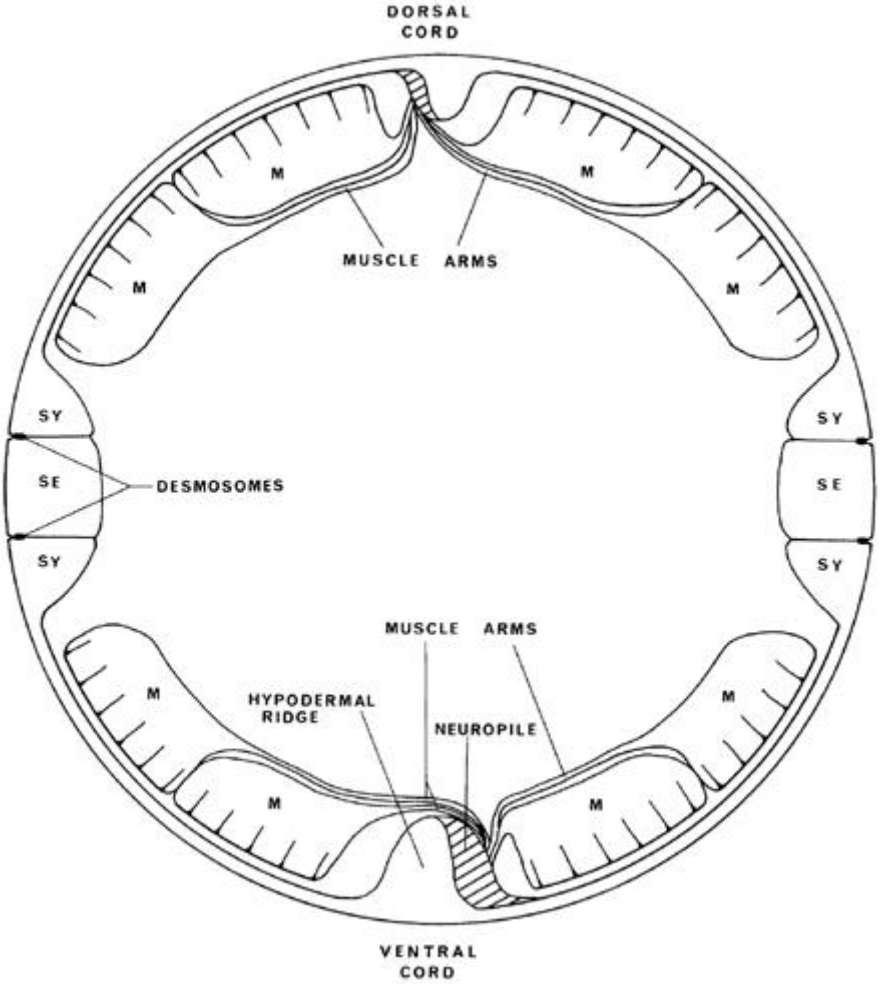


**Figure 1.04. Cross section of *C. elegans* body.** The dorsal and ventral nerve cords are marked. Body wall muscle cells have extensions called extend muscle arms that synapse with excitatory and inhibitory motor neurons in the cords. (From White *et al* 1986).

## 1.05 Neuronal circuit for movement

There are four classes of motor neuron that innervate ventral muscles and four classes of motor neuron that innervate dorsal muscles, VAn, VBn, VDn, VCn and DAn, DBn, DDn, Asn, respectively. Each class of motor neuron consists of multiple members that are repeated along the length of the body. VAn and DAn have anterior projecting axons and can be considered to be of the same class. VBn and DBn have posterior projecting axons and can be considered to be of the same class. These motor neurons receive input from interneurons. VDn and DDn receive synaptic input solely from motor neurons VAn, DAn, VBn and DBn. VCn and ASn are less prominent with regard to their innervation of body wall muscle (White *et al* 1986). VA, DA, VB and DA are excitatory and release ACh, causing muscle contraction

(Johnson and Stretton 1985). DV and DD are inhibitory and release GABA, causing muscle relaxation. The network shown in figure 1.05 shows how relaxation on dorsal and ventral muscles can be coordinated. Ventral excitatory motor neurons (VB and VA) synapse with dorsal inhibitory neurons (DD) (Stretton *et al* 1978, White *et al* 1986). Therefore, when the ventral muscle contracts, the dorsal muscle relaxes. This system of cross inhibition also applies for dorsal excitatory (DA and DB) and ventral inhibitory (VD) motor neurons. These properties of *C. elegans* motor neurons are inferred from studies on *Ascaris lumbricoides* (Stretton *et al* 1978). The idea that this system is present in *C. elegans* is supported by genetic analysis and cell ablation studies. McIntire *et al* (1993) showed that laser ablation of DD and VD in live *C. elegans* prevented sinusoidal movement and resulted in the simultaneous contraction of dorsal and ventral muscles. In the *unc-25* mutant, which is unable to synthesise GABA, simultaneous contraction of dorsal and ventral muscles was observed.

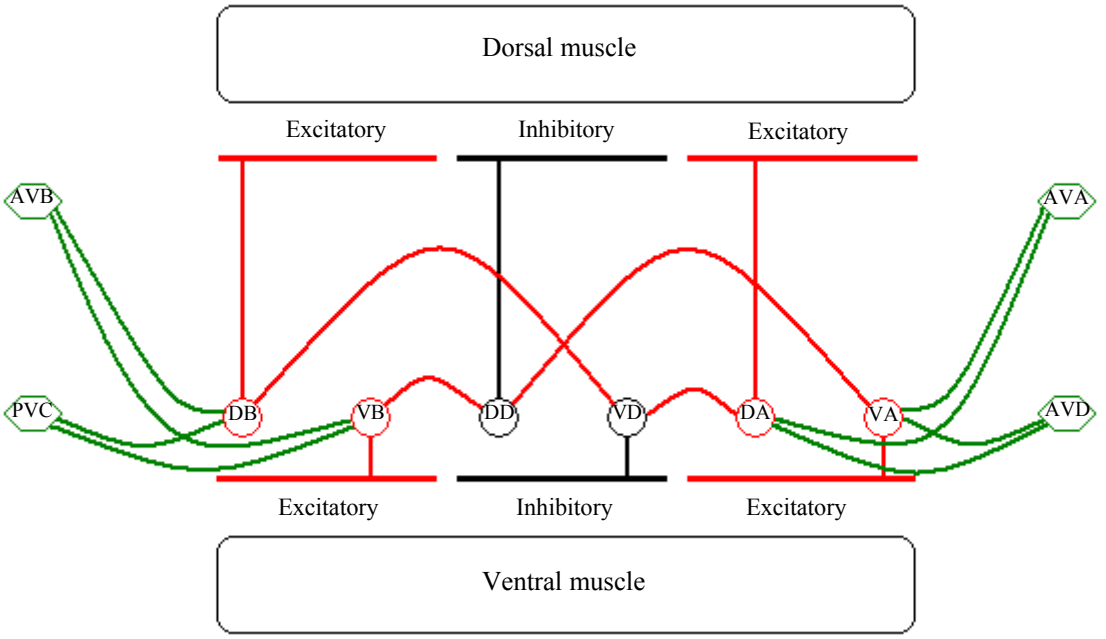


**Figure 1.05. Neuronal network regulating body wall muscle.** The ventral and dorsal muscle cells receive excitatory and inhibitory input from cholinergic motor neurons VB, DB, DA and VA (red) and GABAergic motor neurons DD and VD (black). Interneurons AVA, AVD, AVB and PVC (green) provide input to the motor neurons. (After White *et al* 1986).

In order for this circuit to produce rhythmic sinusoidal locomotion an oscillating pattern of neuronal activity is required. Cells that have oscillating patterns of activity are known as pattern generators. In *Ascaris lumbricoides* the inhibitory neurons, the equivalent of DD and

VD in *C. elegans*, are thought to generate this oscillating pattern (Angstadt and Stretton 1989). Little is known regarding the origin of this oscillating pattern in *C. elegans.*

Synaptic input to the motor neurons of the ventral cord is provided by the interneurons AVA, AVB, AVD, AVE and PVC. These are marked in figure 1.05. DB and VB receive input from PVC and AVB, which drive forward locomotion. DA and VA receive input from AVA and AVD, which drive backward locomotion (Chalfie *et al* 1985). Karbowski *et al* (2008) suggest that the pattern generator is located in the head in *C. elegans*. It is proposed that this signal is propagated downstream by interneurons and/or muscle cell coupling (via gap junctions). As well as requiring a pattern generator for movement, a mechanism for the propagation of the sinusoidal wave is required. The presence of body wall stretch receptors has been proposed. These would act to regulate adjacent motor neurons, thereby allowing propagation of the wave (White *at al* 1986).

## 1.06 Neurotransmitters

*C. elegans* have a variety of classical and non-classical neurotransmitters similar to those in mammalian brain. Similar mechanisms of metabolism and inactivation are also present (Isaac *et al* 1996). *C. elegans* neurotransmitters include 5-HT, dopamine, tyramine, octopamine, ACh, GABA and glutamate as well as a multitude of neuropeptides.

ACh acts at the *C. elegans* NMJ and is the most common excitatory neurotransmitter (Rand 2007). Over a third of neurons in *C. elegans* are cholinergic. *C. elegans* have both nicotinic and muscarinic type ACh receptors. 27 different genes coding for nicotinic ACh receptor subunits have so far been identified. The nicotinic ACh receptors of the body wall muscle have been characterised through expression in *Xenopus* oocytes and electrophysiological recording. There are both levamisole sensitive and levamisole insensitive nicotinic ACh receptors expressed in the body wall muscle. The levamisole sensitive receptors consist of three different types of subunit, UNC-29, UNC-38 and UNC-63, which are thought to form a heteromeric receptor. Both UNC-38 and UNC-63 are ACh binding α subunits, UNC-29 is a non-α subunit. Loss-of-function mutations in these subunits results in resistance to levamisole. Loss-of-function mutations in nicotinic ACh receptor subunits *lev-1* and *lev-8*

results in mild resistance to levamisole (Culetto *et al* 2004, Richmond and Jorgensen 1999). A nicotinic receptor that is levamisole insensitive is also present in the body wall muscle. This is thought to be a homomeric receptor that is made up of ACR-16 α-subunits (Touroutine *et al* 2005). *C. elegans* have three genes that encode receptors with homology to muscarinic receptors, *gar-1 gar-2* and *gar-3*.

Many other genes involved in the regulation of cholinergic transmission have been identified. *C. elegans* have three genes coding for acetylcholine esterase, *ace-1*, *ace-2* and *ace-3*. There is a level of redundancy between these genes, with individual mutants displaying mild phenotypes but a triple mutant of *ace-1*, *ace-2* and *ace-3* being lethal (Johnson *et al* 1988). *unc-17*, initially identified by Brenner *et al* (1974), codes for a vesicular acetylcholine transporter (Alfonso *et al* 1993). *unc-17* loss-of-function mutations are lethal, suggesting that it is essential. Genes coding for choline acetyltransferase (*cha-1*) and choline transporters (*cho-1*) have also been identified (Rand 2007).

GABA acts on *C. elegans* body wall muscle where it causes relaxation and on the enteric muscles to cause contraction (Jorgensen 2005). 26 of the 302 neurons in *C. elegans* are GABAergic. These include the previously mentioned DD and VD body wall muscle motor neurons, RME head motor neurons, AVL and DVB enteric motor neurons and the interneuron RIS. GABA has inhibitory effects on the body wall muscle that are mediated by GABA-gated chloride channels. These $GABA_A$ receptors are encoded by the gene *unc-49* in *C. elegans*. Three distinct $GABA_A$ receptor subunits are generated from this single gene and are thought to co-assemble to form a heteromultimeric GABA receptor (Bamber *et al* 1999). The excitatory effects of GABA on enteric muscles are mediated by a GABA-gated cation channel, *exp-1*. These receptors receive synaptic input from the AVL and DVB motor neurons (McIntire 1993). EXP-1 resembles UNC-49 except in the pore forming domain, which confers cation selectivity (Beg and Jorgensen 2003). Other GABA receptors have been identified through sequence homology. These include a G-protein coupled $GABA_B$ receptors (Jorgensen 2005).

The biogenic amines dopamine, octopamine, 5-HT and tyramine regulate a variety of behaviours in *C. elegans*, including locomotion, egg laying, defecation and foraging. These neurotransmitters act on both neurons and muscle to modulate these behaviours. Genes coding for seventeen putative biogenic amine receptors have been identified in *C. elegans*

(Chase and Koelle 2007). Genes coding for enzymes required for the synthesis of biogenic amines have also been identified. These include: *tph-1* (tryptophan hydroxylase) which is required for the synthesis of 5-HT (Sze *et al* 2000), *tbh-1* (tyramine β-hydroxylase) and *tdc-1*(tyrosine decarboxylase) which are required for octopamine synthesis (Alkema *et al* 2005) and *cat-2* (tyrosine hydroxylase) which is required for dopamine synthesis (Lints and Emmons 1999). The expression pattern of these genes has been used to identify which neurons release specific biogenic amine neurotransmitters.

Glutamate mediates both excitatory and inhibitory synaptic signaling. In *C. elegans,* there are ionotropic and metabotropic glutamate receptors. The ionotropic glutamate receptors are heteromeric ligand-gated ion channels. They can be classified based on their pharmacological properties. There are those that bind N-methyl-D-aspartate (NMDA receptors) and those that do not (non-NMDA receptors). Non-NMDA receptors are further categorised into those that bind α-amino-3-hydroxy-5-methyl-4isoxazole propionic acid (AMPA receptors) and those that bind kainate (kainate receptors). There are thought to be ten ionotropic glutamate receptors in *C. elegans*, two NMDA receptors (*nmr-1* and *nmr-2*) and eight non-NMDA receptors (*glr-1* to *glr-8*), based on sequence homology with pharmacologically characterized mammalian receptors. Expression of these receptors is almost exclusively in interneurons and motor neurons (Brockie *et al* 2001).

As well as cation selective ionotropic glutamate gated channels, there are chloride selective glutamate gated channels. A key role of these channels is the regulation of the timing of pharyngeal muscle relaxation. *avr-15* codes for a glutamate-gated chloride channel that is expressed in extra-pharyngeal neurons and pharyngeal muscle cells PM4 and PM5. The glutamate-containing neuron M3 synapses onto PM4 and acts to regulate the timing of muscle relaxation during pumping (Avery 1993). Inhibitory post synaptic potentials (IPSPs) can be observed in the EPG trace during normal pharyngeal pumping and are not generated when M3 is not functional. The pharynx of the *avr-15* loss-of-function mutant *ad1051* does not generate IPSPs, demonstrating that it is required for glutamate's inhibitory action on the pharynx.

*C. elegans* also have metabotropic glutamate receptors. These are G-protein coupled receptors. Genes coding for three such receptors have been identified, *mgl-1*, *mgl-2* and *mgl-3* (Dillon *et al* 2006). Little is known about the role that these receptors play in glutamatergic signaling in *C. elegans*.

*C. elegans* has over a hundred genes coding for various types of neuropeptides. *C. elegans* neuropeptides include insulin-like peptides (*ins* genes), FMRFamide-related peptides (*flp* genes) and non-insulin like / non-FMRFamide like peptides (*nlp* genes). Neuropeptides are derived from larger precursor molecules that are cleaved to produce active molecules. Neuropeptides are processed by two key enzymes. Protein convertase, which is required for the initial cleavage of the precursor peptide (Kass *et al* 2001), and carboxy-peptidase, which removes a flanking basic sequence from the peptides (Jacob and Kaplan 2003). FLP peptides have been shown to have a variety of physiological effects. Papaioannou *et al* (2005) demonstrated a role for the FLP peptides in the regulation of pharyngeal pumping. Liu *et al* (2007) showed that signaling mediated by the FLP peptides coded for by *flp*-8, *flp*-10, *flp*-12, and *flp*-20 are required for the sensory transduction involved in male turning behaviour. Peptides coded for by *flp*-1 have also been shown to regulate the egg laying interval (Waggoner *et al* 2000). The NLPs occur in the pharyngeal neurons (Li 2005) and excite pharyngeal muscle (Papaioannou *et al* 2008). NLPs have also been implicated in an innate immune response (Couillault *et al* 2004). The insulin-like peptides have been found to have a role in the life span of *C. elegans* (Gami and Wolkol 2006). However, these peptides are likely to be involved in many other processes that have yet to be identified.

## 1.07 Forward and reverse genetics

As well as being a good model for parasitic nematodes, *C. elegans* has the advantage of being amenable to genetic manipulation. Such manipulations include mutagenesis, RNA interference and trans-gene expression. When investigating molecular mechanisms in *C. elegans* either forward or reverse approaches can be taken. Reverse genetic techniques are hypothesis driven. Analysis of the phenotypes of mutants with specific mutations can be used to inform about the role of genes in a drug's mode of action. Alternatively, RNA interference can be used to knock down the expression of specific genes. The drawback of the reverse genetic approach is that prior knowledge about the mechanism is required. In this respect, the forward genetic approach does not have this problem. No prior knowledge about the mechanism is required. Forward genetics also has been successfully used in determining drug mode of action. This technique was pioneered in *C. elegans* by Sidney Brenner. This involves a random mutagenesis followed by screening for a specific phenotype. The mutation resulting

in the phenotype can then be mapped and the gene involved identified. Brenner (1974) generated mutants partially resistant to the effects of the anthelmintic levamisole and identified specific genes involved in these resistance mechanisms. The completion of sequencing of the *C. elegans* genome (The *C. elegans* sequencing consortium 1998) now makes the process of mapping and identification of genes involved much easier. These techniques are further discussed in the methods section.

## 1.08 Human parasitic nematodes and other zoonotic parasites

It is estimated that more than one third of the world's population harbour parasitic worms, of which 300 million suffer permanent ill health as a result (World health report 2000). Parasitic worm infections primarily affect populations in developing countries. Parasitic worms can be divided into three categories: nematodes, cestodes and trematodes, the latter two being platyhelminths. Humans become infected by cestodes through ingestion of under-cooked or raw meat containing larvae or material contaminated by faeces. Nematodes, which include the common round worm (*Ascaris lumbricoides*) thread worm (*Enterobius vermicularis*), hook worm (*Ancylostoma duodenal*) and whip worm (*Trichuris trichiura*), are transmitted through the ingestion of eggs from contaminated soil or by penetration of the skin by larvae. These nematodes and cestodes reside in the gut of their host. Other nematodes reside in various tissues of their hosts, including the lymphatic system, subcutaneous tissue, eye and skeletal muscle. These nematodes include *Wuchereria bancrofti* and *Onchocerca volvulus* which cause the diseases elephantiasis and onchocerciasis (river blindness). Trematodes cause schistosomiasis, infecting humans through penetration of the skin. They reside in the veins of the gut or bladder, resulting in inflammation of these tissues as well as haematuria and loss of blood in the faeces.

The control of parasitic nematodes in humans presents a challenging problem in the developing world. The problem is one of access to treatment. In 2001 the Partners for Parasitic Control (PPC) was launched in order to urge countries with endemic nematode and schistosome infections to tackle the problem, as well as developing a global databank. The PPC is composed of agencies of the United Nations, WHO Members States, research institutes and NGOs. One key goal of the PPC is to provide preventative treatment to 75% of

school aged children at risk of morbidity by 2010. Table 1.02 shows the proportion of the school aged children at risk of morbidity from nematode and schistosome infections that have received treatment from 2003 to 2007. The proportion in 2007 was 5.6%.

| School age children | 2003 | 2004 | 2005 | 2006 | 2007 |
|---|---|---|---|---|---|
| Total treated | 25,844,440 | 40,734,389 | 62,169,783 | 76,751,236 | 49,173,431 |
| Total at risk of morbidity in all endemic countries | 878,209,058 | 877,987,807 | 877,861,438 | 877,082,032 | 878,082,032 |
| Percent coverage achieved | 2.9% | 4.6% | 7.1% | 8.7% | 5.6% |
| No. of countries reported data | 48 | 54 | 59 | 62 | 48 |

**Table 1.02. Preventative treatment of school age children for nematode and schistosome infections in endemic countries.** Total numbers and proportion of school aged children at risk who have been treated for nematode and schistosoma infections in 2003, 2004, 2005, 2006 and 2007. Data compiled by the World Health Organisation.

## 1.09 Nematode infections in live stock

Parasitic nematode infections result in poor food quality, poor animal health and low profitability. Anthelmintics are widely used to treat infections in all areas of agriculture. A 1997 survey conducted by the US department of agriculture revealed that 77% of US beef cattle farmers treat their herds with anthelmintics (Corwin 1997). Ruminants are affected by many different parasitic nematodes that can reside in the abomasum, small intestine, large intestine or lungs. *Haemonchus contortus* resides in the abomasum of sheep and goats and is considered to be one of the most pathogenic parasites. It is a blood sucking parasite that is found predominantly in tropical and sub-tropical climates but has been found in European countries as far north as Sweden (Waller and Chandrawathani 2005). Infection by *H. contortus* may be hyperacute, acute, or chronic. In the hyperacute disease, death may occur within one week of heavy infection without significant signs. The acute disease is characterised by anaemia and oedema (Zajac 2006). *Cooperia oncophora* resides in the small intestine of cattle. *C. oncophora* produces a relatively mild disease state but it can be responsible for weight loss and poor productivity. *Dictyocaulus viviparous*, commonly known as lung worm, affects cattle. It can result in obstruction of the airways and collapse of alveoli. With large numbers of larvae present, the animal may die with severe interstitial emphysema (Zajac 2006). These are just a few examples of the most economically relevant parasitic nematodes that affect the health and productivity of live stock.

## 1.10 Plant parasitic nematodes

Plant parasitic nematodes are one of the greatest threats to crops across the world. The potato cyst nematodes *Globodera rostochiensis* and *Globodera pallida* are such examples. The UK potato industry employs more than 30,000 people and maintains the economic viability of 500,000 hectares of farm land. *G. rostochiensis* and *G. pallida* live and feed on the root tips of potatoes and other plants. This results in damage to the roots and can result in up to an 80% reduction in yield from the crop (Kerry *et al* 2002).

## 1.11 Parasitic nematode infections of companion animals

Companion animals such as cats and dogs are commonly infected with parasitic nematodes. Treatment of infected pets is especially important as there is the potential for infection of humans, who are often in close contact. Domestic cats are commonly infected by the parasitic nematodes *Toxicara cati* and *Toxicara leonina*. Dogs are commonly infected by *T. leonina* and *T. canis*, which can be lethal in pups. The larvae of these nematodes can migrate to the tissues of many species, including humans. Although this is usually asymptomatic, fever, eosinophilia and hepatomegaly can result. This condition is known as viscera larval migrans. A condition known as ocular larva migrans can occur when larva settle in the eye, causing impairment of vision (Fisher 2003).

## 1.12 Treatment of parasitic nematode infections in livestock and domesticated animals

Parasitic nematode infections are treated using a group of compounds known as anthelmintics. There are an increasing number of different anthelmintics available that have a variety of mechanisms of action.

**Nicotinic ACh receptor agonists:** Levamisole and pyrantel are both examples of anthelmintics that are nicotinic ACh receptor agonists. These drugs act at the nematode neuromuscular junction. Through the use of tension and electrophysiological recordings from *Ascaris* muscle strips Acever *et al* (1970) demonstrated that levamisole causes a contraction.

This results in a spastic paralysis of the worms which are then passed out through the faeces. Genetic evidence for the activation of nicotinic ACh receptors comes from work done in *C. elegans*. Fleming *et al* (1997) demonstrated that loss of function of nicotinic ACh receptor subunits *unc-29*, *unc-31* and *lev-1* resulted in a high level of resistance to levamisole.

**GABA agonists:** Piperazine causes flaccid paralysis and paralysed worms are passed out through the faeces alive. Martin (1982) demonstrated that both GABA and piperazine caused in increase in input conductance in *A. suum* muscle. This increase was shown to be reduced when the preparation was bathed in a low chloride Ringer, indicating piperazine increases chloride conductance. Later, patch clamp experiments directly demonstrated that piperazine caused an opening of chloride channels (Martin *et al* 1985).

**Avermectins:** The avermectins include ivermectin, doramectin, moxidectin and abamectin (Martin *et al* 1997). Ivermectin is widely used in veterinary medicine and is used to treat onchocerciasis. Abamectin is used as a pesticide for crop protection. Avermectins have been shown to act as antagonists of the *A. suum* muscle GABA receptors (Holden-Dye and Walker 1990). However, this action was only observed at concentrations that were not clinically relevant. Attention has more recently turned to the glutamate gated chloride channels. Evidence for their role has come from pharmacological studies in *Xenopus* oocytes into which *C. elegans* RNA was injected. It was shown that a chloride dependent inward current could be induced by both glutamate and ivermectin and it was proposed that these currents were mediated by the same channel (Arena *et al* 1992). Activation of chloride dependent inward currents by glutamate and ivermectin was observed in oocytes expressing two specific *C. elegans* glutamate gated chloride channel subunits, α and β (Cully *et al* 1994). These currents could be induced by ivermectin in *Xenopus* oocytes expressing the α-type subunit alone. Mutations in the glutamate gated chloride channel α subunits has been shown to confer resistance to ivermectin. A triple mutant of *avr-14*, *avr-15* and *glc-1* confers a 4000 fold increase in survival when exposed to ivermectin (Dent *et al* 2000). AVR-15 has been shown to mediate ivermectin's response in the *C. elegans* pharynx (Dent *et al* 2000; Pemberton *et al* 2001).

**Praziquantel:** Praziquantel has little effect against nematodes and is used primarily as a treatment for schistosomiasis. Praziquantel causes a slow depolarisation of the tegument that is associated with an influx of calcium ions. This results in paralysis and death of the parasite.

Proposed sites of action for praziquantel include: voltage-activated calcium channels, intracellular messenger activated calcium channels, extracellular receptor operated calcium channels, non-selective cation channels also allowing entry of calcium, sodium / calcium exchanger, calcium ATPase, intrategumental calcium buffers, $IP_3$ releasable store from the sarcoplasmic reticulum, calcium-induced calcium release channels (CICR channel), calcium ATPase pump: sarcoplasmic endoplasmic reticulum calcium (SERCA), electrical junctions between muscle cell and tegument, electrical junctions between muscle cells (Redman *et al* 1996).

**Benzimidazoles:** Benzimidazoles include mebendazole, thiabenazole and albendazole. The mode of action of benzimidazoles involves their binding to β tublin. α and β tublin polymerise to form microtubule structures which are major components of eukaryotic cilia and flagella. Benzimidazoles inhibit the formation of microtubules, resulting in damage to intestinal cells and starvation of the nematode (Van Den Bossche and De Nollin 1973, Sangster *et al* 1985). The time-frame in which these drugs act is therefore longer than anthelmintics that disrupt neuromuscular transmission.

**Novel treatments:** Due to the emergence of resistance to many commonly used anthelmintics, novel ways of combating nematode infections need to be continuously developed. These can be traditional pharmacological therapies or an alternative approach can be taken. There is the potential to vaccinate against nematode infections. A variety of potential antigens have been described for use in vaccination (Knox and Smith 2001, Bakker 2004). Novel classes of anthelmintics include amino-acetonitrile derivatives (AADs) and cyclo-octadepsipeptides. AADs target a specific nicotinic ACh receptor subunit ACR-23 (in *C. elegans*), causing hypercontraction resulting in a spastic paralysis (Kaminsky *et al* 2008). The cyclo-octadepsipeptides are the subject of this thesis and will be discussed in the following sections.

## 1.13 Anthelmintic resistance mechanisms

Resistance to anthelmintics arises through spontaneous mutations in proteins key to their mode of action. Resistance typically arises due to the over use of anthelmintics. Resistant populations can then become established due to selection whilst using a single anthelmintic in

the treatment of parasitic worm infections (Williams 1997). These mutations causing resistance may either affect the binding of an anthelmintic to a receptor or proteins involved in the modulation of this receptor. Alternatively, mutations in proteins unrelated to the anthelmintic's mode of action, such as those involved in drug metabolism, may lead to resistance. Various mechanisms of resistance exist for a number of anthelmintics. In the following section some of these mechanisms are discussed. The nematode *C. elegans* has proved useful in understanding resistance mechanisms.

Mutation in a variety of nicotinic ACh receptor subunits has been shown to confer resistance to levamisole in *C. elegans*. Fleming *et al* (1997) showed that mutations in the α-nACh receptor subunit *unc-38* and the non-α-nACH subunits *lev-1* and *unc-29* conferred a high level of resistance to levamisole. Although the generation of resistant *C. elegans* is useful for mode of action studies, it is not necessarily that informative about resistance in parasitic nematodes. *C. elegans* carrying mutations that confer high levels of resistance often have severe locomotor and egg laying phenotypes that could not be sustained by parasitic nematodes. The mechanisms of levamisole resistance in parasitic worms are not well understood. Sangster *et al* (1998) demonstrated that levamisole has high and low affinity binding sites in *H. contortus* larval and parasitic stage homogenates. Resistant isolates of *H. contortus* had a lower binding affinity for the [$^3$H]*m*-aminolevamisole, suggesting an alteration in the low affinity binding site. Robertson *et al* (1999) analysed levamisole sensitive single channel currents in *Oesophagostomum dentatun* muscle. Currents in both levamisole sensitive and resistant isolates were recorded. Different channel populations were identified in terms of conductance in the resistant and sensitive isolates. This was interpreted as a shift in the proportion of the heterogenous nACh receptor subtypes to receptors less sensitive to the drug. Attempts to identify specific mutations that confer resistance in parasitic nematodes have been made without success. Correlation between *H. contortus* nACh receptor subunit sequence HCA1, a homologue of *C. elegans unc-38*, and levamisole resistance could not be established (Hoekstra *et al* 1997).

Resistance to benzimidazoles has been shown to be due to a reduced binding to β-tubulin (Kohler 2001, Lacey 1988). In *H. contortus* reduced binding has been shown to be due to a point mutation in β-tubulin. A correlation between resistant alleles and a phenylalanine to tyrosine amino acid substitution at position 200 in the β-tubulin was established (Kwa *et al* 1994). It was confirmed that this mutation conferred resistance through the use of the model

organism *C. elegans* (Kwa *et al* 1995). *H. contortus* β-tubulin isotypes of *tub-1* were expressed in *C. elegans ben-1*(*u462*), a β-tubulin mutant resistant to the effects of thiabendazole. Expression of the *tub-1* isotype encoding phenylalanine at amino acid position 200 conferred thiabendazsole sensitivity to the *ben-1*(*u462*) mutant. Expression of the *tub-1* isotype encoding tyrosine at amino acid position 200 failed to confer thiabendazole sensitivity, strongly suggesting that this point mutation is responsible for the resistance observed in *H. contortus*.

Resistance to ivermectin has been widely reported in a variety of species. In *C. elegans* a high level of resistance can be achieved by simultaneous mutation of three α-type glutamate-gated chloride channels, *avr-14*, *avr-15* and *glc-1* (Dent *et al* 2000). Although the phenotypes of this triple mutant are relatively modest, they may be less sustainable in parasitic nematodes. It may be that the lower levels of resistance are more relevant to understanding resistance in parasitic nematodes. A variety of genes were found to have a modulatory role in ivermectin sensitivity in *C. elegans*. These include the gap junction subunits *unc-7* and *unc-9* and mutants that are thought to have reduced permeability to ivermectin (*osm-1*, *osm-5*, *dyf-11* and *che-3*) (Dent *et al* 2000). Genetic analysis of *H. contortus* resistant to ivermectin suggests that a single gene controls the resistance mechanism (Jambre *et al* 2000). Resistance in a *Trichostrongylus colubriformis* isolate was found to be dependent on more than one gene. Multiple mechanisms of resistance are likely to exist in many parasitic nematode species.

Resistance to currently used anthelmintics is continually developing. New anthelmintics that are effective against resistant populations therefore need to be developed in order to maintain an effective arsenal for the treatment of parasitic nematode infections.

## 1.14 Cyclo-octadepsipeptides

The cyclo-octadepsipeptides are a group of compounds that have anthelmintic activity. Emodepside is a derivative of the natural compound PF1022A. PF1022A is a fermentation product of the fungus *Mycelia sterilia*, and is found in the microflora on the leaves of *Camellia japonica*. Sasaki *et al* isolated it and determined its structure in 1992 (Sasaki *et al*, 1992). It belongs to a class of N-methylated, 24-membered cyclo-octadepsipeptides. Figure

1.06 shows the structure of PF1022A and a semi synthetic derivative, emodepside (BAY44-4400).

**A)** **B)**

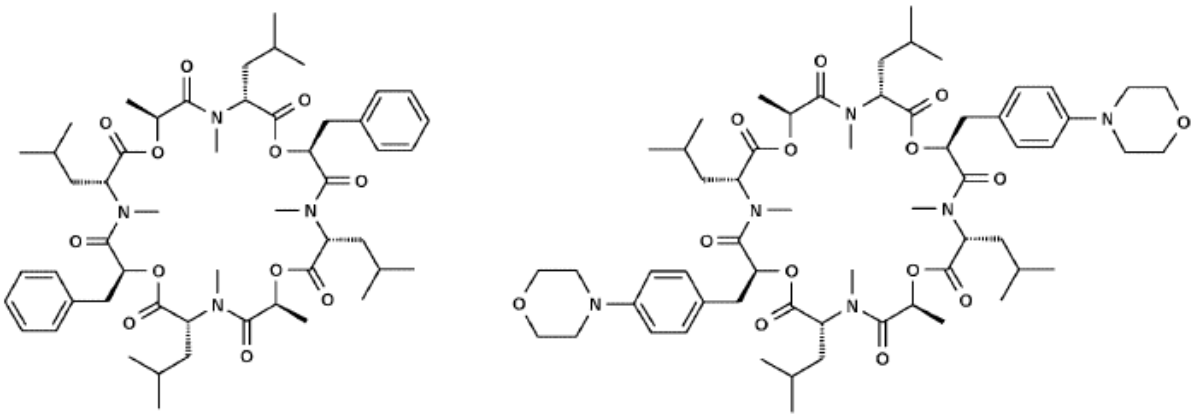

**Figure 1.06. Structure of A) PF1022A and B) emodepside (BAY44-4400)**. (Adapted from Harder & Samson-Himmelstjerna, 2002).

Both of these compounds were patented by the Fujisawa Pharmaceutical Co. in 1993. Both PF1022A and emodepside have been shown to have potent anthelmintic activity in a variety of species. Initial experiments were performed by Tagaki *et al.* in 1991 on *Ascaridia galli* in chickens. Emodepside has now been shown to have efficacy in a variety of nematodes in cattle, sheep, horses, cats, dogs, chickens and rodents (Harder & Samson-Himmelstjerna, 2002). Emodepside has resistance breaking properties. This is of key importance as it permits emodepside to be used to treat parasitic worm infections where other treatments have failed. It also suggests that emodepside has a novel mode of action as resistance often develops to a class of compounds rather than to a single compound. Emodepside was found to be effective against *H. contortus* isolates with resistance to ivermectin and levamisole and against *C. oncophora* isolates with resistance to ivermectin. PF1022A was found to be effective against *H. contortus* isolates with resistance to the benzimidazole, febantel (Harder and Von Samson-Himmelstjerna 2002).

Essential characteristics to the success of the cyclo-octadepsipeptides as marketable anthelmintics include selective toxicity for the parasite and minimal host side effects. Much testing of PF1022A has been carried out against a range of parasitic nematodes and in various hosts, alongside the documentation of any side effects observed. Various methods of

application of the PF1022A have also been tested. No side effects resulted from PF1022A being administered orally to rats (in doses up to 100 mg/kg body weight), dogs (in doses of 5 mg/kg body weight) or cattle (in doses of 5 mg/kg body weight ; Samson-Himmelstjerna *et al* 2000). The intramuscular administration of PF1022A to dogs (in doses of 5 mg/kg body weight) and its intravenous administration to cattle (in doses of 1 mg/kg of body weight) did not result in side effects either (Samson-Himmelstjerna *et al* 2000). In fact, none of the modes of administration of PF1022A to either rats, dogs, sheep, horses or cattle resulted in any side effects (Samson-Himmelstjerna *et al* 2000). Mice were also found to tolerate PF1022A administered orally at concentrations as high as 2000 mg/kg of body weight (Sasaki *et al* 1992). The concentrations used in these experiments were highly effective at clearing parasitic nematode infections in the host animals. The fact that no side effects were observed in the hosts with the oral applications shows that PF1022A has toxicity selective for the parasites. However, it is possible that this could be due to reasons of drug mobility. The fact that no side effects were observed following systemic application suggests that the nature of the selective toxicity is molecular. Emodepside is currently marketed under the trade name Profender, which is a mix of emodepside and praziquantel. It is administered by absorption through the skin, again demonstrating the selective nature of its toxicity.

## 1.15 Emodepside's effects on *C. elegans*

Emodepside's action in *C. elegans*: Emodepside causes inhibition of locomotion, pharyngeal pumping, egg laying and also slows development (Willson *et al* 2004, Amliwala 2005, Bull *et al* 2007). The effects of emodepside on pharyngeal pump rate in *C. elegans* were measured using the EPG technique. Basal pump rate was stimulated using 500 nM 5-HT. The $IC_{50}$ for emodepside on 5-HT stimulated pump rate is 4.1 nM. Amliwala (2005) exposed *C. elegans* eggs to emodepside on agar plates. The effect of emodepside on the rate of locomotion of the adult worms was measured. The $IC_{50}$ for emodepside's effect on locomotion is 4.2 nM in this assay. Bull *et al* (2007) investigated the effect of emodepside on growth rate and egg laying. Growth rate was retarded by emodepside at concentrations of 10 nM or higher. Emodepside concentrations of 20 nM and above were shown to have inhibitory effects on egg laying rate.

## 1.16 Cyclo-octadepsipeptide mode of action

Understanding the molecular mechanism of action of cyclo-octadepsipeptides is of great interest. Knowledge of the molecular target for cyclo-octadepsipeptides provides the opportunity to design compounds with increased effectiveness. Cyclo-octadepsipeptides potentially have a variety of medical, veterinary and agricultural applications. An understanding of their mechanism of action would allow these potential applications to be more easily identified. The following section reviews our current knowledge of the mode of action of cyclo-octadepsipeptides.

**Ionophore characteristics:** Cyclo-octadepsipeptides such as valinomycin, enniatin A and beauvericin have been shown to have ionophore characteristics in planar lipid bilayers. PF1022A might also exert its anthelmintic effect through an ion carrier mechanism. The effects of a number of depsipeptides were investigated using three different approaches (GeBner *et al.*, 1996). 1) *in vivo* activity against a variety of parasitic nematodes, 2) *in vitro* studies using *Ascaris suum* and 3) electrophysiological studies on planar bilayers. It was shown that a number of octa-depsipeptides, which do not have ionophore characteristics, have potent anthelmintic activity. On the other hand, some depsipeptides with ionophore activity did not show any anthelmintic effects. Most notably the PF1022A isomer, PF1022-001, was shown to have similar ionophore activity in planar lipid bilayers but virtually no anthelmintic

activity when tested *in vivo*. The compound SBJ1822 on the other hand shows no pore forming activity in planar lipid bilayers but has a strong anthelmintic activity. The effects of PF1022A, SJB1822 and PF1022-001 on the spike potentials of *A. suum* muscle cells were investigated. It was shown that characteristic irregular potential spikes occurring in these cells were suppressed by a five hour incubation with PF1022A and SJB1822. PF1022-001 on the other hand had no effect on spike activity. Based on these observations it appears that it is not a pore forming activity but a more specific action that is required for anthelmintic activity (GeBner *et al.*, 1996). The following section discusses the effects that emodepside has on neuromuscular transmission.

**GABA-ergic effects of Cyclo-octadepsipeptides:** The mechanism of action of PF1022A has been examined neuropharmacologically using *Angiostrongylus cantonesis*, and a variety of pharmacological agents (Terada, 1992). Paralysis of *A. cantonesis* by PF1022A was shown to be partially reversed by the action of GABA-ergic antagonists such as bicuculline and picrotoxin. This indicated that PF1022A might cause paralysis through stimulation of GABA release and/or by enhancing post-synaptic GABA effects. The effect of N-methylcytisine, which causes ACh release, was to reverse PF1022A-induced paralysis when applied with GABA-ergic antagonists. Additionally, the spasmogenic effects of N-methylcytisine and eserine (an ACh esterase inhibitor) in the presence of GABA-ergic antagonists are inhibited by PF1022A. This suggests that PF1022A causes a decrease in ACh effects. Terada *et al* (1992) suggest that PF1022A produces an inhibition of the cholinergic system whilst synergistically stimulating the GABA-ergic mechanism. Alternatively, these results may be explained by a general inhibitory effect of PF1022A. A decrease in GABA-ergic activity and an increase in cholinergic activity would both counteract a general inhibitory effect of PF1022A on nematode muscle.

Chen *et al* (1996) also suggested that GABA receptors in the muscle of *A. suum* play a role in the mechanism of action of PF1022A. In these experiments, membrane protein was prepared from the homogenate of somatic muscle cells. PF1022A was shown to displace [2,3-$^{3}$H(N)]-GABA and [methyl-$^{3}$H] bicuculline (an antagonist of mammalian $GABA_A$ receptors) in a concentration-dependent way. However, these results may have been misinterpreted as bicuculline has been shown not to antagonize *A. suum* $GABA_A$ receptors (Walker *et al* 1992).

Willson *et al* (2003) investigated the effect of emodepside at the neuromuscular junction, in the parasitic nematode *A. suum*. In these experiments, tension measurements of the dorsal muscle strip (DMS) and sharp electrode recordings from individual muscle cells were performed. 10 μM emodepside was shown to cause a relaxation of basal tension of the DMS. When the DMS was pre-treated with 30 μM ACh, causing rapid contraction, emodepside (1-10 μM) caused a time-dependent reduction in the amplitude of the contraction. To investigate the emodepside-induced relaxation, Willson *et al.* (2003) investigated the effects of the inhibitory neurotransmitters GABA and neuropeptide PF2. In contrast to the slow and partial relaxation caused by emodepside, GABA caused a rapid and complete relaxation (ie. basal level of tension). Neuropeptide PF2, on the other hand, caused slow and incomplete relaxation, similar to that of emodepside.

To investigate if these effects of emodepside were through a direct action on the muscle or via neurotransmitter release, experiments were conducted using a denervated DMS. The response to ACh of a denervated DMS preparation was not significantly inhibited by 10 μM emodepside but neuropeptide PF2 continued to inhibit it, suggesting that emodepside's mode of action involves neurotransmitter release. The sharp electrode recordings from the muscle cells showed that emodepside caused a slow and irreversible hyperpolarisation. This hyperpolarisation was reduced with the removal of calcium ($Ca^{2+}$), and was not observed in the presence of 4-aminopyridine (4-AP) and tetraethylammonium (TEA), both potassium ($K^{+}$) channel blockers. These results are consistent with a role for $Ca^{2+}$-dependent neurotransmitter release in the mechanism of emodepside, or alternatively with the requirement for $Ca^{2+}$ for the activation of a current on the muscle membrane e.g. a $Ca^{2+}$-dependent voltage-activated $K^{+}$ channel.

**Latrophilin receptors:** α-Latrotoxin (αLTX) is a component of the venom of *Lactrodectus* spiders, the most common of which is the black widow spider (Frontali *et al* 1976). It was observed that α-Latrotoxin depleted nerve terminal of vesicles at the frog neuromuscular junction (Frontali *et al* 1976). The effect of this venom is to cause global neurotransmitter release. A component of the mechanism of action of αLTX is through the formation of pores in cell membranes (Lui and Misler 1998, Orlova *et al* 2000), through which cations flow, resulting in depolarisation and the release of synaptic vesicles. Part of αLTX's effects are mediated by receptors. αLTX interacts with two distinct membrane proteins, neurexin and latrophilin. Neurexin is a neuron specific protein that binds αLTX only in the presence of

calcium. They are thought to function as cell adhesion molecules in the synaptic cleft. The *Drosophila* neurexin mutant has been shown to be defective in synapse formation (Zeng *et al* 2007). Neurexin has been shown to bind to another cell adhesion molecule known as neuroligin, bridging the synaptic cleft (Levinson and El-Husseini 2007). The role of neurexin with regard to αLTX is thought to be one of anchoring it in the cell membrane (Bittner 2000). Latrophilin receptors are G-protein-coupled receptors (GPCR) (Krasnopernov *et al* 1999). Binding of αLTX to latrophilin is thought to result in activation of the GPCR and a pathway resulting in neurotransmitter release, this process is calcium independent.

Volynski *et al* (2000) demonstrated a mechanism of αLTX-induced neurotransmitter release independent of its pore forming activity. They performed experiments in which a non pore forming mutant of αLTX, $\alpha LTX^{N4C}$, was used. It was demonstrated to be non pore forming through whole cell recordings in COS7 cells expressing exogenous latrophilin. αLTX caused large inward currents but no current was observed with $\alpha LTX^{N4C}$. Binding levels of αLTX and $\alpha LTX^{N4C}$ cannot account for these differences as it was shown, through Western blotting, that binding levels are similar. It was also demonstrated that $\alpha LTX^{N4C}$ was unable to form tetramers but $\alpha LTX^{WT}$ was. Tetrameric αLTX is thought to have the ability to form pores in the membrane, whereas monomeric and lower oligomeric forms are not. Volynski *et al* (2000) showed that application of $\alpha LTX^{N4C}$ to rat synaptosomes loaded with [$^{14}$C]-glutamate induced transmitter release. To check this release was not due to the presence of a small number of pores formed by $\alpha LTX^{N4C}$, $La^{2+}$, an effective blocker of αLTX pores was added. The amount of [$C^{14}$]-glutamate release was not significantly different. The effect of $La^{2+}$ on $\alpha LTX^{WT}$ treated synaptosomes was to reduce the level of [$C^{14}$]-glutamate release to levels seen using $\alpha LTX^{N4C}$. This demonstrates that αLTX has the ability to induce neurotransmitter release through a mechanism other than through the formation of pores in the membrane.

Saeger *et al* (2001b) identified a *H. contortus* latrophilin receptor HC110-R as a target for emodepside. A cDNA expression library was constructed from *H. contortus* using λZAPII. Nitrocellulose filters were incubated with a PF1022A-keyhole limpet haemocyanin (KLH) conjugate prior to incubation with an anti PF1022A-KLH antibody. Finally, incubation with a secondary antibody was conducted for detection. Sequencing of cDNA resulted in the identification of a 3539 bp cDNA sequence encoding an orphan seven transmembrane receptor. This was termed HC110-R, the structure of which is shown in figure 1.07. The binding of emodepside was shown to occur particularly in the 54 kDa amino-terminal region

of HC110-R. This was demonstrated through expression of the 54 kDa amino-terminal region in *E. coli* followed by poly-acrylamide gel electrophoresis and Western blot analysis. Homologues of HC110-R were identified in *C. elegans* through database and phylogenetic analysis. There are two latrophilin-like receptors in *C. elegans*: *lat-1* (B0457.1) and *lat-2* (B0266.2). LAT-1 has 47% amino acid identity with HC110-R. LAT-2 has homology with HC110-R in the galactose binding lectin domain (22% identity), the hormone receptor domain (19% identity) and the G-protein-coupled receptor proteolytic site and seven transmembrane domains (39% identity). These regions are highlighted in figure 1.07. HC110-R has an overall identity of 20% with LAT-2. LAT-2 has homology with LAT-1 in the galactose binding lectin domain (22% identity), the hormone receptor domain (22% identity) and the G-protein-coupled proteolytic site and seven transmembrane domains (38% identity). Overall, LAT-1 has 20% identity with LAT-2. Although the identity between these G-protein-coupled receptors is relatively low, the *C. elegans* latrophilin receptors, LAT-1 and LAT-2, belong to the same class and sub-class of G-protein coupled receptors. They belong to the class of G-protein-coupled receptors known as the secretin family (family B), and to the sub-class known as the LNB-7TM (B2) (Foord *et al* 2002). The B2 sub-class differs from other G-protein-coupled receptors in that they have a large amino terminal region that can be cleaved at the G-protein-coupled receptor proteolytic site. Of the G-protein-coupled receptors in *C. elegans,* only three fall into the B2 family. LAT-1 and LAT-2 are most closely related. The third, F15B9.7, is more distantly related (Harmar, 2001).

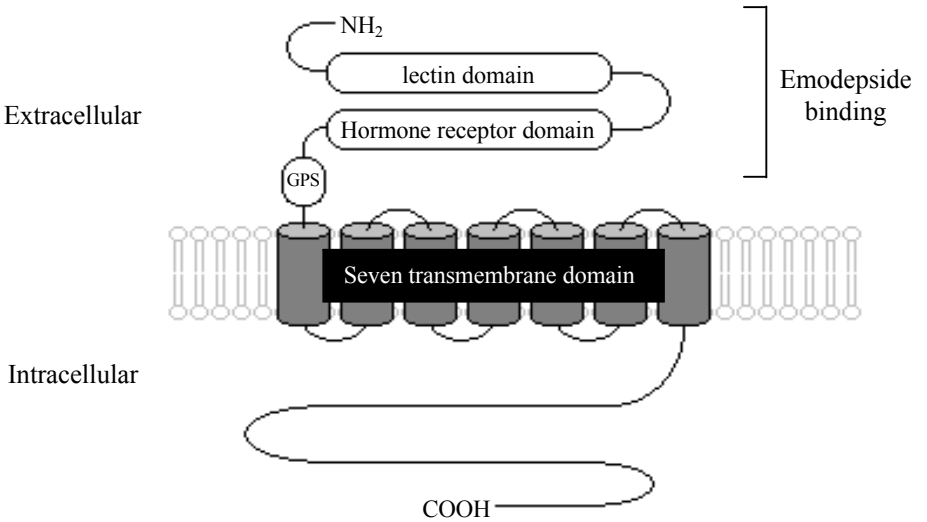


**Figure 1.07. Model of HC110R in the plasma membrane**. The proposed binding region for α-LTX and PF1022A are marked. The conserved galactose binding lectin domain, hormone receptor domain and G-protein proteolytic site domain are highlight. Emodepside binding occurs in the amino terminal region. (Created using NCBI conserved domain search tool / adapted from Saeger *et al* 2001).

Using fluorescence imaging techniques, Saeger *et al* (2001) demonstrated that α-LTX was able to induce an influx of $Ca^{2+}$ in HEK293 cells transformed with HC110-R. PF1022-001 and emodepside did not cause an influx of $Ca^{2+}$ but did antagonise the effect of LTX on $Ca^{2+}$ influx.

A series of experiments employing gene knock down in components of a hypothesized vesicle release pathway in *C. elegans* indicate that emodepside causes release of neurotransmitters, resulting in paralysis (Willson *et al* 2004). Willson *et al* (2004) investigated the role of latrophilin receptors in emodepside's mode of action using the EPG technique. To determine whether the latrophilin receptor was involved in the potent effect of emodepside on the *C. elegans* pharynx, RNA interference (RNAi) was used to knock down the *lat-1* gene. The pharynxes of the *lat-1* RNAi treated *C. elegans* were shown to be resistant to concentrations of up to 100 nM emodepside. RNAi of *lat-1* also led to a reduction in sensitivity to emodepside on locomotion. RNAi of *lat-2* lead to a reduction in sensitivity to emodepside on locomotion and a slight reduction in sensitivity to its effects on pharyngeal pumping (Willson *et al* 2004, Amliwala 2005).

The expression pattern of *lat-1* was also examined. This was done using a *lat-1*::DsRed2 reporter construct. In larval stages, staining was most prominent in the muscle. In adult worms, expression was predominantly in the anterior neurons, both pharyngeal and extra-pharyngeal. This suggests that the role that the LAT-1 receptor plays in emodepside's mode of action is neuronal in adult worms (Willson *et al.*, 2004b). Willson *et al* (2004) went on to screen several mutant strains for emodepside resistance in order to investigate the possibility of emodepside's involvement in latrophilin mediated neurotransmitter release.

LAT-1 is a G-protein coupled receptor. The G-protein subunit Gαq has been shown to have a role in the activation of pharyngeal pumping and locomotion in *C. elegans* (Brundage *et al* 1996). The *C. elegans* Gαq, *egl-30*, activates phospholipase C when expressed in COS-7 cells. The *C. elegans* G-protein subunit Gαo, *goa-1*, appears to negatively regulate synaptic transmission. *goa-1* loss of function mutants have hyperactive locomotion and egg laying. Genetic analysis showed that Gαo negatively regulates Gαq (Miller *et al* 1999). Figure 1.08 shows a simplified diagram illustrating the role of the G-protein subunits Gαq and Gαo in neurotransmitter release. Activation of Gαq results in an increase in diacylglycerol (DAG). Gαq activates PLC-β which hydrolyses phosphatidylinositol-4,5-bisphosphate (PIP2) to

inositol-1,4,5-triphosphate (IP3) and DAG. DAG then binds to the UNC-13, part of the synaptic vesicle release machinery that is responsible for vesicle priming (Hurley *et al* 1997). Binding of DAG to UNC-13 is thought to facilitate neurotransmitter release in *C. elegans* (Lackner *et al* 1999). Activation of Gαo results in a decrease in DAG. Gαo activates DAG kinase, which converts DAG to phosphatidic acid. Reduced DAG binding to UNC-13 would be expected to reduce neurotransmitter release. The role of Gαq, Gαo, PLCβ and UNC-13 in emodepside's mode of action were investigated (Willson *et al* 2004).

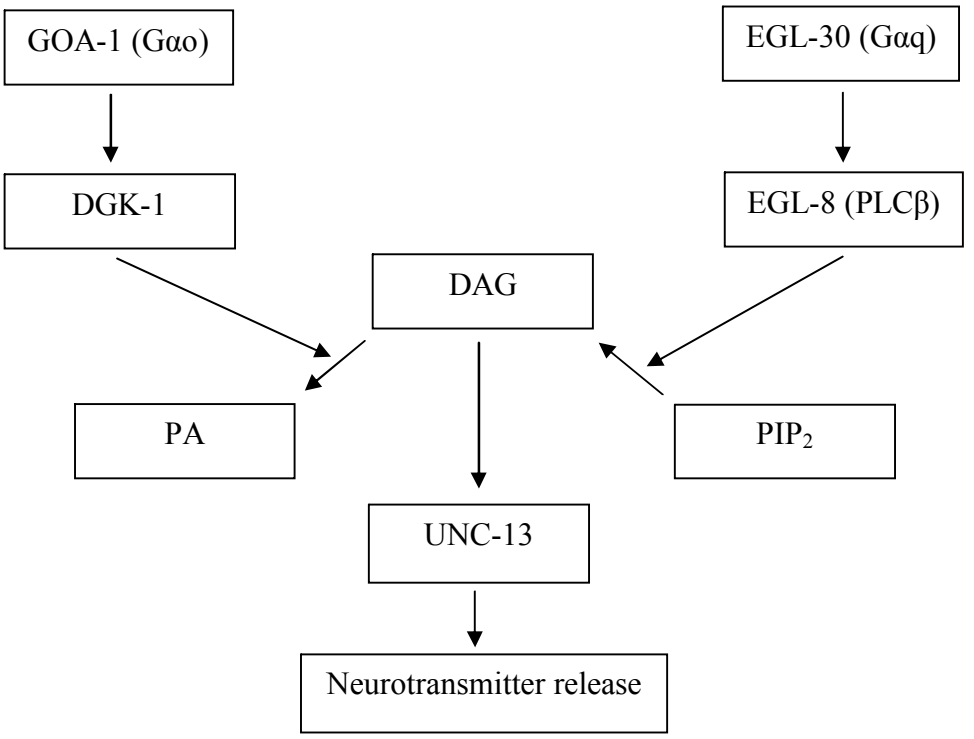


**Figure 1.08. G-protein coupled receptor regulation of neurotransmitter release.** (Adapted from Bastiani and Mendel 2006).

Reduction-of-function Gαq mutant *egl-30*(*ad806*) showed reduced sensitivity to emodepside and a gain-of-function mutant *egl-30*(*tg26*) showed increased sensitivity on both pharyngeal pumping and locomotion. Gαo reduction-of-function mutant *goa-1*(*n1134*) showed increased sensitivity to emodepside both in pharyngeal pumping and locomotion (Willson *et al* 2004). PLC-β reduction-of-function mutants *egl-8*(*md1971*) and *egl-8*(*n488*) were shown to be less sensitive to emodepside's effects on pharyngeal pumping and on locomotion. Two *unc-13* reduction of function alleles, *s69* and *e1091*, showed reduced sensitivity to emodepside. These results support the hypothesis that emodepside binds to latrophilin to activate Gαq. Gαq

activates PLC-β resulting in an increase in the production of DAG. Binding of DAG to UNC-13 results in neurotransmitter release. It is proposed that this release of neurotransmitter results in the paralytic effects of emodepside (Willson *et al.*, 2004a), (Amliwala K *et al.*, 2004). Figure 1.09 shows the proposed mechanism of action of emodepside.

A mechanism of emodepside-induced neurotransmitter release is supported by studies using the fluorescent endocytotic marker FM4-64 (Willson *et al* 2004). FM4-64 is amphiphilic and is believed to be unable cross the cell membrane bilayer. It can become incorporated into cells during endocytosis. Dissected pharynxes were incubated with FM4-64. FM4-64 was found to localize in neuronal puncta, which is consistent with its presence in synaptic regions of the pharyngeal neurons. Vehicle control experiments showed stable fluorescence for up to 30 minutes, whereas addition of 100 nM emodepside caused loss of fluorescence over a 10 minute period. This loss of fluorescence is though to reflect emodepside-induced exocytosis (Willson *et al* 2004).

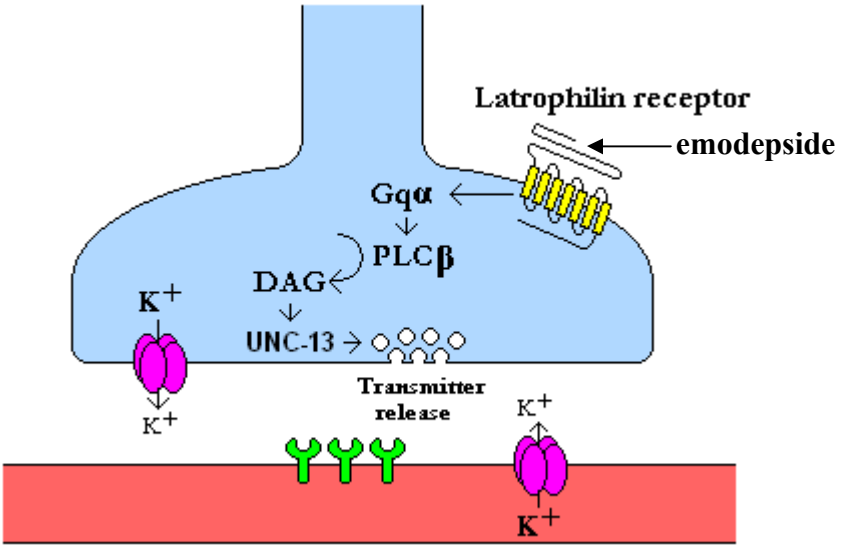


**Figure 1.09. Proposed mechanism of action of emodepside.** It has been proposed the emodepside binds to the *C. elegans* latrophilin receptor (LAT-1) causing activation of Gqα. Gqα activates PLCβ which converts $PIP_2$ to $IP_3$ and DAG. DAG binds to UNC-13 and causes neurotransmitter release. (after Willson *et al* 2004).

However, some unresolved issues remain with regard to this mechanism. Although emodepside has been shown to bind HC110R, it has not been shown to bind to either of the *C. elegans* latrophilin homologues. Also, the low level of resistance to emodepside observed

with RNA interference of the latrophilin receptors suggests that there may be more to the mechanism of action of emodepside. It would be expected that knocking out the emodepside receptor would result in a high level of resistance. The lack of this high level resistance may be explained by incomplete knock down by the RNA interference or it may be due to a functional redundancy between *lat-1* and *lat-2*.

## 1.17 BK channels

Amliwala (2005) conducted a mutagenesis screen in *C. elegans* to look for high level emodepside resistant worms. Mapping and sequencing led to the identification of mutations in the *slo-1* gene. SLO-1 is a large conductance (BK) voltage-sensitive calcium-gated potassium channel.

**BK channels (voltage sensitive calcium gated):** These channels have a variety of names, including Maxi K channels, BK channels, SLO channels (slowpoke) but will be referred to as BK channels. They consist of a tetramer of α subunits that create a selective pore in the membrane. The α subunits have domains involved in voltage and calcium gating of the channel. The first BK channel gene to be identified was the *Drosophila melanogaster slo* (or slowpoke). The *D. melanogaster slo* gene mutant was generated through random mutagenesis and selected from a screen for temperature sensitivity. Intracellular recording from the dorsal longitudinal flight muscles revealed lengthened action potentials and reduction in the initial outward current. This implicated the BK channel in early repolarisation of muscle action potentials (Elkins *et al* 1986). The *D. melanogaster* BK channel genomic DNA and cDNA sequence were isolated and sequenced by Atkinson *et al* (1991). Hydropathy analysis of the amino acid sequence revealed a seven transmembrane region at the N-terminal. Sequence comparison with voltage-gated potassium channels showed homology with the fourth (S4) transmembrane domain. This region is thought to act as a voltage sensor (Papazian *et al* 1991). There is also strong homology with voltage gated potassium channels in the region between transmembrane domains S5 and S6. This forms the ion pore (MacKinnon and Yellen 1990). The *D. melanogaster* BK channel sequence is distinct from other potassium channel sequences other than in these two regions.

BK channels have several key domains. These include, seven transmembrane domains (S0 to S6), the S4 voltage sensor, the pore domain (S5/S6 linker), regulators of potassium conductance domains (RCK1 and RCK2) and the calcium bowl. Figure 1.10 shows a single channel α subunit with these key regions highlighted.

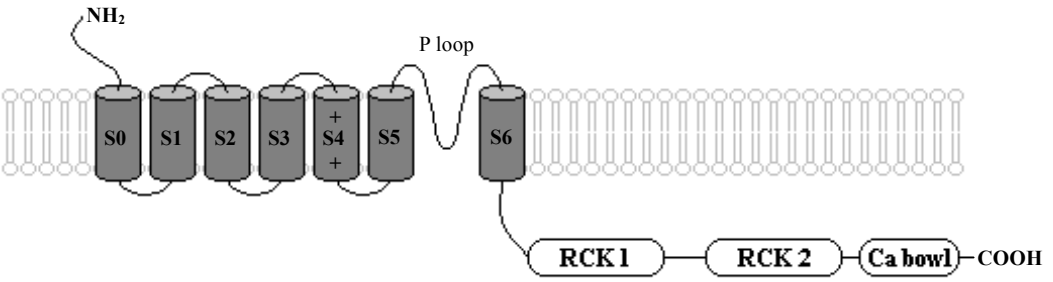


**Figure 1.10. BK channel α subunit.** Key features of the α subunit are highlighted. The S4 voltage sensor controls voltage gating. The RCK1, RCK2 and calcium bowl control calcium regulation. The P-loop forms the pore through which potassium ions pass when a tetramer of α subunits assembles. (After Salkoff *et al* 2006, Wang *et al* 2001).

**Voltage sensor and pore domain:** The seven transmembrane domain includes the voltage sensor and the pore domain. The major difference compared to voltage-gated potassium channels is the presence of an extra transmembrane domain, S0. The presence of the S0 domain places the N-terminus outside the cell. Meera *et al* (1997) demonstrated that antibodies targeted against epitope tags introduced into the amino terminal of the human BK channel *KCNMA1* were able to bind in non- permeablised cells, suggesting the N-terminus is extracellular. The S4 voltage sensor consists of a sequence repeat of one positively charged amino acid (arginine or lysine) followed by two hydrophobic amino acids. The idea that this region acts as a voltage sensor is supported by the fact that mutations within the S4 domain alter voltage sensitivity (Lichtinghagen *et al* 1990). Direct evidence for a role of this domain in voltage sensing came from experiments that employed fluorescent probes attached to different positions in S4 domain. Changes in the fluorescence of these probes correlated with channel gating, suggesting a change in confirmation (Larrson *et al* 1996). The pore domain is also encompassed in the seven transmembrane domain. This pore domain sits between transmembrane domains S5 and S6. This region is highly conserved across all families of potassium channels and is responsible for the channel's ion selectivity. Crystallography has been used to determine the structure of this region in the Kcsa channel (a homologue of the eukaryotic voltage-gated potassium channel) from *Streptomyces lividans* (Doyle *et al* 1998, Zhou and MacKinnon 2003, Nishida *et al* 2007). In the tetramer of α subunits, four pore domains come together to form a selective filter through which potassium ions can pass. Potassium ions approach the selectivity filter in a hydrated state but pass through it un-hydrated. The selectivity filter is lined with carbonyl oxygen atoms, the orientation of which mimic the hydration of potassium ions. This allows for potassium ions to selectively pass through the channel. The single channel conductance of BK channels (~250 pS) is much

greater than that of other potassium channels, yet they share the same selectivity filter. It is thought that the flux of potassium ions is influenced by a ring of negatively charged residues in the vestibule of the channel. These residues may cause an increase in the local potassium concentration, resulting in an increased availability of potassium ions for transit through the channel (Salkoff *et al* 2006).

**Calcium sensing domains:** The intracellular C-terminal region of BK channels contains regions involved in calcium gating. The main sites of calcium sensing are known as the calcium bowl and the regulator of conductance for potassium domains, RCK1 and RCK2. The calcium bowl was implicated in calcium sensing through the analysis of currents in BK channels containing mutations in this region. Deletion of a stretch of three aspartate residues results in a reduced calcium sensitivity of the channel, requiring a higher concentration of calcium for activation (Schreiber and Salkoff 1997). It is now thought that the calcium bowl acts to inhibit voltage activation of BK channels in the absence of calcium. Binding of calcium to the calcium bowl overcomes this inhibition (Schreiber *et al* 1999). This was demonstrated through the analysis of currents in BK channel chimeras. Chimeras were generated in which portions of the calcium bowl in BK channels were replaced with sequence from a non-calcium-activated homologous channel. Chimera channels lacking all endogenous calcium bowl sequence were voltage sensitive but did not require calcium for activation. Calcium sensitivity was restored in chimera channels containing specific regions of the calcium bowl, suggesting a role in inhibition of voltage activation in the absence of calcium (Salkoff 2006).

The RCK1 domain has a role in calcium sensing. Mutations affecting the RCK domains were examined by patch clamp analysis of BK channel currents in *Xenopus* oocytes. Mutations of conserved residues in the RCK1 domain (D362A and D367A) were found to reduce calcium sensitivity (Xia *et al* 2002). A triple mutant of D362A, D367A and a mutation abolishing calcium bowl function lack almost all calcium sensitivity, suggesting these two regions account for the majority of calcium sensing function of BK channels. Analysis of the crystal structure of the RCK domains of the MthK channels from bacteria *Methanobacterium thermoautotrophicum* revealed how these RCK domains link to channel gating. In the tetramer of subunits it is proposed that the RCK domains form an intracellular gating ring. On the binding of calcium between adjacent RCK domains in the tetramer, there is a widening of the gating ring. This widening causes the channel to open through a pulling of the linkers that

connect the gating ring to the channel (Jiang *et al* 2002). Figure 1.11 shows a cartoon of how the BK channel is envisaged based on these studies.

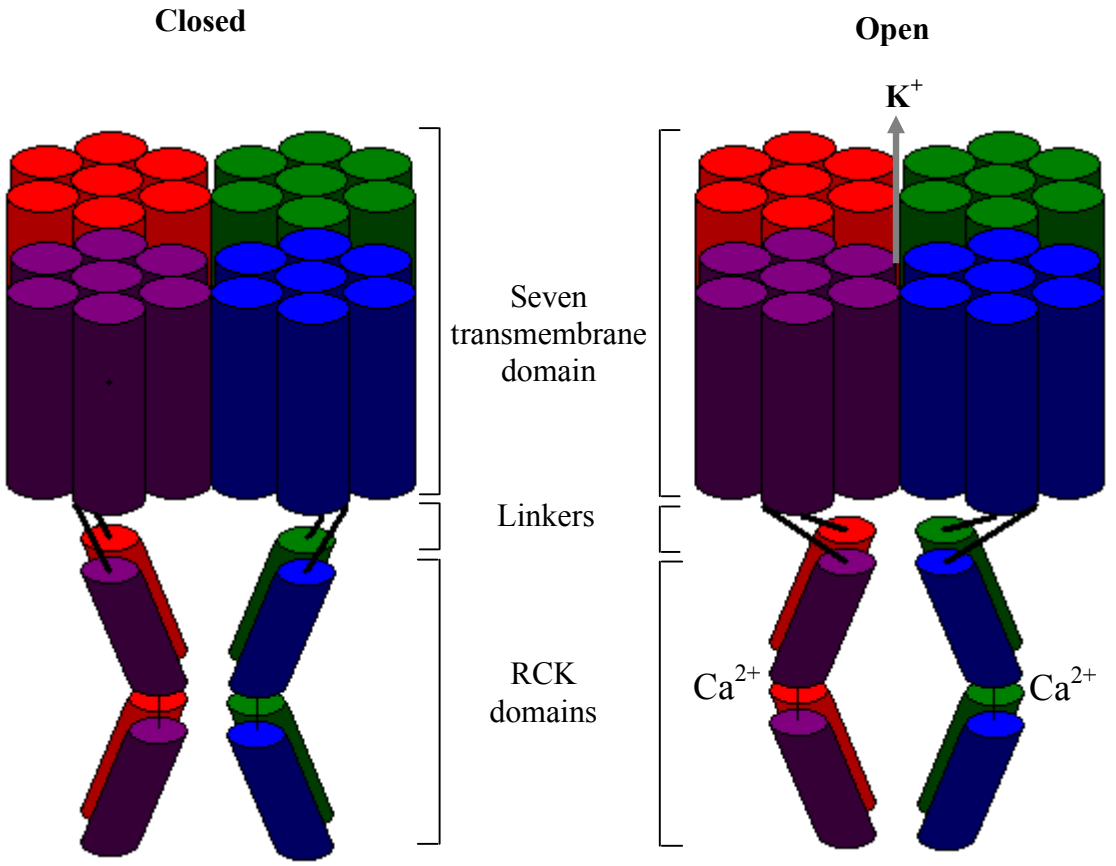


**Figure 1.11. BK channel activation via RCK domains.** Each of the four BK channel α subunits are coloured (red, green, blue and purple). Binding of calcium between adjacent RCK domains results in a conformational change that pulls on the linkers and opens the channel. (After Salkoff *et al* 2006).

## 1.18 *C. elegans* BK channels

***slo-1:*** It has been demonstrated that *slo-1* is involved in the regulation of neurotransmitter release (Wang *et al* 2001). *slo-1* mutants were isolated based on their ability to relieve the block in neurotransmitter release of an *unc-64*(*e246*) syntaxin reduction-of-function mutant. The *unc-64*(*e246*) mutant has defects in its locomotion, only moving briefly when prodded. They are described as lethargic (Saifee *et al* 1998). *unc-64* are resistant to the acetylcholine esterase inhibitor aldicarb but have wild type sensitivity to the nicotinic agonist levamisole. Aldicarb resistance is indicative of a reduction in ACh release. Aldicarb blocks the hydrolysis of ACh by ACh esterase resulting in a build up of ACh and paralysis. Reduced ACh release therefore results in a reduction in sensitivity to aldicarb. No change in levamisole sensitivity indicates that that this is not a post-synaptic effect. *slo-1* alleles were found to suppress the lethargic phenotype of *unc-64*(*e246*), indicating *slo-1* also has a role in regulating neurotransmitter release or mediating its response. *slo-1*(*js379*) was able to rescue the aldicarb resistance of *unc-64*(*e246*) and defects in pharyngeal pumping. EPG traces for *unc-64*(*e246*) show reduced inhibitory activity, which can be rescued by *slo-1*(*js379*).

SLO-1 potentially has a role in either neurons or muscle in suppressing *unc-64* phenotypes. Wang *et al* (2001) looked at the expression pattern of *slo-1* using both *gfp* reporter constructs and a polyclonal antibody with specificity for the calcium bowl. Both reporter construct and antibody showed expression in the nerve ring, nerve cords, body wall muscle and vulval muscle. Tissue specific expression of wild type *slo-1* in an *unc-64*(*e246*), *slo-1*(*js379*) double mutant was used to determine the tissue in which expression of *slo-1* restores the *unc*-64 lethargic phenotype. Expression of wild type *slo-1* in neurons, but not body wall muscle, restored the lethargic phenotype in the double mutant. This indicates SLO-1 acts to regulate neurotansmitter release, rather than the response of the muscle to neurotransmitter release. The effects of *slo-1* and *unc-64* mutations on neurotransmitter release were also assessed by recording excitatory post synaptic currents (EPSC) from the body wall muscle using whole cell patch clamp. The *unc-64*(*e246*), *slo-1*(*js379*) was found to have an increased duration of EPSC as well as an increased frequency of mEPSC compared to *unc-64*(*e246*). This supports the idea that SLO-1 acts as a brake to neurotransmitter release. From this screen, several genes previously implicated in the regulation of neurotransmitter release were identified, as well as the potassium channel SLO-1. Interestingly, only SLO-1 potassium channels were

pulled out of the screen, suggesting that it differs from other $K^+$ channels in its ability to regulate neurotransmitter release. The activity of BK channels has been shown to be closely coupled to voltage-gated $Ca^{2+}$ channels (Marrion and Travalin 1998). It is thought that this close interaction may be the mechanism by which SLO-1 $K^+$ channels regulate transmitter release.

The SLO-1 BK channel has also been shown to be important in the behavioural response of *C. elegans* to ethanol (Davies *et al* 2003). Ethanol acts to inhibit locomotion, egg laying, pharyngeal pumping and development (Davies *et al* 2003, Mitchell *et al* 2007). Thirteen ethanol resistant strains, which mapped to the *slo-1* locus, were identified through a mutagenesis screen. These mutants were resistant to ethanol's effects on locomotion and egg laying. Davies *et al.* performed rescue experiments using *slo-1* constructs with neuronal and muscle promoters to determine if ethanol resistance was due to lack of expression in neurons or body wall muscle. Expression of SLO-1 in neurons was shown to fully restore ethanol sensitivity in mutant *slo-1*(*js118*). Expression of SLO-1 in the muscle of *slo-1*(*js118*) caused no significant restoration of ethanol sensitivity. It was also shown that the effect of ethanol on SLO-1 was specific, rather than an indirect suppression of the depressive effects by hyperactive neurotransmission. *In vivo* patch clamp recordings identified a SLO-1-dependent current in *C. elegans* neurons (CEP). Ethanol was shown to selectively and reversibly increase the amplitude of the outward-rectifying current in neurons in *N2* animals. This action should in turn inhibit neuronal excitability and reduce transmitter release. Ethanol had no effect on currents in *slo-1* mutants, indicating a direct mechanism of ethanol resistance. In addition, SLO-1 gain-of-function mutants displayed depression of locomotion and egg laying frequency in a similar way to that of ethanol treated worms. This similarity suggests that SLO-1 activation is a major cause of ethanol intoxication in *C. elegans* (Davies *et al.*, 2003).

Figure 1.12 illustrates a mechanism by which ethanol may have its intoxicating effect in *C. elegans*. An action potential arrives at the nerve terminal. There is a $Ca^{2+}$ influx through voltage-dependent $Ca^{2+}$ channels, which stimulates transmitter release. The increase in the $Ca^{2+}$ concentration in the nerve terminal increases the probability of the SLO-1 channel being in the open confirmation. There is an outward flow of $K^+$, and repolarisation of the cell, which produces a feedback inhibition on the voltage-dependent $Ca^{2+}$ channel, thereby reducing neurotransmitter release. Ethanol potentiates SLO-1 activity, leading to an inhibition of transmitter release (Crowder, 2004). However, the ethanol sensitivity of *slo-1*(*js379*) has been

shown not to be significantly different from that of *N2* (personal communication with Phillipa Mitchell). Subtle differences in assay techniques may account for these observations or genetic differences between *slo-1*(*js379*) and the *slo-1* alleles isolated in the ethanol resistance screen may exist. It is possible that mutations tightly linked to *slo-1* may be required in combination with mutations in *slo-1* to cause ethanol resistance.

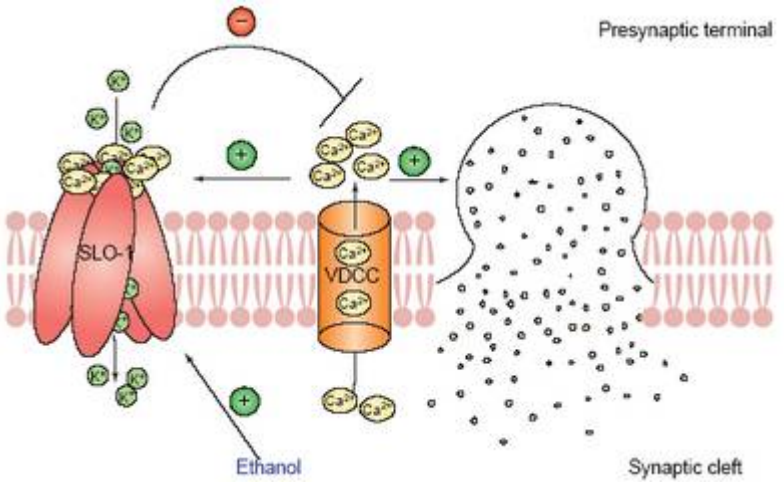


**Figure 1.12. Ethanol activation of SLO-1.** Ethanol is thought to activate SLO-1 either directly or indirectly activate SLO-1. This results in potentiation of feedback inhibition on the voltage-dependent calcium channels (VDCC) and a reduction in neurotransmitter release. (from Davies *et al* 2003).

The BK channel SLO-1 also has a role in mediating the effects of volatile anaesthetics. The *slo-1*(*js380*) loss-of-function mutant is resistant to the effects of volatile anaesthetics (Hawalsi *et al* 2004). The mechanism by which *slo-1*(*js380*) confers resistance is thought to be indirect. It has been postulated that an increase in the level of ACh, as described by Wang *et al* (2001), acts to counteract the effect of the volatile anaesthetics.

SLO-1 has also been shown to have a role in regulating muscle cell excitability. SLO-1 in the body wall muscle of *C. elegans* acts to reduce cell excitability. Carre-Pierrat *et al* (2006) identified hypercontraction and hyperactive head bending phenotypes in *slo-1* mutants. These mutants were also found to cause muscle degeneration when in a *hlh-1* sensitised background. *hlh-1* is a transcription factor involved in control of skeletal muscle myogenesis (Chen *et al* 1994). All of these phenotypes could be rescued by the expression of *slo-1*(+) in the body wall muscle but not in the neurons.

***slo-2:*** The second of the *C. elegans* BK channel homologues is encoded by the gene *slo-2*. The overall sequence identity between SLO-1 and SLO-2 is relatively low at 10% (Lim *et al* 1999). The SLO-1 and SLO-2 channels are, however, structurally similar in that they both consist of a multi-transmembrane domain and a large cytoplasmic C-terminal domain. The membrane topology of SLO-2, predicted by hydropathy analysis, is like that of SLO-1, except for the lack of a S0 transmembrane domain in SLO-2. The most striking differences between SLO-1 and SLO-2 are the absence of several features in SLO-2 that are critical to normal SLO-1 function. The S4 domain of SLO-2 lacks the sequence of positively charged amino acids that comprise the voltage sensor in SLO-1. The calcium sensing region in SLO-1 is known as the calcium bowl and consists of a series of negatively charged residues. It is absent in SLO-2 and replaced by a series of positively charged residues (Lim *et al* 1999, *Yuan* et al 2000). The absence of these domains indicates that the mechanism of activation of SLO-2 must differ from that of SLO-1. SLO-2 has a mammalian homologue known as Slack. The rat homologue of SLO-2 has an identity of 35% with *C. elegans* SLO-1 (Lim *et al* 1999), much higher than the percentage identity between *C. elegans* SLO-1 and SLO-2. SLO-2 channels have been identified in mammalian cardiomyocytes (Kameyama *et al* 1984) and neurons (Dryer 1994). They have been shown to be activated by sodium and are thought to be important under ischaemic conditions (Kameyama *et al* 1984). Factors involved in the activation of *C. elegans* SLO-2 have been studied by Yuan *et al* (2000), who found these channels to be calcium and chloride sensitive. With SLO-2 expressed in *Xenopus* oocytes, large currents could not be evoked in the absence of either calcium or chloride. However, in the presence of both calcium (100 μM) and chloride (50 mM), macroscopic currents were observed. These currents were also found to be voltage dependent, although the source of this dependence is unknown (Yuan *et al* 2000). Yuan *et al* (2003) further studied the sensitivity of the mammalian SLO-2, rSLO-2. As well as being sensitive to sodium (Dryer *et al* 1994), mammalian rSLO-2 has been shown to have sensitivity to chloride (Yuan *et al* 2003). The rSLO-2 chloride dependence was only seen in the presence of sodium, similar to the situation observed in *C. elegans* SLO-2 (Yuan *et al* 2000). The observed calcium dependence of *C. elegans* SLO-2, rather than sodium, is likely to reflect the greater reliance on voltage dependent calcium channels for inward currents.

It is thought that the mechanism for chloride sensing may be located in a region of SLO-2 that is equivalent to the SLO-1 calcium bowl. This region of *slo-2* contains many positively charged residues, rather than the series of negatively charged residues present in the SLO-1

calcium bowl. Mutation of these positively charged residues to negative or neutral residues results in either a reduction or loss of chloride sensitivity, supporting the theory that this region is important for chloride sensing (Yuan *et al* 2003).

SLO-2 has been shown to be expressed in the body wall muscle, vulval muscle, nerve ring and motor neurons through the use of a *slo-2:gfp* fusion construct (Yuan *et al* 2000). This expression pattern is comparable to that of *slo-1*. The similar expression patterns of *slo-1* and *slo-2* raise the possibility that the two subunits may have overlapping function or form heteromultimers. This was investigated using a dominant negative *slo-2* mutant expressed in *Xenopus* oocytes. Co-expression of *N2 slo-2* and the *slo-2* mutant resulted in a thirteen fold reduction in the amplitude of currents compared with *N2 slo-2* alone. Co-expression of *N2 slo-1* and the *slo-2* mutant resulted in a five fold reduction in the amplitude of currents compared with *N2 slo-1* alone. The dominant negative effect of the *slo-2* mutant on *slo-1* suggests that the formation of heteromultimers is occurring.

The role of SLO-2 *in vivo* has been investigated by Santi *et al* (2003). Through the use of deletion mutants and RNAi, it was demonstrated that, under normal physiological conditions, the majority of the outward current in body wall muscle cells was made up from the gene products of the voltage gated potassium channels *shl-1* and *shk-1*. No SLO-2 component of the outward current was identified with intracellular calcium and chloride at physiological concentration (10 nM and 4 mM, respectively). However, under conditions where intracellular calcium and chloride were raised above physiological concentrations (200 μM and 128 mM, respectively), a greatly increased outward current was observed. SLO-2 represented 87% of the total outward current (Santi *et al* 2003). It may be the case that SLO-2 only becomes active under such conditions, which can occur during hypoxia, remaining dormant under normal conditions.

## 1.19 The role of BK channels in cell excitability

BK channels are strongly implicated in the regulation of cell excitability. The studies of *slo-1* mutants in *C. elegans* strongly suggest that it acts to put a brake on neurotransmitter release (Wang *et al* 2001) as well as reducing body wall muscle cell excitability (Carre-Pierrat *et al* 2006). However, voltage-sensitive calcium-activated BK channels have been implicated in both increasing and decreasing cell excitability and neurotransmitter release.

Warbington *et al* (1996) performed electrophysiological experiments in which they measured excitatory junctional potentials (EJPs) and excitatory junctional current (EJCs) from *D. melanogaster* abdominal muscle cells. BK mutants were shown to have decreased EJPs size at external $Ca^{2+}$ concentrations ranging between 0.1 and 1.0 mM. The largest EJP inhibition (70%) was seen at 0.15 mM. This reduced EJP size suggests that a reduction in transmitter release has occurred. At higher concentrations of $Ca^{2+}$ it was shown that the *slo-1* EJPs had an increased duration. The broadening of the EJP can either be due to presynaptic effects in which there is a slower repolarisation, leading to an increased duration of $Ca^{2+}$ influx. Alternatively it may be due to a post-synaptic delay in repolarisation of the EJP. Warbington *et al* tested this by looking at EJCs, which would be expected to be broader if the *slo-1* mutation acts exclusively presynaptically, or the same if acting exclusively postsynaptically (with the muscle cell held under voltage clamp to prevent activation). The EJC was shown not to be broader, suggesting that the broadening of the EJP that occurs at higher $Ca^{2+}$ concentrations is due to BK channel inactivity in the muscle. BK mutants were also shown to partially suppress increased transmitter release seen with application of 4-aminopyridine (4-AP) and in shaker mutants as well as the enhanced effect of 4-AP in *eag* (ether a go go). The BK *shaker* double mutant was shown to have a six fold decrease in EJP amplitude compared with *shaker* alone. This study shows that mutation of BK confers a reduction in transmitter release, rather than an increase (Warbington *et al* 1996).

Xu *et al* (2005) have also provided evidence for SLO-1 having a function that facilitates transmitter release. In the salamander rod synapse light evoked EPSCs can be recorded. In the light, the rod hyperpolarizes, inhibiting glutamate release. In post-synaptic off bipolar and horizontal cells this results in a hyperpolarisation and in on bipolar cells this results in a depolarisation (Hensley *et al* 1993, Wu 1985). This mechanism is shown in figure 1.13. BK

channel block suppresses the amplitude of EPSC, suggesting there is a reduction in neurotransmitter release. This reduction in EPSC is not thought to reflect block of BK in post-synaptic cells, which were held at –60 mV, therefore making activation of BK unlikely. Also, in the off bipolar and horizontal cells and on bipolar cells, changes in the dark holding currents had opposite polarities. I.e. BK block results in an increase in dark holding current in horizontal and off bipolar cells and a decrease in on bipolar cells. If the effect of BK block in post-synaptic cells was being recorded, the dark holding current would increases in all post-synaptic cells. A possible mechanism by which transmitter release is reduced is that BK block reduces the light response of the rods. However, BK block had little effect on the light response of the rods, suggesting this is not the mechanism. BK block was found to suppress the inward calcium current in the rods. Xu *et al* (2005) therefore hypothesised that BK block was having a local effect at the rod synapse. They proposed a mechanism where by an increase in the local potassium concentration in the synapse, through activation of BK, resulted in activation of calcium channels and an increase in neurotransmitter release. The confined structure of the ribbon synapse is thought to limit the diffusion of potassium ions, allowing its accumulation. In isolated rods the calcium current was not suppressed, supporting this hypothesis.

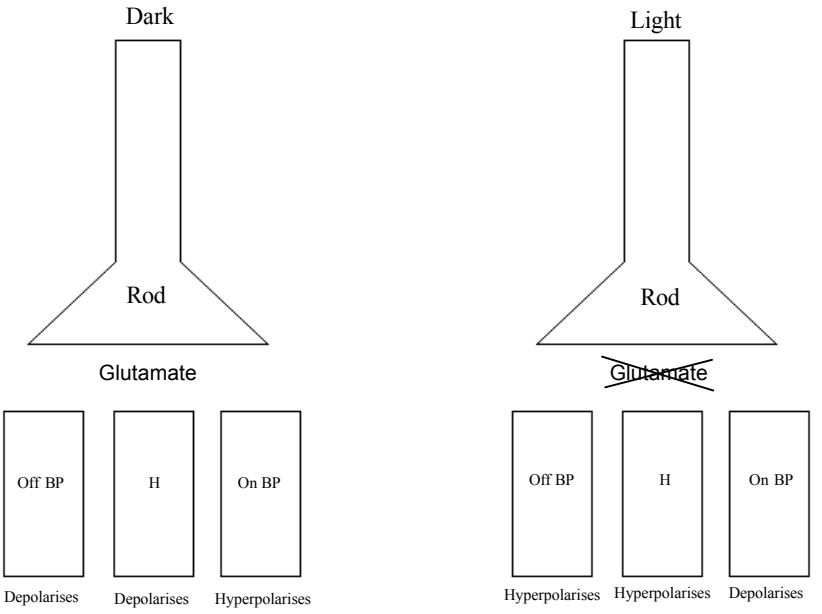


**Figure 1.13. Salamander rod synapse.** In the dark the rod is depolarised and releases glutamate. In the light the rod hyperpolarizes inhibiting glutamate release. Off bipolar (Off BP) and horizontal (H) cells depolarise in response to glutamate. On bipolar (On BP) hyperpolarize in response to glutamate. (After Hensley *et al* 1993, Wu 1985)

The fact that SLO-1 is required for emodepside sensitivity suggests that emodepside signals through SLO-1. Although there is evidence that knocking out *slo-1* can result in a decreased transmitter release in certain cases (Warbington *et al* 1996 and Xu *et al* 2005), it seems likely that in *C. elegans* it results in an increase in transmitter release (Wang *et al* 2001). If this is the case then one would expect that the action of emodepside is to reduce transmitter release, contrary to the evidence produced by Willson *et al* (2004) which outlined a latrophilin signalling pathway resulting in transmitter release. Emodepside induces a flaccid paralysis in *C. elegans.* This is consistent with the role of SLO-1 in the *C. elegans* body wall muscle, which appears to be to reduce cell excitability (Carre-Pierrat *et al* 2006).

## 1.20 Project aims

The overall aim of the project was to further understand the mode of action of emodepside, in particular, the relative role of latrophilin and SLO-1 in emodepside's inhibitory effects on *C. elegans* locomotion. This was achieved through a number of inter-related objectives as follows: Amliwala (2005) demonstrated that targeting of *lat-1* and *lat-2* with RNAi resulted in a reduction in emodepside sensitivity. The suggestion is that LAT-1 and LAT-2 are receptors for emodepside. If all of emodepside's effects are associated with these receptors, knock down of them would be expected to result in a high level of resistance. The level of resistance observed by Amliwala (2005) is not consistent with this. This could be due to an incomplete effect of the RNAi and/or could indicate that there is redundancy between *lat-1* and *lat-2*. Alternatively it may indicate the presence of another mechanism by which emodepside acts, e.g. SLO-1. Available mutants of the *lat-1* and *lat-2* genes will be used to investigate the roles of these receptors in emodepside's mode of action. A double *lat-2*, *lat-1* mutant will be constructed in order to investigate the possibility of redundancy.

In order to investigate whether further genes regulate the response to emodepside, forward genetic screens were conducted to generate mutant *C. elegans* that have high level resistance to the effects of emodepside. The genes carrying mutations that confer resistance to emodepside would be characterised.

To confirm the role of SLO-1 in emodepside's mode of action and to more precisely define its role, expression of wild type *slo-1* in a *slo-1* mutant background will be used, as well as the use of complementation tests. The mechanism of *slo-1* involvement will be investigated using tissue specific expression of wild type *slo-1* in a *slo-1* mutant background. Analysis of mutant phenotypes will be conducted in order to relate SLO-1 function to the level of emodepside resistance. Pharmacological studies will be conducted in order to investigate the effect that emodepside has on neurotransmitter release.

Finally, the project aims to investigate whether or not SLO-1 is an emodepside receptor. The potential effect of emodepside on BK channel currents will be investigated using a heterologous expression system and electrophysiological analysis. The *C. elegans* BK channel *slo-1* and the human BK channel *kcnma1* will be investigated.

# Chapter 2

# Methods

## 2.01 Nematode growth medium plates

*C. elegans* are maintained on nematode growth medium (NGM). NGM consists of 15g NaCl, 12.5g peptone and 85g Agar per 5L $H_2O$. This autoclaved solution is supplemented with sterile aqueous solutions of 1 M $CaCl_2$ (5 ml), 1 M $MgSO_4$ (5 ml), 1 M $KPO_4$ (125 ml) and an ethanol solution of 5 mg/ml cholesterol (5ml) (Brenner 1974). Plates were poured using Jencons perimatic gp pump to a consistant volume (13 ml). Plates were dried for a minimum of 24 hours before seeding with 50 µl of a fresh *E. coli* OP50 culture. OP50 was cultured on NGM plates for minimum of 24 hours before use. Plates were stored at room temperature for up to two weeks before use.

## 2.02 *C. elegans* bacterial food source

The food source for *C. elegans* is *E. coli* OP50. *E. coli* OP50 were grown on 9 cm LB agar containing plates. To maintain the OP50, bacteria from the lawn were streaked onto fresh LB plates and grown overnight (~16 hours) at 37$^{o}$C. Single colonies were then selected and grown in 10 ml of LB media overnight (~16 hours) at 37$^{o}$C and 225 rpm in a platform shaker.

## 2.03 Drug containing NGM plates

Drug-containing plates were made up fresh for each assay. 150 ml of NGM was prepared and cooled to 50$^{o}$C in a water bath following autoclaving. Drugs were added to the warm liquid NGM. Serial dilutions of stock solutions were made before addition to NGM. 1 in 200 dilutions of the stock solutions were made in NGM. Emodepside stock solutions were 100% ethanol, whereas all other stock solutions were aqueous. The 1 in 200 dilution of emodepside stock solutions would have given a 0.5 % (86 mM) ethanol concentration in the plate, not allowing for evaporation. Ethanol vehicle control plates were made in the same way as for emodepside-containing plates with the omission of emodepside. After addition of drug the media was mixed robustly to enable even distribution of the drug.

## 2.04 NGM ethanol concentration

Ethanol affects *C. elegans* behaviour (Morgan and Sedensky 1995, Davies *et al* 2003). For this reason the ethanol concentration of the emodepside-containing plates was tested using the "NAD-ADH Reagent Multiple Test Vial" kit from Sigma. This kit contains nicotinamide adenine dinucleotide (NAD) and alcohol dehydrogenase (ADH). ADH calalyses the following reaction.

$$\text{Ethanol} + \text{NAD} \xrightarrow{\text{ADH}} \text{Acetaldehyde} + \text{NADH}$$

The consequent increase in absorption at 340 nm due to the production of NADH is directly proportional to the ethanol concentration. The following reaction mixture was set up to generate a calibration curve (Table 2.01). NAD/ADH was dissolved in 0.5 M glycine buffer pH9.

**5 M Glycine buffer pH9:** 500 nM glycine, 1 M NaCl

| **Reagent** | **Volume / 620 µl reaction** |
|---|---|
| NAD / ADH (≥ 0.625 mM / ≥ 53 units/ml) | 600 µl |
| Ethanol (5, 10, 20, 50 or 100 mM) | 20 µl |

**Table 2.01. Reaction mixture for ethanol oxidation reaction.**

The reaction was incubated at 25 $^{o}$C for ten minutes. Absorbance was measured at 340 nm. A calibration curve was generated. Figure 2.01 shows the absorbance of NADH produced in a reaction with NAD and 5, 10, 20, 50 and 100 mM ethanol.

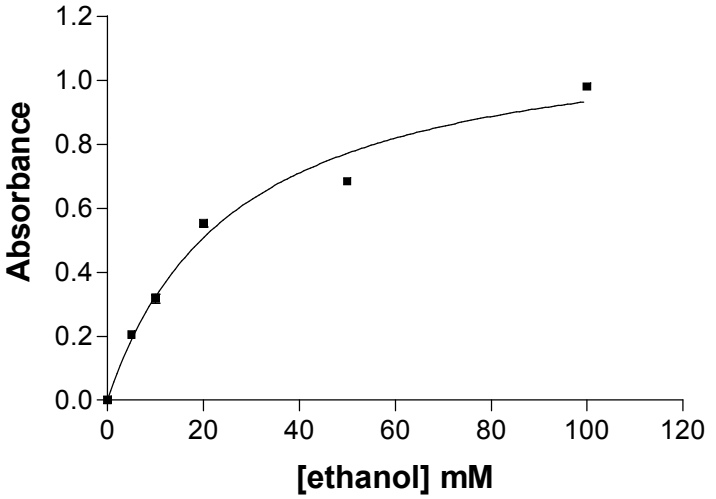


**Figure 2.01. Ethanol assay calibration curve for.** Absorbance of NADH at 340 nm produced in ethanol oxidation reaction. Absorbance of NADH produced in a reaction with NAD and 5, 10, 20, 50 and 100 mM ethanol.

To test the concentration of ethanol in drug-containing NGM plates, chunks (~ 0.5g) of agar were sonicated in 1ml of $H_2O$ for 1 hour. This allows the ethanol in the agar to equilibrate with the $H_2O$. A reaction with a sample of this $H_2O$ was set up and the absorbance measured. The average absorbance of three readings from three replicates was found to be 0.406. Reading off the curve, this equates to 13.9 mM ethanol. The concentration of ethanol in the agar was calculated to be 40 mM. This is below the concentration where effects of ethanol on locomotion become apparent (Davies *et al* 2003) and is substantially lower than the 86 mM that was added. Never-the-less, ethanol vehicle controls were included for all emodepside assays.

## 2.05 Emodepside solubility

Emodepside stocks are made up in ethanol due to its low solubility in aqueous solution. These are then diluted in M9, Dent's saline or NGM to obtain emodepside at the required concentrations. Therefore, assays were conducted to test whether at assay concentrations, emodepside remains in aqueous solution or is held in a suspension. Spectrophotometry of emodepside in ethanol and aqueous solutions (0.5 % ethanol) at assay concentrations was conducted to determine which the case was. It was established that peak absorbance of emodepside is at 256 nm. Emodepside solutions were made up in triplicate. Using an Eppendorf BioPhotometer spectrophotometer, the absorbance of 10 μM emodepside in 100 % ethanol and aqueous solution (0.5 % ethanol) was measured. Solutions were then spun in 1.9

ml Eppendorf tubes at 16000 x g for 15 minutes. Solution was carefully removed from the top of the tube to avoid taking any undissolved emodepside. The absorbance was the measured, again (Figure 2.02.). The Eppendorf BioPhotometer spectrophotometer is limited to reading absorbance at 260, 280 and 320 nm.

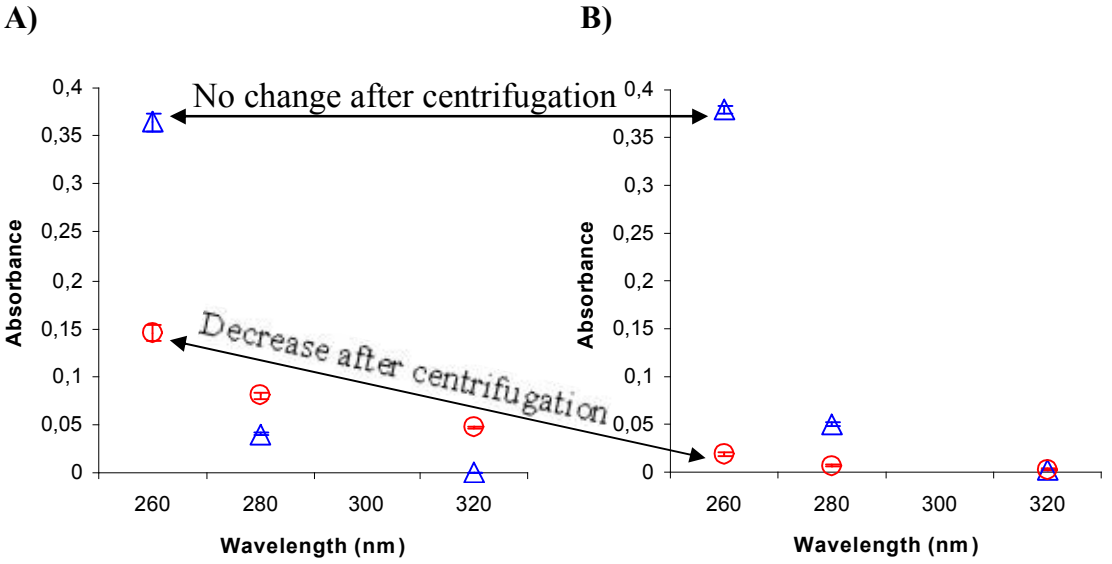


**Figure 2.02. Analysis of emodepside solubility.** Spectrophotometric analysis of emodepside solubility in either 100 % ethanol or 0.5 % ethanol aqueous solution. **A)** Absorbance of 10 µM emodepside in 100 % ethanol (△) and 10 µM emodepside in 0.5 % ethanol (○). **B)** Absorbance of 10 µM emodepside in 100 % ethanol (△) and 10 µM emodepside in 0.5 % ethanol (○) after a 15 minute spin at 16000 xg. Each point is the average of 9 readings (from 3 samples) ± SEM.

Absorbance at 260 nm is close to the peak absorbance of emodepside (256 nm). Absorbance of 10 µM emodepside at 260 nm is 0.364 when dissolved in 100 % ethanol and 0.145 when in 0.5 % ethanol. This suggests there is less dissolved emodepside in the 0.5 % ethanol solution. After spinning at 16000 x g for 15 minutes the absorbance of emodepside in the 100% ethanol solution remained approximately the same, 0.379 at 260 nm. Absorbance in the 0.5 % ethanol solution dropped to 0.019 at 260 nm. This suggests that the emodepside precipitates in the 0.5 % ethanol solution and is pelleted during the spin step. The absorbance of emodepside in the 0.5 % ethanol solution at 280 nm and 320 nm appears to be higher than in the 100 % ethanol solution. This is probably pseudo-absorbance, resulting from light scattering due to the presence of insoluble particles. Indeed, absorbance at these wavelengths is greatly reduced after centrifugation, indicating these particles have been pelleted. Both batches of emodepside, MK400022 and KP00JFT, behaved identically in this assay.

Due to the insolubility of emodepside in aqueous solutions at assay concentrations, plate assays are the most suitable way to investigate emodepside's effects on locomotion. The set NGM will allow for even dispersal of emodepside throughout the plate.

## 2.06 Locomotion assays: Plate assay

As a measure of locomotion, the number of wave forms a worm traces out in a given time can be counted. The definition of a single body bend is the path traced out by a worm where the head, or tail depending on direction of travel, returns to the same point in the wave form from which it started. Body bends are counted from the head of the worm if it is moving forwards and the tail of the worm if it is moving backwards. The wave form traced out by the worm may vary in shape in different strains or with different treatments, but the same definition is applied for this study.

Locomotion was assayed on NGM agar plates. In these assays, worms at L4 stage were selected and exposed to drug-containing plates for 24 hours on food. Worms were then individually transferred to unseeded drug-containing plates for 1 minute. The purpose of this step is to deposit OP50 that adheres to the worm and prevent transfer of OP50 to the assay plate. The presence of food impacts on locomotion. Worms move more freely in the absence of food and this allows for shorter assay times. Finally worms were individually transferred to a drug-containing assay plate and left for 1 minute before body bend were counted for 1 minute. At each step worms were transferred using 0.2 mm diameter pins to reduce the transfer of *E. coli* OP50.

Inter-assay variability in the rate of locomotion was observed. Inter-assay variability may arise due to slight variations in temperature at which the assay is conducted. Intra assay variability did not occur. All assays were therefore conducted in parallel with controls. The inter-assay variability and inter assay consistency is demonstrated in figure 2.03. This shows the rate of locomotion of *N2* animals on 100 nM emodepside from assays conducted on A) separate days and B) in parallel. Each bar represents the average rate of locomotion of a population of worms from individual NGM plates.

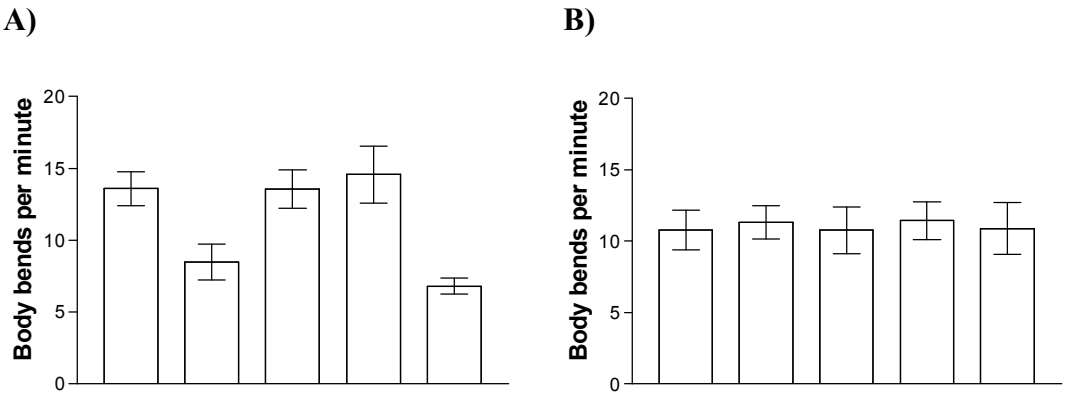


**Figure 2.03. Inter-assay variability. A)** The mean rate of locomotion of *N2* worms on 100 nM emodepside. Each bar represents an independent population assayed on different days. **B)** The mean rate of locomotion of *N2* worms on 100 nM emodepside. Each bar represents an independent population assayed in parallel with each other. For each bar n≥7 +/- SEM.

## 2.07 Locomotion assays: Reversal assay

Worms move in a stereotyped fashion, forward movement being interspersed with reversals. When worms are removed from food the frequency of reversal increases. This increase in reversal is a foraging behavior (Gray and Bargmann 2005, Zhao *et al* 2003, Zheng *et al* 1999). Worms were assayed off food so that foraging behavior would be initiated and reversal frequency increased, thereby reducing the assay time required. Worms were selected at L4 stage and kept on food for 24 hours. Worms were then individually transferred to an unseeded plate to reduce the amount of *E. coli* OP50 transferred to the assay plate. After 1 minute each worm was then transferred to an unseeded assay plate. After five minutes of acclimatization, the number of reversals the worm made in 1 minute was recorded.

## 2.08 Locomotion assays: Aldicarb assay

Aldicarb is an anticholinesterase (ACE) inhibitor. ACE metabolises ACh in the synaptic cleft to control the duration of response to ACh. Aldicarb blocks ACE, resulting in a build up of ACh and spastic paralysis of the muscle. Figure 2.04 illustrates this mechanism. The sensitivity of mutant or drug treated worms to aldicarb can be used to provide an indication of the level of ACh release (Miller *et al* 1996).

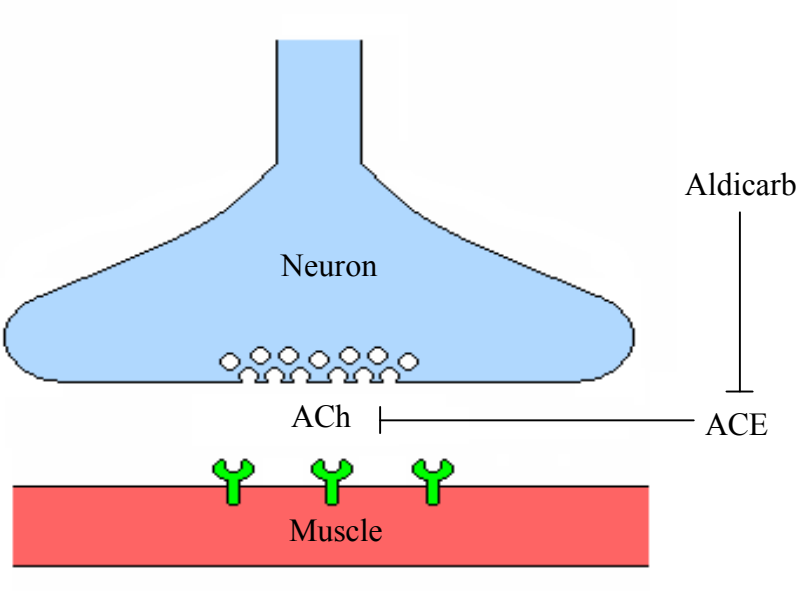


**Figure 2.04. Aldicarb mechanism of action.** Aldicarb inhibits ACE in the neuromuscular junction, preventing the break down of ACh. ACh continues to activate post-synaptic receptors, leading to spastic paralysis of the muscle.

To test aldicarb sensitivity, L4 worms were selected 24 hours prior to the assay. Fifteen 24 hour post L4 worms were exposed to aldicarb on a seeded 0.5 mM aldicarb-containing plate. This was defined as a single trial. At 30 minute intervals the number of paralysed worms on the plate were recorded. Worms were defined as paralysed if a single prod with a platinum wire pick failed to elicit forward or backward movement. Paralysed worms were removed from the plate. All trials were done blind.

For experiments looking at the effect of emodepside on aldicarb sensitivity, L4 worms were selected and pre-exposed to either emodepside or vehicle (0.5 % ethanol) for 24 hours. They were then exposed to either 0.5 mM aldicarb and 100 nM emodepside or 0.5 mM aldicarb and vehicle (0.5 % ethanol) or 100 nM emodepside alone. The number of paralysed worms was

recorded every 30 minutes until all worms were paralysed. Paralysed worms were removed from the assay plate.

## 2.09 Locomotion assays: Levamisole assay

Levamisole is a nicotinic ACh receptor agonist (Lewis *et al* 1980). It causes hyper-contraction and paralysis of the body wall muscle through activation of post-synaptic nicotinic ACh receptors (Lewis *et al* 1980, Fleming *et al* 1997, Culetto *et al* 2004). The post-synaptic sensitivity of mutants and emodepside treated worms was investigated using levamisole.

For experiments looking at the effect of emodepside on levamisole sensitivity, L4 worms were selected and pre-exposed to either emodepside or vehicle (0.5 % ethanol) for 24 hours. They were then exposed to either 100 μM levamisole and 100 nM emodepside or 100 μM levamisole and vehicle (0.5 % ethanol) or 100 nM emodepside alone. The number of paralysed worms was recorded every 30 minutes until all worms were paralysed. Paralysed worms were removed from the assay plate.

## 2.10 *C. elegans* genomic DNA extraction

DNA was extracted from both populations of worms and from single worms. To extract DNA from a population, worms were washed off a 5 cm plate with 1 ml of M9. Plates contained populations of several hundred worms at various stages of development. The worms were then transferred to a 1.9 ml Eppendorf tube and incubated at 5 $^{o}$C for 5 minutes to pellet the worms. The supernatant (containing OP50) was removed leaving a worm pellet. Extra wash steps were conducted when necessary to ensure OP50 were removed. 100 µl of worm-lysis buffer/proteinase K (100 µg/ml) mix was added to the worm pellet. This was incubated at -80 $^{o}$C for 15 minutes followed by an incubation at 65 $^{o}$C for 1 hour (vortexing every 15 minutes), resulting in cell lysis and digestion of protein. A final incubation of 95 $^{o}$C for 15 minutes was used to denature the proteinase K. DNA was diluted with 400 µl 10 mM Tris (pH 8.1).

To extract DNA from single worms, they were first cleaned by transferring to a non-seeded plate for ~ 2 minutes. They were then picked into 3 µl of worm-lysis buffer/proteinase K mix (100 µg/ml) in a well of a PCR plate. The same procedure for DNA extraction from a population was then followed. PCR reaction mix was added directly to the lysed worm.

**M9 Buffer:** $KH_2PO_4$ 22 mM, $Na_2HPO_4$ 42 mM, NaCl 85 mM, $MgSO_4$ 1 mM

**Lysis buffer:** Tris HCl 10 mM pH 8.3, KCl 50 mM, $MgCl_2$ 2.5 mM, NP40 0.45 %, Tween 20 0.45 %, Gelatine 0.01 %.

## 2.11 *C. elegans* RNA extraction

RNA was extracted from five 5 cm plates of worms (as described for DNA extraction). Worms were washed from each plate with 1 ml of M9 and transferred to 1.9 ml Eppendorf tubes. These were incubated at 5 $^{o}$C for 5 minutes to pellet the worms. The supernatant was removed leaving a worm pellet and 100 µl of supernatant. Extra wash steps were conducted when necessary to ensure OP50 were removed. Worms from the 5 plates were pooled in a single 1.9 ml Eppendorf tube. This was incubated at 5 $^{o}$C for five minutes to pellet the worms. The supernatant was removed leaving the worm pellet.

1 ml of Trizol was added and incubated at room temperature for 1 hour, vortexing every 10 minutes. It was then spun at 16000 x g for 10 minutes at 4 $^{o}$C to pellet insoluble material. The supernatant was transferred to a fresh tube. 200 µl of chloroform was added and the tube was vortexed for 15 seconds. This was centrifuged at a RCF of 16110 x g for 15 minutes at 4 $^{o}$C. The upper aqueous phase was transferred to a fresh tube and 500 µl of isopropanol was added. This was incubated at room temperature for 10 minutes and then spun at 14 g at 4 $^{o}$C to pellet the RNA. The supernatant was removed and the pellet washed in 100 µl 75 % ethanol (made up in diethylpyrocarbonate (DEPC) treated $H_2O$). A further spin at a RCF of 16110 x g for 10 minutes was done and supernatant removed, followed by a second wash with 100 µl of 100 % ethanol. The supernatant was removed and the pellet allowed to air dry. The pellet was then re-suspended in 50 µl of DEPC treated $H_2O$.

Reverse transcription was carried out immediately to avoid loss of RNA due to RNAse degradation. RNA was frozen at -80 $^{o}$C in DEPC treated $H_2O$.

## 2.12 Polymerase chain reaction

Polymerase chain reaction (PCR) was used for a variety of applications. Deletions in genomic DNA were detected using PCR. This allowed the confirmation of the genotype of deletion mutants as well as the tracking of deletions during out-crossing. Genomic DNA was PCR amplified for sequencing of point mutations in mutant strains. PCR was used to confirm the presence of plasmids in transfected worms. *slo-1* cDNAa was PCR amplified in order to generate a vector for *slo-1* expression in HEK293 cells. Regions around snip-SNPs were PCR amplified for snip-SNP mapping.

**Primer design –** Gene specific primers were used for all PCR. Primers sequences were designed to be between 18 and 30 nucleotides long, and to have a GC content of between 40 and 60 %. The following rules were followed when designing primers: avoid runs of 3 or more G or C at the 3` end, avoid a T at the 3` end, avoid complementary sequences within and between primers. The following equation was used to determine an annealing temperature for primers.

**Annealing temperature = ($2^oC$ x (A + T)) + ($4^oC$ x (C+G))**

Primer pairs were designed to have similar annealing temperatures where possible. An average of annealing temperatures was taken for primer pairs. A list of primers used is shown in the appendix.

**PCR mixture –** Expand long template PCR system (Roche) was used for all PCR. dNTPs from Invitrogen were used for all PCR. Table 2.02 shows the reaction mixture used for PCR. PCR were optimised through variation of the $Mg^{2+}$ concentration in the PCR buffer and variation of annealing temperature.

| **Reagent** | **Volume / 25 µl reaction** |
|---|---|
| dNTPs 25 mM | 0.25 µl |
| DNA | 3 µl |
| Expand long template PCR system 5 Units/µl | 0.125 µl |
| PCR buffer 10 X | 2.5 µl |
| Sense primer 10 µM | 5 µl |
| Anti-sense primer 10 µM | 5 µl |
| $ddH_2O$ (DEPC) | 9.125 |

**Table 2.02. Components of the PCR reaction mixture**.

**10 X PCR buffer:** 17.5 mM to 27.5 mM $MgCl_2$, 500 mM KCl, 100 mM Tris HCl pH 8.3, gelatine 200 µg/ml

**PCR conditions –** Table 2.03 shows the cycling conditions used for PCR. Annealing temperature varied depending on the primers being used. Elongation time varied depending on the size of the DNA template. Expand long template PCR system (Roche) elongates at a rate of 1 kb per minute. Cycle number varied depending on the quantity of PCR product required.

| Step | Temperature | Duration | Cycles |
|---|---|---|---|
| **Initial denaturation** | 94 $^{o}$C | 2 minutes | 1 X |
| **Denaturation**<br>**Annealing**<br>**Elongation** | 94 $^{o}$C<br>50 - 60 $^{o}$C<br>68 $^{o}$C | 30 seconds<br>30 seconds<br>1 minute / Kb | 10-30 X |
| **Final elongation** | 68 $^{o}$C | 7 minutes | 1 X |

**Table 2.03. PCR cycle conditions.**

PCR were run using an M J research PTC-200 Peltier thermal cycler. Expand long template PCR system (Roche) can amplify DNA fragments up to 20 kb in size. It has proof-reading activity and copies DNA threefold more accurately than Taq DNA polymerase.

**Reverse Transcription PCR -** Reverse Transcriptase PCR (RT-PCR) reactions were carried out using the SuperScript III One-Step RT-PCR system with Platinum Taq DNA Polymerase (Invitrogen). RT-PCR was used to amplify *slo-1* cDNA from *slo-1*(*js379*) non-complementing strains. Table 2.04 shows the reaction mixture for the RT-PCR. Table 2.05 shows the conditions for the RT-PCR. RT-PCR were run using an M J research PTC-200 Peltier thermal cycler.

| **Reagent** | **Volume / 25 µl reaction** |
|---|---|
| 2 X reaction mix: | 25 µl |
| RNA | 5 µl |
| SuperScript III RT / Platinum Taq mix | 2 µl |
| Sense primer 10 µM | 1 µl |
| Anti-sense primer 10 µM | 1 µl |
| dd$H_2O$ (DEPC) | 16 µl |

**Table 2.04. Components of the RT-PCR reaction mixture.**

**2 X reaction mix:** 0.4 mM of each dNTP, 3.2, mM $MgSO_4$

| | Temperature | Time | Cycle number |
|---|---|---|---|
| cDNA synthesis | 60 $^oC$ | 30 minutes | 1 x |
| Initial denaturation | 94 $^oC$ | 2 minutes | 1 x |
| Denaturation<br>Annealing<br>Elongation | 94 $^oC$<br>55 $^oC$<br>68 $^oC$ | 15 seconds<br>30 seconds<br>3.5 minutes | 40 x |
| Final elongation | 68 $^oC$ | 7 minutes | 1 x |

**Table 2.05. RT-PCR cycle conditions**

## 2.13 PCR purification

PCR products were purified when required for use in further enzymic reactions. PCR purification was carried out using a QIAquick PCR Purification Kit as per instructions. The purification process removes: primers and nucleotide less than 100 bp, enzymes, oil and salts.

## 2.14 Gel electrophoresis

Agarose gels of between 0.8 and 1.5 % were used depending on the size of the DNA fragment being run. Agarose was dissolved by heating in TBE buffer. Ethidium bromide (10 mg/ml) was added to the dissolved agarose and the solution was set in a casting tray. 5x loading buffer was added to DNA. Gels were run at 120 V (200 ml and 140 ml gels) or at 90 V (50 ml gels) in TBE buffer. All gels were run with a 1kb ladder (MBI Fermentas) (Figure 2.05). 5 µl of ladder were run making the 1.6 kb band 50 ng. DNA was visualised using AlphaImager transilluminator and digitally photographed.

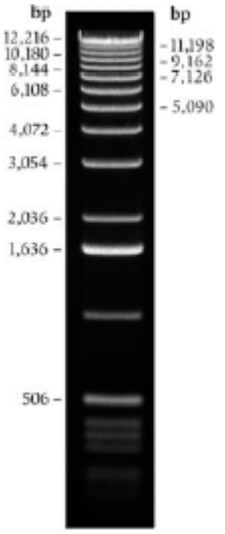


**Figure 2.05. 1 kb ladder used in gel electrophoresis.** Invitrogen 1 kb DNA ladder (www.invitrogen.com). 1636 bp band was loaded at 50 ng.

**TBE:** 45 mM Tris-borate, 1 mM EDTA

**5 X loading buffer:** 5 % bromophenol Blue 250 µl, Glycerol 30 %, $H_2O$ 70% ml

## 2.15 Transformation of chemically competent cells

Subcloning Efficiency DH5α (Invitrogen) chemically competent cells were used. 25 µl aliquots (1.9 ml Eppendorf tubes) of DH5α were thawed on ice. 1-10 ng of DNA was gently mixed with DH5α cells and incubated on ice for 30 minutes. Cells were then heat shocked at 42$^{o}$C for 20 seconds, followed by a further 2 minute incubation on ice. 200 µl of SOC (GIBCO BRL) was added to the cells and incubated at 37$^{o}$C and at 225 rpm in a platform shaker for 1 hour. 50 µl and 150 µl of DH5α culture was spread on antibiotic containing LB plates. Ampicillin was used at 50 ng/µl and kanamycin at 50 ng/µl. The plates were incubated for 16 hours at 37$^{o}$C.

## 2.16 Plasmid / Cosmid preparation

Plasmids and cosmids were extracted from DH5α cells. The antibiotics ampicillin (50 ng/µl) and kanamycin (50 ng/µl) in LB media and LB agar were used for selection.

Plasmids (pPD118.33, pBK3.1 and pBK4.1) for use in *C. elegans* transfection were isolated using the QIAprep Spin Miniprep Kit (Qiagen). Single colonies were picked from a freshly streaked selective plate. 5 ml of LB media, containing the appropriate antibiotic, was inoculated and incubate for 16 h at 37°C and at 225 rpm in a platform shaker. Bacterial cells were harvested by centrifugation at 16000 x g for 1 minute. LB media supernatant was removed and DNA was extracted. DNA yield using QIAprep Spin Miniprep Kit was in general approximately 15 µg.

Plasmids (pCMV4-XL6 and pIRES2-EGFP) for HEK293 cell transfection were isolated using QIAGEN Plasmid Mini Kits (Qiagen). Single colonies were picked from a freshly streaked selective plate. 5 ml of LB media, containing the appropriate antibiotic, was inoculated and incubated for 16 h at 37°C and at 225 rpm in a platform shaker. Bacterial cells were harvested by centrifugation at 16000 x g for 1 minute. LB media supernatant was removed and DNA was extracted. DNA yield with QIAGEN Plasmid Mini Kits was in general approximately 15 µg. QIAGEN Plasmid Mini Kits yields transfection grade plasmid DNA.

The BO457 cosmid for use in *C. elegans* transfection was isolated using Sigma microprep (Sigma). Single colonies were picked from a freshly streaked selective plate. 2 ml starter cultures were set up and incubated for 8 hours at 37 $^{o}$C and at 225 rpm in a platform shaker. 50 µl of starter culture was used to inoculate 25 ml of LB media, containing the appropriate antibiotic. This was incubated for 16 h at 37°C and at 225 rpm in a platform shaker. Bacterial cells were harvested by centrifugation at 6000 x g for 15 minute. LB media supernatant was removed and DNA was extracted.

## 2.17 Restriction Endonucleases

Restriction digest banding patterns were used to confirm the identity of plasmids and cosmids. Restriction digests were used for the identification of *N2* and CB4856 DNA in snip-SNP mapping. Restriction enzymes were also used to generate sticky ends on *slo-1* cDNAa for insertion into pIRES2-EGFP. Restriction enzymes from New England Biolabs Ltd were used. Table 2.06 shows the reaction mixture used in restriction digests. 1 unit of restriction enzyme completely digests 1 µg of DNA in 1 hour. All enzymes used were incubated at 37 $^{o}$C for a minimum of 1 hour to ensure a complete digest. Enzymes were either heat inactivated (65 $^{o}$C for 15 minutes) or removed using PCR purification (QIAquick PCR Purification Kit).

| **Reagent** | **Volume / 20 µl reaction** |
|---|---|
| DNA (~500 ng/ µl) | 1 µl |
| Buffer 10 X (1, 2, 3 or 4) | 2 µl |
| BSA (1 µg/µl) if required | 2 µl |
| Enzyme (1 unit) | 1 µl |
| dd$H_2O$ | 14 µl |

**Table 2.06. Reaction mixture for restriction digests.**

Optimal conditions for digests were achieved using the following NEB buffers. NEB recommended buffers were used for double digests.

**10X Buffer 1:** 100 mM Bis-Tris-Propane-HCl, 100 mM $MgCl_2$, 10 mM Dithiothreitol
**10X Buffer 2:** 500 mM NaCl, 100 mM Tris-HCl, 100 mM $MgCl_2$, 1 mM Dithiothreitol
**10X Buffer 3:** 1 M NaCl, 500 mM Tris-HCl, 100 mM $MgCl_2$, 10 mM Dithiothreitol
**10X Buffer 4:** 500 mM potassium acetate, 200 mM Tris-acetate, 100 mM Magnesium Acetate, 10 mM Dithiothreitol

## 2.18 Shrimp alkaline phosphatase (SAP)

SAP (USB) was used in the construction of pIRES2-EGFP + *slo-1* cDNAa vector. PCR purified digested (EcoRI and NheI) pIRES2-EGFP was treated with SAP to prevent religation. The following reaction mixture was used (Table 2.07). One unit of SAP catalyses the hydrolysis of 1 µmol of 5'-phosphates in one minute. Reactions were incubated at 37 $^{o}$C for one hour. SAP was inactivated by incubation at 65$^{o}$C for 15 minutes.

| **Reagent** | **Volume / 20 µl reaction** |
|---|---|
| 10 X SAP reaction buffer | 2 µl |
| DNA | 15 µl (75 ng, ~ 0.0214 pmoles) |
| $ddH_2O$ | 2 µl |
| SAP (0.1 unit / µl) | 1 µl (0.1 units) |

**Table 2.07. Shrimp alkaline phosphatase reaction mix.**

**10 X SAP Reaction Buffer:** 200mM Tris-HCl (pH 8.0), 100mM $MgCl_2$.

## 2.19 T4 DNA ligase

T4 DNA ligase (NEB) was used in the construction of pIRES2-EGFP + *slo-1* cDNAa vector. *slo-1* cDNAa was ligated into pIRES2-EGFP in EcoRI and NheI restriction sites. *slo*-1 cDNAa was mixed with pIRES2-EGFP in a three fold molar excess. The following reaction mixture was set up (Table 2.08). Reactions were incubated overnight at 15 $^{o}$C.

| **Reagent** | **Volume / 20 µl reaction** |
|---|---|
| pIRES2-EGFP (5 ng/µl ) | 10 µl (~50 ng) |
| *slo-1* cDNAa insert (17 ng/µl) | 6 µl (~100 ng) |
| T4 DNA Ligase | 1 µl |
| 10 x T4 DNA Ligase reaction buffer | 2 µl |
| dd$H_2O$ | 1 µl |

**Table 2.08. T4 DNA Ligase reaction mixture.**

**10 X T4 DNA Ligase reaction buffer:** 500 mM Tris-HCl, 100 mM $MgCl_2$, 10 mM ATP, 100 mM Dithiothreitol

Subcloning Efficiency DH5α (Invitrogen) were inoculated with ligation product in the way previously described.

## 2.20 Sequencing

Sequencing was done by MWG Biotech. Dry DNA (20 ng/100bp) samples and primers (10 mM) were sent. MWG Biotech "value read" service was used, which can sequence up to a 900 bp stretch.

## 2.21 *C. elegans* genetic nomenclature

**Strain names:** Strains have non-italicised names consisting of two uppercase letters followed by a number.

**Genotypes:** Genes have italicised names in the format of three lower case letters, hyphen, number. Alleles have italicised names in the format of one or two lower case letters followed by a number. When gene and allele names are written together they are in the format *gene*(*allele*). Mutants with more than one mutation are written by listing the gene and allele in left-right order on the genetic map. Different linkage groups are separated by a semicolon and given in the order *I*, *II*, *III*, *IV*, *V*, *X*. Heterozygotes are designated by separating mutations on the two homologous chromosomes with a slash. wild-type alleles are designated by a plus sign.

**Transgenes:** Extrachromosomal arrays are given italicised names consisting of the laboratory allele prefix, the two letters *Ex*, and a number. Integrated transgenes are designated by italicised names consisting of the laboratory allele prefix, the two letters *Is*, and a number. Both *Ex* and *Is* can optionally be followed by genotypic or molecular information describing the transgene, in square brackets. Gene fusions incorporated in transgenes that consist of a *C. elegans* gene fused to a reporter are indicated by the *C. elegans* gene name followed by two colons and the reporter, all italicised.

## 2.22 Chemical mutagenesis screen

*N2* worms were mutagenised with the chemical mutagen ethlymethanesulphonate (EMS) at a concentration of 0.05 M, using the method described by Sulston and Hodgkin (1988). The average mutation frequency of EMS is $5x10^{-4}$ per gene. About 13 % of mutations produced by EMS are deletions, the rest are point mutations (Anderson 1995). This procedure was carried out in a fume cupboard and double gloves were worn due to the toxic nature of EMS. 1M NaOH was used for rinsing gloves and 4M NaOH is used for cleaning contaminated plastic. A dedicated Gilson was used.

5 cm plates containing *N2* animals at various growth stages were washed off with 1 ml of M9 buffer and transferred to a 20 ml tube (Sterilin). The worms were left to settle for 15 minutes before the majority of the supernatant was removed, leaving 2ml. In a separate tube 2 ml of M9 buffer was mixed with 20 µl of EMS, giving a concentration of 0.1 M. This was then added to the 2ml of M9 containing the worms, giving a final EMS concentration of 0.05 M. The tube was placed on its side for 4 hours, mixing every ½ hour by gently rocking it. The worms were then put through 5 wash steps. The volume up was made up to 20ml with M9, left for 15 minute to allow the worms to settle, before removing the supernatant and repeating the wash. After the final wash the supernatant was removed, leaving 2 ml of M9 containing the worms. 0.5 ml of this was then pipetted to the edge of 4 seeded NGM plates. L4 worms that were healthy enough to reach the bacterial lawn within half an hour were selected and placed on individual plates.

Most mutations are likely to be recessive (Brenner 1974). Mutated worms must therefore be propagated in order to select homozygous mutants (F3). 120 L4 F1 worms exposed to the mutagen were picked to individual plates. These were incubated for 4 to 5 days at 20 $^{o}$C. Once the F1 had laid eggs that had matured to gravid F2 adults the F3 eggs were extracted in the following process. The worms were washed off each plate with 1 ml of M9 buffer and transferred to separate 1.9 ml Eppendorf tubes. They were allowed to settle for 5 minutes before the supernatant was removed, leaving a pellet of worms. 100 µl of the following solution, 1.25 % NaOCl, 2 M NaOH, was added to the Eppendorf and left for 2 minutes to break up the F2 worm. 1 ml of M9 buffer was added and then spun for 20 seconds at 16000 x g before removing the supernatant. Another 1 ml of M9 buffer was added and the spin

repeated. The majority of the supernatant was removed, leaving ~ 100 µl. The extracted eggs were then pipetted on a 1 µM emodepside NGM plate and screened for resistance. This concentration of emodepside slows development and inhibits movement of adult worms. The screen selected animals that 1) reached adulthood within *N2* time frame, 2) retained *N2* sinusoidal patterns of movement. The mutagenesis screen is estimated to be of ~ 7500 genomes.

## 2.23 Out-crossing

EMS produces random mutations. Therefore a strain containing a desired mutation will also contain many other unwanted mutations. These mutations can be removed through a process of out-crossing. This process allows mutant DNA to be replaced with *N2* DNA whilst retaining the desired mutation. Mutant strains are mated with *N2* to produce heterozygous progeny (F2). F3 progeny homozygous for the desired mutation are then selected. These worms are said to be 1 x out-crossed. This process can be repeated to further reduce the number of mutations. Homozygous progeny are detected either through a phenotype linked to the mutation of interest, by PCR amplification of a deletion or sequencing of a point mutation.

Males were generated through heat-shock of L4 hermaphrodites for 7 hours at 30 $^{o}$C. This increases the proportion of male progeny to ~2 %. F1 Mutant L4 males were then picked and crossed with *N2* hermaphrodites. The cross was set up at L4 stage to reduce self-fertilization. L4 F2 progeny resulting from the first cross were then placed on individual plates and selfed. F3 progeny were then screened for the mutation of interest, either by phenotype, PCR or sequencing. Populations were then established from worms homozygous for the mutation. Multiple crosses were set up at each step to ensure the desired genotypes were obtained. Figure 2.06 shows the process of out-crossing. Strains were out-crossed between 3 to 5 times.

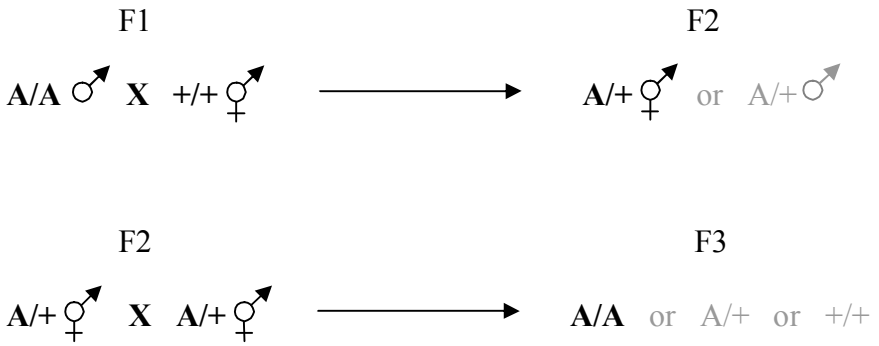


**Figure 2.06. Out-crossing of mutant worm strains.** This process is repeated multiple times to remove unwanted mutations. "A" represents the mutant allele and + represents *N2*. Selection of, A/A is based on phenotype or on PCR or sequencing of the mutation.

## 2.24 *lat-2 lat-1* double mutant

The strains VC965, carrying *lat-1*(*ok1465*), and XA3727, carrying *lat-2*(*tm463*), were used to generate *lat-2 lat-1* double mutants. *lat-1*(*ok1465*) has a developmental defect and is therefore balanced. *lat-1*(*ok1465*) was balanced using the mIn1 balancer (Edgely and Riddle 2001). mIn1 is an inversion of a large central portion of chromosome II, extending from *lin-31* to *rol-1*, that includes most of the genes on the chromosome. *lat-1* and *lat-2* are both covered by mIn1. mIn1 has integrated GFP and *dpy-10*(e128). *dpy-10*(*e128*) is recessive and *gfp* is semi-dominant. Figure 2.07 highlights the key features of mIn1.

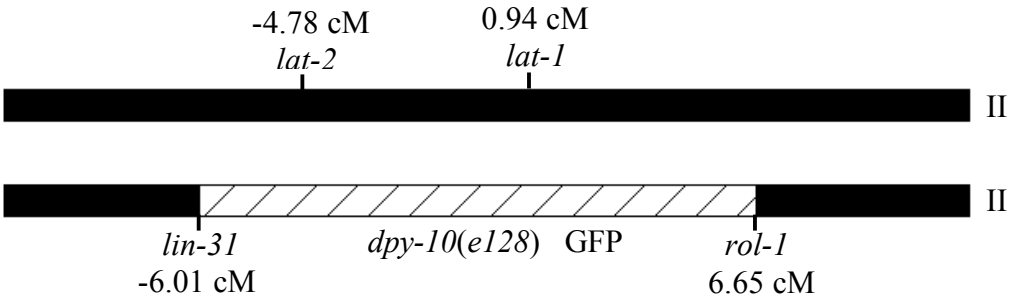


**Figure 2.07. mIn1 balancer.** mIn1 is an inversion of a large central portion of chromosome II, extending from *lin-31* to *rol-1*, that includes most of the genes on the chromosome (Edgely and Riddle 2001). *lat-1* and *lat-2* are both covered by mIn1. The strain VC965 carries the Chromosome II balancer mIn-1 and *lat-1*(*ok1465*). mIn1 has GFP integrated and *dpy-10*(*e128*). Genetic map positions of the above mention genes are marked (www.wormbase.org 08/01/08).

The following crosses were set up in order to obtain a *lat-2*, *lat-1* double mutant (Figure 2.08).

**Cross 1)**

**+ *lat-1* II / mIn1 II ♀ X *lat-2* + II / *lat-2* + II ♂ ⟶**

Select non-*gfp*, non-dumpy

⟶ **+ *lat-1* II / *lat-2* + II**

**Cross 2)**

**+ *lat-1* II / *lat-2* + II ♀ X + *lat-1* II / mIn1 II ♂ ⟶**

Select non-dumpy, *gfp* expressing

⟶ ***lat-2 lat-1* II / mIn1 II** or + *lat-1* II / mIn1 II

or *lat-2* + II/ mIn1 II or + + II / mIn1 II

**Figure 2.08. Construction of *lat-2 lat-1* II / mIn1 II.** Only genotypes of the selected cross progeny are show. Selection is based on dumpy and gfp phenotypes. Progeny from cross 2 were selected and screened for the presence of both *lat-2*(*tm463*) and *lat-1*(*ok1465*). Progeny of the desired phenotype are shown in bold.

Non-dpy, *gfp* expressing worms were selected from cross 2 progeny. They were then screened for worms carrying both *lat-2*(*tm463*), *lat-1*(*ok1465*) using PCR to detect deletions. The probability of recombination between *lat-2* and *lat-1* is 1/17.48 as they are 5.72 cM apart on chromosome II. The probability of obtaining *lat-2*, *lat-1* // mIn1 from cross 2 is 1/34.96.

## 2.25 Snip-SNP mapping

Mutations conferring resistance to emodepside were mapped using a technique known as snip-SNP (single nucleotide polymorphisms) mapping. This technique exploits the SNPs that exist between *N2 C. elegans* and the Hawaiian strain CB4856. SNPs can result in the creation or destruction of restriction enzyme sites across the genome. There are predicted to be 6222

SNPs in CB4856 with reference to *N2*, with 3457 of these modifying restriction sites (snip-SNPs). 493 of these have been confirmed experimentally (Wicks *et al* 2001). These snip-SNPs are used as markers for mapping. A fragment of genomic DNA containing the snip-SNP is PCR amplified and then digested with the appropriate restriction enzyme.

In order to map using this technique a visible marker mutation was first introduced into the emodepside resistant (ER) mutant background. The *dpy-20*(*e1282*) was used for this purpose. *dpy-20*(*e1282*) results in the dumpy appearance of the worm. The following crosses, shown in figure 2.09, were set up in order to obtain ER, *dpy-20*(*e1282*) double mutants.

**Cross 1)**

***dpy-20* IV / *dpy-20* IV♀ X ER / ER ♂ →**

Select non-dumpy

**→ *dpy-20* IV; + / + IV; ER**

**Cross2)**

***dpy-20* IV; + / + IV; ER ♀ X *dpy-20* IV; + / + IV; ER♀ →**

Select dumpy worms

**→ *dpy-20* IV; ER / *dpy-20* IV; ER** or *dpy-20* IV; ER / *dpy-20* IV; +

or *dpy-20* IV; + / *dpy-20* IV; +

**Figure 2.09. Introduction of *dpy*-20 in mutant background.** Crosses set up in order to obtain *dpy-20* IV; ER / *dpy-20* IV; ER. Only genotypes of the selected cross progeny are show. Selection is based on dumpy phenotypes. Progeny from cross 2 were selected and screened for resistance to 1 µM emodepside. Progeny of the desired phenotype are shown in bold.

Selection of *dpy-20* IV; ER / *dpy-20* IV; ER was based on dumpy phenotype. Progeny from these worms were screened for emodepside resistance using the same screening method as described for the mutagenesis screen.

Worms with the *dpy-20* IV; ER / *dpy-20* IV; ER genotypes were used to set up the crosses with CB4856 shown in figure 2.10. These crosses allow for the introduction of CB4856 DNA whilst retaining the mutation that confers resistance. The *dpy-20* marker was used to confirm that the cross was successful.

**Cross 1)**

***dpy-20* IV; ER / *dpy-20* IV; ER ♀ X CB / CB ♂ →**

Select non-dumpy

**→ *dpy-20* IV; ER / CB; CB**

**Cross 2)**

***dpy-20* IV; ER / CB; CB ♀ X *dpy-20* IV; ER / CB; CB ♂ →**

Select emodepside resistant

**→ *dpy-20* IV; ER / *dpy-20* IV; ER** or **_dpy-20_ IV; ER / CB IV; ER**

or **CB IV; ER / CB IV; ER**

**Figure 2.10. Crosses set up in order to introduce CB DNA into ER / ER.** Non-dumpy progeny were selected from cross 1 to ensure the cross was successful. Progeny resistant to 1 μM emodepside were selected from cross 2 irrespective of their dumpy phenotype. Progeny of the desired phenotype are shown in bold.

All progeny were selected from cross 2 in figure 2.10, and individually placed on 1 μM emodepside plates. Populations were established from individual progeny and screened for emodepside resistance using the method previously described for the mutagenesis screen. Genomic DNA was then extracted from these populations as previously described. Cross 2 in figure 2.10 follows Mendelian genetics. i.e. ¼ will be CB / CB, ½ will be CB / + and ¼ will be + / +. However, due to the selection based on resistance to 1 μM emodepside, the region of the mutation conferring resistance will always be *N2* DNA. Recombination events allow CB DNA to be introduced to the chromosome that carries the mutation conferring resistance. These recombination events become increasingly less frequent nearer the mutation. Using the DNA from the strains generated in the cross in figure 2.10, the mutation conferring resistance can be mapped using the snip-SNPs.

## 2.26 Complementation tests

Complementation tests are genetic tests that can be used to determine if mutation of a particular gene is responsible for a certain phenotype. This test requires a candidate gene and a strain with an appropriate mutation within this gene. *slo-1*(*js379*) was used for this purpose. The following cross was set up (figure 2.11).

***dpy-20* IV; ER / *dpy-20* IV; ER ♀ X *slo-1* V / *slo-1* V ♂ →**

Select non-dumpy

***dpy-20* IV; ER / *slo-1* V**

**Figure 2.11. Cross set up in order to generate heterozygous *slo-1*(*js379*) and ER.** The progeny from this cross were then tested for sensitivity to 1 μM emodepside in the body bends assay.

*slo-1*(*js379*) are resistant to emodepside. If *dpy-20* IV; ER / *slo-1* V are resistant, then the emodepside resistant strain is said to be a non-complement of *slo-1*(*js379*). This suggests it is an allele of *slo-1*. Complementation tests were conducted on all emodepside resistant strains. Emodepside resistance was tested on 1 μM emodepside in the body bends assay as previously described.

## 2.27 Transgenic worms

Transgenic worms were generated by micro-injection of DNA vectors into the syncytium of young adult worms (1 day post L4). Vectors were co-injected with the injection marker pPD118.33. pPD118.33 contains *gfp* behind the *myo-2* pharyngeal muscle promoter. The technique used is illustrated in figure 2.12.

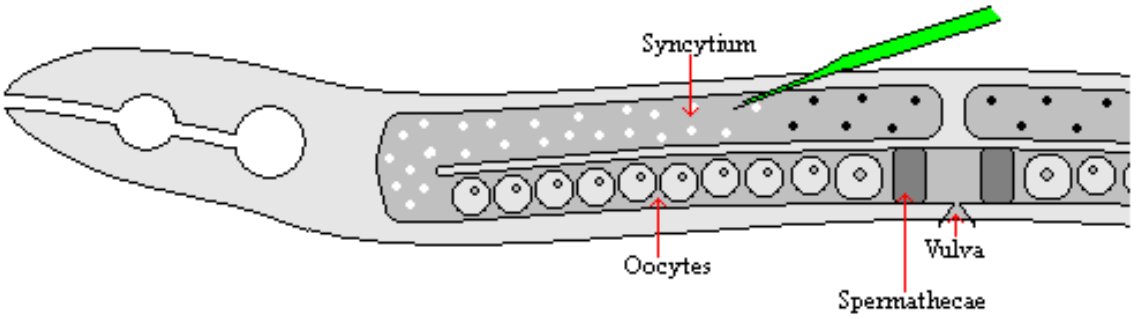


**Figure 2.12. Micro-injection of *C. elegans*.** The distal part of the gonad was injected with the vectors to be expressed. These become incorporated as extra chromosomal arrays in the progeny of the injected worm. (After White *et al* 1988)

To obtain needles for micro-injection, 1mm diameter aluminosilicate glass capillaries were pulled using the P-2000 Sutter Instrument electrode puller. DNA solutions were made up in $ddH_2O$ at concentrations of 50 ng/µl for injection marker vectors and at 25 ng/µl for all other vectors. DNA solutions were spun for 10 minutes at 16000 x g to pellet any debris and then transferred to a fresh tube. Micro-injection needles were placed in the tube containing the DNA solution and filled by capillary action for 10 minutes. The needle was then mounted on a micro-manipulator (Eppendorf TransferMan NK2). Viewing the needle under X40 magnification, it was then broken against the edge of a cover slip immersed in oil. This creates a jagged edge suitable for injection.

2 % agarose pads were used to stick the worms in position. These were made by pipetting 50 µl of molten 2 % agarose in $ddH_2O$ onto a microscope slide. This was then flattened using a cover slip and dried at 60 $^{o}$C for 1 hour. Worms were picked to these pads, and a drop of oil was placed on them to prevent them drying out. Worms were then injected with DNA solution under X40 magnification. They were recovered by pipetting 10 µl of M9 buffer on to them.

Worms were transferred onto NGM plates. Transgenic progeny were selected using the pPD118.33 *gfp* marker and stable lines established these worms.

## 2.28 Cell culture

**Cell culture** - HEK293 cells (Graham *et al* 1977) were cultured at 37$^{o}$C and 5% $CO_2$. 25 $cm^2$ flasks (Greiner bio-one) were routinely used, as was Dulbecco's Modified Eagle Medium (DMEM) + Glutamax (Gibco). DMEM was supplemented with Foetal Calf Serum (10%) (Gibco) and penicillin/streptomycin (100 units/ml /100 µg/ml) (Gibco). Medium was replaced every two days.

**Passaging cells -** Cells were passaged when at approximately 80% confluence. Culture media was aspirated form the flask. 2 ml of Phosphate buffered solution (PBS) (Gibco) pH7.4 was added to rinse the cells. The PBS was aspirated and 1 ml of trypsin (2.5 g/l) versene (2g/l) mix was added. This was then incubated at 37 $^{o}$C for three minutes. 10 ml of DMEM was added to dilute the trypsin. This was then spun at 1000 x g for two minutes to pellet the cells. DMEM was aspirated and the cells were re-suspended in fresh DMEM. The volume of DMEM cells were re-suspended in depended on the percentage confluence required. 0.5 ml of re-suspended cells was then added to 4.5 ml DMEM in 25 $cm^2$ flasks. Alternatively, re-suspended cells were added to 6 well plates (Greiner bio-one) containing cover slips for transfection and patch clamp experiments. 13 mm cover slips (Raymond A Lamb) were washed in 100 % ethanol and then air dried. Covers slips were placed in six well plates (Greiner bio-one). 2 ml of DMEM and 0.5 ml of re-suspended cells were added to each well. Cells were added at approximately 20 percent confluence and grown for a minimum of 24 hours before transfection.

## 2.29 HEK293 transfection

HEK293 cells were transfected when approximately 20 percent confluent. Cells must not be too confluent as single cells are required for patch clamp experiments. 6 µg of DNA was mixed with 1500 µl of Opti-MEM (with GlutaMAX) (Gibco). 12 µl of Lipofectamine 2000 (Invitrogen) was mixed with 1500 µl of Opti-MEM. These two mixes were incubated at room

temperature for five minutes and then combined and incubated for 20 minutes at room temperature.

DMEM was aspirated from the six well plate and replaced with 2 ml of Opti-MEM. 0.5 ml of the DNA, Lipofectamine 2000 mix was added per well. Plates were incubated at 37 $^{o}$C for six hours before Opti-MEM was replaced with DMEM. Cells were used in patch clamp experiments 24 hours after transfection.

Transfected cell were identified by *gfp* expression. *C. elegans slo-1* cDNAa was cloned into pIRES2-EGFP which contains *gfp* driven by pCMV. Human Kcnma1 variant 2 cDNA was cloned in pCMV6-XL4, which contains no marker for eukaryote transfections. It was therefore co-transfected with pIRES2-EGFP in a 3:1 molar ratio. Transfection efficiency was estimated to be between 20 % and 50 %.

## 2.30 Patch clamp analysis

Whole cell patch clamp experiments were conducted on HEK293 cells. HEK293 cells attached to cover slips were transferred to a bath containing an external solution. These were stuck down using silicone grease (ACE Silicones) Cells were viewed using a Zeiss Axioskop2 under x 10 and x 40 water immersion lens. Patch pipettes containing internal solution were manoeuvred towards the membrane single cells. The patch pipette was held at -80 mV. Positive pressure sufficient to form a slight depression (~1 μm) in the cell membrane was applied through the patch pipette. This positive pressure was then turned off, creating a backflow sufficient to suck the cell membrane onto the patch pipette. Stable seals generally formed instantaneously. Attempts to open cells were made when seal resistance was more than 1 GΩ. Cells were opened using a combination of suction and voltage pulse (1.5 V for 0.5 ms). Recordings were taken from open cells with a seal resistance of more than 1 GΩ.

**External solution:** 137 mM NaCl, 5.9 mM KCl, 2.2 mM $CaCl_2$, 1.2 mM $MgCl_2$, 14 mM glucose, 10 mM HEPES. pH 7.4 (with NaOH)

**Internal solution:** 140 mM KCl, 1 mM $MgCl_2$, 10 mM HEPES, 2 mM $Na_2ATP$, 5 mM EGTA, 300 μM $CaCl_2$. pH 7.2 (with KOH)

Equipment and software – The Axopatch 200B (Axon Instruments) patch clamp amplifier was used in combination with CU203BU headstage (Axon Instruments). Digidata1322A was used for conversion of analogue to digital data and interface with a PC. Clampex version 9.2.0.09 was used for recording of data.

Patch pipettes – Patch pipettes were made from 1.3 mm melting point capillaries (CAP-MPO-75 Bilbate). They were pulled in a Narishige vertical puller in two steps. Patch pipettes of between 3.5 and 5 MΩ resistance were used. Electrode resistance was obtained using Clampex 9.2 seal test function, which applies a 5 mV step to calculate resistance.

Electrodes – A silver chloride coated silver wire recording electrode was used. The reference electrode was a silver chloride pellet electrode connected to the recording chamber via an agar bridge containing bathing solution. This was used to minimise junction potentials and to prevent changes in the ionic composition of the bath solution.

Voltage step protocol – A voltage step protocol was set up using Clampex version 9. From a resting potential of -80 mV, voltage steps were made to: -90, -80, -70, -60, -50, -40, -30, -20, -10, 0, +10, +20, +30, +40 and +50 mV. Each step lasted 100 ms. Current required to maintain the potential at each voltage step was recorded. Leak subtraction was routinely applied using the P/N leak subtraction facility of Clampex. Four sweeps were automatically applied prior to execution of the step protocol in the opposite polarity. The average leak was automatically subtracted.

Pharmacology – Drugs were applied to the bath. 0.5 ml of external solution was removed from the bath and replaced with 0.5 ml of drug dissolved in bath solution. 4-AP, IBTX and emodepside were added to a final concentration of 10 mM, 100 nM, and 100 nM respectively.

# Chapter 3

# The role of latrophilin receptors in emodepside's mode of action

## 3.1 Introduction

Evidence has previously been put forward for a role of the latrophilins in the mode of action of emodepside (Saeger *et al* 2001, Wilson *et al* 2004). This evidence is based on expression cloning of latrophilin from *H. contortus* and RNA interference studies in *C. elegans*.

In all RNAi studies targeting latrophilins (Willson *et al* 2003, Amliwala 2005), the effect was to cause a reduction in sensitivity to emodepside rather than complete resistance. There are several possible explanations for this. It may be that the knock down of the LAT-1 and LAT-2 receptors by RNAi is incomplete and therefore they are only partially resistant to emodepside's effects. Alternatively, redundancy between LAT-1 and LAT-2 may exist. This would mean that the action of emodepside can be directed through either LAT-1 or LAT-2. If LAT-1 is knocked down then emodepside's effects go through LAT-2, and if LAT-2 is knocked down then emodepside's effects go through LAT-1. Therefore latrophilin RNAi targeted worms would not show a high level of resistance. Another possibility is that there is a tissue limited affect of the RNAi. Effective silencing of genes by RNAi in neurons has been shown to be variable (Esposito *et al* 2007). Inefficient silencing of latrophilin receptors in some tissues would result in partial resistance. Alternatively, the effects seen with RNAi targeting the latrophilins may only modulate emodepside's effects and a distinct mechanism of action may exist.

The availability of deletion mutants for both *lat-1* and *lat-2*, during the course of this project, provided the opportunity for a more robust analysis of the role of the latrophilins in the mode of action of emodepside. Investigation of the effects of emodepside on these mutant strains was undertaken. In this chapter, characterisation and phenotypic analysis of these mutants is described. A double *lat-2 lat-1* mutant was generated to address the question of functional redundancy between *lat-1* and *lat-2* in terms of emodepside resistance.

## 3.2 Developmental defect of the latrophilin mutant strain VC965

The strain VC965 carries *lat-1*(*ok1465*) balanced by the insertion *mIn1*. The *mIn1* balancer has an inverted region that carries *dpy-10*(*e128*) and *gfp* (see methods, page 66). *lat-1*(*ok1465*) is balanced in this way as development of homozygous *lat-1*(*ok1465*) arrests. A small proportion of *lat-1*(*ok1465*) are able to escape this developmental arrest. Homozygous *lat-1*(*ok1465*) are identifiable in a population of VC965 as they lack expression of *gfp*. In order to obtain a homozygous *lat-1*(*ok1465*) population, 75 larvae not expressing *gfp* were selected, one of which developed to adult. It was possible to establish a homozygous population through propagation of this single worm. The developmental defect was defined more precisely using this population. The development of synchronised *N2* and *lat-1*(*ok1465*) eggs was observed over a 96 hour period. Figure 3.01 shows the proportion of animals at each stages of development. Worms were staged, based on vulva appearance under a dissecting microscope (x 63 max).

94 % of the synchronised *N2* had developed to adult at 72 and 96 hours. The 6 % that failed to develop are likely to have been damaged during transfer of the eggs. At 72 hours, 98.4 % *lat-1*(*ok1465*) remained at L1 stage, 0.8 % were eggs, 0.4 % were L2 and 0.4 % were L3. At 96 hours, 98.4 % *lat-1*(*ok1465*) remained at L1 stage, 0.8 % were eggs, 0.4 % were L4 and 0.4 % were adult. There were significantly fewer *lat-1*(*ok1465*) adults ($P<0.001$) and significantly more *lat-1*(*ok1465*) L1 ($P<0.001$) at 72 and 96 hours compared to *N2*. These groups were compared using Fisher's exact test.

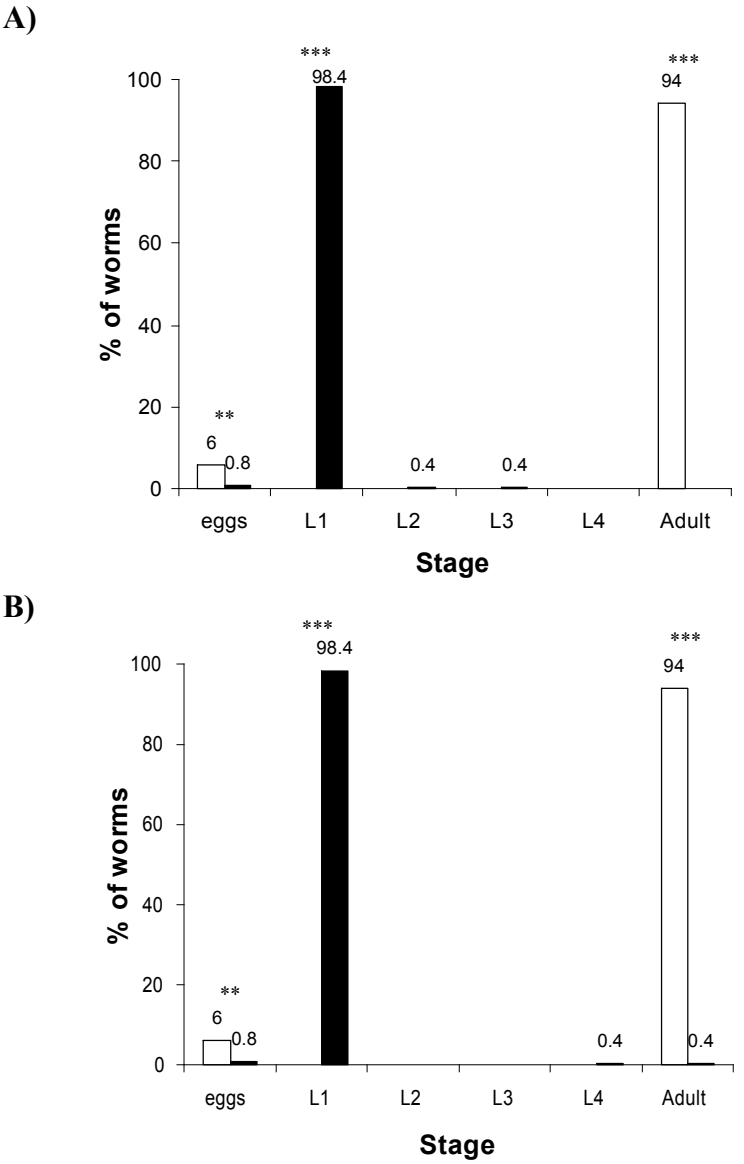


**Figure 3.01. Quantification of *lat-1*(*ok1465*) growth defect.** Percentage of homozygous *lat-1*(*ok1465* ) (■) and *N2* (□) worms at each growth stage at **A)** 76 hours **B)** 94 hours after synchronised eggs were selected. Larval stage was determined by stage of vulva development. For *lat-1*(*ok1465*) (■) n=250, for *N2* (□) n=100. Differences between *N2* and *lat-1*(*ok1465*) were compared at each stage using a two-tailed Fisher's exact test. ** indicates $P<0.01$ and *** indicates $P<0.001$.

Twenty of the *lat-1*(*ok1465*) identified as L1 were observed under x 1000 power to more stringently analyse the stage of vulva development. All twenty proved to be at the L1 stage of development. Figure 3.02 shows an example of the vulva at L1. Four vulva precursor cells are visible, Z1, Z2, Z3 and Z4. The vulva of *N2* worms is at this stage of development in the L1 moult.

**A)**

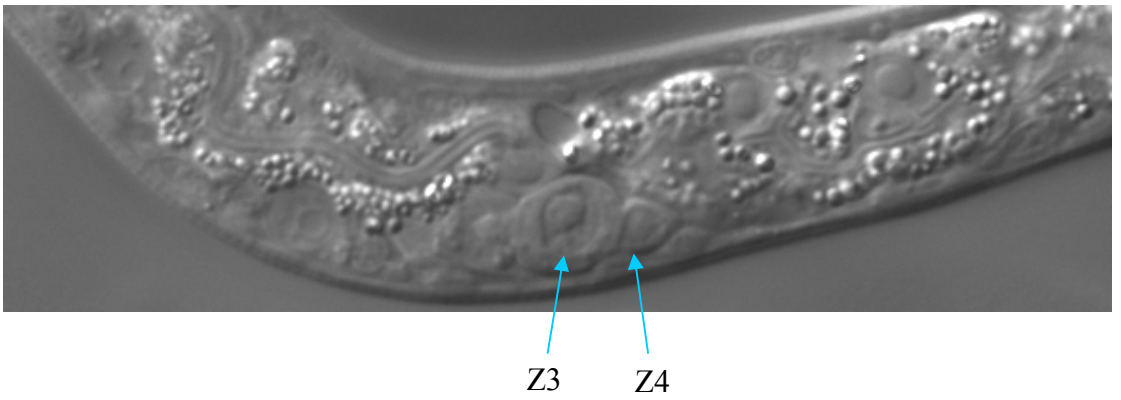


**B)**

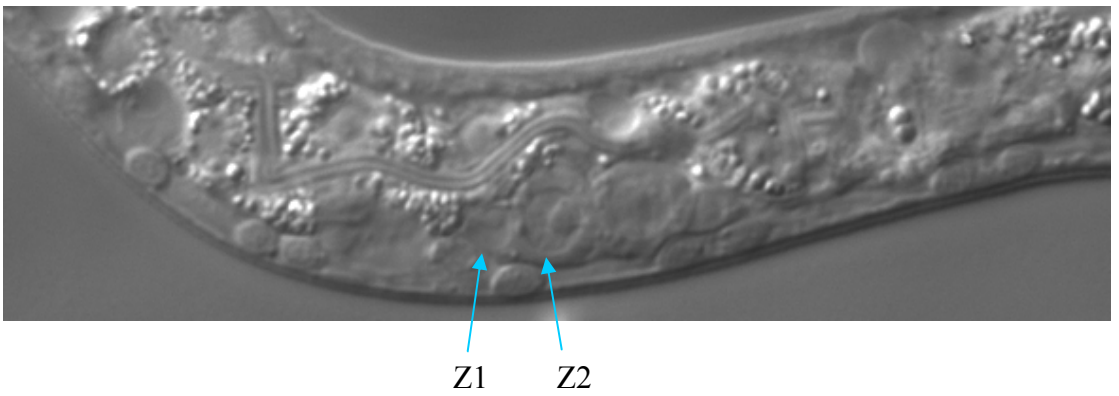


**Figure 3.02. Vulval development of *lat-1*(*ok1465*).** Homozygous *lat-1*(*ok1465*) after 94 hours development at x 1000 magnification. The vulva precursor cells are marked. **A)** Shows the lateral view of Z3 and Z4. **B)** Shows the lateral view of Z1 and Z2. This stage of vulva development occurs during L1.

Attempts to rescue the developmental defect of *lat-1*(*ok1465*) were made. The cosmid BO457 was co-injected with the genetic marker $_{p}$*myo-2::*GFP (pPD118.33). Transgenic F1 progeny from injected animals were obtained but the developmental defect did not rescue.

## 3.3 *lat-1*(*ok1465*) contains a 2209 bp deletion

The strain VC965 carries *lat-1*(*ok1465*), which has a 2209 bp deletion. The presence of this deletion in the VC965 strain was confirmed using PCR. Primers either side of the deletion were used to amplify *lat-1*(+) DNA fragments of 3604 bp and *lat-1*(*ok1465*) DNA fragments of 1395 bp. PCR was also used to demonstrate that VC956 animals not expressing *gfp* were homozygous for *lat-1*(*ok1465*). Primers within and either side of the deletion were used. A *lat-1*(*ok1465*) DNA fragment of 1395 bp was amplified. The primer within the deletion results in the amplification of a 732 bp fragment in *lat-1*(+). The lack of this product from DNA of worms not expressing *gfp* confirms that they are homozygous for *lat-1*(*ok1465*). Figure 3.03 shows a gene model of *lat-1* with the *ok1465* deletion marked (adapted from www.wormbase.org), as well as gel electrophoresis for the PCR described.

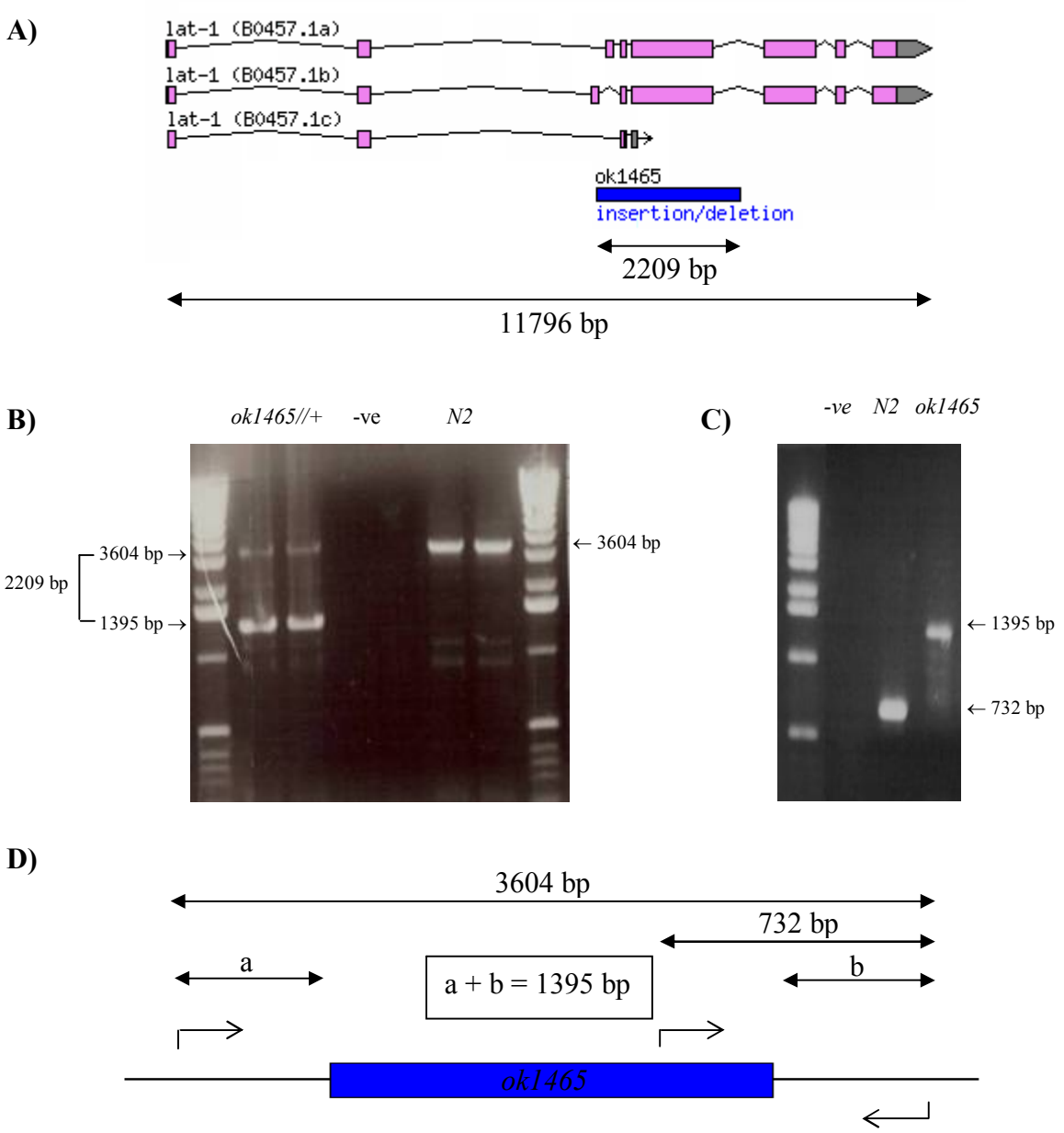


**Figure 3.03. Genotypic analysis of the strain VC965. A)** *lat-1* gene model (www.wormbase.org). The three splice variants have been identified. The allele *ok1465* has a 2209 bp deletion spanning exons 3, 4 and 5 of splice variants a and b and exons 3 and 4 of splice variant c. **B)** PCR of genomic DNA from *N2* and *lat-1*(*ok1465*) / *lat-1*(+) using primers either side of the deletion. *N2* gives a band of 3604 bp and *lat-1*(*ok1465*) / *lat-1*(+) gives bands of 3604 bp and 1395 bp. **C)** PCR of genomic DNA from *N2* and *lat-1*(*ok1465*) / *lat-1*(*ok1465*) using primers within and either side of the deletion. *N2* gives a band of 732 bp and *lat-1*(*ok1465*) / *lat-1*(*ok1465*) gives a band of 1395 bp. **D)** *lat-1*(*ok1465*) model highlighting regions PCR amplified. Bold arrows mark regions amplified by PCR. Faint arrow denote primers.

Three splice variants of *lat-1* have been identified. *ok1465* results in the loss of regions coding for 41 % of the galactose binding lectin domain in splice variant a and 10 % in splice variant b, the hormone receptor domain, the GPCR proteolytic site domain and the first transmembrane domain in splice variant a. In splice variant a the deletion is in frame. In splice variant b, exon 3 reads in intron 5 and encounters a stop codon. In splice variant c, *ok1465* results in the loss of 25 % of the galactose binding lectin domain, its only domain. Figure 3.04 shows the amino acid sequence for splice variant a with the *ok1465* deletion and domains highlighted.

MRRNKTTYSLLQTILVACLLTVTPTFASNKPTTDESGTISHTICDGEAAE
LSCPAGKVISIVLGNYGRFSVAVCLPDNDIVPSNINCQNHKTKSILEK**KC**
**NGDSMCYFTVDKKTFTEDPCPNTPKYLEVKY**NCVVPATTTTTTTTTSTTT
**TDSSLIVDEEEEAQKDALNSDVIKPVKKK**EDVFCSATNRRGVNWQNTKSG
**TTSSAPCPEGSSGKQLWACTEEGQWLTEFPNSAGCESNWISSRN**SVLSGV
**ISSEDVSGLPEFLRNLGSETRRPMVGGDLPKVLHLLEKTVNVIAEESWAY**
**QHLPLSNKGAVEVMNYMLRNQEIWGSWDVTKRKEFASRFILAAEKAMVAS**
**AKGMMTSAESNVIVQPAITVEISHKIKMSSQPTDYILFPSAALWNGQNVD**
**NVNIPRDAILKINKDETQVFFSSFDNLGAQMTPSDVTVAIAGTDQTEVRK**
**RRVVSRIVGASLIENGKERRVENLTQPVRITFYHKESSVRHL**SNPTCVWW
**NHHELKWKPSGCKLSYHNKTMTSCDCTHLTHFAVLMDVRGH**DLNEID**QTL**
**LTLLTYVGCIISIICLLLTFFAYLIFSRNGGD**RVFIHENLCLSLAIAEIT
FLAGITRTEDSLQCGIIAVALMYMFLSALTWMLLEGYHIHRMLTEVFPSD
PRRFTYLLVGYIPPAIITLVAYLYNSDGFGTPDHCWLSTQNNFIWFFAGP
ACFIFCANSLVLVKTLCTVYQHTSGGYLPCRHDVDSGRSIRNWVKGSLAL
ASLLGVTWIFGLFWVEDSRSIVMAYVFTISNSLQGLFIFLFHVVFAEKMR
KDVGHWMYRRGCGGSSNSSPNHKRHNVQRDLMSPGVNSSTGSDFLYNTND
KYLTNSDTTNRLVYNGIMNHPNQMSVYQQHPHHQIYEQQPGTYDYATIAY
GDMMPGHRVAAPPAYQRLAVAEGRYGSQHQLYQGWHHRPPPEFSPPPPPL
STGPPNSRHYGTGSSGRRPPSSKMSDDSAYSDGSSSMLTTEVTPQGQTVL
RIDLNKPSMYCQDL

**Figure 3.04. LAT-1 amino acid sequence.** Amino acid sequence of *lat-1* splice variant a. The underlined section highlights the deleted region in *lat-1*(*ok1465*). Yellow highlights the galactose binding lectin domain. Blue highlights a domain present in hormone receptors. Purple highlights G-protein-coupled receptor proteolytic site domain. Green highlights a seven transmembrane domain.

It has been proposed that emodepside binds to the amino terminus of HC110-R (Saeger *et al* 2001). In *lat-1*(*ok1465*) the majority this region is deleted. It therefore seems unlikely that LAT-1 would be functional with regard to emodepside's proposed mode of action. It would

also be predicted that the loss of the first transmembrane domain would result in the protein being incorrectly orientated in the membrane. It would be expected that loss of function of LAT-1 would prevent activation of the vesicle release pathway by emodepside and therefore result in resistance.

The deleted region in *lat-1*(*ok1465*) reported on Wormbase was confirmed by sequencing of genomic DNA. The break point was found to be at 6585 bp from the start codon. This lies in intron 2 in splice variants a and c and in exon 3 in splice variant b. The deletion finishes in intron 5 at 8794 bp. Figure 3.05 shows the sequencing of *lat-1*(*ok1465*).

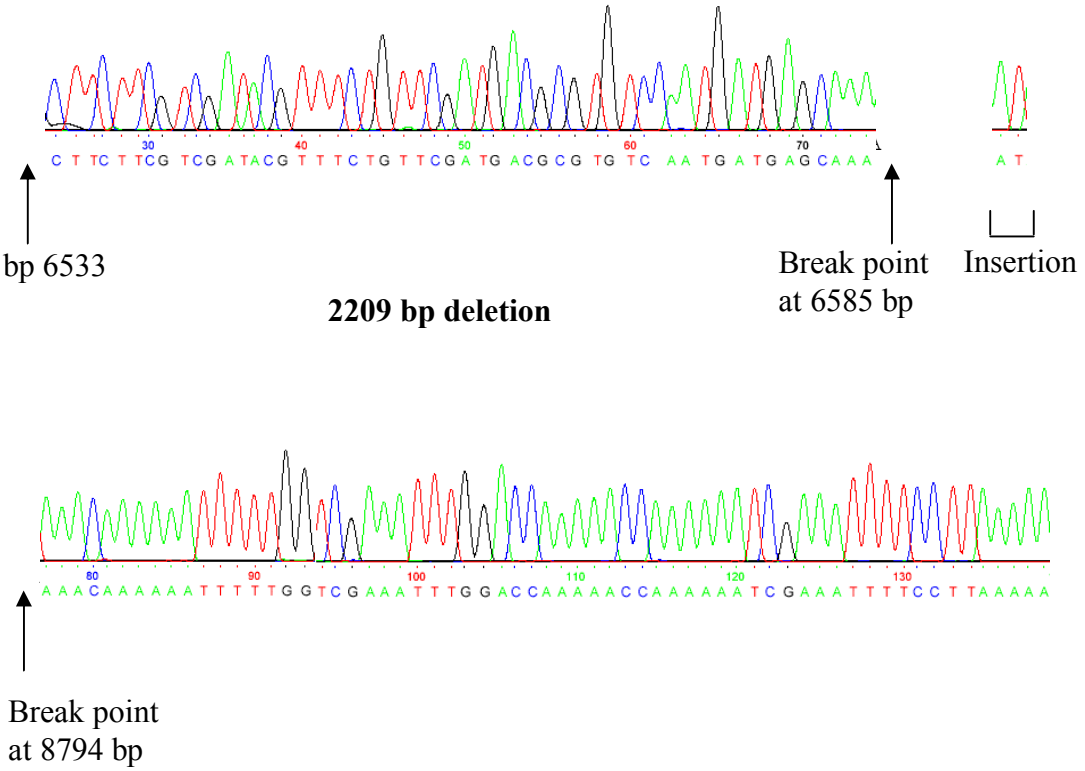


**Figure 3.05. *lat-1*(*ok1465*) sequence.** Sequencing of a PCR amplified fragment of genomic DNA from homozygous *lat-1*(*ok1465*). The deleted portion of *lat-1* is between 6585 bp and 8794 bp of the *lat-1* gene. There is an AT insertion in this region. The deleted region is 2209 bp.

## 3.4 *lat-1*(*ok1465*) are not resistant to emodepside's effects on locomotion

The sensitivity of *lat-1*(*ok1465*) to emodepside's effect on locomotion was tested using the body bends assay. Animals were exposed to emodepside for 24 hours and then assayed off food. The inhibition of locomotion in *N2* and *lat-1*(*ok1465*) by emodepside at 1 nM, 10 nM, 100 nM, 1 μM and 10 μM was not significantly different. Figure 3.06 shows a dose response for *N2* and *lat-1*(*ok1465*). *N2* have an $IC_{50}$ of 100 nM, 95 % confidence limits 68 nM to 146, compared with a *lat-1*(*ok1465*) $IC_{50}$ of 230 nM, 95 % confidence limits 96 nM to 552 nM.

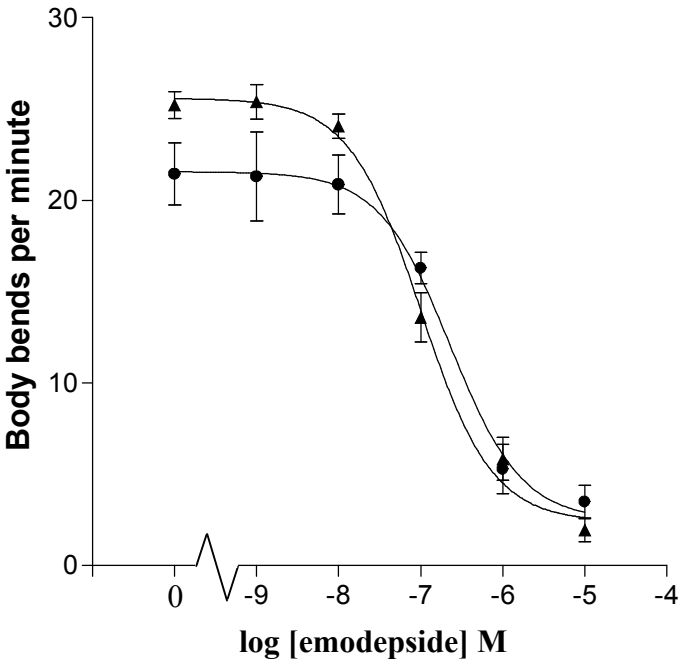


**Figure 3.06. *lat-1*(*ok1465*) dose response.** Dose response for emodepside on homozygous *lat-1*(*ok1465*) (●) and *N2* (▲). For each point n≥7 and is the mean ± S.E.Mean.

In contrast to the RNAi studies (Wilson *et al* 2003, Almliwala 2005), *lat-1*(*ok1465*) displayed a similar sensitivity to emodepside as *N2*. To further investigate the role of the latrophilins in emodepside's mode of action, *lat-2* was investigated.

## 3.5 *lat-2* deletion mutants

Two strains with *lat-2* deletions were available, VC158 which carries *lat-2*(*ok301*) and TM463 which carries *lat-2*(*tm463*). Neither strain displayed any obvious behavioural or developmental phenotype. PCR was used to confirm the presence of the deletions in these strains. For *lat-2*(*ok301*), primers either side of the deletion were used to amplify *lat-2*(+) DNA fragments of 3159 bp and *lat-2*(*ok301*) DNA fragments of 2076 bp. For *lat-2*(*tm463*), primers either side of the deletion were used to amplify *lat-2*(+) DNA fragments of 2908 bp and *lat-2*(*tm463*) DNA fragments of 1530 bp. PCR was also used to confirm that both strains were homozygous using primers within and either side of the deletion. For *lat-1*(*ok301*), a DNA fragment of 2076 bp was amplified and for the *N2* control, a DNA fragment of 1100 bp was amplified. The lack of the 1100 bp band in *lat-1*(*ok301*) demonstrates it is homozygous. For *lat-1*(*tm463*), a DNA fragment of 1530 bp was amplified and for the *N2* control, a DNA fragment of 852 bp was amplified. The lack of the 852 bp band in *lat-1*(*tm463*) demonstrates it is homozygous. Figure 3.07 shows a gene model for *lat-2* with *ok301* and *tm463* deletions highlighted as well as gel electrophoresis for the PCR described.

Two *lat-2* splice variants have been identified (www.wormbase.org). The deletion in *lat-1*(*tm463*) cover exons 4, 5, 6, 7, 8 and 9 of splice variant a. This results in the loss of coding sequence for 20 % of the C-type lectin-like domain and the galactose binding lectin domain in splice variant a. The deletion in *lat-2*(*tm463*) begins in exon 4 and reads into intron 9, subsequently encountering a stop codon in splice variant a. The product of splice variant b, which consists of a 15 amino acid amino terminal region, a seven transmembrane domain and a 200 amino acid C-terminal tail, is not covered by this deletion. The deletion in *lat-2*(*ok301*) covers part of 3' un-translated region of *lat-2*. Figure 3.08 shows the amino acid sequence for *lat-2* splice variant a with the *tm463* deletion and domains highlighted.

The deletion in *lat-2*(*tm463*) covers a large portion of the amino terminal which is proposed to be the binding site for emodepside in HC110-R (Seager *et al* 2001). It would therefore be expected that emodepside would be unable to bind. The deletion also results in the introduction of an early stop codon, which is likely to truncate the protein.

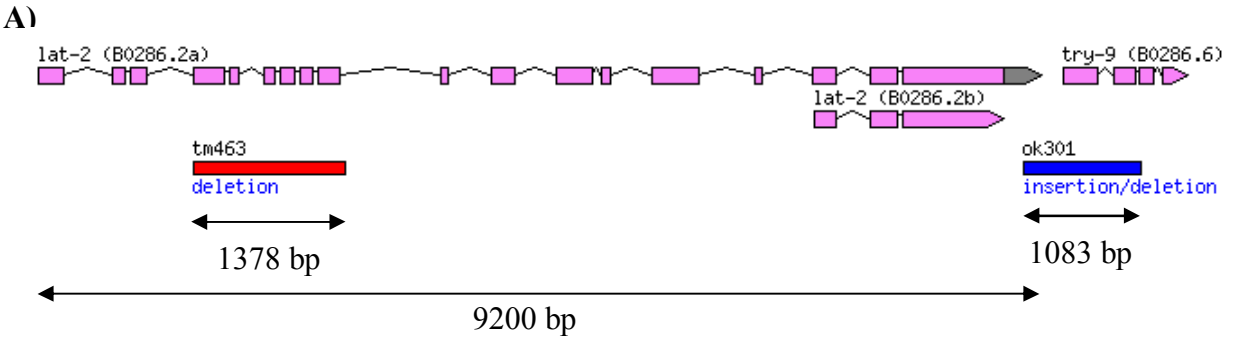
A)
lat-2 (B0286.2a)
try-9 (B0286.6)
lat-2 (B0286.2b)
tm463
deletion
ok301
insertion/deletion
1378 bp
1083 bp
9200 bp

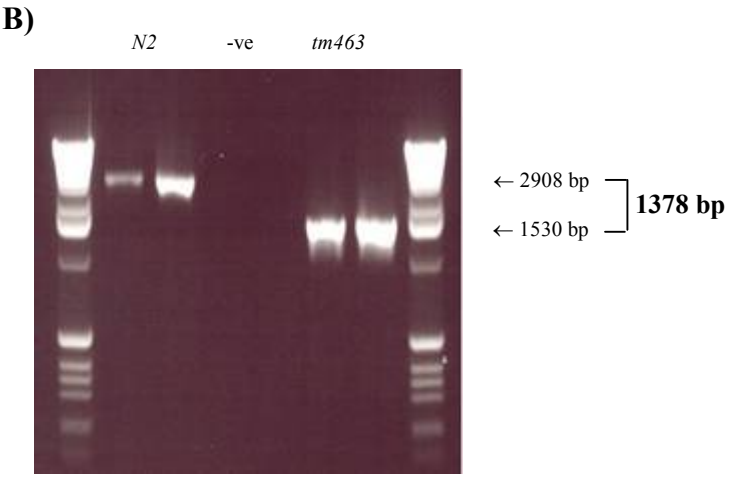
B)
N2
-ve
tm463
← 2908 bp
← 1530 bp
1378 bp

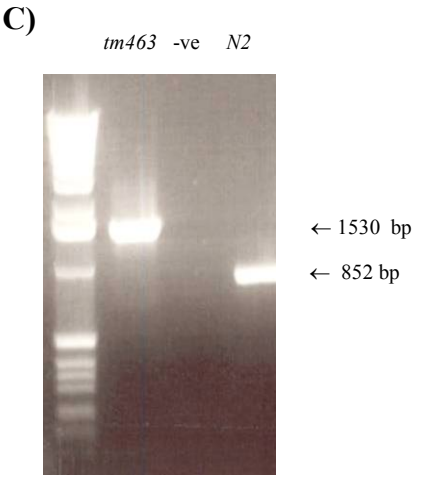
C)
tm463
-ve
N2
← 1530 bp
← 852 bp

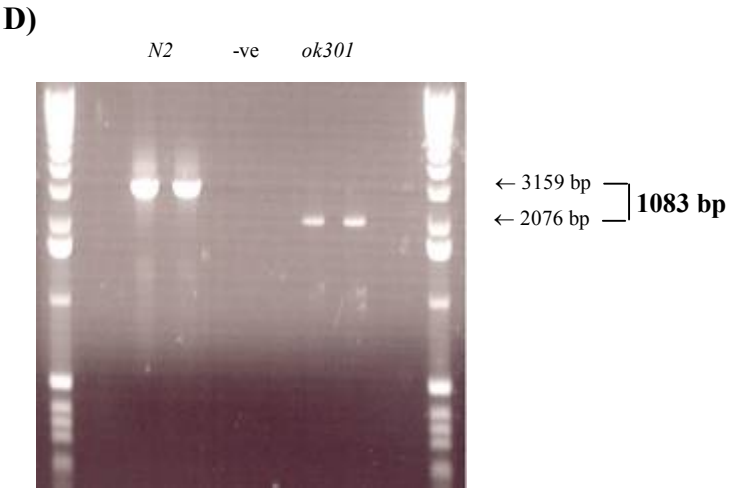
D)
N2
-ve
ok301
← 3159 bp
← 2076 bp
1083 bp

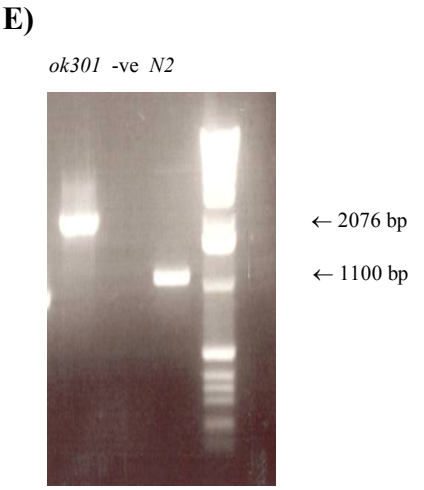
E)
ok301
-ve
N2
← 2076 bp
← 1100 bp

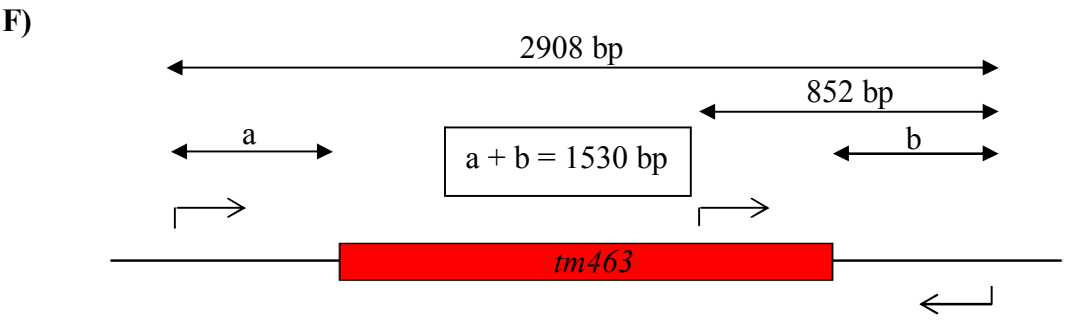
F)
2908 bp
852 bp
a
a + b = 1530 bp
b
tm463

**G)**

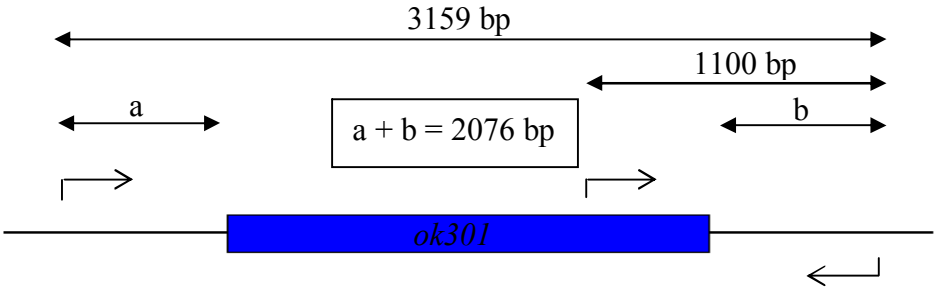


**Figure 3.07. Genotypic analysis of *lat-2*(*ok301*) and *lat-2*(*tm453*). A)** *lat-2* gene model (www.wormbase.org). The two splice variants are shown. The allele *tm463* has a 1379 bp deletion spanning exons 4, 5, 6, 7, 8 and 9 of splice variant a. The allele *ok301* spans part of the 3' UTR of splice variant a. **B)** PCR of genomic DNA from *N2* and *lat-2*(*tm463*) using primers either side of the deletion. *N2* gives a band of 2908 bp and *lat-2*(*tm463*) gives a bands of 1530 bp. **C)** PCR of genomic DNA from *N2* and *lat-2*(*tm463*) using primers within and either side of the deletion. *N2* gives a band of 852 bp and *lat-2*(*tm463*) give a band of 1530 bp. **D)** PCR of genomic DNA from *N2* and *lat-2*(*ok301*) using primers either side of the deletion. *N2* gives a band of 3159 bp and *lat-2*(*ok301*) gives a band of 2076 bp. **E)** PCR of genomic DNA from *N2* and *lat-2*(*ok301*) using primers within and either side of the deletion. *N2* gives a band of 1100 bp and *lat-2*(*ok301*) give a band of 2076 bp. **F)** *lat-2*(*tm463*) model highlighting regions PCR amplified. Bold arrows mark regions amplified by PCR. Faint arrow denote primers. **G)** *lat-2*(*ok301*) model highlighting regions PCR amplified. Bold arrows mark regions amplified by PCR. Faint arrow denote primers.

MAKQLKYPFLIFIISLAQCQVSNQNVNLCQSNICQNGGTCLVASSVPATA
TCPKNSIYYMGSCYVFDTTLRNWNDAALYCNNMNSATLPLVESAEDQAFF
AGYLQAMIPSNPPADMRPPPDGIWTAVRGVNNVTRASWVYYPGSFLVTDT
FWAPQEPNIYVNYNDVC**VALQSDSFYREWTTALCTILKYTVCKV**APTQIQ
**AKYVAQCSCPNGYGGQTCETQSTTNQQASTQRTCGSNDFQFSCPNDQTIT**
**VDFASFGAQESSMCNQASQSREQTCSNVNSLQTVINACQGLQSCEIRNLT**
**STFSNTPCPVPQEQYLETRMRCETAQQPSCLSGLIQFDSRCYSMTIETNE**
**KKQRTMEDAQTYCSQSGGSIITSPPDALLQQIVQKVNAETKKTVNFWIGT**
**PNNCQLLMVTGSSTSYSQCPSSPSSTANVICSTVPQSTASVSARPTQSAP**
**VDPVSQTMARREVYTGVQP**PSVPDSINKPRYCKKEKKDGITYEQTRACML
HEQPCPDPQNVEGTVTRYCNCQTAKWETPDTTNCTHRWVAEMETAIKDNQ
PVEDISSTVNRQLKSTIERTLFGGDITGTVRLSNDMLSLARNQFSVLNDR
NLRENKARNFTENLGGSGDQLLSPVAATVWDQLSSTIRIQHASKLMSVLE
QSVLLLGDYMTDQKLNLQYINWAMEVERSEPEVQTFGAAASPNVQDDMGM
MRVMAAAPPAPQPETNTTIMFPSLKLSPTITLPSASLLSSLASPTPVAGG
GPSILSSFQDDTPVGMASTPNLNRNPVKLGYYAFAGFGQLLNNNNDHTLI
NSQVIGASIQNATQSVTLPVDHPVTFTFQHLTTKGVSNPRCVYWDLMESK
WSTLGCTLIATSSNSSQCSCTHLTSFAILMDISGQVGRLSGGLASALDVV
STIGCAISIVCLALSVCVFTFFRNLQNVRNSIHRNLCLCLLIAELVFVIG
MDRTGNRTGCGVVAILLHYFFLSSFCWMLLEGYQLYMMLIQVFEPNRTRI
FLYYLFCYGTPAVVVAISAGIKWEDYGTDSYCWIDTSTPTIWAFVAPIIV
IIAANIIFLLIALKVVLSVQSRDRTKWGRIIGWLKGSATLLCLLGITWIF
GFLTAVKGGTGTAFAWIFTILNCTQGIFIFVLHVVLNEKVRASIVRWLRT
GICCLPETSSAAYNSRSFLSSRQRILNMIKVNGHSYPSTASTDDKEKQLT
PITKTTDWLSRLPNQDSVSIPESNFNNLNGTLENSNLNSAEIKEEDEIPE
LRRRVTVDLNPMIVSNNEIERMSHASSDPRGSQIIEVTAVEKKAPVKRIK
FPLGAKQSERGSQHRTKAKVIAPPESPVSESGSKDYRF

**Figure 3.08. LAT-2 amino acid sequence.** Amino acid sequence of *lat-2* splice variant a. The underlined section highlights the deleted region in *lat-2*(*tm463*). Red highlights a C-type lectin-like domain. Yellow highlights a galactose binding lectin domain. Blue highlights a domain present in hormone receptors. Purple highlights a G-protein-coupled receptor proteolytic site domain. Green highlights a seven transmembrane domain.

In order to confirm the sequence of *lat-2* in *lat-2*(*tm463*) reported on Wormbase, sequencing of genomic DNA across the deleted region was done. The break point was found to be at 1423 bp from the start codon. This lies at the beginning of exon 4. The deletion finishes in intron 9 at 2801 bp. Figure 3.09 shows the sequencing of *lat-2*(*tm463*).

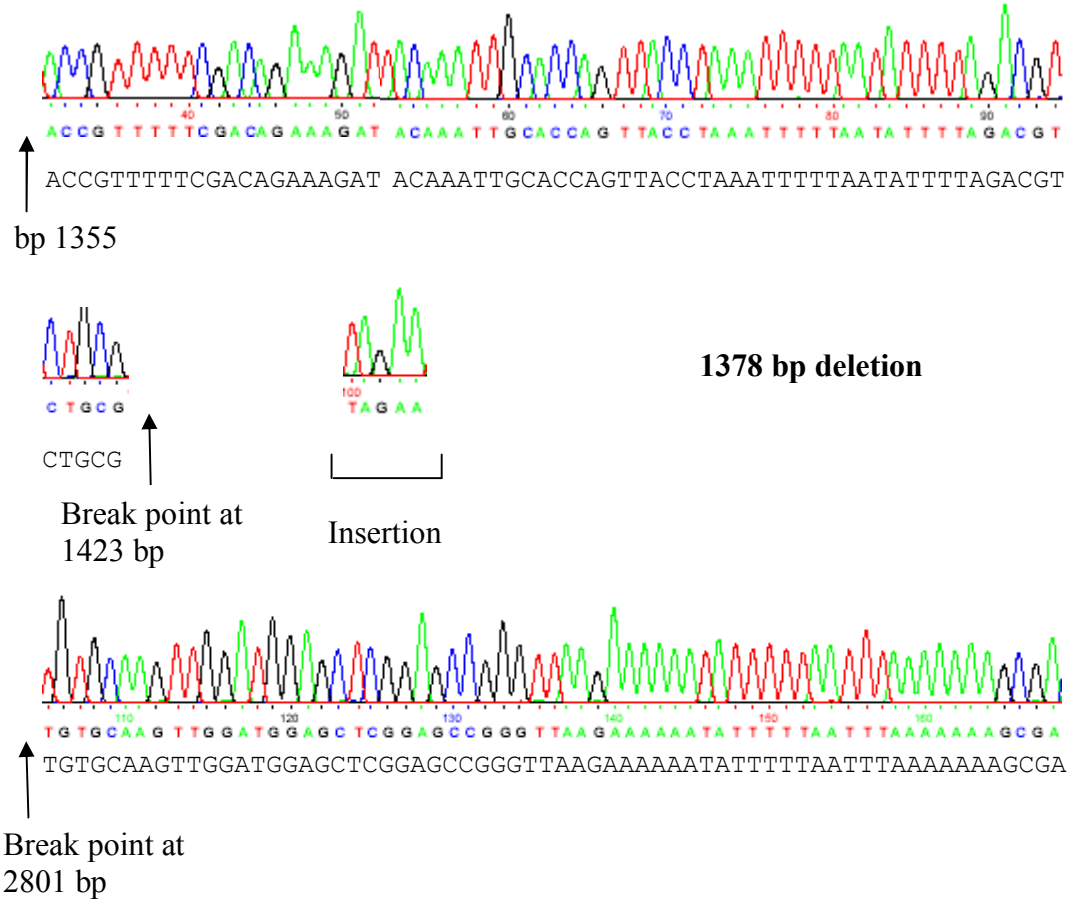


**Figure 3.09. *lat-2*(*tm463*) sequence** Sequencing of a PCR amplified fragment of genomic DNA from homozygous *lat-2*(*tm463*). The deleted portion of *lat-2* is between 1423 bp and 2801 bp of the *lat-2* gene. There is a TAGAA insertion in this region. The deleted region is 1378 bp.

Although *lat-2*(*ok301*) may produce a functional LAT-2, the effect of emodepside on both deletion mutants was investigated as *lat-2*(*ok301*) had previously shown decreased sensitivity (Amliwala 2005). Both *lat-2*(*ok301*) and *lat-2*(*tm463*) were out-crossed five times prior to analysis of emodepside sensitivity. Both alleles were followed by PCR during out-crossing (see methods, page 65). Out-crossed strains *lat-2*(*ok301*) and *lat-2*(*tm463*) were designated strain names XA3726 and XA3727 respectively.

## 3.6 Emodepside sensitivity of *lat-2*(*ok301*) and *lat-2*(*tm463*)

The sensitivity of *lat-2*(*ok301*) and *lat-2*(*tm463*) to emodepside's affect on locomotion was tested using the body bends assay. Animals were exposed to emodepside for 24 hours and then assayed off food. The inhibition of locomotion in *N2*, *lat-2*(*ok301*) and *lat-2*(*tm463*) by emodepside at 1 nM, 10 nM, 100 nM, 1 μM and 10 μM was not significantly different. Figure 3.10 shows a dose response for *N2*, *lat-2*(*ok301*) and *lat-2*(*tm463*). *N2* have an $IC_{50}$ of 163 nM, 95 % confidence limits 57 nM to 460 nM, compared with a *lat-2*(*ok301*) $IC_{50}$ of 320 nM, 95 % confidence limits 100 nM to 849 nM and a *lat-2*(*tm463*) $IC_{50}$ of 244 nM, 95 % confidence limits 74 nM to 804 nM.

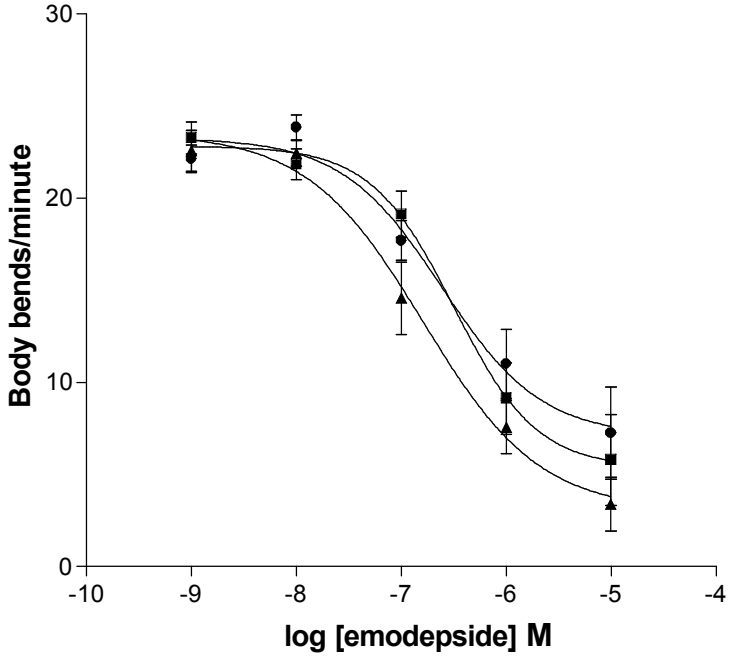


**Figure 3.10. *lat-2* dose response.** Dose response curves for emodepside on *lat-2*(*tm463*) (•), *lat-2*(*ok301*) (■) and *N2* (▲). Each point is the mean ± S.E.Mean of 7 determinants (except at $1x10^{-5}$ M where n=5).

Neither *lat-2*(*ok301*) nor *lat-2*(*tm463*) showed a significant decrease in sensitivity to emodepside. In order to investigate the possibility of redundancy between *lat-1* and *lat-2* a double mutant was constructed.

## 3.7 *lat-2 lat-1* double mutant

Figure 3.11 A) shows the crosses set up in order to generate the *lat-2 lat-1* double mutant. The mIn1 balancer provided useful dumpy and GFP markers for selecting the correct progeny. mIn1 also covers both *lat-1* and *lat-2* and could therefore be used to balance the double mutant once it was obtained. *lat-1* and *lat-2* are both on chromosome II, 5.64 cM apart. The probability of a recombination event resulting in both *lat-1*(*ok1465*) and *lat-2*(*tm463*) alleles being carried on the same chromatid is 1/17.7. The odds of recovering *lat-2 lat-1* on the same chromatid balanced by mIn1 are 1/35.5. The process of generating the *lat-2 lat-1* double mutant is described in the methods in greater detail.

Figure 3.11 B) shows gel electrophoresis of the PCR products resulting for amplification *lat*-1 and *lat-2* from genomic DNA (extracted from single worms) of *gfp* expressing progeny from cross 2. Primer flanking the *lat-1*(*ok1465*) and *lat-2*(*tm463*) were used to amplify DNA fragments of 1395 bp and 1530 bp, respectively, in the way previously described. 1/48 progeny selected from cross 2 carried both *lat-1*(*ok14165*) and *lat-2*(*tm463*).

**A)**

Cross 1) + *lat-1* II / mIn1 II ♀ × *lat-2* + II / *lat-2* + II ♂ ⟶ + *lat-1* II // *lat-2* + II

Cross 2) + *lat-1* II / *lat-2* + II ♀ × + *lat-1* II / mIn1 II ♂ ⟶ *lat-2 lat-1* II / mIn1 II

**B)**

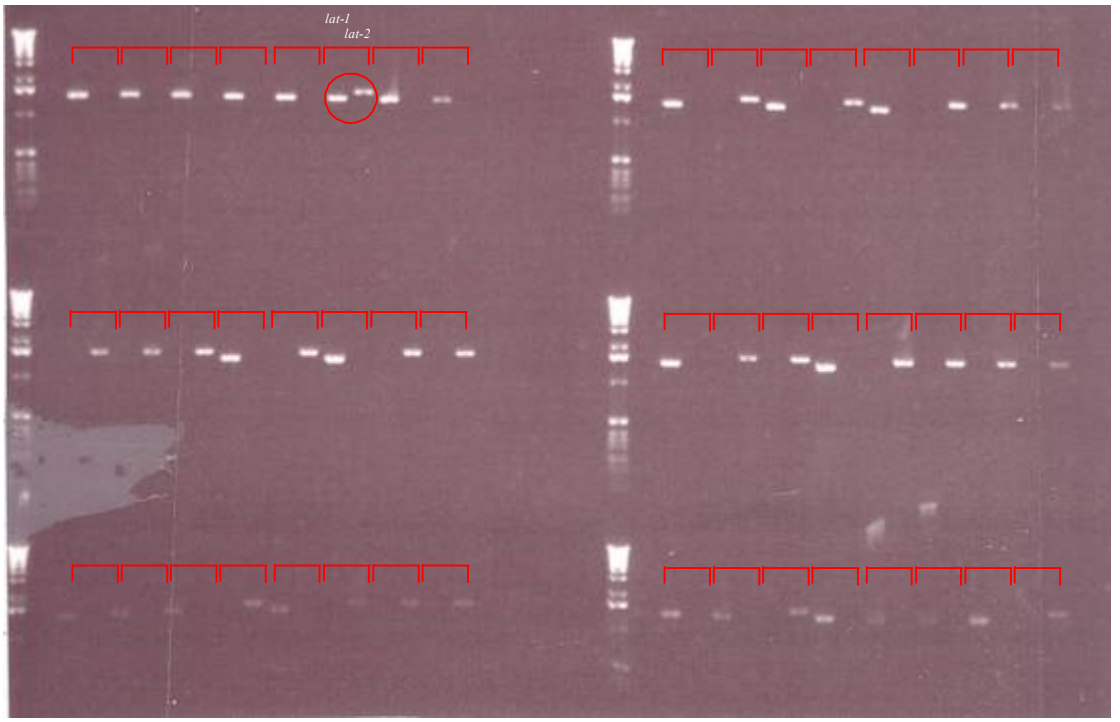


**Figure 3.11. *lat-2 lat-1* double mutant construction. A)** Crosses set up in order to obtain *lat-2 lat-1* II / mIn1 II. **B)** PCR of genomic DNA from 48 single worms resulting from cross 2. Primers flanking the deletions in *lat-1*(*ok1465*) and *lat-2*(*tm463*) were used to generate 1395 and 1530 bp fragments, respectively. Each bracket encloses PCR products generated using *lat-1* and *lat-2* primers from genomic DNA of a single worm. The circled bands are generated from genomic DNA carrying both *lat-1*(*ok1465*) and *lat-2*(*tm463*).

A population was established from the single animal carrying *lat-2 lat-1* II / mIn1 II generated in cross 2. The developmental defect linked to *lat-1*(*ok1465*) was retained. In order to generate a homozygous *lat-2 lat-1* population, approximately 200 L1 not expressing *gfp* were selected. A homozygous population was established from a single animal that reached adult.

Although the chromosomal location of *lat-1* and *lat-2* makes the chance that non *gfp* animals selected from the balanced strain do not carry both *ok1465* and *tm463* extremely unlikely, the genotype of this population was confirmed using PCR. Primers within and either side to the *lat-1*(*ok1465*) and *lat-2*(*tm463*) were used in the way described previously. A DNA fragment

of 1395 bp was generated in *lat-2*(*tm463*) *lat-1*(*ok1465*) and of 732 bp in *N2*, using *lat-1* primers. The lack of the 732 bp band in *lat-2*(*tm463*) *lat-1*(*ok1465*) confirms it is homozygous for *lat-1*. A DNA fragment of 1530 bp was generated in *lat-2*(*tm463*) *lat-1*(*ok1465*) and of 852 bp in *N2*. The lack of the 852 bp band in *lat-2*(*tm463*) *lat-1*(*ok1465*) indicates it is homozygous for *lat-2*(*tm463*). Figure 3.12 shows a gel for the above mentioned PCR reactions.

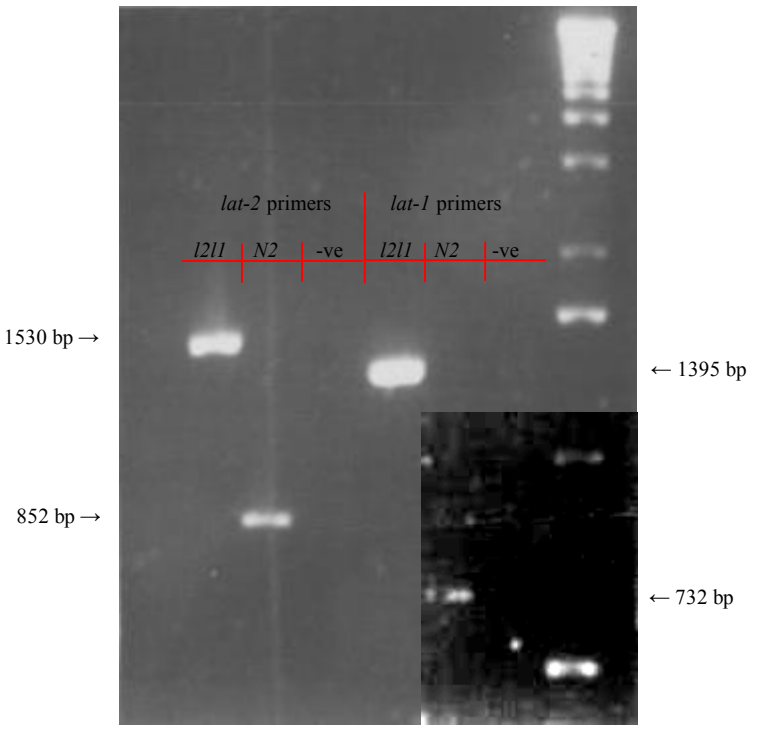


**Figure 3.12. Confirmation of *lat-2 lat-1* genotype.** PCR of genomic DNA from homozygous *lat-2*(*tm463*)*lat-1*(*ok1465*) using primers flanking and within the deletions in *lat-2*(*tm463*) and *lat-1*(*ok1465*). PCR using primers flanking and within the deletion of *lat-2*(*tm463*) produces *lat-2*(*tm463*) and *N2* products of 1530 bp and 852 bp, respectively. PCR using primers flanking and within the deletion of *lat-1*(*ok1465*) produces *lat-1*(*ok1465*) and *N2* products of 1395 bp and 732 bp, respectively. The contrast has been increased in the bottom right hand corner of this gel due to the low intensity of some bands.

## 3.8 Emodepside sensitivity of *lat-2*(*tm463*) *lat-1*(*ok1465*)

The sensitivity of *lat-2*(*tm463*) *lat-1*(*ok1465*) to emodepside's affect on locomotion was tested using the body bends assay. Animals were exposed to emodepside for 24 hours and then assayed off food. The inhibition of locomotion in *N2* and *lat-2*(*tm463*) *lat-1*(*ok1465*) by emodepside at 1 nM, 10 nM, 100 nM, 1 μM and 10 μM was not significantly different. Figure 3.13 shows a dose response for *N2* and *lat-2*(*tm463*) *lat-1*(*ok1465*). *N2* have an $IC_{50}$ of 14 nM, 95 % confidence limits 9 nM to 19, compared with a *lat-2*(*tm463*) *lat-1*(*ok1465*) $IC_{50}$ of 19 nM, 95 % confidence limits 11 nM to 33 nM.

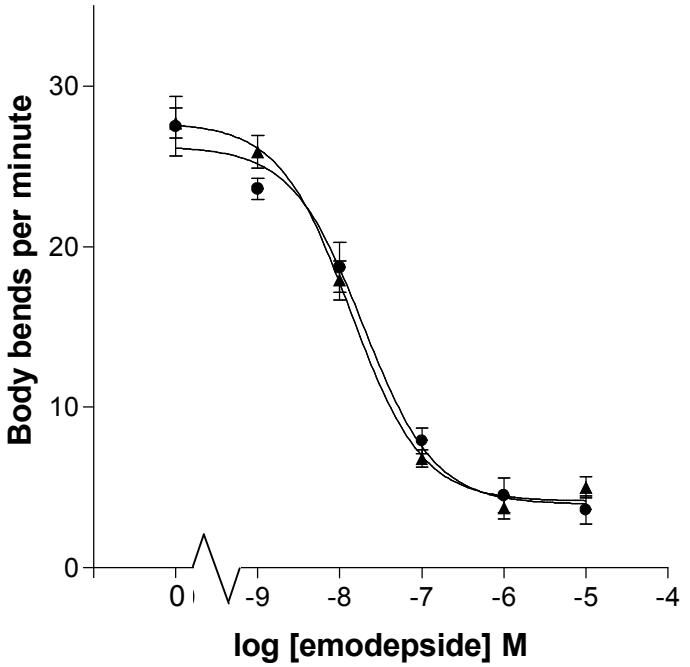


**Figure 3.13. *lat-2* (*tm463*) *lat-1*(*ok1465*) dose response.** Dose response curves for emodepside on *lat-2*(*tm463*)*lat-1*(*ok1465*) (●) and *N2* (▲). For each point n=10 and is the mean ± S.E.Mean.

## 3.9 Discussion

Saeger *et al* (2001) demonstrated binding of emodepside to the amino terminal of the latrophilin receptor of *Haemonchus contortus*, HC110-R. HEK293 cells transfected with HC110-R showed a decreased response to αLTX in the presence of emodepside, indicating there is a competitive interaction with HC110-R. Wilson *et al* (2004) proposed that emodepside acts though LAT-1 in neurons, to cause vesicle release and paralysis of the pharyngeal muscle. Components of a latrophilin vesicle-mediated neurotransmitter release pathway (Davletov *et al* 1998) were knocked down, using either mutant *C. elegans* strains or RNAi, resulting in decreases in sensitivity to emodepside. Amliwala (2005) demonstrated that RNAi targeting of *lat-1* and *lat-2* in *C. elegans* resulted in a deceased sensitivity to emodepside. The *lat-2*(*ok301*) mutant strain VC158 was also shown to have reduced sensitivity to emodepside. These decreases in sensitivity to emodepside have not been observed in the locomotion assays conducted on *lat-1*(*ok1465*) and *lat-2*(*tm463*). There are a variety of possible reasons for these inconsistencies. There may be a non specific effect of the RNAi that resulted in a decrease in emodepside sensitivity. Alternatively, variability in the emodepside thrashing assay may have given misleading results with regard to the effect of *lat-1* and *lat-2* RNAi on emodepside sensitivity.

The studies investigating the effects of RNAi targeting of *lat-1* and *lat-2* on emodepside sensitivity were conducted in liquid. These assays look at the thrashing rate of worms over the course of one hour. They are exposed to 10 μM emodepside during this time period. Attempts to use these assays to investigate the sensitivity of *lat-2*(*tm463*) and *lat-2*(*ok301*) were made. However, these assays produced inconsistent results. *lat-2*(*tm463*) was tested in three independent assays. In one assay *lat-2*(*tm463*) was found to be significantly less sensitive to emodepside than *N2*. In two further assays *lat-2*(*tm463*) was found to be as sensitive as *N2* to emodepside. *lat-2*(*ok301*) was found to be as sensitive as *N2*. These results are shown in the appendix.

The inconsistency seen with the thrashing assay may be explained by the low solubility of emodepside at 10 μM concentrations (see methods) as well as the relatively short exposure period. Attempts to keep the suspension of emodepside well mixed prior to the assay were made. However, there is the potential for animals to be exposed to varying amounts of

emodepside. For this reason an alternative assay was used. A 24 hour exposure period on NGM plates followed by analysis on NGM plates was used (see methods, page 49). Although there was inter assay variability in the NGM plate assays, results were consistent relative to controls when performed in parallel (see methods, page 50).

*lat-2*(*ok301*) was previously shown to have decreased sensitivity to emodepside's effect on locomotion in the body bends assay (Amliwala 2005). However the out-crossed *lat-2*(*ok301*) was not found to have decreased sensitivity to emodepside. Out-crossing results in the loss of many mutations present in strains generated by random mutagenesis. The differences in sensitivity between out-crossed and not out-crossed strains may be explained by the loss of a mutation(s) during out-crossing. The un-out-crossed *lat-2*(*ok301*) was re-tested in the body bends assay and was found to have a slight but significant decrease in emodepside sensitivity (see appendix).

As no reduction in emodepside sensitivity was seen in *lat-1*(*ok1465*) or *lat-2*(*tm463*), it was postulated that a redundancy might exist between the two genes with regard to emodepside's mode of action. In order to investigate this possibility, a double *lat-2 lat-1* mutant was constructed. The *lat-2 lat-1* double mutant showed no decrease in sensitivity to emodepside in the locomotion assay. The data indicate that the latrophilins do not play a role in emodepside's mode of action with regard to its effect on locomotion.

The developmental arrest phenotype of *lat-1*(*ok1465*), which was also observed in the *lat-2*(*tm463*) *lat-1*(*ok1465*) double mutant, could not be rescued by expressing *lat-1*(+) in the *lat-1*(*ok1465*) background. However, any rescue may have been masked due to the presence of the genetic marker $_{p}$*myo-2::*GFP (pPD118.33). It has been observed that pPD118.33 can cause developmental arrest, similar to that observed in *lat-1*(*ok1465*), when expressed with no other vectors present. It may be that very high levels of *gfp* expression in the pharyngeal muscle inhibit pumping, resulting in developmental arrest. The presence of the developmental arrest phenotype in the *lat-2*(*tm463*) *lat-1*(*ok1465*) double mutant illustrates its tight genetic linkage to *lat-1*(*ok1465*).

Analysis of the effects of emodepside on *lat-1*(*ok1465*), *lat-2*(*tm463*) and *lat-2*(*t,463*) *lat-1*(*ok1465*) in the electropharyngeogram assay were performed by Kate Bull. *lat-2*(*tm463*) was not found to have a significantly different sensitivity to emodepside than *N2*. *lat-1*(*ok1465*)

and *lat-1*(*ok1465*) *lat-2*(*tm463*) were both found to be significantly less sensitive to emodepside compared with *N2*, consistent with findings by Willson *et al* (2003). This indicates there is a role for *lat-1* in the response of the pharynx to emodepside.

The lack of any reduction in sensitivity to emodepside's effects on locomotion in the latrophilin mutants demonstrate that other genes must be involved in it's mechanism of action. The following chapters investigate the role of SLO-1 in emodepside's effects on locomotion.

# Chapter 4

# Forward genetic screens for emodepside resistance: characterisation of resistant strains identifies *slo-1* as a major determinant of emodepside's action

## 4.1 Introduction

Forward genetic approaches in *C. elegans* have been successfully used to identify molecular targets for anthelmintic drugs and other compounds. The technique was initially used by Sidney Brenner in 1974. He isolated mutants that were resistant to the effects of the ACh esterase (ACE) inhibitor, lannate, and the anthelmintic, levamisole. Using complementation tests he was able to assign genes to a number of these resistant strains. With the sequencing of the *C. elegans* genome and the advancement of mapping techniques, forward genetic approaches are now widely used. Forward genetics has the great advantage of being an un-biased approach with the potential to generate and select mutant animals that are highly resistant to the effects of emodepside.

This approach was taken in an earlier study (Amliwala 2005). A mutagenesis screen identified seven emodepside resistant strains (Amliwala 2005). Five of these had linkage to chromosome V. Of these five, two (*pd18* and *pd20*) were mapped to a locus at ~16.8 cM. *slo-1*(*js379*), which lies in this region of chromosome V, was found to be highly resistant to emodepside (Amliwala 2005). SLO-1 is a calcium-activated voltage sensitive potassium channel. It is one of two BK channels in *C. elegans*, SLO-1 and SLO-2. The role of a calcium-activated potassium channel was previously suggested as a possible reason for an emodepside-induced calcium-dependent hyperpolarisation of *Ascaris suum* muscle strip (Willson *et al* 2003).

The aim of this chapter is to produce further emodepside resistant strains and identify the mutations conferring resistance. Snip-single nucleotide polymorphism (SNP) mapping, complementation tests and sequencing are used in the identification of mutations that cause high level resistance to emodepside.

Ethlymethanesulphonate is a chemical mutagen that is routinely used for mutagenesis of *C. elegans*. Figure 4.01 shows the process by which emodepside resistant mutants were generated as selected. The majority of mutations produced are point mutations (~87 %), the rest are deletions (~13 %) (Anderson 1995). Generally the mutations produced are recessive (Brenner 1974). Therefore the F3 progeny were screened for emodepside resistance (Figure 4.01).

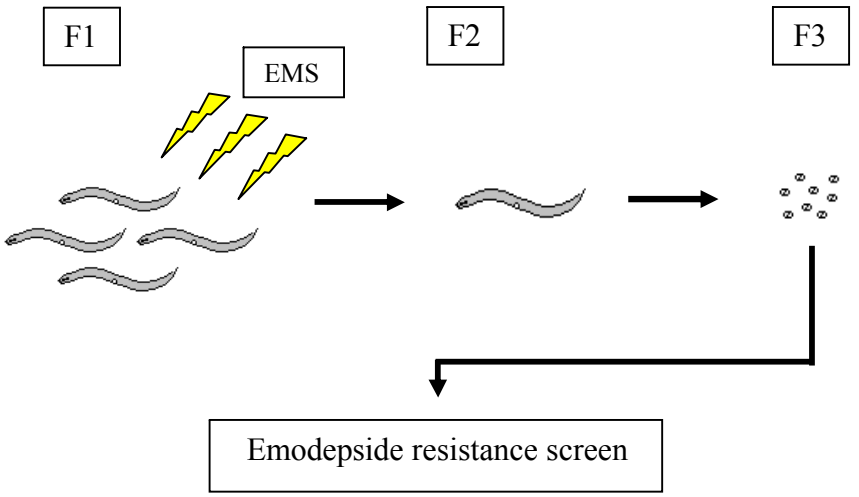


**Figure 4.01. *C. elegans* mutagenesis.** EMS mutagenesis of *C. elegans*. L4 *C. elegans* are mutagenised using the chemical mutagen EMS. F3 progeny are selected and screened for emodepside resistance. Most mutations are recessive and F2 progeny are unlikely to display resistance.

Snip-SNPs (single nucleotide polymorphisms) are SNPs that alter restriction sites. There are a predicted 6222 SNPs in the *C. elegans* strain CB4856, of which 3457 are predicted be snip-SNPs (Wicks *et al* 2001). These snip-SNPS can be used for the mapping of experimentally derived mutations. Snip-SNPs can be easily detected using restriction fragment length polymorphisms (RFLP). These are amplified using PCR and digested with the appropriate restriction enzyme. By analysis of snip-SNPs in the DNA of progeny resulting from crosses between CB4856 and emodepside resistant *N2* animals (see methods), mutations can be mapped.

Complementation tests are a genetic test that can be used to show if mutations are alleles of the same or different genes (Brenner *et al* 1974). These tests allow for mutations in genes to be identified without a lengthy mapping process. The test relies on the mutation being recessive in nature. Different emodepside-resistant strains are crossed with each other and the progeny are tested for emodepside resistance. If the progeny are resistant, the strains are said to be non-complements. This indicates that they are alleles of the same gene.

## 4.2 Mutagenesis screen

A screen of approximately 7500 genomes was conducted. The selection of resistant mutants was based on the ability to develop from eggs to adult on 1 μM emodepside within 96 hours as well as an ability to move in a sinusoidal pattern. Three emodepside-resistant mutants were isolated from this screen. In total, seven emodepside-resistant mutants from this screen and the previous screen (Amliwala 2005) were investigated. The following allele names were assigned to the emodepside resistant mutants: *pd19, pd23, pd21, pd17, pd24, pd47* and *pd46*.

## 4.3 Snip SNP mapping

*pd19* was isolated by Amliwala (2005) but had not been decisively mapped to a chromosome. Initial indications suggested linkage to chromosome I. The appropriate crosses were set up in order to obtain resistant animals carrying CB DNA (see methods). DNA was extracted from the progeny of 51 emodepside resistant carrying CB and *N2* DNA. 14 of these DNA extracts were used for the initial mapping steps to determine chromosomal linkage. Three snip-SNPs on chromosome I were used at – 27.45 cM, -6.15 cM and 8.84 cM. DNA was *N2* homozygous in 36, 21 and 14 percent of samples at -27.45 cM, -6.15 cM and 8.84 cM respectively. These values are close to what would be expected with Mendelian segregation, indicating that *pd19* is not linked to chromosome I. Figure 4.02 A) shows digested PCR products for the three snip-SNPs on chromosome I. Control digests for *N2* and CB are shown for each snip-SNP. Figure 4.02 B) shows the proportion of *N2*, CB and *N2* / CB in each DNA sample at the three snip-SNPs.

**A)**

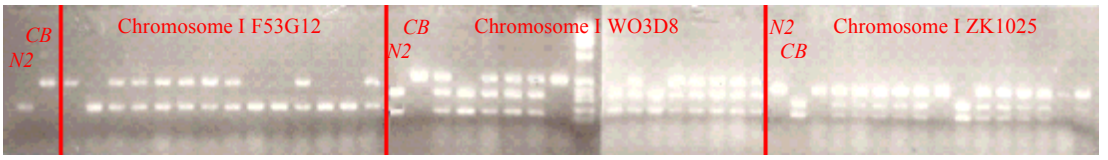


**B)**

| ***pd19*** | Chromosome 1 | Chromosome I | Chromosome I |
|---|---|---|---|
| SNP location Cosmid:nucleotide | F53G12:8422 | WO3D8:34384 | ZK1025:21353 |
| Genetic map position (cM) | -27.45 | -6.15 | 8.84 |
| | CB | H | ***N2*** |
| | ***N2*** | ***N2*** | H |
| | H | H | H |
| | H | H | H |
| | H | H | H |
| | H | CB | H |
| | H | ***N2*** | ***N2*** |
| | H | H | CB |
| | ***N2*** | ***N2*** | H |
| | ***N2*** | H | H |
| | H | H | H |
| | ***N2*** | H | H |
| | ***N2*** | H | ? |
| | H | H | H |
| **% *N2*** | **36** | **21** | **14** |

**Figure 4.02. Chromosome I mapping data for *pd19*. A)** Restriction digest of PCR fragments generated from genomic DNA containing SNPs. SNPs at the following genetic map positions on chromosome I were used; -27.45, -6.15 and 8.84. Dde1 cuts at SNP F53G12:8422 in *N2* to give fragments of 220bp and 220 bp. Dra1 cuts at SNP WO3D8:34384 in *N2* to give fragments of 334 and 175. Nde1 cuts at SNP ZK1025:21353 in CB to give fragments of 251 bp and 149 bp. **B)** Percentage of resistant F2 progeny with *N2* DNA at SNPs F53G12:8422, WO3D8:34384 and ZK1025:21353 (see text for details).

**A)**

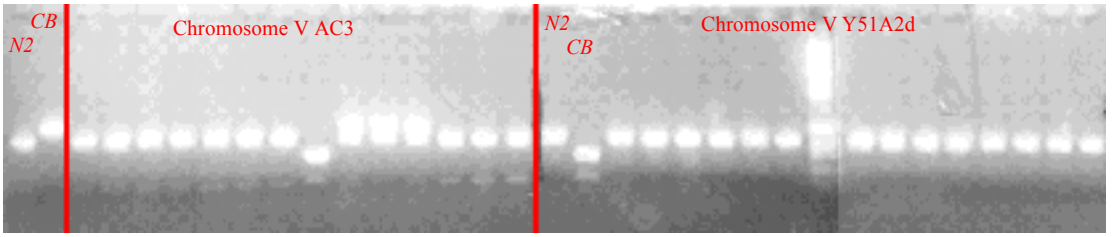


**B)**

| ***pd19*** | Chromosome V | Chromosome V |
|---|---|---|
| SNP location<br>Cosmid nucleotide | AC3:3025 | Y51A2D:92865 |
| Genetic map position (cM) | 2.53 | 16.92 |
| | ***N2*** | ***N2*** |
| | ***N2*** | ***N2*** |
| | ***N2*** | ***N2*** |
| | ***N2*** | ***N2*** |
| | ***N2*** | ***N2*** |
| | ***N2*** | ***N2*** |
| | ***N2*** | ***N2*** |
| | ? | ***N2*** |
| | H | ***N2*** |
| | H | ***N2*** |
| | H | ***N2*** |
| | ***N2*** | ***N2*** |
| | ***N2*** | ***N2*** |
| | ***N2*** | ***N2*** |
| **% *N2*** | 71 | 100 |

**Figure 4.03. Chromosome V data for *pd19*. A)** Restriction digest of PCR fragments generated from genomic DNA containing SNPs. SNPs at the following genetic map positions on chromosome V were used; 2.53 and 16.92. Dra1 cuts at SNP AC3:3025 in *N2* to give fragments of 105 and 387. Dra1 cuts at SNP Y51A2d in CB to give fragments of 273 and 121. **B)** Percentage of resistant F2 progeny with *N2* DNA at SNPs AC3:3025 and Y51A2d:92865 (see text for details).

Possible linkage of *pd19* to chromosome V was tested using snip-SNPs at 2.53 cM and 16.92 cM. DNA was *N2* homozygous in 71 and 100 percent of samples at 2.53 cM and 16.92 cM respectively. These values do not reflect Mendelian segregation, indicating that *pd19* is linked to chromosome V. Figure 4.03 A) shows digested PCR products for the two snip-SNPs on chromosome V. Control digests for *N2* and CB are shown for each snip-SNP. Figure 4.03 B) shows the proportion of *N2*, CB and *N2* / CB in each DNA sample at the two snip-SNPs.

Mapping revealed linkage to chromosome V in all alleles tested. This indicated that all were alleles of the same gene. This was confirmed through the use of complementation tests.

## 4.4 Complementation tests

Complementation tests allow genes containing mutations that result in a phenotype to be rapidly identified. The test relies on the mutations being recessive. The strain NM1968, which has the *js379* mutation in *slo-1*, was used in complementation tests with emodepside resistant strains. The *dpy-20*(*e1282*) mutation was introduced into the background of the emodepside resistant mutants for use as a marker when generating cross progeny for complementation tests. Initially the sensitivity of *slo-1*(*js379*), *slo-1*(*js379*) / *slo-1*(+) and *N2* to 1 μM emodepside was tested using the body bends assay. The locomotion of emodepside treated animals is shown as a percentage of the locomotion on vehicle containing plates. Figure 4.04 shows the percentage control response of worms with these genotypes. The locomotion of *slo-1*(*js379*) / *slo-1*(+) and *N2* is significantly inhibited compared with *slo-1*(*js379*), with $P<0.001$. *slo-1*(*js379*) / *slo-1*(+) is as sensitive to 1 μM emodepside as *N2*. This demonstrates that a single copy of *slo-1*(+) is sufficient to confer emodepside sensitivity. The recessive nature of *slo-1*(*js379*) makes it suitable for use in complementation tests.

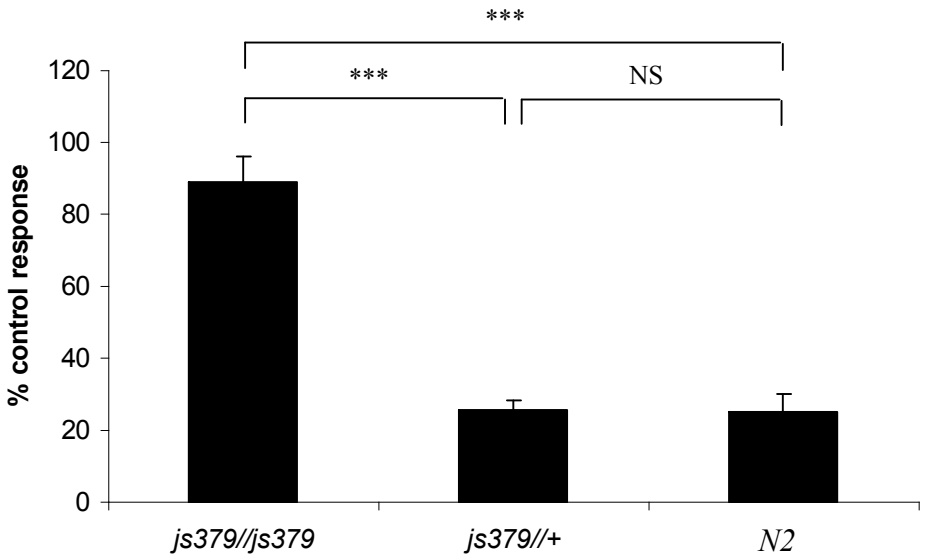


**Figure 4.04. *slo-1*(*js379*) is recessive.** % control response (body bends) of *js379*/*js379, js379*/+ and *N2* after 24 hour exposure to 1 μM emodepside. "% control response" is the number of body bends per minute after exposure to emodepside as a percentage of the number of body bends on vehicle for each strain. For each bar n≥7 and is the mean ± S.E.Mean. *** indicates $P<0.001$.

Emodepside-resistant strains were crossed with either *slo-1*(*js379*) or alleles that were shown to be non-complements of *slo-1*(*js379*). Cross progeny that carry non-complementing emodepside resistant alleles would be expected to be resistant to emodepside. Emodepside resistant strains were crossed with *N2* to check that mutations causing emodepside resistance were recessive, as a dominant mutation may falsely indicate non-complementation.

**Complementation of *pd19***

Figure 4.05 shows the percentage control response of *pd19 / pd19*, *pd19 / +* and *pd19 / js379* on 1 μM emodepside. The locomotion of *pd19 / +* is significantly more inhibited by 1 μM emodepside than *pd19 / pd19* ($P<0.001$). This demonstrates that *pd19* is recessive. The locomotion of *pd19 / +* is also significantly more inhibited than *pd19 / js379* ($P<0.001$). This demonstrates that *pd19* and *js379* are non-complements, indicating that they are alleles of the same gene.

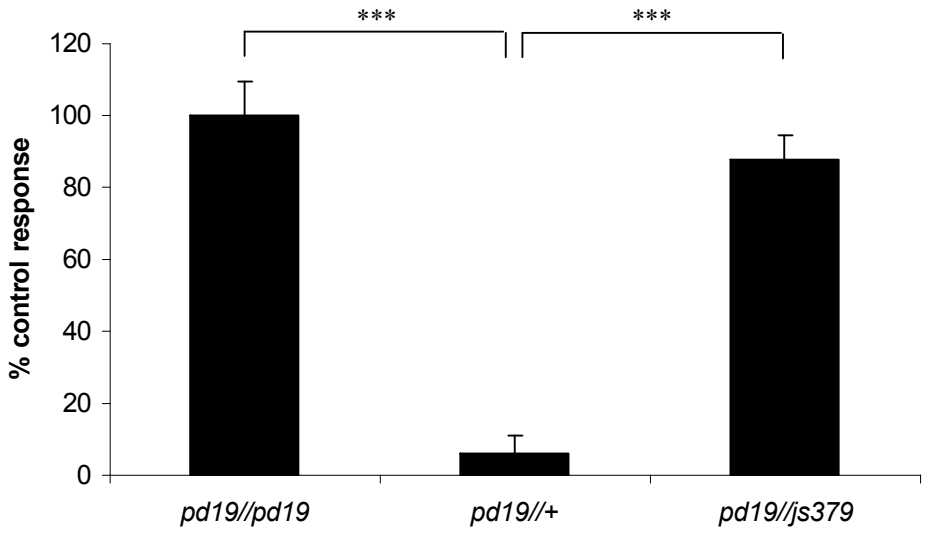


**Figure 4.05. *pd19* is a non-complement of *slo-1*(*js379*).** % control response (body bends) of *pd19*//*pd19, pd19*//+ and *pd19*//*js379* after 24 hour exposure to 1 μM emodepside. "% control response" is the number of body bends per minute after exposure to emodepside as a percentage of the number of body bends on vehicle for each strain For each bar n≥5 and is the mean ± S.E.Mean. *** indicates $P<0.001$.

**Complementation of *pd23***

Figure 4.06 shows the percentage control response of *pd23 / pd23*, *pd23 /* + and *pd23 / js379* on 1 μM emodepside. The locomotion of *pd23 /* + is significantly more inhibited by 1 μM emodepside than *pd23 / pd23* ($P$<0.001). This demonstrates that *pd23* is recessive. The locomotion of *pd23 /* + is also significantly more inhibited than *pd23 / js379* ($P$<0.001). This demonstrates that *pd23* and *js379* are non-complements, indicating that they are alleles of the same gene.

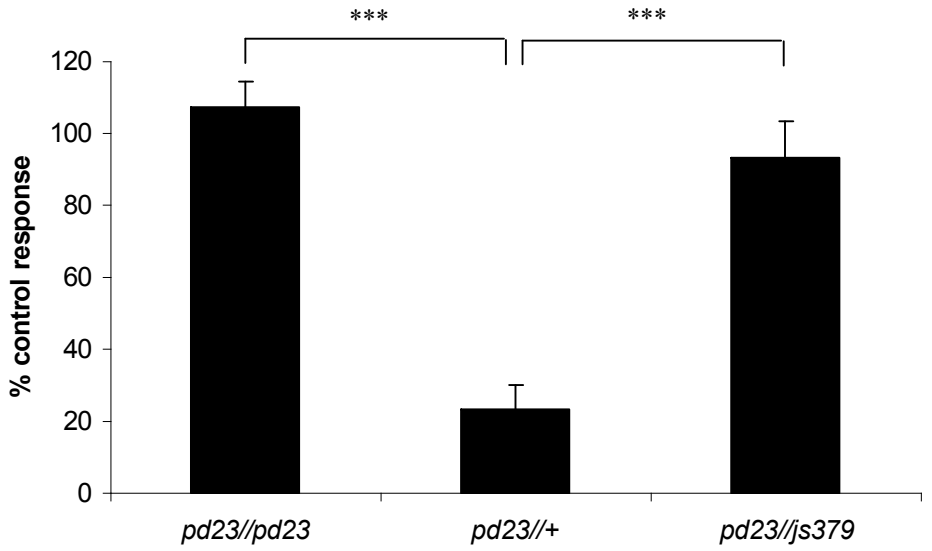


**Figure 4.06. *pd23* is a non-complement of *slo-1*(*js379*).** % control response (body bends) of *pd23*//*pd23, pd23*//+ and *pd23*//*js379* after 24 hour exposure to 1 μM emodepside. "% control response" is the number of body bends per minute after exposure to emodepside as a percentage of the number of body bends on vehicle for each strain For each bar n≥7 and is the mean ± S.E.Mean. *** indicates $P$<0.001.

**Complementation of *pd21***

Figure 4.07 shows the percentage control response of *pd21 / pd21*, *pd21 / +* and *pd21 / js379* on 1 μM emodepside. The locomotion of *pd21 / +* is significantly more inhibited by 1 μM emodepside than *pd21 / pd21* ($P<0.001$). This demonstrates that *pd21* is recessive. The locomotion of *pd21 / +* is also significantly more inhibited than *pd21 / js379* ($P<0.001$). This demonstrates that *pd21* and *js379* are non-complements, indicating that they are alleles of the same gene.

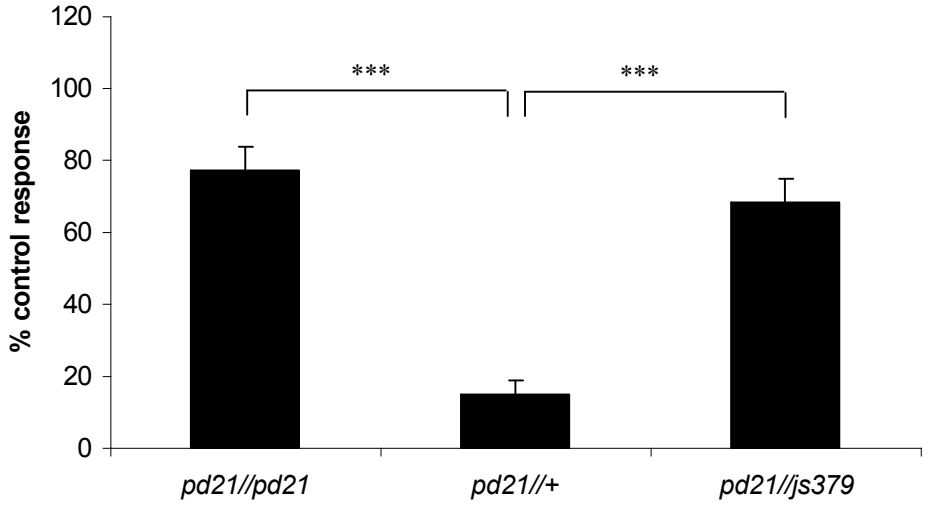


**Figure 4.07. *pd21* is a non-complement of *slo-1*(*js379*).** % control response (body bends) of *pd21*//*pd21, pd21*//+ and *pd21*//*js379* after 24 hour exposure to 1 μM emodepside. "% control response" is the number of body bends per minute after exposure to emodepside as a percentage of the number of body bends on vehicle for each strain For each bar n≥5 and is the mean ± S.E.Mean. *** indicates $P<0.001$.

**Complementation of *pd17***

Figure 4.08 shows the percentage control response of *pd17 / pd17*, *pd17 / +* and *pd17 / js379* on 1 μM emodepside. The locomotion of *pd17 / +* is significantly more inhibited by 1 μM emodepside than *pd17 / pd17* ($P<0.01$). This demonstrates that *pd17* is recessive. The locomotion of *pd17 / +* is also significantly more inhibited than *pd17 / js379* ($P<0.001$). This demonstrates that *pd17* and *js379* are non-complements, indicating that they are alleles of the same gene.

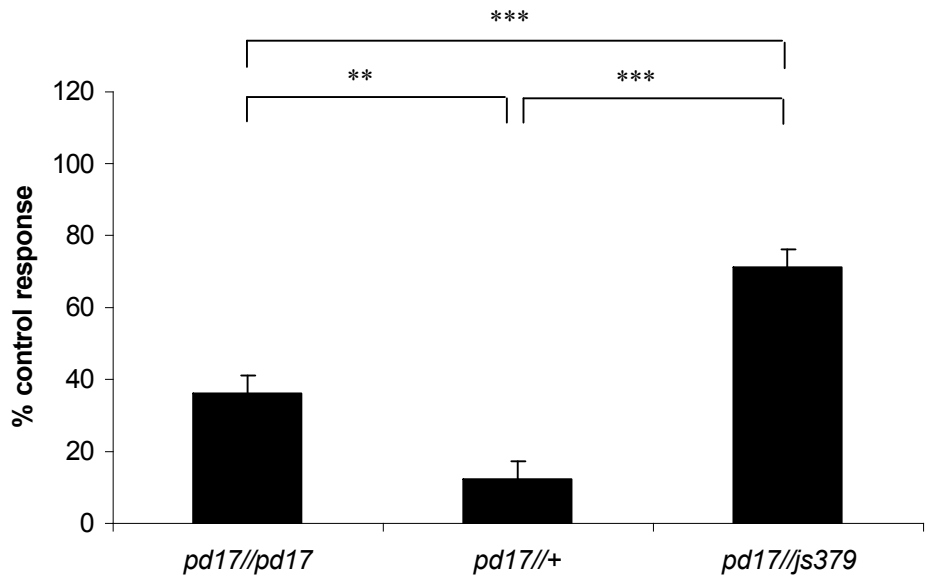


**Figure 4.08. *pd17* is a non-complement of *slo-1*(*js379*).** % control response (body bends) of *pd17*//*pd17, pd17*//+, and *pd17*//*js379* after 24 hour exposure to 1 μM emodepside. "% control response" is the number of body bends per minute after exposure to emodepside as a percentage of the number of body bends on vehicle for each strain For each bar n≥7 and is the mean ± S.E.Mean. ** indicates $P<0.01$ and *** indicates $P<0.001$.

**Complementation of *pd24***

Figure 4.09 shows the percentage control response of *pd24 / pd24*, *pd24 / +* and *pd24 / pd23* on 1 μM emodepside. The locomotion of *pd24 / +* is significantly more inhibited by 1 μM emodepside than *pd24 / pd24* ($P<0.001$). This demonstrates that *pd24* is recessive. The locomotion of *pd24 / +* is also significantly more inhibited than *pd24 / pd23* ($P<0.001$). This demonstrates that *pd24* and *pd23* are non-complements, indicating that they are alleles of the same gene.

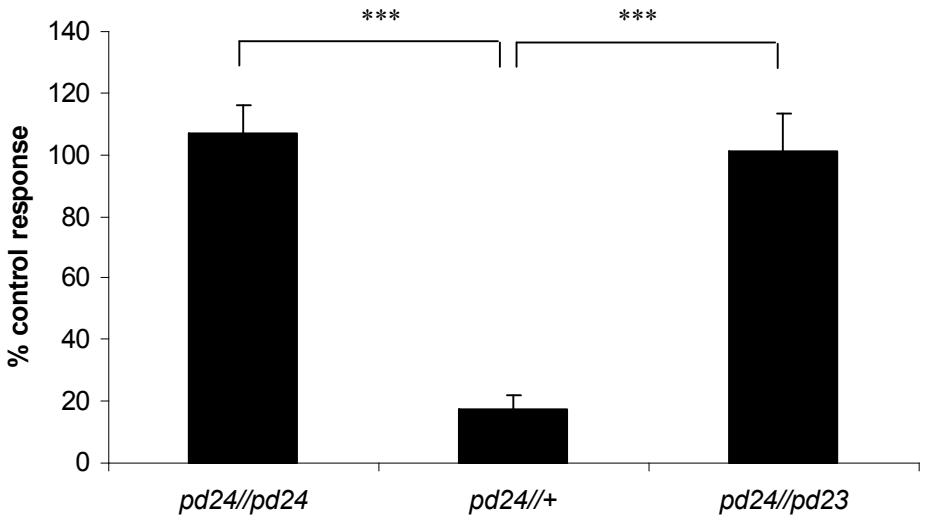


**Figure 4.09. *pd24* is a non-complement of *slo-1*(*pd23*).** % control response (body bends) of *pd24*//*pd24, pd24*//+ and *pd24*//*pd23* after 24 hour exposure to 1 μM emodepside. "% control response" is the number of body bends per minute after exposure to emodepside as a percentage of the number of body bends on vehicle for each strain For each bar n≥6 and is the mean ± S.E.Mean. *** indicates $P<0.001$.

**Complementation of *pd47***

Figure 4.10 shows the percentage control response of *pd47 / pd47*, *pd47 / +* and *pd47 / pd23* on 1 μM emodepside. The locomotion of *pd47 / +* is significantly more inhibited by 1 μM emodepside than *pd47 / pd47* ($P<0.001$). This demonstrates that *pd47* is recessive. The locomotion of *pd47 / +* is also significantly more inhibited than *pd47 / pd23* ($P<0.001$). This demonstrates that *pd47* and *pd23* are non-complements, indicating that they are alleles of the same gene.

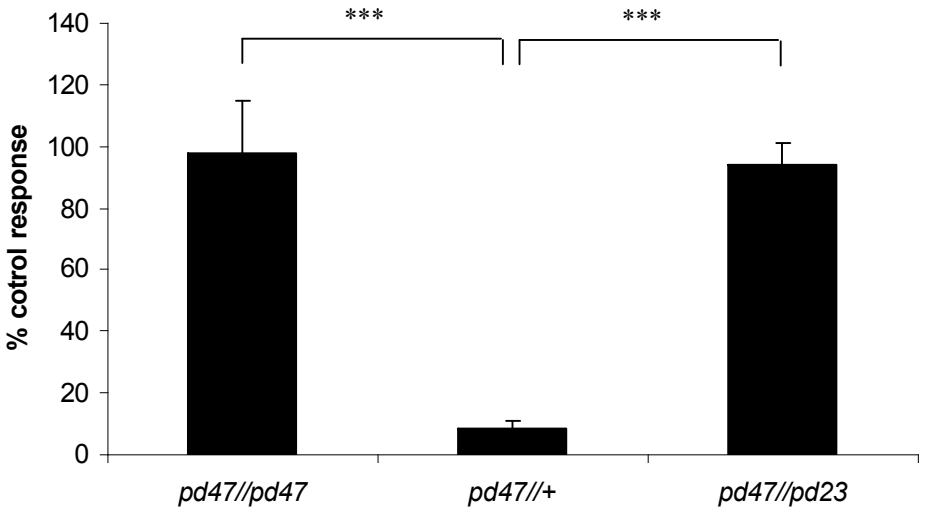


**Figure 4.10. *pd47* is a non-complement of *slo-1*(*pd23*).** % control response (body bends) of *pd47*//*pd47, pd47*//+ and *pd47*//*pd23* after 24 hour exposure to 1 μM emodepside. "% control response" is the number of body bends per minute after exposure to emodepside as a percentage of the number of body bends on vehicle for each strain For each bar n≥5 and is the mean ± S.E.Mean. *** indicates $P<0.001$.

**Complementation of *pd46***

Figure 4.11 shows the percentage control response of *pd46 / pd46*, *pd46 /* + and *pd46 / pd23* on 1 μM emodepside. The rate of locomotion of *pd46 /* + is not inhibited more than the locomotion of *pd46 / pd46*. This however reflects the low level of resistance of *pd46* / *pd46* rather than indicating that it has a dominant phenotype. *pd46* was defined as resistant based on the parameters of the screen, not on its rate of locomotion. A sinusoidal shape of locomotion was observed in *pd46 / pd46* (6 out 6 of animals) on 1 μM emodepside. This sinusoidal shape of locomotion was not observed in *pd46 /* + (6 out 6 of animals), indicating that *pd46* is recessive. The rate of locomotion of *pd46 /* + on 1 μM emodepside is not significantly different from that of *pd46 / pd23*. However, *pd46 / pd23* (6 out of 6 animals) displayed a sinusoidal shape of locomotion whereas *pd46 /* + did not (6 out of 6 animals). This demonstrates that *pd46* and *pd23* are non-complements, indicating that they are alleles of the same gene.

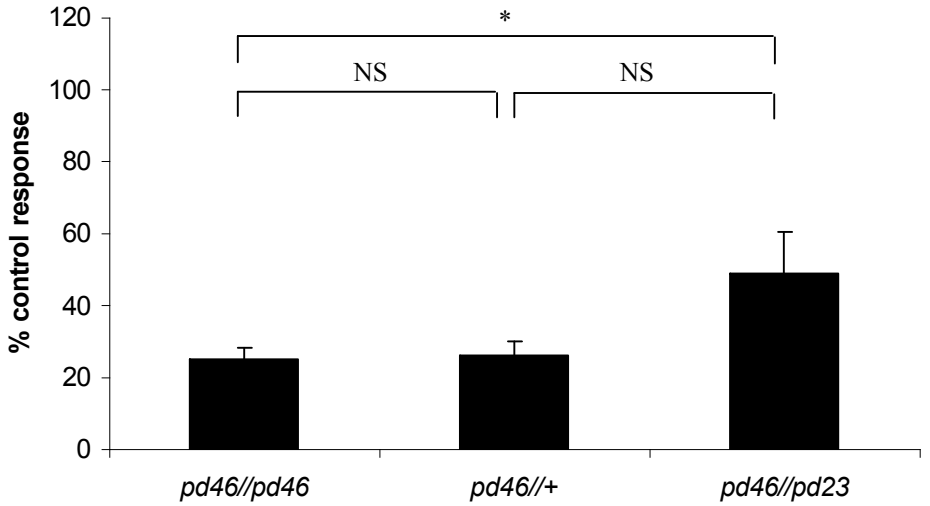


**Figure 4.11. *pd46* is a non-complement of *slo-1*(*pd23*).** % control response (body bends) of *pd46*//*pd46, pd46*//+ and *pd46*//*pd23* after 24 hour exposure to 1 μM emodepside. "% control response" is the number of body bends per minute after exposure to emodepside as a percentage of the number of body bends on vehicle for each strain For each bar n≥6 and is the mean ± S.E.Mean. * indicates $P<0.05$.

## 4.5 Sequencing of *slo-1* cDNA from emodepside resistant animals

The data from the complementation tests strongly indicates that each strain carries an allele of *slo-1*. In order to identify mutations conferring resistance to emodepside, the cDNA of *slo-1* was sequenced in the resistant strains. RNA was extracted from each emodepside-resistant strain. *slo-1* cDNA was generated from total RNA using the SuperScript III One-Step RT-PCR system and gene specific primers. Nested primers, located immediately upstream of the start codon and downstream of the stop codon, were used for generating *slo-1* cDNA from *pd17*, *pd19*, *pd21* and *pd24*. An alternate 3' primer with better specificity, 170 bp downstream of the stop codon was used for generating *slo-1* cDNA from *pd24*, *pd46* and *pd47*. Figure 4.12 shows the products produced in RT-PCR reactions using the primers described. DNA fragments that appear to be of the predicted *N2* sizes (~3400) are generated in *pd17, pd19, pd21, pd23, pd24, pd46* and *pd47*. As well as the predicted band size, fainter bands of ~1600bp were generated in *pd17*, *pd19*, *pd21* and *pd23* and of ~1800 bp in *pd24* (see appendix, page 206).

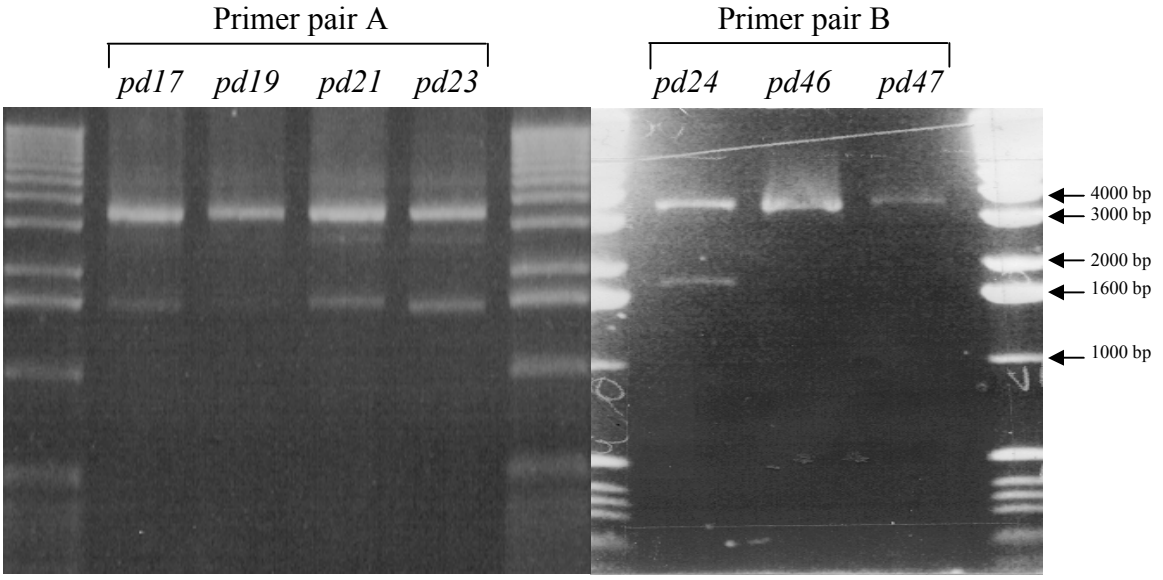


**Figure 4.12. Gel electrophoresis of *slo-1* cDNA.** RT-PCR products for *slo-1* from resistant strains *pd17*, *pd19*, *pd21*, *pd23*, *pd24*, *pd46* and *pd47*. Nested primer upstream of the start and downstream of the stop codon were used to generate *slo-1* cDNA. *N2* fragments are predicted to be of either 3423 (primer pair A) or 3593 (primer pair B) for splice variant a.

cDNA was amplified in two successive rounds of PCR for each allele. *slo-1* cDNA consistently failed to amplify for *pd47* in the second round PCR. This may indicate the presence of a mutation in a region complementary to the primers used.

The cDNA was sequenced. Sequencing primers spaced at 370 bp intervals across the cDNA were used. The primers used were complementary to *slo-1* cDNA sequences common to all identified splice variants. Three splice variants of *slo-1* have been identified in *C. elegans* (Wei *et al* 1996, Zhao *et al* 2001). Figure 4.13 shows a gene model for *slo-1* (www.wormbase.org). Splice variant a has 20 exons. Splice variant b lacks exon 13 compared with splice variant a. Splice variant c has an alternate exon 9, an extra exon (exon 11a) between exons 11 and 12 and lacks exon 13 compared with splice variant a.

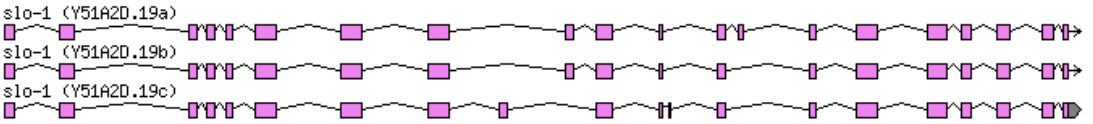


**Figure 4.13. *slo-1* gene model.** Adapted from www.wormbase.org. Three splice variants of *slo-1* have been identified (Wei *et al* 1996, Zhao *et al* 2001). Comparing with splice variant a: splice variant b lacks exon 13; splice variant c has an alternate exon 9, an extra exon (exon 11a) between exons 11 and 12 and lacks exon 13.

In some sequencing reactions for *slo-1* the presence of a mixture of sequences was observed. This was due to the presence of alternate splice variants in the cDNA. By reading off the overlapping sequence, both sequences for splice variants a/b and splice variant c could be identified. When the sequence produced from sequencing of cDNA was not of sufficient quality, individual exons or groups of exons were PCR amplified from genomic DNA and sequenced. Table 4.01 shows the sequence coverage of *slo-1* for each allele.

| Allele | *slo-1* cDNAa | *slo-1* cDNAb | *slo-1* cDNAc |
|---|---|---|---|
| ***pd17*** | **93.6 %** | **95.4 %** | **89.6 %** |
| ***pd19*** | **93.8 %** | **96.0 %** | **90.6 %** |
| ***pd21*** | **90.5 %** | **92.3 %** | **91.0 %** |
| ***pd23*** | **78.4 %** | **80.0 %** | **79.9 %** |
| ***pd24*** | **96.4 %** | **98.0 %** | **94.7 %** |
| ***pd46*** | **98.8 %** | **98.8 %** | **98.8 %** |

**Table 4.01. *slo-1* sequencing coverage.** Percentage of sequence covered for alleles *pd17, pd19, pd21, pd23, pd24* and *pd46*. Percentage of sequence covered for each splice variant is shown.

Mutations were identified in *slo-1* in four of the alleles. The sequencing for the mutated regions for each allele are shown in the following section. Mutations identified in the cDNA were confirmed through sequencing of genomic DNA for each allele. *N2* sequence was obtained from www.wormbase.org for alignment with *slo-1* from the emodepside resistant alleles.

Figure 4.14 shows sequencing for two regions of *slo-1*(*pd17*) cDNA in which mutations were identified. C1572T and C2583T result in semi-conservative changes in the amino acid sequence. Both nucleotides changes result in alanine to valine substitutions in the amino acid sequence at aa 524 and 870.

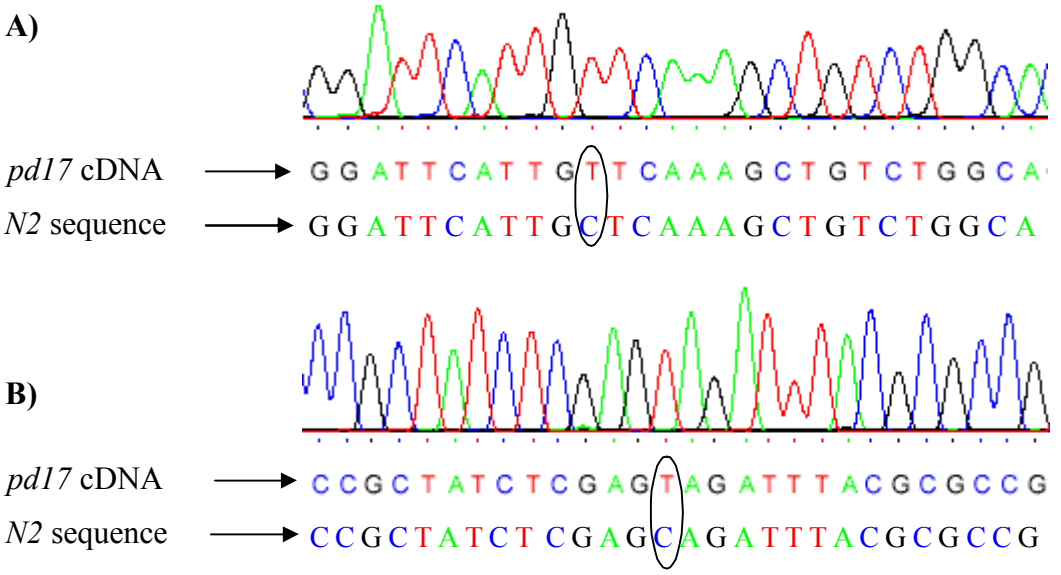


**Figure 4.14. Sequencing of *pd17 slo-1* cDNA.** Mutations **A)** C1572T and **B)** C2583T were identified in *pd17 slo*-1 cDNA. These were confirmed through sequencing of the regions in *pd17* genomic DNA.

Figure 4.15 shows sequencing for a region of *slo-1*(*pd19*) cDNA in which a mutation was identified. *pd19* carries the mutation G1294A. This result in a change in the amino acid sequence from glycine to arginine at 432.

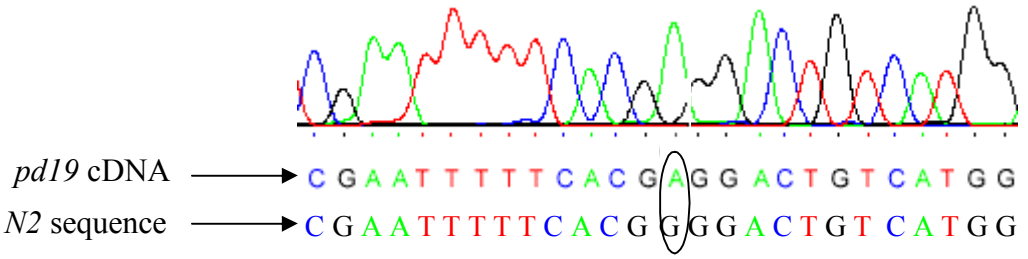


**Figure 4.15. Sequencing of *pd19 slo-1* cDNA.** Mutation G1294A was identified in *pd19 slo*-1 cDNA. This was confirmed through sequencing of the region in *pd19* genomic DNA.

Figure 4.16 shows sequencing for a region of *slo-1*(*pd23*) cDNA in which a mutation was identified. *pd23* carries the mutation G1511A. This results in a change in the amino acid sequence from tryptophan to a stop at 504.

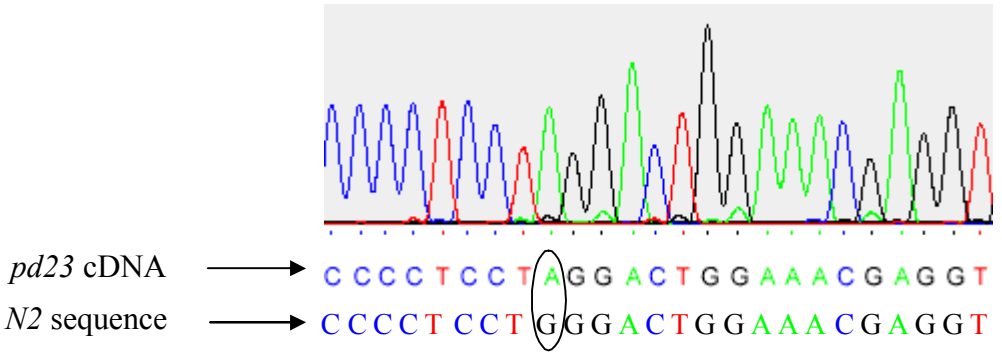


**Figure 4.16. Sequencing of *pd23 slo-1* cDNA.** Mutation G1511A was identified in *pd23 slo-1* cDNA. This was confirmed through sequencing of the region in *pd23* genomic DNA.

Figure 4.17 shows sequencing for a region of *slo-1*(*pd24*) cDNA in which a mutation was identified. *pd24* carries the mutation C1861T. This results in a change in the amino acid sequence from glutamine to a stop at 620.

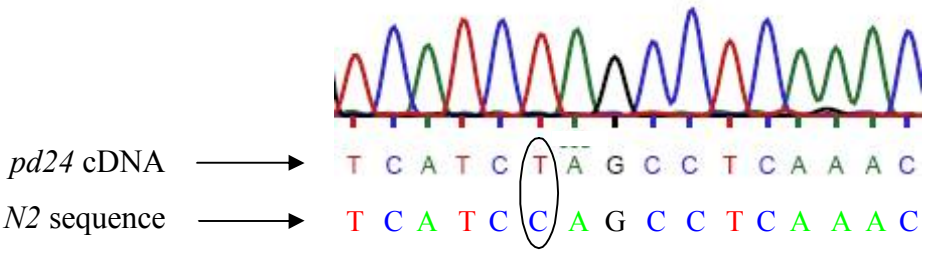


**Figure 4.17. Sequencing of *pd24 slo-1* cDNA.** Mutation C1861T was identified in *pd24 slo-1* cDNA. This was confirmed through sequencing of the region in *pd24* genomic DNA.

Table 4.02 summarises the mapping, complementation and sequencing data for emodepside-resistant alleles. The region in which these mutations lie are also noted. All alleles on which snip-SNP mapping was conducted were found to map to chromosome V, on which *slo-1* lies. All alleles were found to be non-complements of *slo-1* alleles *js379* or *pd23*. All mutations identified were found to lie in RCK1 and RCK2 (regulator of potassium conductance) C-terminal domains. *js379* lies in between transmembrane domains 4 and 5.

| Allele | Chromosomal linkage | *slo-1* non-complement | *slo-1* aa change | Region of mutation |
|---|---|---|---|---|
| *pd17* | V | ✓ | **A524V A870V** | **RCK1 αF RCK2** |
| *pd19* | **V** | ✓ | **G432R** | **RCK1 βC** |
| *pd21* | V | ✓ | **-** | **-** |
| *pd23* | V | ✓ | **W504Stop** | **RCK1 αE** |
| ***pd24*** | - | ✓ | **Q620Stop** | **RCK1 βI to βJ** |
| ***pd47*** | - | ✓ | - | - |
| ***pd46*** | - | ✓ | **-** | - |

**Table 4.02. Summary of emodepside resistant allele particulars.** Chromosomal linkage, complementation data, *slo-1* mutation and region of alleles isolated in screens for emodepside resistance. Particulars written in grey had previously been identified (Amliwala 2005).

Figure 4.18 shows the amino acid sequence and a model of SLO-1. The three alternate splice variants are highlighted. Mutations in *pd17, pd19, pd23, pd24* and *js379* are marked. Mutations in these alleles are present in all three splice variants. The transmembrane domains, RCK domains, voltage sensor, pore domain (P loop) and $Ca^{2+}$ bowl are marked.

**A)**

MGEIYSPSQSKGFNQPYGYPMNCNLSRVFMEMTEEDRKCLEERKYWCFLLSSITTFCASMILVVIWRVVTHLCCQRREKE

FVEPIPAPEAVQINMNGSKHAPSETDPFLKQQEEKHLGWMTEAKDWAGELISGQSLTGRFLVLLVFILSIGSLIIYFYDA

SFQNFQVETCIPWQDSPSQQIDLGFNIFFLVYFFIRFIAASDKVWFLLEMYSWIDFFTIPPSFVAIYLQRNWLGFRFLRA

LRLMTVPDIL**Q/Stop**YLNILKTSSSIRLTQLVTIFVAVCLTGAGLVHLLENSGDFFKGFINPHRITYADSVYFVLVTMS

***js379***

TVGYGDIYCTTLCGRLFMIFFILFGLAMFASYVPEIADLIGNRQKYGGEYKGEHGKKHIVVCGHITYDSVSHFLQDFLHE

DRDDVDVEVVFLHRVVPDLELEGLFKRHFTKVEFFT**G/R**TVMDSLDLSRVKIGDADACLVLANKYSTNPDAEDAANIMRV

***pd19***

ISIKNYSSDIRVIVQLMQYHNKAYLLNIPS**W/Stop**DWKRGDDVICLAELKLGFI**A/V**QSCLAPGFSTMMANLFAMRSFK

***pd23*** ***pd17***

TSQTTPDWLNLYLCGAGMEMYTDTLSHSFVGMTFPEAVDLLFNRLGLLLLAIELKDEENKECNIAINPGPHIVI**Q/Stop**

PHTPLWLNDYLRGAGMEMYTESLSPSFANMSFPEAAN ***pd24***

Splice c alternate exon 9

PQTQGFFIAQSADEVKRAFFWCKQCHDDIKDVSLIKKCKCKNLALFRRNTKHSTAAR**********ARATDVLQQF

DYSDFDALFYQND

Splice c exon 11a

QPQAPAGPMGHLGQQVQLRMINQQ**********PSSGGRRNSMSIPPDGRGVDFSKDFEQQFQDMK

SSTSDTHLNTKSLRFAYEIKKLM

Splice a exon 13

YDSTGMFHWCPSRNLEDCVLERHQAAMTVLNGHVVVCLFADQDSPLIGLRNFIMPLRSSNFHYHELKHVVIVGDLEYLRK

EWKTLYNLPKISILNGSPLSR**A/V**DLRAVNINLCDMCVIISARVPNTEDTTLADKEAILASLNIKAMQFDDTLGFFPMRH

***pd17***

QTGDRSPLGSPISMQKKGAKFGTNVPMITELVNDSNVQFLDQDDDDDPDTELYLTQPFACGTAFAISVLDSLMSTTYFND

SALTLIRTLVTGGATPELELILAEGAGLRGGYSTPETLSNRDRCRIAQISLQDNPYDGVVHNTTYGAMFTIALRRYGQLC

IGLYRLHDQDNPDSMKRYVITNPPAELRIKNTDYVYVLEQFDPGLEYEPGKRHF*

Transmembrane domains

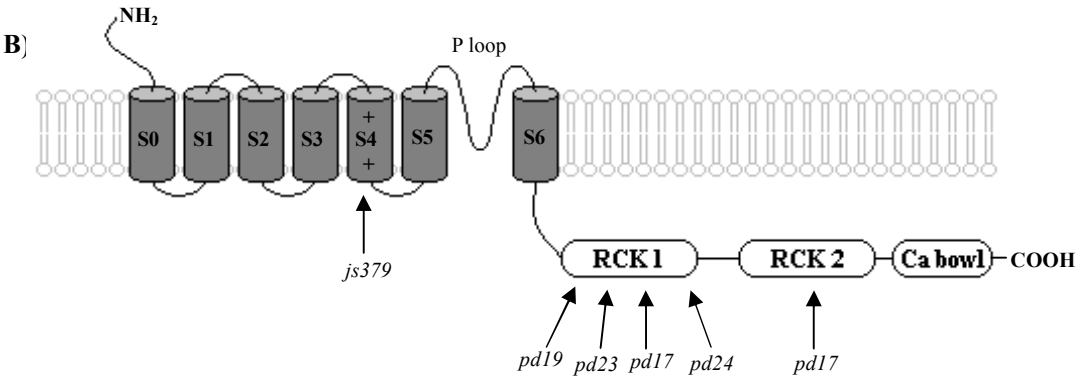


**Figure 4.18. SLO-1 amino acid sequence and structure. A**) SLO-1 amino acid sequence. There are three splice variants and the sequence of these are indicated. The location of the *slo-1* mutations for: *js379*, *pd19*, *pd23*, *pd17*, *pd24* are indicated. The RCK domains are underlined, the voltage sensor is marked with a broken line, the pore domain (P loop) is highlighted in black and the $Ca^{2+}$ bowl is highlighted in grey. **B)** cartoon of the SLO-1 protein showing the location of the mutations. The voltage sensor (S4), the P loop and $Ca^{2+}$ sensor ($Ca^{2+}$ bowl) are also marked. (After Wang *et al* 2001, Salkoff *et al* 2006 / based on sequence similarity).

## 4.6 Discussion

This chapter presents evidence that all highly resistant emodepside strains are alleles of the same gene, *slo-1*. The mapping of *pd19* shows that it has linkage to chromosome V. All mapped emodepside resistant alleles (Amliwala 2005) showed linkage to chromosome V. Two alleles, *pd18* and *pd20*, were shown to map to a region close to *slo-1* (~16.8 cM) (Amliwala 2005). The mapping data suggest that all the emodepside resistant alleles are likely to be alleles of the same gene. All alleles were tested in complementation tests. The emodepside resistant strains *pd19, pd23, pd21, pd17, pd24, pd47* and *pd46* are all non-complements of *slo-1*(*js379*) or *pd23* (itself a non-complement of *js379*). The fact that all alleles fall into the same complementation group suggests that they are all alleles of the same gene.

The fact that all resistant strains carry alleles of *slo-1* indicates that it is key to emodepside's mode of action. *slo-1*(*js379*), which has a premature stop codon in the S4 domain, is predicted to be a loss-of-function mutant. This implies that it is the loss of SLO-1 function that confers resistance to emodepside in *slo-1*(*js379*). This suggests that emodepside's effect on the SLO-1 channel would be to activate it. Of the mutations identified, all five lie in parts of the *slo-1* gene that code for regions known as regulators of conductance of potassium (RCK) domains. There are two RCK domains per SLO-1 α-subunit, RCK1 and RCK2. Both *pd23* and *pd24* result in the generation of premature stop codons in the RCK1 domain. *pd19* results in a glycine to alanine substitution in RCK1. *pd17* results in two alanine to valine substitutions in RCK1 and RCK2 domains. A tetramer of SLO-1 α-subunits is required to form a functional channel. In this tetramer of subunits it is proposed that the RCK domains (4 x RCK1 and 4 x RCK2) form an intracellular gating ring (Jiang *et al* 2002). It is thought that this gating ring changes conformation on ligand binding, resulting in opening of the channel (Jiang *et al* 2002). Jiang *et al* (2002) proposed a model whereby calcium binds in clefts between adjacent RCK domains in the tetramer, resulting in a widening of the gating ring. This widening causes the channel to open through a pulling of the linkers that connect the gating ring to the channel. It is thought that different channels can be gated by a variety of different ligands. It is possible that emodepside may affect this mechanism either directly of indirectly to open the channel. Second round amplification of *slo-1* cDNA in *pd47* consistently failed. This could indicate

that there is mutation at the site of primer annealing. Mutations upstream of the start codon could potentially disrupt the promoter and prevent expression.

A BLAST of RCK1 and RCK2 domains from *C. elegans slo-1* revealed homology of these domains in calcium-activated potassium channels across species. The amino acid identities for RCK ranged from 100% in *Caenorhabditis briggsae* to 22 % in *Trypanosoma cruzi*. In RCK2 the amino acid identity ranged from 100 % in *Caenorhabditis briggsae* to 22 % in *Dictyostelium discoidem*. Alignment of *C. elegans slo-1* RCK domains with the homologues revealed that residue glycine 432 was always conserved. In the allele *pd19*, glycine 432 is substituted for arginine. The alanine residues at position 524 and 870, which are substituted for valines in *pd17*, were less conserved. It is interesting that glycine 432 is always conserved as it suggests that it may be important for normal function of this RCK domain. The less substantial conservation of alanines 524 and 870 suggests they may be less important for normal RCK domain function.

The mutations in *pd24* and *pd23* are also of interest. The stop codon in *pd23* lies approximately half way through RCK1. It seems unlikely that a channel with a functional gating ring would form with this mutation. It has been shown that BK channels truncated after the seventh trans-membrane domain can retain their function when expressed in HEK 293 cells and *Xenopus* oocytes (Piskorowski *et al* 2002). It is therefore possible that a functional channel that lacks the majority of RCK1 and all of RCK2 is expressed in *pd23*. If this is the case, it would indicate that the RCK domains are required for emodepside's mode of action. However, Piskorowski *et al* (2002) also showed that the expression level of the truncated BK channel was a 1000 fold lower compared with *N2*. If this is the case with *C. elegans slo-1* in *pd23*, the low level of expression could explain the resistance to emodepside, rather than the lack of a gating ring. The same can be said of *pd24*, which has a stop codon in the latter half of RCK1.

Understanding the nature of these mutations may help to understand the mechanism of emodepside. It may be that in some cases that the mutations that confer resistance to emodepside do not affect SLO-1 function, potentially providing an insight to an emodepside binding site on SLO-1. This is further investigated in the following chapter.

# Chapter 5

# Behavioural analysis of *slo-1* alleles

## 5.1 Introduction

The BK channel SLO-1 is a key mediator of emodepside's effects. The fact that only *slo-1* mutants were isolated from the screens for emodepside resistance supports this idea. In order to further understand the role of *slo-1* in emodepside's mode of action an investigation of the phenotypes of *slo-1* mutants has been undertaken. Through a comparison of *slo-1* allele phenotypes and the nature of the *slo-1* mutations, information on emodepside's mode of action can be obtained.

It might be expected that if emodepside signals through SLO-1, the highest level of drug resistance would be seen in those mutants predicted to be functional nulls. If emodepside binds to SLO-1, high levels of emodepside resistance may also be seen in SLO-1 mutants that retain their function but have mutations in an emodepside binding site. These theories were tested by measuring the level of sensitivity to emodepside and two read outs of SLO-1 function, the reversal frequency of direction of movement and aldicarb sensitivity. The emodepside sensitivity, reversal frequency and aldicarb sensitivity of eight *slo-1* alleles is investigated. *slo-1* mutants were reported to have an increased sensitivity to the ACh esterase (ACE) inhibitor aldicarb as well as having an increased tendency to reverse (Wang *et al* 2001). The emodepside sensitivity of two *slo-1* gain-of-function alleles, *ky399* and *ky389*, is also investigated. If emodepside acts through SLO-1, the gain of function mutants would be predicted to have the same level of sensitivity to emodepside as *N2*. If loss of SLO-1 function acts to oppose emodepside's action then the effect of gain of SLO-1 function and emodepside would be predicted to additive. Figure 5.01 shows the two possible mechanisms of SLO-1 involvement in emodepside's mode of action.

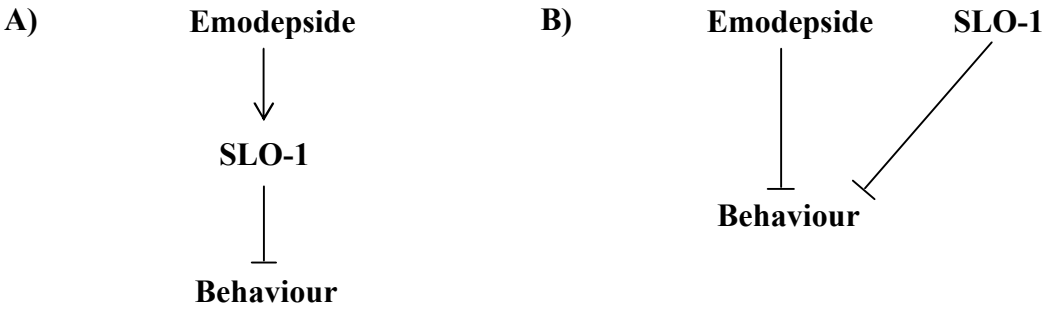


**Figure 5.01. Alternative hypothesises for SLO-1 involvement in emodepside's mode of action. A)** Emodepside acts directly through SLO-1 resulting in paralysis. **B)** SLO-1 function complements emodepside's effects.

The forward movement of *C. elegans* is interspersed with spontaneous reversals (Chiba and Rankin 1990). The neuronal circuit controlling forward and backward movement was first described in the context of mechano-sensation (Chalfie *et al* 1985, White *et al* 1986). The command interneurons AVA, AVB, AVD/E and PVC receive input from a variety of sensory neurons and inter-neurons. The output from the command inter-neurons is directed to a subset of motor-neurons, initiating either forward or backward movement (Chalfie *et al* 1895, Zheng *et al* 1999). The command inter-neurons AVA and AVD/E control backward movement and AVB and PVC control forward movement. It is thought that the command interneurons have an intrinsic activity and that reversal frequency is regulated by the level of neuronal depolarisation (Zheng *et al* 1999). The increased reversal frequency of *slo-1*(*js379*) suggests that there is an increase in neuronal activity within the command inter-neurons. Increased neuronal activity may result from loss of SLO-1 function. If this is the case, reversal frequency provides a read-out for the level of SLO-1 function.

Reduced aldicarb sensitivity in *C. elegans* is thought most likely to reflect defects in synaptic transmission (Miller *et al* 1996). Mutants with hyperactive neurotransmission have been shown to be hypersensitive to the effects of aldicarb (Nurrish *et al* 1999). Wang *et al* (2001) showed that *slo-1* loss-of-function mutants were hypersensitive to aldicarb. Davies *et al* (2003) showed that *slo-1* gain-of-function mutants had reduced sensitivity to aldicarb. These increases and decreases in aldicarb sensitivity are likely to reflect changes in the level of ACh release resulting from altered neuronal activity. In this case, aldicarb should also provide a read-out for the level of SLO-1 function. However, the apparent effect of SLO-1 loss of function on aldicarb sensitivity should be viewed with caution. Rescue of aldicarb sensitivity of *slo-1* mutants has not been demonstrated and the aldicarb sensitivity of hypomorphic *slo-1* alleles is not consistent (Wang *et al* 2001).

Prior to phenotypic analysis, the *slo-1* alleles *pd17*, *pd19*, *pd21*, *pd23*, *pd24*, *pd46* and *pd47* were out-crossed three times into the *N2* genetic background to remove extraneous mutations. *slo-1* homozygous outcrossed animals were selected based on resistance to emodepside. The parameters used to define emodepside resistance in the mutagenesis screen were used for this selection. The *slo-1*(*js379*) strain NM1968 was obtained from the CGC, outcrossed five times. The strains CX3940 and CX3933, which carry *ky399* and *ky389*, respectively, were obtained from the CGC. CX3933 was obtained outcrossed three times. CX3940 was obtained outcrossed once and carrying *rol-6*(*e187*). In order to assay CX3940, *rol-6*(*e187*) was

outcrossed. Outcrossed *ky399* were selected based on egg laying and locomotion phenotypes (Davies *et al* 2003). Due to the semi dominant nature of *ky399*, selection of homozygous *ky399* was confirmed by the absence of *N2* like egg laying and locomotion phenotypes in the progeny. *ky399* retain eggs and have sluggish locomotion.

Out crossed alleles were used in all assays excluding aldicarb assays. This was due to the emergence of aldicarb hypersensitivity in the *N2* strain propagated in house during the course of this project. This aldicarb hypersensitivity is likely to be due to spontaneous mutation. The out crossed alleles therefore potentially carry this mutation. This highlights the need for caution when interpreting aldicarb sensitivity data. In order to allow for this, un-outcrossed *slo-1* alleles were compared to an *N2* from which they were generated from prior to the emergence of aldicarb hypersensitivity. Outcrossed *slo-1* alleles were compared to the *N2* with which they were outcrossed. *N2* and the aldicarb hypersensitive *N2* displayed the same reversal frequency and emodepside sensitivity as each other. Therefore, the presence or absence of the mutation conferring aldicarb hypersensitivity in the out crossed strains will not influence the outcome of these assays.

## 5.2 *slo-1*(*js379*) is emodepside insensitive

Previously, sensitivity of *slo-1*(*js379*) to emodepside's effects on locomotion had been assessed using the thrashing assay (Amliwala, 2005). Due to problems with the solubility of emodepside, this project adopted the body bends assay was used in order to assess emodepside sensitivity. Further more, all assays were performed in parallel with *N2* controls. Figure 5.02 shows a dose response curve for *N2* and *slo-1*(*js379*). Animals were exposed to emodepside for 24 hours and then assayed off food. Emodepside significantly inhibited the locomotion of *N2* and at 100 nM, 1 µM and 10 µM. *slo-1*(*js379*) was not significantly inhibited at these concentrations. *N2* have an $IC_{50}$ of 100 nM, 95 % confidence limits 68 nM to 146. No $IC_{50}$ for *slo-1*(*js379*) could be measured as emodepside does not inhibit its locomotion. This illustrates the high level of resistance that *slo-1*(*js379*) have to emodepside.

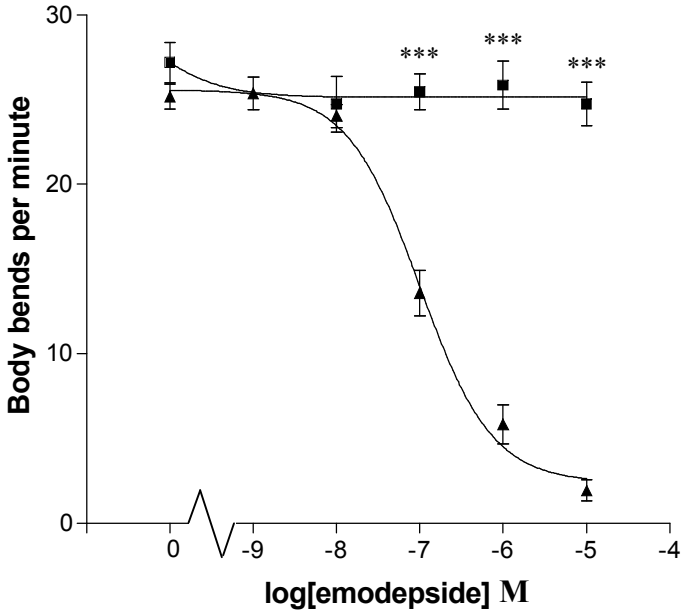


**Figure 5.02. *slo-1*(*js379*) dose response for emodepside.** *slo-1*(*js379*) (■) and *N2* (▲). For each point n≥12 and is the mean ± S.E.Mean. *** indicates $P<0.001$.

*slo-1*(*js379*) are unaffected by concentrations as high as 10 µM. This high level of resistance is also reflected in the lack of effect that emodepside has on the sinusoidal shape of movement of *slo-1*(*js379*). Figure 5.03 shows the effect of 24 hour exposure to 1 µM emodepside on the sinusoidal movement of *N2* and of *slo-1*(*js379*) on food. Photographs show 24 hour post L4 worms. *N2* lose their sinusoidal shape on 1 µM emodepside and extend their anterior in a straight line. *slo-1*(*js379*) retain their sinusoidal shape on 1 µM emodepside.

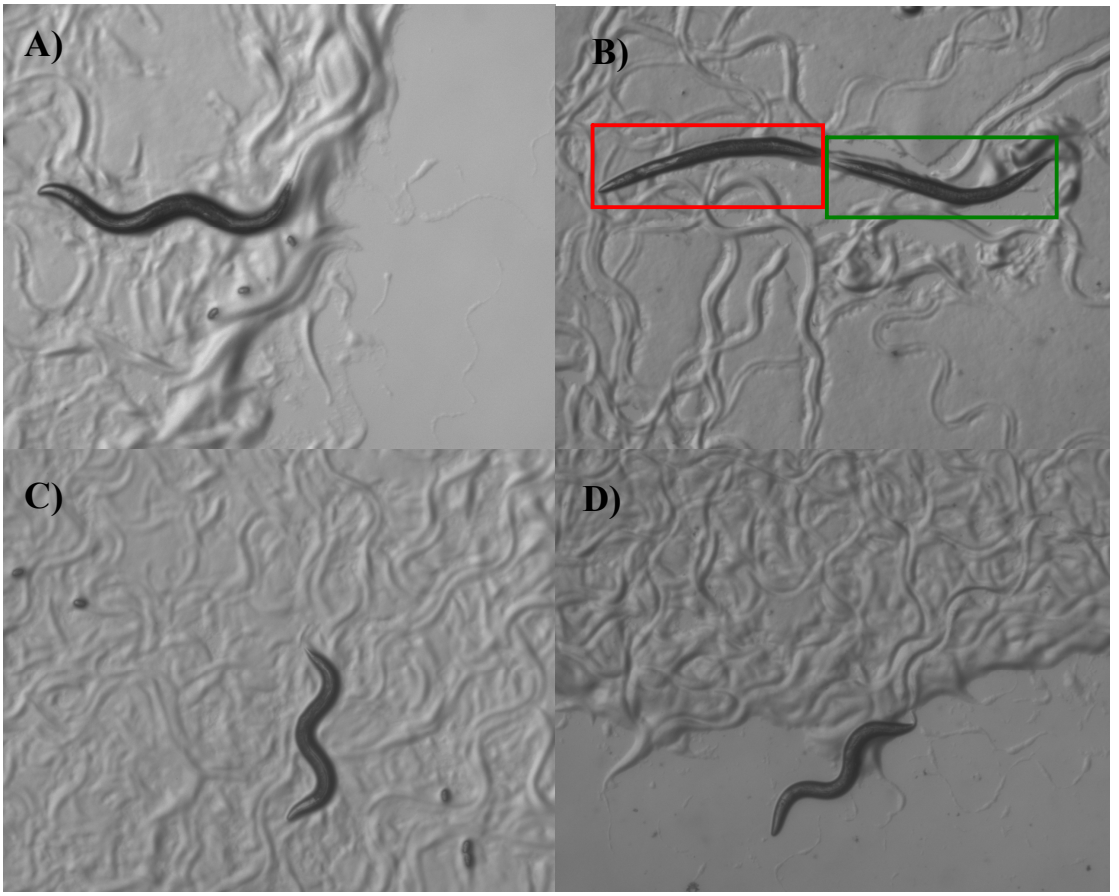


**Figure 5.03. Emodepside's effects on *N2* and *slo-1*(*js379*) body posture.** All photograph show 24 hour post L4 worms. **A)** *N2* exposed to vehicle for 24 hours, **B)** Two *N2* exposed to 1 µM emodepside for 24 hours, **C)** *slo-1*(*js379*) exposed to vehicle for 24 hours, **D)** *slo-1*(*js379*) exposed to 1 µM emodepside for 24 hours.

## 5.3 Quantification of emodepside resistance in *slo-1* alleles

The level of resistance to emodepside of *slo-1* alleles *js379*, *pd17*, *pd19*, *pd21*, *pd23*, *pd24*, *pd46* and *pd47* was tested in the body bends assay. L4 worms were picked onto 1 µM emodepside-containing NGM plates for 24 hours on food. They were also picked onto 0.5 % ethanol vehicle NGM plates. After 24 hours the young adults were picked onto an un-seeded NGM plate for one minute in order to remove any OP50. They were then picked to an un-seeded assay plate and left to recover for one minute. Finally body bends were counted for one minute. Figure 5.04 shows effect of 1 µM emodepside on these animals. This illustrates that not all *slo-1* alleles exhibit the same high level of emodepside resistance observed in *js379*.

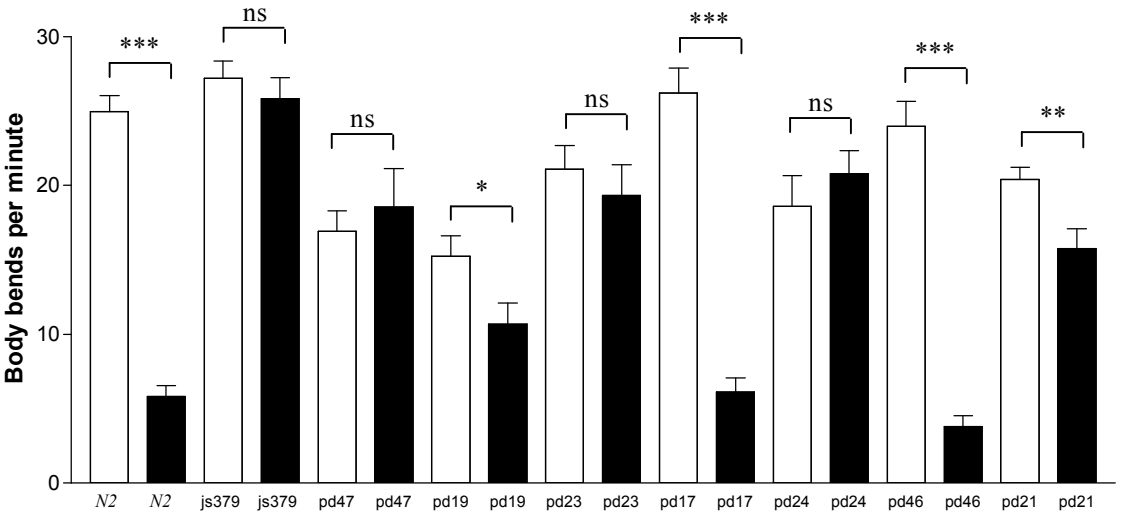


**Figure 5.04. *slo-1* allele emodepside sensitivities.** The effect of 24 hour exposure to 1 μM emodepside on locomotion of *N2*, *js379*, *pd47*, *pd19*, *pd23*, *pd17*, *pd24*, *pd46* and *pd21*. □ shows animals exposed to vehicle and ■ shows animals exposed to 1μM emodepside. For each bar n≥8 and is the mean ± S.E. Mean. * indicates *P<0.05*, ** indicates *P*<0.01 and *** indicates *P*<0.001

The locomotion of *N2*, *pd17*, *pd46* is significantly inhibited by 1 μM emodepside, with *P*<0.01. *pd17* and *pd46* appear to be as sensitive to 1 μM emodepside as *N2* with regard to their rate of locomotion. However, they retain a sinusoidal pattern of movement on 1 μM emodepside as observed in strains with stronger resistance. The locomotion of *pd19* and *pd21* is significantly inhibited by 1 μM emodepside, although to a lesser extent, with *P* values of *P<0.05* and *P*<0.01, respectively. The locomotion of *js379*, *pd47*, *pd23* and *pd24* is not inhibited by 1 μM emodepside.

## 5.4 Reversal frequency of *slo-1* alleles

Worms were assayed off food so that foraging behaviour would be initiated and reversal frequency increased, thereby reducing the assay time required. Worms were selected at L4 stage and kept on food for 24 hours. Worms were then individually transferred to an unseeded plate to reduce the amount of *E. coli* OP50 transferred to the assay plate. After 1 minute each worm was then transferred to an unseeded assay plate. After five minutes of acclimatization, the number of reversals the worm made in 1 minute was recorded. Assays were performed blind and conducted in parallel with *N2* controls.

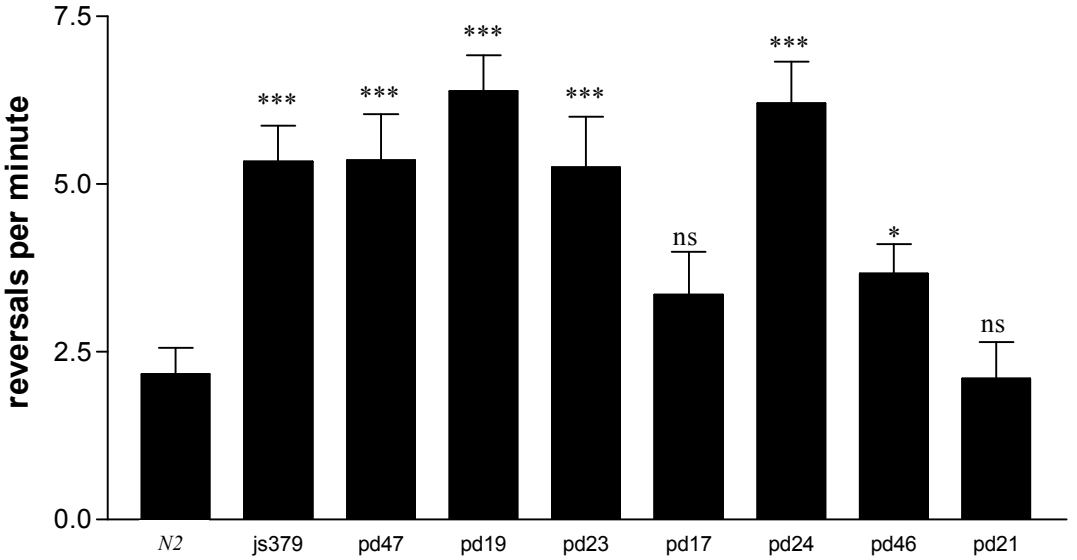


**Figure 5.05. *slo-1* allele reversal frequencies.** Number of reversals in one minute of *N2*, *js379*, *pd47*, *pd19*, *pd23*, *pd17*, *pd24*, *pd46* and *pd21* after five minutes off food. For each bar n≥10 and is the mean ± the S.E. Mean. * indicates *P<0.05* and *** indicates *P*<0.001 compared with *N2*.

Figure 5.05 show average reversal frequency of each *slo-1* allele compared with the average reversal frequency of *N2*. The reversal frequencies of *pd17* and *pd21* do not significantly differ from that of *N2*. The reversal frequency of *pd46* is slightly but significantly increased compared to *N2* (*P<0.05*). The reversal frequencies of *pd47*, *pd19*, *pd23* and *pd24* are significantly increased compared with *N2* (*P*<0.001). In general there is a correlation between reversal frequency and emodepside sensitivity. However, *pd21* has a reversal frequency comparable to that of *N2* whereas its has strong resistance to emodepside.

## 5.5 Aldicarb sensitivity of *slo-1* alleles

L4 worms were selected 24 hours before the assay. The assay was performed blind. Young adults were transferred to 0.5 mM aldicarb containing NGM plates seeded with OP50. Worms were assayed on food to prevent the worms from moving off the plate. 15 worms were placed on each plate. The number of paralysed worms was recorded every 30 minutes. Paralysis was assessed through a single prod with a platinum wire pick. Multiple trials were conducted for each strain. One trial refers to a single plate of worms assayed. Experiments were run with parallel controls. Paralysed worms were removed from the plate.

Figure 5.06 A) shows the average percentage of animals paralysed by 0.5 mM aldicarb from 16 trials. *slo-1*(*js379*) are paralysed by 0.5 mM aldicarb at a quicker rate that *N2*. A significantly higher proportion of *slo-1*(*js379*) are paralysed after 60, 90 and 120 minutes on 0.5 mM aldicarb ($P<0.001$). This result is similar to that observed by Wang *et al* (2001). Figure 5.06 B) shows the average percentage of animals paralysed by 0.5 mM aldicarb from ≥10 trials. *slo-1*(*pd24*) are paralysed by 0.5 mM aldicarb at a quicker rate that *N2*. A significantly higher proportion of *slo-1*(*pd24*) are paralysed after 60, 90 and 120 minutes on 0.5 mM aldicarb with $P<0.05$, $P<0.001$ and $P<0.01$, respectively. Figure 5.06 C) shows the average percentage of animals paralysed by 0.5 mM aldicarb from ≥4 trials. *slo-1*(*pd19*) are paralysed at the same rate as *N2* by 0.5 mM aldicarb. Figure 5.06 D) shows the average percentage of animals paralysed by 0.5 mM aldicarb from ≥4 trials. *slo-1*(*pd23*) are paralysed at the same rate as *N2* by 0.5 mM aldicarb. Figure 5.06 E) shows the average percentage of animals paralysed by 0.5 mM aldicarb from ≥4 trials. *slo-1*(*pd17*) are paralysed by 0.5 mM aldicarb at a quicker rate that *N2*. A significantly higher proportion of *slo-1*(*pd17*) are paralysed after 30, 60 and 90 minutes on 0.5 mM aldicarb with $P<0.01$, $P<0.001$ and $P<0.001$, respectively. Figure 5.06 F) shows the average percentage of animals paralysed by 0.5 mM aldicarb from ≥3 trials. *slo-1*(*pd47*) are paralysed by 0.5 mM aldicarb at a quicker rate that *N2*. A significantly higher proportion of *slo-1*(*pd47*) are paralysed after 60 and 90 minutes on 0.5 mM aldicarb with $P<0.05$ and $P<0.01$. Figure 5.06 G) shows the average percentage of animals paralysed by 0.5 mM aldicarb from ≥2 trials. *slo-1*(*pd21*) are paralysed at the same rate as *N2* by 0.5 mM aldicarb. Figure 5.06 H) shows the average percentage of animals paralysed by 0.5 mM aldicarb from ≥2 trials. *slo-1*(*pd46*) are paralysed by 0.5 mM

aldicarb at a quicker rate that *N2*. A significantly higher proportion of *slo-1*(*pd46*) are paralysed after 90 minutes on 0.5 mM aldicarb ($P<0.01$).

No correlation can be drawn between the level of resistance to emodepside and the sensitivity to aldicarb. In the cases of *js379*, *pd24* and *pd47*, strong resistance to emodepside and high sensitivity to aldicarb are observed. However, *pd23* is strongly resistant to emodepside but its sensitivity to aldicarb is not significantly different to that of *N2*. *pd17* and *pd46* are weakly resistant to emodepside yet both are significantly more sensitive to aldicarb than *N2*. *pd19* and *pd21* have an intermediate level of resistance to emodepside but are not significantly more sensitive to aldicarb than *N2*. Although mutations present in the background of these strains may affect their aldicarb sensitivity, the lack of any correlation suggests an uncoupling between emodepside resistance and aldicarb hypersensitivity.

**A) *js379***

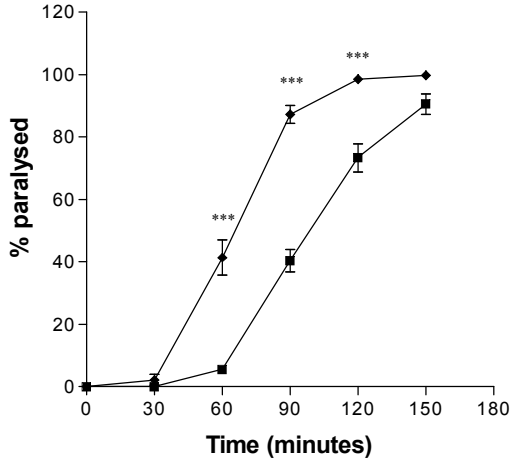


**B) *pd24***

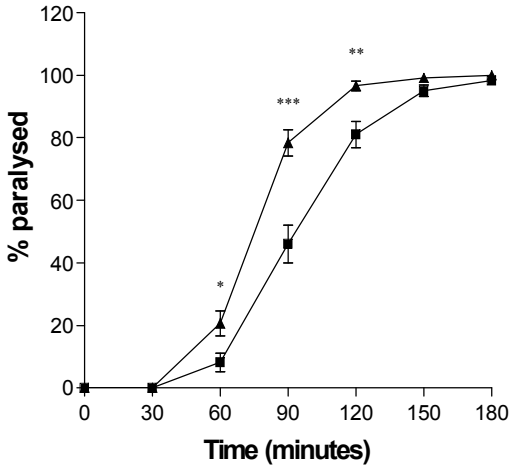


**C) *pd19***

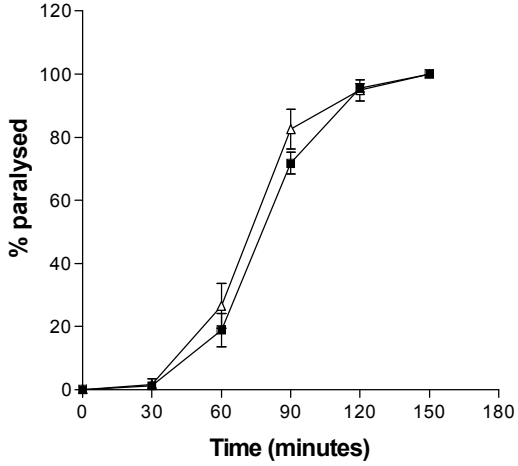


**D) *pd23***

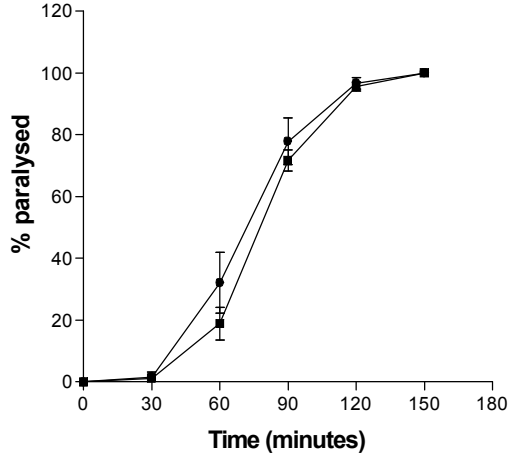


**E) *pd17***

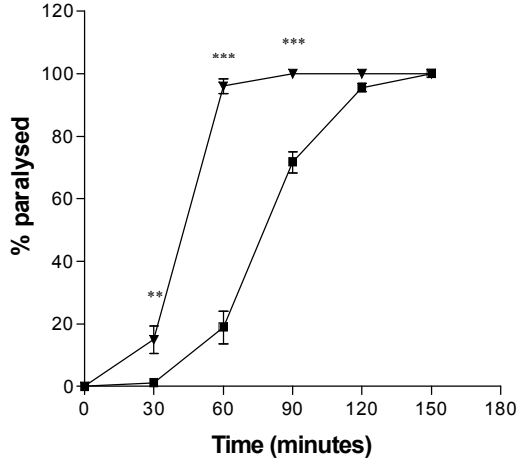


**F) *pd47***

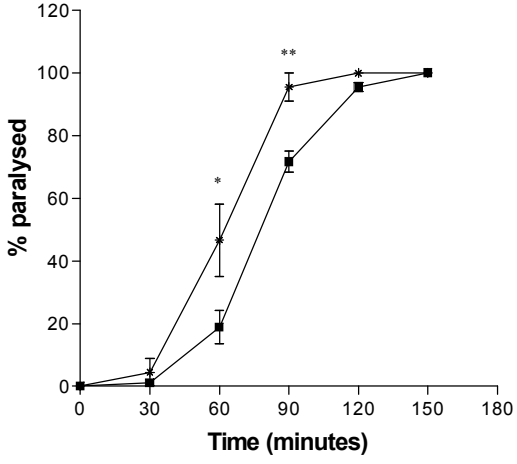

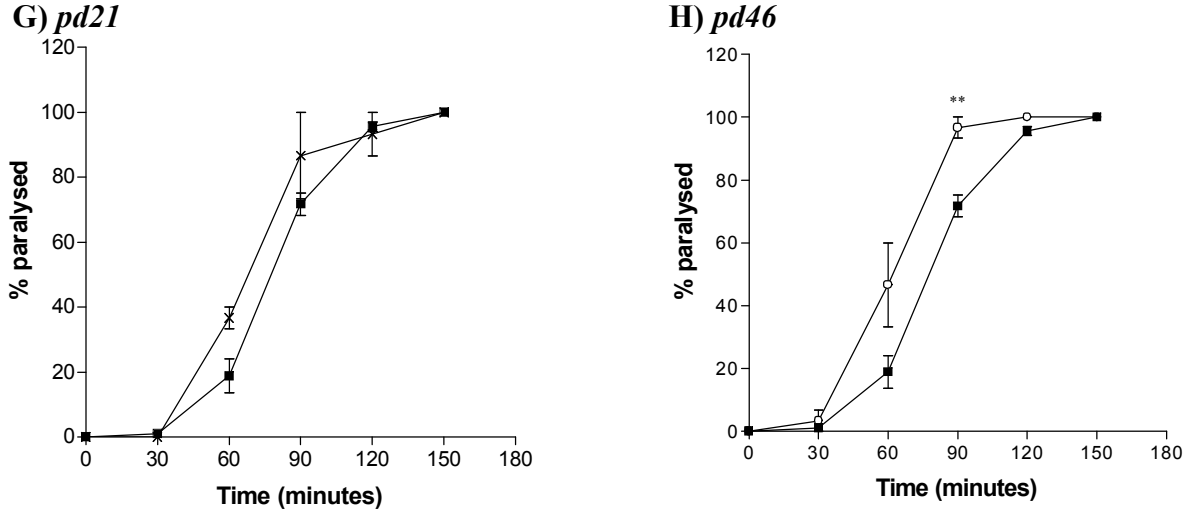


**Figure 5.06. *slo-1* allele aldicarb sensitivities.** Time until paralysis on 0.5 mM aldicarb of 24 hour post L4 worms on food: **A)** *N2* (■) and *js379* (♦), each point is the mean ± S.E.Mean of 16 trials, **B)** *N2* (■) and *pd24* (▲), each point is the mean ± S.E.Mean of ≥ 10 trials, **C)** *N2* (■) and *pd19* (△), each point is the mean ± S.E.Mean of ≥ 4 trials, **D)** *N2* (■) and *pd23* (●), each point is the mean ± S.E.Mean of ≥ 4 trials, **E)** *N2* (■) and *pd17* (▼), each point is the mean ± S.E.Mean of ≥ 4 trials, **F)** *N2* (■) and *pd47*, each point is the mean ± S.E.Mean of ≥ 3 trials, **G)** *N2* (■) *pd21* (×), each point is the mean ± S.E.Mean of ≥ 2 trials, **H)** *N2* (■) and *pd46* (○), each point is the mean ± S.E.Mean of ≥ 2 trials. * indicates *P<0.05*, ** indicates *P*<0.01 and *** indicates *P*<0.001.

## 5.6 *slo-1*(*ky399*) and *slo-1*(*ky389*) gain-of-function mutants phenocopy emodepside treated *N2* and are not emodepside hypersensitive

The *slo-1* gain-of-function mutants *ky399* and *ky389* were previously isolated as *nsy-3* mutants in a screen of neuronal symmetry (Tromel *et al* 1999). Both *slo-1*(*ky389*) and *slo-1*(*ky399*) have defects in locomotion and egg laying (Davies *et al* 2003).

The sensitivity of *slo-1*(*ky399*) and *slo-1*(*ky389*) to emodepside's effect on locomotion was tested using the body bends assay. Animals were exposed to emodepside for 24 hours and then assayed off food. Most notably, the basal rate of locomotion of *slo-1*(*ky399*) and *slo-1*(*ky389*) is significantly lower than that of *N2*. this is consistent with the suggestion that these *slo-1* gain of function mutants phenocopy the effects of emodepside. Despite this lower locomotion rate, the $IC_{50}$ for emodepside was not altered. Figure 5.07 shows a dose response for *N2* and *slo-1*(*ky399*) and *slo-1*(*ky389*). The $IC_{50}$ of *N2*, *slo-1*(*ky399*) and *slo-1*(*ky389*) are not significantly different.. *N2* have an $IC_{50}$ of 52 nM (95 % confidence limits 32 nM to 84nM). *slo-1*(*ky399*) have an $IC_{50}$ of 130 nM (95 % confidence limits 48 nM to 347 nM). *slo-1*(*ky389*) have an $IC_{50}$ of 130 nM (95 % confidence limits 62 nM to 273 nM).

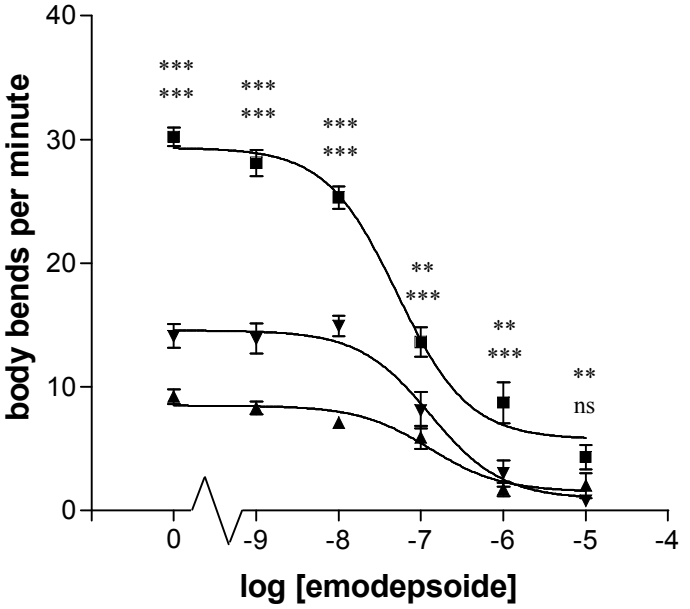


**Figure 5.07. Emodepside dose response for *slo-1* gain-of-function mutants.** *slo-1*(*ky399*) (▲), *slo-1*(*ky389*) (▼) and *N2* (■). For each point n=10 and is the mean ± S.E.Mean. ** indicates $P<0.01$ and *** indicates $P<0.001$. Comparison are made between *N2* vs *slo-1*(*ky389*) (shown above) and *N2* vs *slo-1*(*ky399*) (shown below).

A more detailed consideration of the phenotype of *slo-1* gain of function showed that both *slo-1*(*ky399*) and *slo-1*(*ky389*) phenocopy the effects of emodepside on *N2*. As well as the effects on its locomotion, egg laying is significantly decreased in both *slo-1*(*ky399*) and *slo-1*(*ky389*) (Davies *et al* 2003). Similarly, emodepside inhibits egg laying and locomotion in *N2* (Bull *et al* 2007, Wilson *et al* 2003). The appearance of the locomotion of *slo-1*(*ky399*) and *slo-1*(*ky389*) resembles that of *N2* exposed to 10 nM or 100 nM emodepside, with shallower bends and a tendency to elongate their anterior.

## 5.7 Discussion

The high level of emodepside resistance observed in the putative null *slo-1*(*js379*) suggests that emodepside activates SLO-1 dependent pathway. If loss of SLO-1 function only acted to oppose the paralytic action of emodepside, it would be expected that the resistance would be less substantial. However, emodepside appears to have no effect on *slo-1*(*js379*) at concentrations as high as 10 μM. Effects of emodepside on *N2* are apparent at concentrations lower than 10 nM in the body bends assay.

The phenotypes of the *slo-1* alleles are presented in table 5.01. There is a correlation between the level of emodepside resistance and reversal frequency, with some exceptions. The alleles *js379*, *pd23*, *pd24* and *pd47* confer insensitivity to 1 μM emodepside. *js379*, *pd23*, *pd24* and *pd47* all display a frequency of reversal that is significantly increased compared to *N2* ($P<0.001$). *pd17* and *pd46* confer a low level of resistance to emodepside. The reversal frequency of *pd17* is not significantly different from that of *N2*. The reversal frequency of *pd46* is only slightly increased compared to that of *N2* ($P<0.05$). In general, alleles that show the highest resistance have the strongest *slo-1* loss of function phenotype.

The exception to this is *pd21*. *pd21* has an intermediate level of resistance but has a reversal frequency not significantly different to that of *N2*. This suggests that SLO-1 function is retained in *pd21* while emodepside sensitivity is reduced. This may indicate a directed action of emodepside on SLO-1. *pd19* also has an intermediate level of resistance to 1 μM emodepside, although the statistical significance of this is low ($P<0.05$). The frequency of reversal of *pd19* is significantly greater than that of *N2* ($P<0.001$). This could suggest that loss of SLO-1 acts to oppose emodepside's effects. Alternatively the mutation in *pd19* may reduce SLO-1 function to a level sufficient to result in a reversal frequency that is significantly different from *N2* whilst retaining some emodepside sensitivity. The bulk of the evidence suggests an action of emodepside through SLO-1.

| Allele | **1)** Emodepside resistance level | **2)** Reversal frequency increase – compared to *N2* | **3)** Aldicarb sensitivity at T90 |
|---|---|---|---|
| *js379* | ++++ (High) | *** | *** |
| *pd23* | ++++ (High) | *** | ns |
| *pd24* | ++++ (High) | *** | *** |
| *pd47* | ++++ (High) | *** | ** |
| *pd19* | +++ (intermediate) | *** | ns |
| *pd21* | ++ (intermediate) | ns | ns |
| *pd17* | + (low) | ns | *** |
| *pd46* | + (low) | * | ** |

**Table 5.01. *slo-1* allele phenotype summary. 1)** Level of resistance to 1 μM emodepside. Comparisons made between 1 μM emodepside and 0.5 % ethanol vehicle treated worms. ++++ indicates ns (most resistant), +++ indicates $P<0.05$, ++ indicates $P<0.01$, + indicates $P<0.001$ (least resistant). **2)** The statistical significance of increases in reversal frequency for each *slo-1* allele are shown. **3)** The statistical significance of increases in aldicarb sensitivity after 90 minutes exposure for each *slo-1* allele are shown. . * indicates $P<0.05$, ** indicates $P<0.01$ and *** indicates $P<0.001$.

The level of aldicarb sensitivity in these mutants does not correlate well with the reversal frequency or emodepside resistance. The lack of any correlation between emodepside resistance / reversal frequency and aldicarb hyper-sensitivity might indicate that these phenotypes do not originate through the same mechanism. This could either be through a different mechanism involving *slo-1* or alternatively, a mechanism unrelated to *slo-1*.

*js379* is a putative null mutant that is hypersensitive to aldicarb. However, the relationship between *slo-1* function and aldicarb sensitivity does not appear to be consistent. Of the two mutants that have premature stop codons generated in the emodepside resistance screen, two are aldicarb hypersensitive (*js379* and *pd24*) and one is not (*pd23*). The mutation in *pd23* would be expected to result in truncation of *slo-1* earlier in the sequence than *pd24*. If loss of SLO-1 function results in aldicarb hypersensitivity, both *pd24* and *pd23* would be expected to be aldicarb hypersensitive. The fact that they are not suggests that the aldicarb hyper-sensitivity may be un-related to these mutations in *slo-1*. In a similar way, *slo-1* suppressors of the *unc*-64 lethargic phenotype also had large variations in their aldicarb sensitivity (Wang *et al* 2001). The allele *md1745* has an early stop codon between the S0 and S1 transmembrane domains (Q134Stop), compared with *js379* which has an early stop codon in the S4 transmembrane domain (W850Stop). However, *js379* is substantially more sensitive to

aldicarb than *md1745*. Expression of *slo-1*(+) in aldicarb hypersensitive *slo-1* loss of function mutants is required to definitively address this question.

The available evidence suggests that greater loss of SLO-1 function result in stronger emodepside resistance and reversal frequency phenotypes. Alleles with premature stop codons (*js379*, *pd24*, *pd23*) have a high level of emodepside resistance (++++) and a reversal frequency highly significantly increased compared to *N2* (***). The amino acid change G432R in *pd19* results in a lower level of emodepside resistance (+++) and a reversal frequency highly significantly increased compared to *N2* (***). The amino acid changes A524V and A870V in *pd17* result in a low level of emodepside resistance (+) and a reversal frequency not significantly different compared to *N2* (ns). It seems likely that reversal frequency reflects the level of SLO-1 function. However, if emodepside acts through SLO-1 directly, it may be possible to generate emodepside resistant alleles that do not affect SLO-1 function. Mutation of a possible emodepside binding site on SLO-1 could result in a high level of resistance whilst leaving SLO-1 function unaffected. It is possible that this is the case with *pd21*. Unfortunately, sequencing of *pd21 slo-1* cDNA is yet to identify a mutation.

The *slo-1* gain-of-function mutants *ky399* and *ky389* are not hypersensitive to emodepside. If loss of SLO-1 function confers emodepside resistance by indirectly opposing its paralytic effects, it would be expected that the effects of SLO-1 gain-of-function and emodepside would be additive. The fact that it is not suggests that emodepside acts directly through SLO-1, or a SLO-1 dependent pathway.

The effect of *slo-1* function on aldicarb sensitivity is unclear. The lack of correlation between emodepside resistance / reversal frequency and aldicarb sensitivity and the unexplained variability in aldicarb sensitivity of *slo-1* alleles shows that further investigation is required. Importantly, rescue of this phenotype through the generation of *slo-1*(*js379*) expressing *slo-1*(+) was not demonstrated directly by Wang *et al* (2001). Therefore the suggestion that SLO-1 loss of function increases aldicarb sensitivity is in doubt. Attempts to address this are made in the following chapter.

# Chapter 6

# Tissue specific analysis of the role of SLO-1 in emodepside's mode of action

## 6.01 Introduction

The genetic evidence suggests that emodepside causes activation of the BK channel SLO-1. Activation may result from direct binding of emodepside or activation via a pathway. As BK channels provide a mechanism for cell repolarisation, activation of SLO-1 channels would be expected to reduce cell excitability. The aim of this chapter is to investigate the effect that emodepside has on cell excitability and how this results in inhibition of locomotion. This was addressed using two approaches. A pharmacological analysis was used to test whether emodepside increases or decreases the activity of cholinergic motor neurons or body wall muscle. In addition, cell specific expression of wild type *slo-1* in the *slo-1*(*js379*) null genetic background was used to assess whether emodepside requires *slo-1* in neurons and/or muscle to inhibit locomotion.

In neurons reduced cell excitability would impact on neurotransmitter release. However, it is unclear whether BK channel activation reduces or increases neurotransmitter release. Warbington *et al* (1996) found that loss of function of *Drosophila melanogaster* SLO channel results in a decrease in neurotransmitter release. Xu *et al* (2005) demonstrated that specific block of BK channels in the salamander rod synapse could decrease transmitter release. This is possible in the salamander rod synapse as its confined structure prevents diffusion of the potassium ions out of the synaptic cleft, resulting in a high local concentration (Towns-Anderson *et al* 1985). However, the morphology of *C. elegans* synapses does not resemble that of the salamander rod synapse. In fact, the structure of *C. elegans* synapses is far simpler. Synapses in *C. elegans* occur *en passant*. The pre-synaptic specialisations vary in size and complexity. The post-synaptic elements have no visible specialisation and are often quite ambiguous (White *et al* 1986). It is hard to imagine that the potassium induced calcium currents that occur in the salamander rod synapse could occur by the same mechanism at these synapses, where ions could easily diffuse. The most relevant evidence for the role of SLO-1 in neurotransmitter release comes from a paper by Wang *et al* (2001). *slo-1* was identified in a screen for *C. elegans* mutants that would suppress the lethargic phenotype of the syntaxin hypomorph *unc-64*. *unc-64*(*e246*) has reduced neurotransmitter release, which has been demonstrated using the acetylcholine esterase (ACE) inhibitor aldicarb. *unc-64*(*e246*) has a reduced aldicarb sensitivity which can be rescued by *slo-1*. Although the role of *slo-1* in aldicarb sensitivity is not clear, *slo-1* does rescue the *unc-64* lethargic phenotype.

Neuronal expression of *slo-1*(+) in the *unc-64*, *slo-1* double mutant abolished rescue of the lethargic phenotype. This suggests the role of SLO-1 in *C. elegans* is to reduce neurotransmitter release. Therefore, it would be expected that emodepside would cause a reduction in neurotransmitter release.

Pharmacological compounds can be used as tools to inform about cell excitability. Aldicarb and levamisole have been used in this way in the following chapter. Aldicarb is an ACE inhibitor. ACE metabolises ACh in the synaptic cleft to control the duration of its response. Block of ACE results in a build up of ACh and paralysis of the muscle. The sensitivity of mutants or drug treated worms to aldicarb can be used to provide an indication of changes in ACh release (Miller *et al* 1996). An increased sensitivity to aldicarb indicates there is an increase in ACh release. Levamisole is a nicotinic ACh receptor agonist (Lewis *et al* 1980). It cause hyper-contraction and paralysis of the body wall muscle through activation of post-synaptic nicotinic ACh receptors (Lewis *et al* 1980, Fleming *et al* 1997, Culetto *et al* 2004). The sensitivity of a mutant or drug treated worm to levamisole can be used to provide an indication of changes in muscle cell excitability. An increased sensitivity to levamisole indicates an increase in muscle cell excitability. The mechanisms of action of both aldicarb and levamisole are illustrated in figure 6.01.

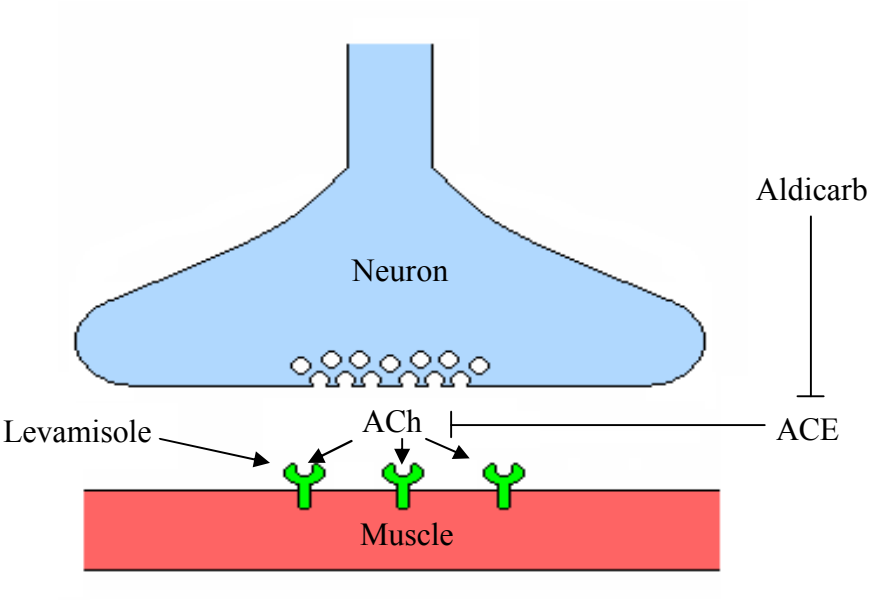


**Figure 6.01. Aldicarb and levamisole modes of action.** Aldicarb inhibits ACE in the neuromuscular junction, preventing the break down of ACh. ACh continues to activate post-synaptic receptors, leading to paralysis of the muscle. Levamisole in an ACh agonist that activates post-synaptic nicotinic ACh receptors, leading to paralysis of the muscle.

In this chapter the effect of emodepside pre-treatment on the sensitivity to aldicarb and levamisole has been used to provide an indirect indicator of how it might influence neuromuscular transmission.

## 6.02 *C. elegans* transformations

In order to understand the role of SLO-1 in emodepside's mode of action, tissue specific rescue of *slo-1* in the neurons or body wall muscle of *slo-1*(*js379*) was undertaken. The vectors pBK3.1 and pBK4.1 for these experiments were kindly provided by Lawrence Salkoff (Wang *et al* 2001). pBK3.1 contains *slo-1* cDNAa under the control of the neuronal promoter $_{p}$*snb-1* (Nonet 1999). pBK4.1 contains *slo-1* cDNAa under the control of the body wall muscle $_{p}$*myo-3*. These were injected into the syncytium of young adults *slo-1*(*js379*) in order to generate transgenic progeny. The injection marker pPD118.33 was used. pPD118.33 contains *gfp* under control of the pharyngeal muscle promoter $_{p}$*myo-2*. This was co-injected with pBK3.1 and pBK4.1. Co-injected vectors that share homology undergo frequent recombination reactions. These reactions drive the assembly of large contiguous arrays which become heritable if they attain a sufficient size (Mello *et al* 1991). pBK3.1 and pBK4.1 have 3168 bp and 3377 bp of identity with pPD118.33, respectively. Transgenic animals that express $_{p}$*myo-2::gfp* are therefore likely to carry the co-injected vectors within the extra-chromosomal array. Once the extra-chromosomal arrays are formed, the frequency of recombination is greatly reduced and they are propagated indefinitely with little further rearrangement (Mello *et al* 1991). Stable lines, in which the extra-chromosomal array is propagated, were used in all assays.

Initial control experiments were conducted to confirm that the pPD118.33 marker did not confer sensitivity to emodepside in *slo-1*(*js379*). Stable lines of *slo-1*(*js379*) carrying pPD118.33 were established. The sensitivity of worms expressing the marker to 10 µM emodepside was tested in a locomotion assay. L4 worms expressing the $_{p}$*myo-2::gfp* marker were exposed to 10 µM emodepside on food containing NGM plates for 24 hours. Body bends of the young adult worms were then counted for one minute off food on 10 µM emodepside NGM plates (see methods). Figure 6.02 shows the rate of locomotion of *N2*, *slo-1*(*js379*) and *slo-1*(*js379*) expressing $_{p}$*myo-2::gfp* with and without exposure to 10 µM emodepside.

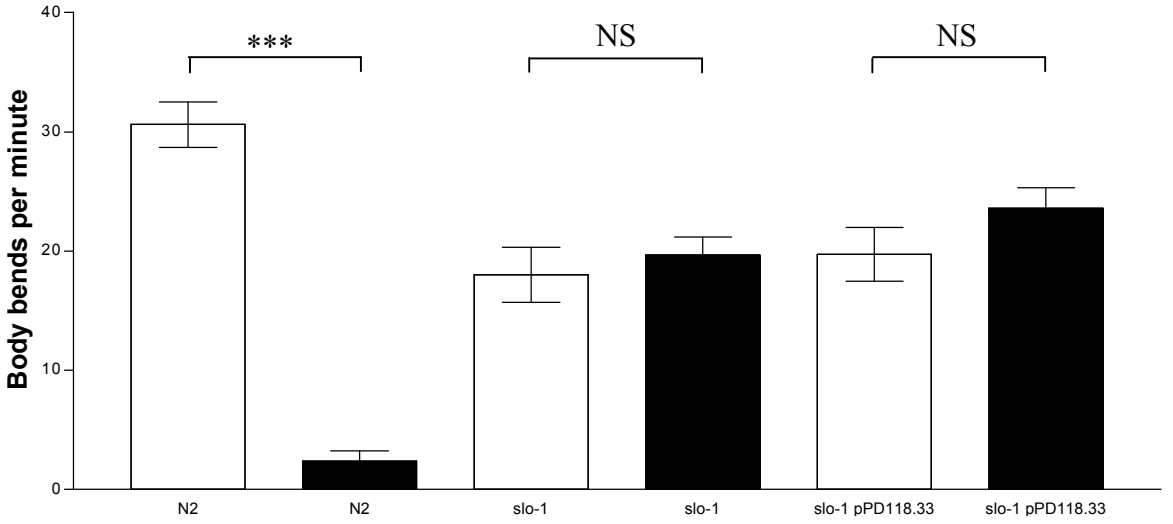


**Figure 6.02. Transfection marker control assay.** Rate of locomotion of *N2*, *slo-1*(*js379*) and *slo-1*(*js379*) transformed with pPD118.33 ($_{P}$*myo-2*::GFP). Clear bars show the rate of locomotion off emodepside (on vehicle) and filled bars show the rate of locomotion on 10 µM emodepside. N=6 for *slo-1*(*js379*) on emodepside and N=8 for the rest.. Each bar is the mean ± S.E.Mean. *** indicates $P<0.001$.

*N2* worms are significantly inhibited by 10 µM emodepside ($P<0.01$) compared with the vehicle control. The locomotion of *slo-1*(*js379*) on 10 µM emodepside is not significantly different to locomotion on vehicle control. The locomotion of *slo-1*(*js379*) expressing $_{p}$*myo-2::gfp* on 10 µM emodepside is not significantly different to locomotion on vehicle control. This demonstrates that the expression of $_{p}$*myo-2::gfp* does not affect the sensitivity of *slo-1*(*js379*) to emodepside. It seems unlikely that expression of *gfp* in the pharyngeal muscle would directly effect sensitivity to emodepside. However, it has been observed that strong expression of $_{p}$*myo-2::gfp* can slow development and this could potentially have implications for emodepside sensitivity (Bull *et al* 2007).

Before assays were conducted on the transgenic *slo-1*(*js379*) carrying either pBK3.1 or pBK4.1, the presence of these vectors was confirmed using PCR. Figure 6.03 shows maps for these plasmids as well as the PCR products obtained using DNA extracted from transgenic worms, the vector and *N2* worms.

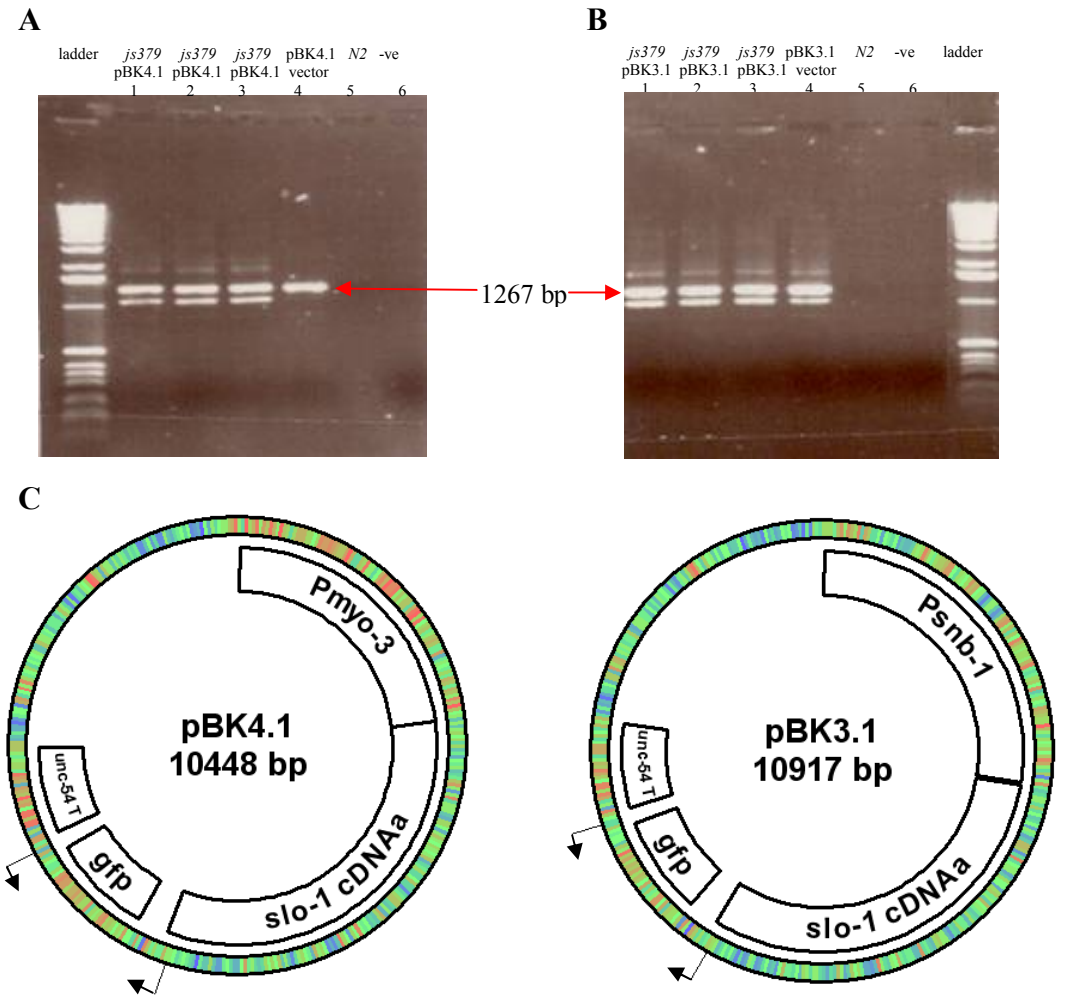


**Figure 6.03. Confirmation of presence of vectors pBK3.1 and pBK4.1 by PCR. A** and **B** shows 1267 bp PCR amplified fragments from the vectors pBK4.1 and pBK3.1, respectively. Primers complementary for sequences in the *slo-1* cDNA and terminator sequence of these vectors were used. **A)** Template DNA for this reaction was taken from 3 populations of *slo-1*(*js379*) transformed with pBK4.1 (1, 2 and 3), pBK4.1 (4) and *N2* (5). Number 6 is a $H_2O$ control. **B)** Template DNA for this reaction was taken from populations of *slo-1*(*js379*) transformed with pBK3.1 (1, 2 and 3), pBK3.1 (4) and *N2* (5). Number 6 is a $H_2O$ control. **C)** Shows vector maps for pBK4.1 and pBK3.1. The PCR amplified regions are marked with arrow heads.

The vectors were detected in the transgenic animals using primers within the *slo-1* cDNA and in the *unc-54* terminator sequence contained in these vectors (see vector maps figure 6.03). DNA was extracted from three populations of worms expressing the $_{p}$*myo-2::gfp* marker for both pBK3.1 and pBK4.1 stable lines. The expected size band produced using the primers marked in figure 6.03 is 1267 bp. Figure 6.03 A) shows that the expected 1267 bp band is produced with DNA extracted from stable lines carrying pBK4.1 and the pBK4.1 vector but is not produced with control *N2* DNA or negative water control. Figure 6.03 B) shows that the expected 1267 bp band is produced with DNA extracted from stable lines carrying pBK3.1

and the pBK3.1 vector but is not produced with control *N2* DNA or negative water control. A *slo-1*(*js379*) expressing $_{p}$*myo-2::gfp* control was also found not to produce the 1267 bp band in this reaction (see appendix). These PCRs demonstrate the presence of the pBK3.1 and pBK4.1 vectors in the $_{p}$*myo-2::gfp* expressing stable lines.

## 6.03 Neuronal expression of *slo-1* restores emodepside sensitivity to *slo-1*(*js379*)

Locomotion assays were conducted on worms expressing *slo-1* cDNAa in neurons. L4 *slo-1*(*js379*), *N2* and *slo-1*(*js379*) expressing *slo-1*(+) in the neurons were picked to 1 nM, 10 nM, 100 nM, 1 µM and 10 µM emodepside containing NGM plates for 24 hours on food. They were also picked to 0.5 % ethanol vehicle NGM plates for 24 hours on food. After 24 hours the young adults were picked to an un-seeded NGM plate for one minute in order to remove any OP50. They were then picked to an un-seeded assay plate and left to recover for one minute. Finally body bends were counted for one minute. Figure 6.04 shows a dose response curve for these animals.

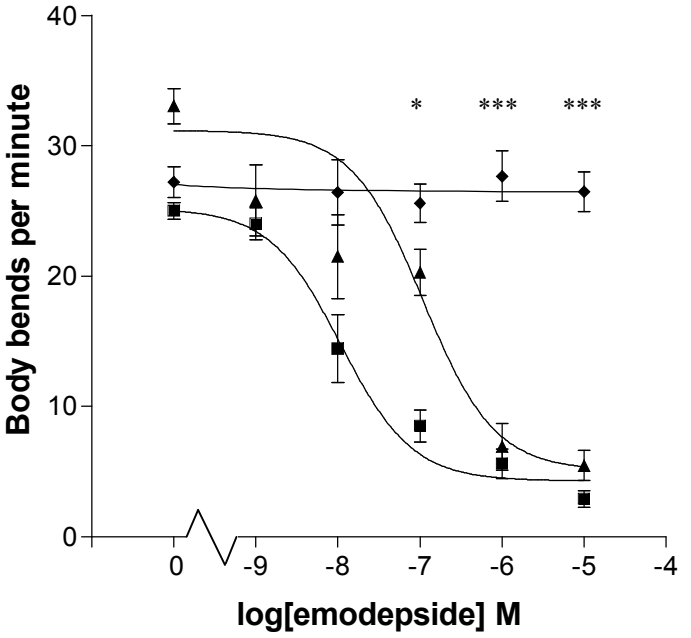


**Figure 6.04. *slo-1* neuronal rescue of emodepside sensitivity.** Dose response curves for emodepside on *N2* (■), *slo-1*(*js379*) (♦) and *slo-1*(*js379*) expressing *slo-1*(+) from the neuron specific promoter $_{p}$*snb-1* (▲). For each point n is between 6 and 32. Each point is the mean ± S.E.Mean. * indicates $P<0.05$ and *** indicates $P<0.001$. Comparisons are made between *slo-1*(*js379*) (♦) and *slo-1*(*js379*) expressing *slo-1*(+) from the neuron specific promoter $_{p}$*snb-1* (▲).

The dose response for *slo-1*(*js379*) expressing *slo-1*(+) in the neurons is pooled data from two independent lines. *N2* and *slo-1*(*js379*) controls were run in parallel with the transgenic lines. The $IC_{50}$ for *N2* in this assay is 11 nM. *slo-1*(*js379*) are uninhibited at all concentrations of emodepside. The $IC_{50}$ for *slo-1*(*js379*) expressing *slo-1*(+) in the neurons is 109 nM. *slo-1*(*js379*) expressing *slo-1*(+) in the neurons is significantly inhibited by 100 nM, 1 μM and 10 μM emodepside compared to *slo-1*(*js379*) with $P<0.05$, $P<0.001$ and $P<0.001$, respectively. *N2* is significantly more sensitive to emodepside than *slo-1*(*js379*) expressing *slo-1*(+) in the neurons at 100 nM with $P<0.001$.

A different phenotype to that of *N2* was observed in the *slo-1*(*js379*) expressing *slo-1*(+) in the neurons when on 10 μM emodepside. The photographs in figure 6.05 show these phenotypes. On 10 μM emodepside *slo-1*(*js379*) has a normal sinusoidal pattern of movement (Figure 6.05 A). *N2* looses the ability to move in a normal sinusoidal manner as emodepside causes a flaccid paralysis (Figure 6.05 B). *slo-1*(*js379*) expressing *slo-1*(+) in the neurons displayed a coiling phenotype in many cases (Figure 6.05 C).

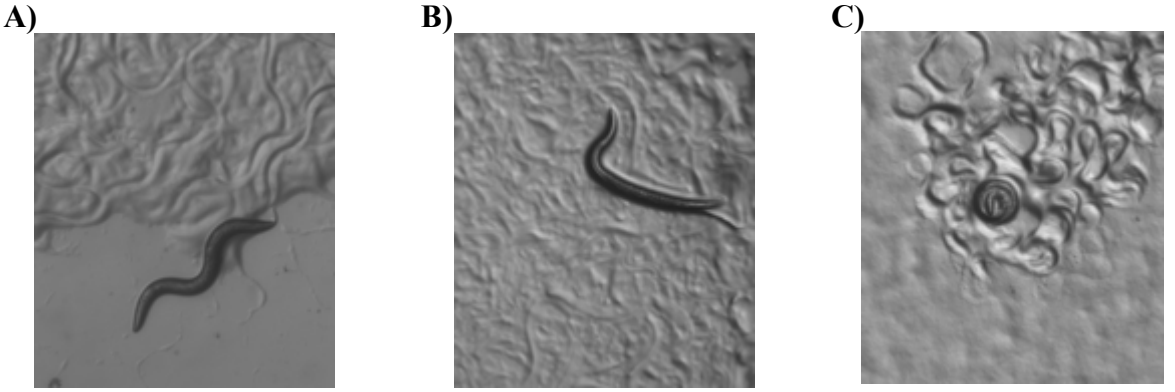


**Figure 6.05. Neuronal rescue phenotype on emodepside.** Strain phenotypes on 10 μM emodepside. **A)** *slo-1*(*js379*) on 10 μM emodepside. **B)** *N2* on 10 μM emodepside. **C)** *slo-1*(*js379*) expressing *slo-1*(+) in the neurons displays a coiling behaviour not observed in *N2* or *slo-1*(*js379*) on 10 μM emodepside.

## 6.04 Body wall muscle expression of *slo-1* restores emodepside sensitivity

Locomotion assays were conducted on worms expressing *slo-1* cDNAa in body wall muscle. L4 *slo-1*(*js379*), *N2* and *slo-1*(*js379*) expressing *slo-1*(+) in the body wall muscle were picked to 1 nM, 10 nM, 100 nM, 1 µM and 10 µM emodepside containing NGM plates for 24 hours on food. They were also picked to 0.5 % ethanol vehicle NGM plates for 24 hours on food. After 24 hours the young adults were picked to an un-seeded NGM plate for one minute in order to remove any OP50. They were then picked to an un-seeded assay plate and left to recover for one minute. Finally body bends were counted for one minute. Figure 6.06 shows a dose response curve for these animals.

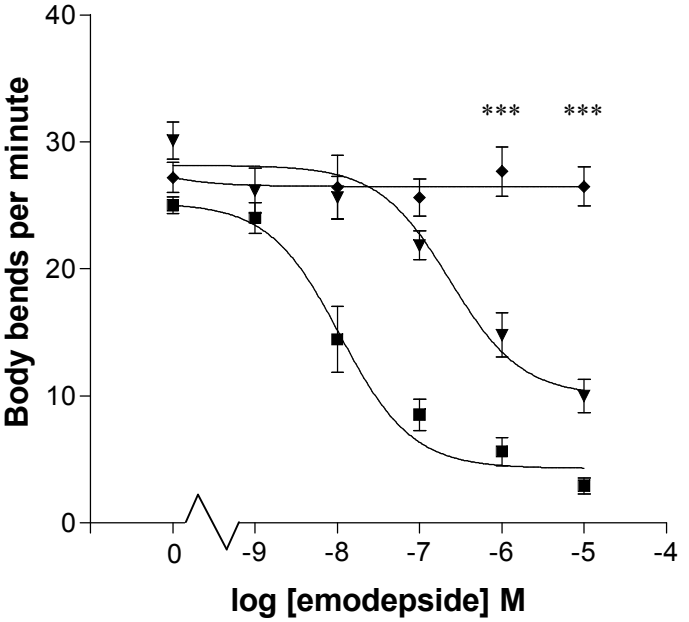


**Figure 6.06. *slo-1* body wall muscle rescue of emodepside sensitivity.** Dose response curves for emodepside on *N2* (■), *slo-1*(*js379*) (♦) and *slo-1*(*js379*) expressing *slo-1*(+) from the body wall muscle specific promoter $_{p}$*myo-3* (▼). For each point n is between 6 and 34. Each point is the mean ± S.E.Mean. *** indicates $P<0.001$. Comparisons are made between *slo-1*(*js379*) (♦) and *slo-1*(*js379*) expressing *slo-1*(+) from the body wall muscle specific promoter myo-3 (▼).

The dose response for *slo-1*(*js379*) expressing *slo-1*(+) in the body wall muscle is pooled data from two independent lines. *N2* and *slo-1*(*js379*) controls were run in parallel with the transgenic lines (controls same as in figure 6.05). The $IC_{50}$ for *N2* in this assay is 11 nM. *slo-1*(*js379*) are uninhibited at all concentrations of emodepside. The $IC_{50}$ for *slo-1*(*js379*) expressing *slo-1*(+) in the body wall muscle is 234 nM. *slo-1*(*js379*) expressing *slo-1*(+) in the

body wall muscle is significantly inhibited by 1 µM and 10 µM emodepside compared to *slo-1*(*js379*) with *P<0.001*. *N2* is significantly more sensitive to emodepside than *slo-1*(*js379*) expressing *slo-1*(+) in the neurons at 100 nM with *P*<0.001. *slo-1*(*js379*) expressing *slo-1*(+) in the body muscle displayed a phenotype similar to that of *N2* on 10 µM emodepside. No coiling phenotype was observed unlike with expression of *slo-1*(+) in the neurons.

## 6.05 Expression of *slo-1*(+) in neurons and body wall muscle restores emodepside sensitivity

Locomotion assays were conducted on worms expressing *slo-1* cDNAa in body wall muscle and neurons. L4 *slo-1*(*js379*), *N2* and *slo-1*(*js379*) expressing *slo-1*(+) in the body wall muscle and neurons were picked to 1 µM emodepside containing NGM plates for 24 hours on food. They were also picked to 0.5 % ethanol vehicle NGM plates. After 24 hours the young adults were picked to an un-seeded NGM plate for one minute in order to remove any OP50. They were then picked to an un-seeded assay plate and left to recover for one minute. Finally body bends were counted for one minute. Figure 6.07 shows the response of these animals to emodepside.

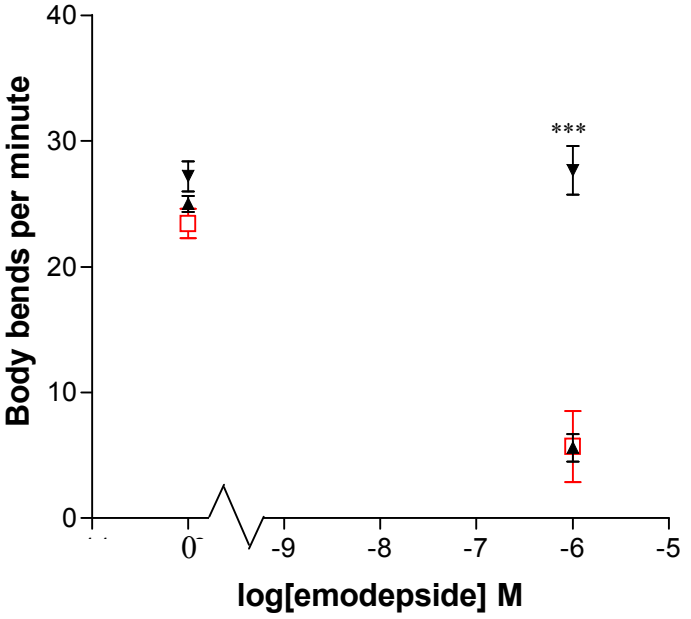


**Figure 6.07. *slo-1* body wall muscle and neuron rescue of emodepside sensitivity.** Response to 1 µM emodepside of *N2* (□), *slo-1*(*js379*) (♦) and *slo-1*(*js379*) expressing *slo-1*(+) from the body wall muscle specific promoter $_{p}$*myo-3* and neuron specific promoter $_{p}$*snb-1* (▼). For each point n is between 7 and 34. Each point is the mean ± S.E.Mean. *** indicates *P*<0.001. Comparisons are made between *slo-1*(*js379*) (♦) and *slo-1*(*js379*) expressing *slo-1*(+) from the body wall muscle specific promoter $_{p}$*myo-3* and neuron specific promoter $_{p}$*snb-1* (▼).

*slo-1*(*js379*) expressing *slo-1*(+) in the body wall muscle and neurons is significantly inhibited by 1 µM emodepside compared to *slo-1*(*js379*) with $P<0.001$. The sensitivity of *slo-1*(*js379*) expressing *slo-1*(+) in the body wall muscle and neurons is not significantly different to *N2* on 1 µM emodepside. However, *slo-1*(*js379*) expressing *slo-1*(+) in the body wall muscle and neurons did not resemble *N2* when exposed to 1 µM emodepside but displayed the coiling phenotype observed in *slo-1*(*js379*) expressing *slo-1*(+) in the neurons. The phenotype produced by expression of *slo-1*(+) in the neurons has a dominant effect.

## 6.06 Aldicarb sensitivity assays

The ACE inhibitor aldicarb was used to investigate if emodepside affects ACh release in *N2* and *slo-1*(*js379*). Aldicarb causes hyper-contraction of *C. elegans* body wall muscle which results in paralysis. It has been previously shown that *slo-1*(*js379*) are aldicarb hyper-sensitive (Wang *et al* 2005). In order to investigate the effect of emodepside on aldicarb sensitivity of *N2* and *slo-1*(*js379*), their rate of paralysis on 0.5 mM aldicarb was assayed. L4 worms were selected 24 hour before the assay. The assay was performed blind. Young adults were transferred to 0.5 mM aldicarb containing NGM plates seeded with OP50. 15 worms were placed on each plate. The number of paralysed worms was recorded every 30 minutes. Multiple trials were conducted for each strain. One trial refers to a single plate of worms assayed. Experiments were run with parallel controls. Data from individual experiments was pooled.

## 6.07 *slo-1*(*js379*) is aldicarb hypersensitive

*N2* and *slo-1*(*js379*) were assayed in the way described above. Figure 6.08 shows the average percentage of animals paralysed by 0.5 mM aldicarb from multiple trials. Each trial is for 15 animals. *slo-1*(*js379*) are paralysed by 0.5 mM aldicarb at a quicker rate that *N2*. A significantly higher proportion of *slo-1*(*js379*) are paralysed after 60, 90 and 120 minutes on 0.5 mM aldicarb ($P<0.001$). This result is similar to what was observed by Wang *et al* (2001).

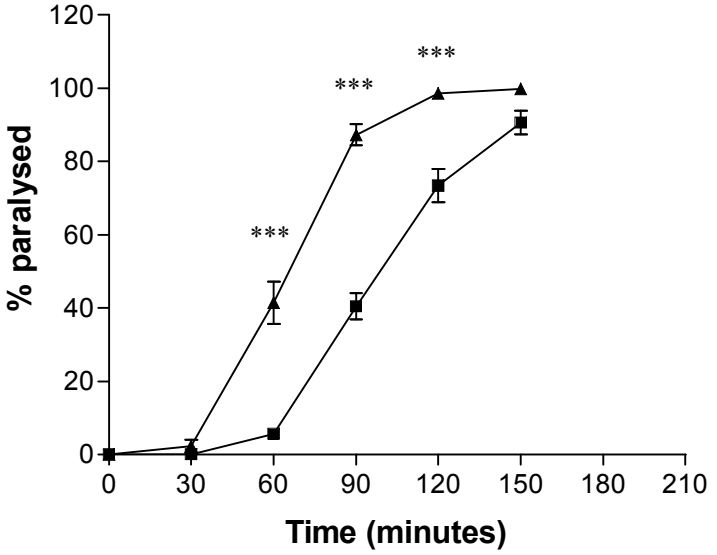


**Figure 6.08. *slo-1*(*js379*) aldicarb sensitivity.** Time until paralysis on 0.5 mM aldicarb for *N2* (■) and *js379* (▲). % paralysed is the average proportion of paralysed animals from multiple trials. Each point is the mean ± S.E.Mean of 16 trials of 15 animals for *N2* and the mean ± S.E.Mean of 16 trials of 15 animals for *slo-1*(*js379*). *** indicates $P<0.001$ compared to *N2* control.

## 6.08 Emodepside decreases *N2* sensitivity to aldicarb

To test whether emodepside affects ACh release, the aldicarb sensitivity of emodepside treated *N2* worms was tested. If emodepside acts to increase ACh release, an increase in aldicarb sensitivity would be predicted. L4 worms were placed on NGM plates containing either sub-paralysing concentrations of emodepside (10 nM or 100 nM) or 0.5 % ethanol vehicle. After 24 hours exposure, treated and un-treated worms were transferred to seeded 0.5 mM aldicarb containing NGM plates, that also contained either emodepside (10 nM or 100 nM) or 0.5 % ethanol vehicle. Emodepside treated worms were also assayed on emodepside NGM plates to confirm the concentrations used were sub-paralysing. The number of paralysed worms was recorded every 30 minutes. Experiments were run with parallel controls. Data from individual experiments was pooled.

Figure 6.09 shows the average percentage of animals paralysed by 0.5 mM aldicarb from multiple trials. *N2* animals pre-treated with 100 nM emodepside paralyse at a significantly slower rate than *N2* animals pre-treated with vehicle (0.5 % ethanol) on 0.5 mM aldicarb. The

percentage of paralysed animals is significantly higher in the control group at 90, 150, 180 and 210 minutes with $P<0.001$ and at 120 minutes with $P<0.01$. The rate of paralysis of *N2* with vehicle (0.5 % ethanol) pre-treatment is comparable to that of *N2* without vehicle pre-treatment (compare to *N2* in figure 6.08), suggesting this concentration of ethanol does not impact on aldicarb sensitivity. *N2* animals pre-treated with 100 nM emodepside and assayed off aldicarb and on 100 nM emodepside did not paralyse, demonstrating that 100 nM is a sub-paralysing concentration of emodepside on *N2*.

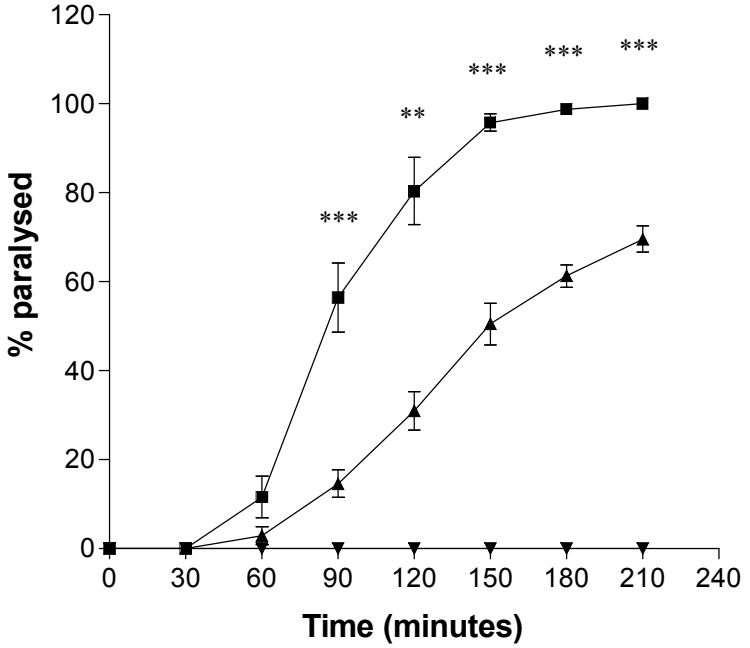


**Figure 6.09. 100 nM emodepside affects *N2* aldicarb sensitivity.** Time until paralysis on 0.5 mM aldicarb**.** *N2* on 0.5 mM aldicarb without pre-exposure to emodepside (■), *N2* on 0.5 mM aldicarb with pre-exposure to 100 nM emodepside (▲) and *N2* without exposure to 0.5 mM aldicarb but with pre-exposure to 100 nM emodepside (▼). Each point is the mean ± S.E.Mean of 8 trials of 15 animals (■), 7 trials of 15 animals (▲) and 3 trials of 15 animals (▼). ** indicates $P<0.01$ and *** indicates $P<0.001$.

Similar effects were observed when pre-treating with 10 nM emodepside (figure 6.10). *N2* animals pre-treated with 10 nM emodepside paralyse at a significantly slower rate than *N2* animals pre-treated with vehicle (0.5 % ethanol) on 0.5 mM aldicarb. The percentage of paralysed animals is significantly higher in the control group at 90, 120 and 150 minutes with $P<0.05$ and at 180 minutes with $P<0.01$.

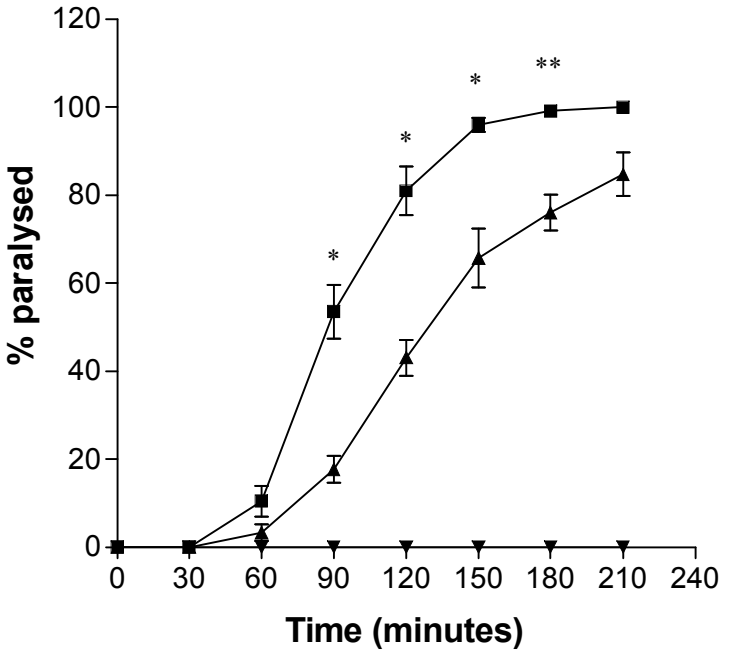


**Figure 6.10. 10 nM emodepside affects *N2* aldicarb sensitivity.** Time until paralysis on 0.5 mM aldicarb. *N2* on 0.5 mM aldicarb without pre-exposure to emodepside (■), *N2* on 0.5 mM aldicarb with pre-exposure to 10 nM emodepside (▲) and *N2* without exposure to 0.5 mM aldicarb but with pre-exposure to 10 nM emodepside (▼). Each point is the mean ± S.E.Mean of 8 trials of 15 animals (■), 4 trials of 15 animals (▲) and 3 trials of 15 animals (▼). * indicates $P<0.05$ and ** indicates $P<0.01$.

It was observed that worms co-exposed to 100 nM emodepside and 0.5 mM aldicarb had a different morphology to worms co-exposed to vehicle (0.5 % ethanol) and 0.5 mM aldicarb. Aldicarb causes hyper-contraction of body wall muscle, resulting in a shortening of body length. Figure 6.11 shows photographs of *N2* worms co-exposed to emodepside and aldicarb or vehicle and aldicarb after 80 minutes. Vehicle and aldicarb co-exposed worms display a shortening of body length to a greater extent than emodepside and aldicarb co-exposed worms. These results indicate that treatment with emodepside results in a decrease ACh release. In emodepside treated worms on aldicarb, it seems likely that the build up of ACh in the synaptic cleft is slowed. The onset of paralysis and the hyper-contracted phenotype due to aldicarb treatment is therefore slowed.

**A)** **B)**

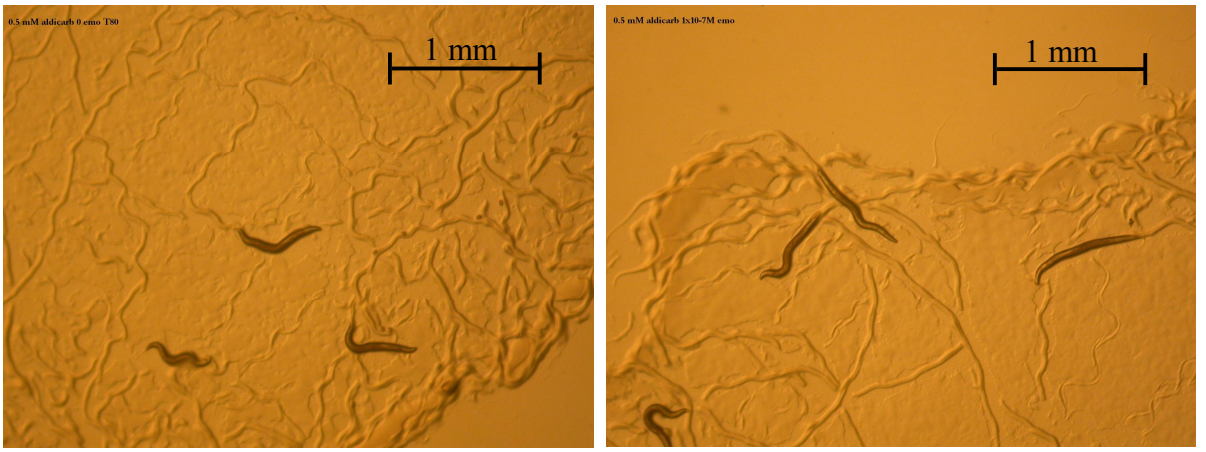


**Figure 6.11. Emodepside affects the onset of aldicarb induce changes in morphology.** Effect of 100 nM emodepside and 0.5 mM aldicarb co-exposure on body length. **A)** *N2* vehicle (0.5 % ethanol) and aldicarb (0.5 mM) co-exposure after 80 minutes, **B)** *N2* emodepside (0100 nM) and aldicarb (0.5 mM) co-exposure after 80 minutes.

## 6.09 Emodepside does not affect *slo-1*(*js379*) aldicarb sensitivity

Assays were conducted to determine if the emodepside induced reduction in aldicarb sensitivity observed in *N2* also occurs in *slo-1*(*js379*). L4 worms were placed on NGM plates containing either a sub-paralysing concentration of emodepside (100 nM) or 0.5 % ethanol vehicle. After 24 hours exposure, treated and un-treated worms were transferred to seeded 0.5 mM aldicarb containing NGM plates, that also contained either emodepside (100 nM) or 0.5 % ethanol vehicle. Emodepside treated worms were also assayed on emodepside NGM plates to confirm the concentrations used were sub-paralysing. The number of paralysed worms was recorded every 30 minutes. Experiments were run with parallel controls. Data from individual experiments was pooled.

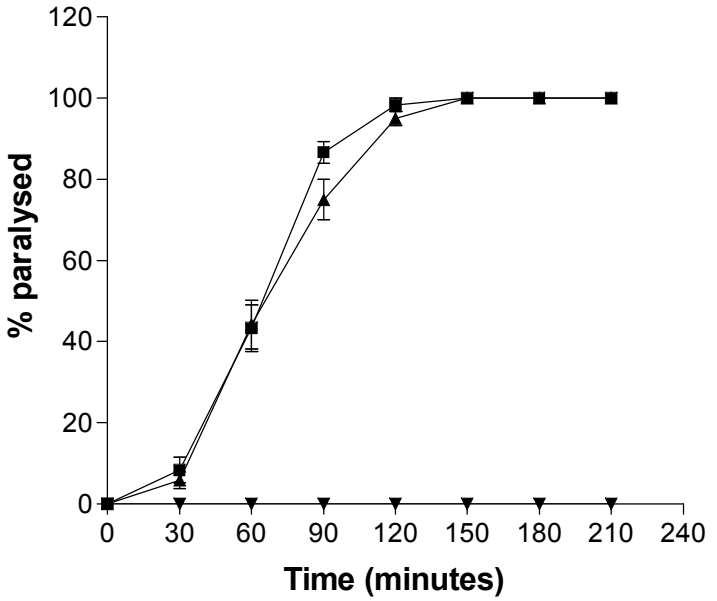


**Figure 6.12. *slo-1*(*js379*) aldicarb sensitivity is unaffected by 100 nM emodepside.** Time until paralysis on 0.5 mM aldicarb. *slo-1*(*js379*) on 0.5 mM aldicarb without pre-exposure to 100 nM emodepside (■), *slo-1*(*js379*) on 0.5 mM aldicarb with pre-exposure to 100 nM emodepside (▲) and *slo-1*(*js379*) without exposure to 0.5 mM aldicarb but with pre-exposure to 100 nM emodepside (▼). Each point is the mean ± S.E.Mean of 4 trials of 15 animals (■), 4 trials of 15 animals (▲) and 3 trials of 15 animals (▼).

Figure 6.12 shows the average percentage of animals paralysed by 0.5 mM aldicarb from multiple trials. *slo-1*(*js379*) animals pre-treated with 100 nM emodepside paralysed at the same rate as *slo-1*(*js379*) animals pre-treated with vehicle (0.5 % ethanol) on 0.5 mM aldicarb. This demonstrates that *slo-1* is required for emodepside's effect on aldicarb sensitivity. *slo-1*(*js379*) animals pre-treated with 100 nM emodepside and assayed off aldicarb and on 100 nM emodepside did not paralyse, demonstrating that 100 nM is a sub-paralysing concentration of emodepside on *slo-1*(*js379*).

The fact that SLO-1 is required for emodepside sensitivity and for emodepside's effects on aldicarb sensitivity suggests that the mechanisms involved are the same. This therefore indicates that emodepside causes paralysis through a reduction in cell excitability.

## 6.10 *slo-1*(*js379*) expressing *slo-1*(+) in neurons are aldicarb hypersensitive

Expressing *slo-1*(+) in the neurons of *slo-1*(*js379*) restores emodepside sensitivity, although in a way not resembling *N2*. The aldicarb hypersensitivity of *slo-1*(*js379*) indicates that SLO-1 negatively regulates ACh release. The emodepside induced reduction in aldicarb sensitivity observed in *N2* does not occur in *slo-1*(*js379*). This suggests that emodepside leads to a reduction in ACh release and that it requires SLO-1 for this. Wang *et al* did not demonstrate rescue of the aldicarb hyper-sensitivity observed in *slo-1*(*js379*). To further understand the role of SLO-1 in ACh release and in emodepside's mode of action, the aldicarb sensitivity of *slo-1*(*js379*) expressing *slo-1*(+) in neurons was investigated.

24 hours post L4 worms were assayed in the way previously described. Figure 6.13 shows the average percentage of animals paralysed by 0.5 mM aldicarb from multiple trials. *slo-1*(*js379*) are paralysed by 0.5 mM aldicarb at a quicker rate that *N2* as previously shown. A significantly higher proportion of *slo-1*(*js379*) are paralysed after 60 and 120 minutes $P<0.01$ and 90 minutes $P<0.001$ on 0.5 mM aldicarb compared with *N2*. The rate of paralysis on 0.5 mM aldicarb of *slo-1*(*js379*) expressing *slo-1*(+) in the neurons is not significantly different from that of *slo-1*(*js379*).

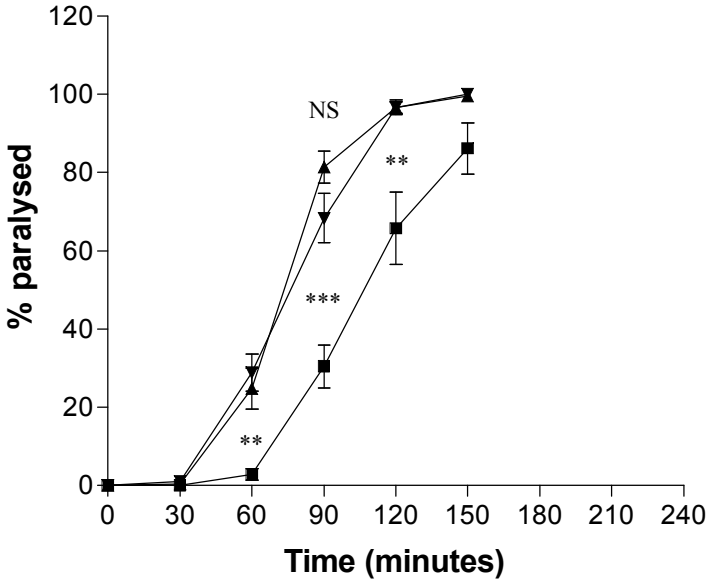


**Figure 6.13. *slo-1* neuronal expression does not rescue aldicarb hyper-sensitivity.** Time until paralysis on 0.5 mM aldicarb. *N2* (■), *slo-1*(*js379*) (▲), and *slo-1*(*js379*) expressing *slo-1*(+) from the neuron specific promoter snb-1 (▼). Each point is the mean ± S.E.Mean of 7 trials of 15 animals (■), 7 trials of 15 animals (▲) and 6 trials of 15 animals (▼). ** indicates $P<0.01$ and *** indicates $P<0.001$. Comparisons marked are between *slo-1*(*js379*) and *slo-1*(*js379*) expressing *slo-1*(+) in neurons (above) and *slo-1*(*js379*) and *N2* (below).

Wang *et al* (2001) demonstrated that *slo-1*(*js379*) has an increased duration, amplitude and frequency of EPSP indicating it has an increased transmitter release. The aldicarb hypersensitivity of *slo-1*(*js379*) also indicates it has increased ACh release. Rescue of the *unc-64*(*e246*) lethargic phenotype by *slo-1*(*js379*) was reversed when *slo-1*(+) was expressed in the neurons, but not in the muscle, of *unc-64*(*e246*); *slo-1*(*js379*) double mutants. This indicates that the reduced neurotransmitter release in *unc-64*(*e246*) is reversed by the loss of *slo-1* in the neurons. However, it was not directly shown that loss of *slo-1* in the neurons causes an increase in transmitter release. Rescue of the increase EPSCs duration, amplitude and frequency or aldicarb hypersensitivity in *slo-1* loss of function mutants was not demonstrated by Wang *et al* (2001). The fact that expressing *slo-1*(+) in the neurons of *slo-1*(*js379*) does not rescue aldicarb hypersensitivity may indicate that *slo-1* in the body wall muscle may play a role in *slo-1*(*js379*) aldicarb hypersensitivity. Loss of *slo-1* in the body wall muscle could potentially result in or contribute to increased EPSC duration, amplitude and frequency and aldicarb hypersensitivity.

## 6.11 *slo-1*(*js379*) expressing *slo-1*(+) in body wall muscle are aldicarb hypersensitive

*slo-1*(*js379*) expressing *slo-1*(+) in the body wall muscle were tested in the aldicarb assay in order to investigate the role of muscle cell excitability in aldicarb sensitivity. 24 hours post L4 worms were assayed in the way previously described. Figure 6.14 shows the average percentage of animals paralysed by 0.5 mM aldicarb from multiple trials. *slo-1*(*js379*) are paralysed by 0.5 mM aldicarb at a quicker rate that *N2* as previously shown. A significantly higher proportion of *slo-1*(*js379*) are paralysed after 60, 90 and 120 minutes $P<0.001$ on 0.5 mM aldicarb compared with *N2*. The rate of paralysis on 0.5 mM aldicarb of *slo-1*(*js379*) expressing *slo-1*(+) in the body wall muscle is significantly different from that of *slo-1*(*js379*) at 60 minutes $P<0.05$.

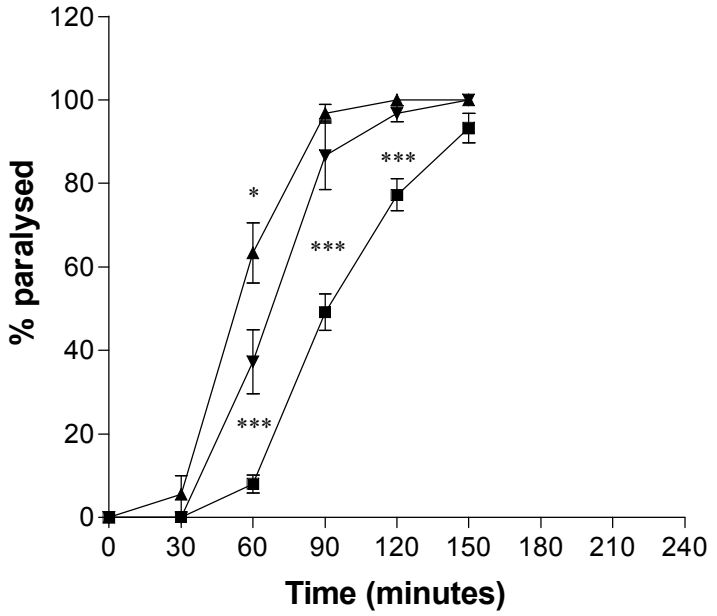


**Figure 6.14. *slo-1* body wall muscle expression does not rescue aldicarb hypersensitivity.** Time until paralysis on 0.5 mM aldicarb. *N2* (■), *slo-1*(*js379*) (▲), and *slo-1*(*js379*) expressing *slo-1*(+) from the body wall muscle specific promoter myo-3 (▼). Each point is the mean ± S.E.Mean of 6 trials of 15 animals (■), 6 trials of 15 animals (▲) and 4 trials of 15 animals (▼). * indicates $P<0.05$ and *** indicates $P<0.001$.

The slight but significant decrease in aldicarb sensitivity of *slo-1*(*js379*) expressing *slo-1*(+) in the body wall muscle compared with *slo-1*(*js379*) indicates that aldicarb sensitivity is affected by the presence of *slo-1* in the muscle.

The nature of the aldicarb hypersensitivity of *slo-1*(*js379*) is subtle. It may be that the lack of rescue observed when expressing *slo-1*(+) in the neurons and the minimal rescue observed when expressing *slo-1*(+) in the body wall muscle is due to the non-native expression of *slo-1*(+). These results do however indicate that aldicarb sensitivity can be affected by SLO-1 in the body wall muscle. This suggests that the reduced aldicarb sensitivity of emodepside treated worms could stem from its effects on SLO-1 neurons or body wall muscle. The effect of the nicotinic ACh receptor agonist levamisole on emodepside sensitivity has therefore been investigated.

## 6.12 Emodepside increases levamisole sensitivity

Levamisole is a nicotinic ACh receptor agonist. It causes spastic paralysis of nematode body wall muscle (Martin *et al* 2005). Levamisole was used to investigate the effect of emodepside on muscle cell excitability. The sensitivity of *N2* pre-treated with 100 nM emodepside or vehicle (0.5 % ethanol) to 100 µM levamisole was tested. L4 worms were placed on NGM plates containing either a sub-paralysing concentration of emodepside (100 nM) or 0.5 % ethanol vehicle. After 24 hours exposure, treated and un-treated worms were transferred to seeded 100 µM levamisole containing NGM plates, that also contained either emodepside (100 nM) or 0.5 % ethanol vehicle. Emodepside treated worms were also assayed on emodepside NGM plates to confirm the concentrations used were sub-paralysing. The number of paralysed worms was recorded every 30 minutes. Experiments were run with parallel controls. Data from individual experiments were pooled.

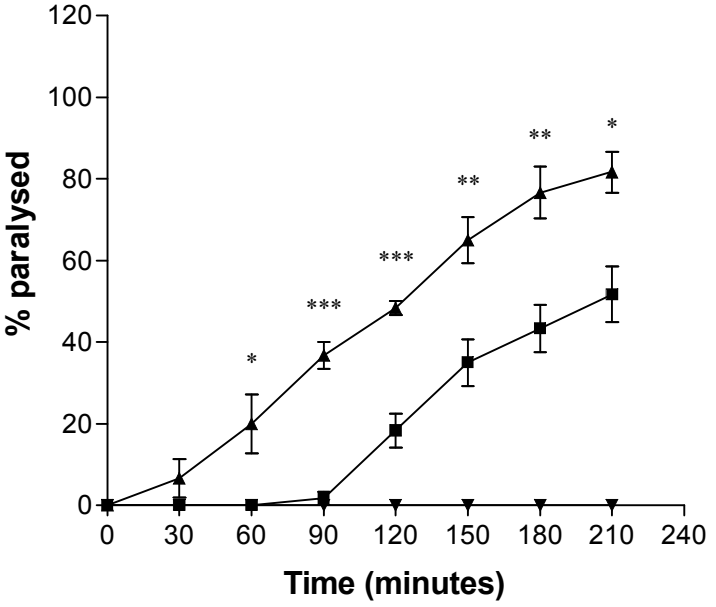


**Figure 6.15. 100 nM emodepside affects *N2* levamisole sensitivity.** Time until paralysis on 100 µM levamisole**.** *N2* on 100 µM levamisole without pre-exposure to emodepside (■), *N2* on 100 µM levamisole with pre-exposure to 100 nM emodepside (▲) and *N2* without exposure to 100 µM levamisole but with pre-exposure to 100 nM emodepside (▼). Each point is the mean ± S.E.Mean of 4 trials of 15 animals (■), 4 trials of 15 animals (▲) and 3 trials of 15 animals (▼). * indicates $P<0.05$, ** indicates $P<0.01$ and *** indicates $P<0.001$.

Figure 6.15 shows the average percentage of animals paralysed by 100 µM levamisole from four trials. *N2* animals pre-treated with 100 nM emodepside paralyse at a significantly faster rate than *N2* animals pre-treated with vehicle (0.5 % ethanol) on 100 µM levamisole. The

percentage of paralysed animals is significantly higher in the emodepside treatment group at 60 and 210 minutes with $P<0.05$, 150 and 180 minutes with $P<0.01$ and 90 and 120 minutes with $P<0.001$. *N2* animals pre-treated with 100 nM emodepside and assayed off aldicarb and on 100 nM emodepside did not paralyse, demonstrating that 100 nM is a sub-paralysing concentration of emodepside on *N2*.

This result is surprising as levamisole is thought to cause spastic paralysis due to increased excitability. If emodepside acts to reduce muscle cell excitability, it would be expected that pre-treated worms would have reduced levamisole sensitivity. If emodepside acts to reduce excitability only in neurons it might be expected that sensitivity to levamisole would remain the same. In order to better understand this result, the sensitivity of *slo-1*(*js379*) to levamisole was investigated.

## 6.13 *slo-1*(*js379*) has reduced levamisole sensitivity

L4 worms were selected 24 hour before the assay. The assay was performed blind. Young adults were transferred to 100 µM levamisole containing NGM plates seeded with OP50. 15 to 20 worms were placed on each plate. The number of paralysed worms was recorded every 30 minutes. Four trials were conducted for each strain. Experiments were run with parallel controls. Figure 6.16 shows the average percentage of animals paralysed by 100 µM levamisole for four trials. *slo-1*(*js379*) are paralysed by 100 µM levamisole at a significantly slower rate that *N2*. A significantly lower proportion of *slo-1*(*js379*) are paralysed after 60, 90, 120, 150 and 180 minutes on 100 µM levamisole with $P<0.001$.

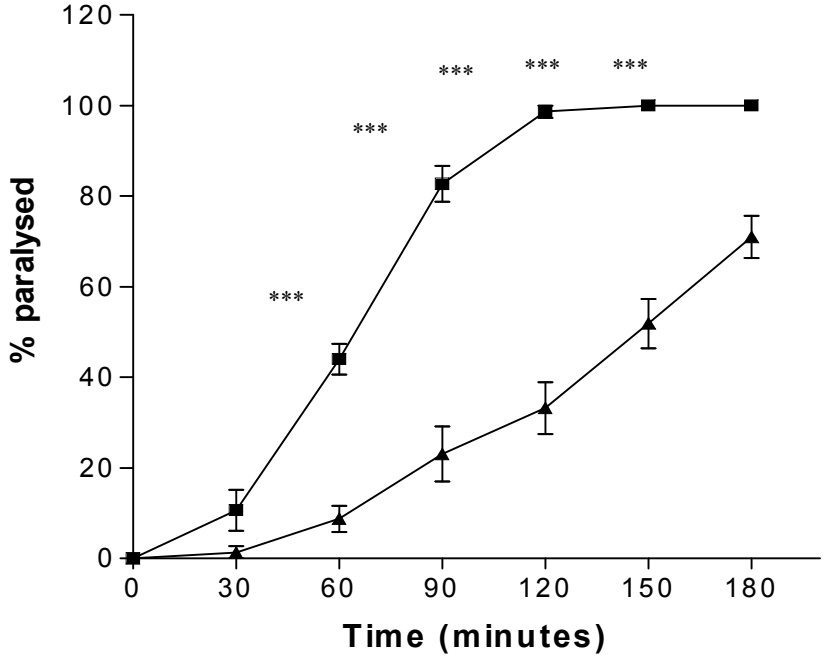


**Figure 6.16. *slo-1*(*js379*) levamisole sensitivity.** Time until paralysis on 100 μM levamisole**.** *N2* on 100 μM levamisole (■) and *slo-1*(*js379*) on 100 μM levamisole (▲). Each point is the mean ± S.E.Mean of 4 trials. *** indicates $P<0.001$.

## 6.14 Discussion

Expression of *slo-1*(+) in either the body wall muscle or neurons of *slo-1*(*js379*) results in rescue of emodepside's inhibitory actions on locomotion. As well as confirming that it is *slo-1* that is required for emodepside sensitivity, it also demonstrates that emodepside can exert effects through SLO-1 both in the body wall muscle and the neurons. Endogenous expression of *slo-1* has been characterised using both immuno-staining and expression of *slo-1*::*gfp*. Wang *et al* (2001) demonstrated that *slo-1* is expressed in the nerve ring, nerve cords, body wall muscle and vulval muscle. This was done using both a mouse polyclonal antibody and a *slo-1::gfp* reporter. Carre-Pierrat *et al* (2006) found expression of *slo-1* in body wall muscle using a *slo-1::gfp* reporter but found the antibody used by Wang *et al* (2001) to be non-specific. Expression of *slo-1* has also been found in most of the pharyngeal neurons, again using a *slo-1::gfp* reporter (Chiang *et al* 2006).

The rescue observed in *slo-1*(*js379*) expressing *slo-1*(+) in the body wall muscle and neurons is consistent with the expression pattern of *slo-1* in *N2*. The ability of *slo-1*(+) to rescue emodepside sensitivity in both tissues shows that it can act through SLO-1 in body wall muscle and neurons to inhibit locomotion. Neither *slo-1*(*js379*) expressing *slo-1*(+) in body wall muscle nor in neurons resulted in complete rescue of emodepside sensitivity. As it seems likely that SLO-1 plays a role in both the body wall muscle and neurons in emodepside's inhibitory effects on locomotion, it is not surprising that expression in one or the other does not completely rescue the phenotype. However, when *slo-1*(+) was expressed in body wall muscle and neurons simultaneously the rescue still did not resemble *N2*. The coiling phenotype observed with the neuronal rescue was still present.

There are several possible explanations for this incomplete rescue. Genes in extra-chromosomal arrays can have a patchy expression across the tissue in which it is driven (Stinchcomb *et al* 1985). This is evident with the *gfp* transfection marker, which sometimes is present throughout the pharyngeal muscle and at other times has a patchy expression. Mosaic expression of *slo-1* could result in incomplete rescue of emodepside's effects. It is also possible that the use of a single *slo-1* splice variant (cDNAa) in these rescue experiments prevents full rescue of emodepside's effects. Another possibility is that the use of the *snb-1* and *myo-3* promoters, rather than the endogenous *slo-1* promoter, results in a different level or

pattern of expression. This seems most likely as expression of *slo-1*(+) (cDNAa) using the endogenous *slo-1* promoter resulted in complete rescue of emodepside effects on locomotion (Personal communication with Nina Krüger).

Expressing *slo-1*(+) in the body wall muscle or neurons of *slo-1*(*js379*) results in a quantitatively similar rescue of emodepside's inhibitory effect on locomotion, with $IC_{50}$ of 234 nM and 109 nM, respectively. There are however qualitative differences between these strains when exposed to emodepside. *slo-1*(*js379*) expressing *slo-1*(+) in the body wall muscle exhibits a phenotype similar to that of *N2*. Emodepside causes a flaccid paralysis. The worm loses its sinusoidal shape of movement and extends its anterior forward by propelling itself through shallow wave-like movement of its posterior. Expression of *slo-1*(+) in the neurons results in a tight coiling not observed in *N2* animals when on 10 μM emodepside. Using the pan-neuronal promoter *snb-1* (Nonet 1999) may have resulted in expression of *slo-1* in neurons that do not usually express it. Imbalances in neurotransmitter release have been shown to result in coiling phenotype (Walthall *et al* 1993). It is possible that an emodepside-induced activation of SLO-1 in neurons that do not normally express SLO-1 causes an imbalance in neurotransmitter release and a coiling of the worm.

The rescue of emodepside sensitivity through expression of *slo-1* in either body wall muscle or neurons suggests SLO-1 is important for emodepside's effects in both these tissues. The emodepside resistance in *slo-1* loss-of-function mutants suggests that emodepside causes an activation of SLO-1. Activation of SLO-1 would be expected to cause a reduction in cell excitability. Levamisole and aldicarb were used in order to indirectly investigate the effect of emodepside on the excitability of muscle and neurons.

Reduced aldicarb sensitivity in *C. elegans* is thought most likely to reflect defects in synaptic transmission (Miller *et al* 1996). *slo-1*(*js379*) was shown to be aldicarb hypersensitive in the previous chapter and by Wang *et al* (2001). In the previous chapter, aldicarb sensitivity was found to be unaltered in many of the *slo-1* mutants. The relevance of *slo-1* loss of function in increasing aldicarb sensitivity was investigated. Expression of *slo-1*(+) in the neurons of *slo-1*(*js379*) does not result in rescue of the aldicarb hypersensitivity, suggesting the increased aldicarb hypersensitivity is either independent of *slo-1*(*js379*) or is due to loss of SLO-1 function in other tissues. The lack of correlation between aldicarb hypersensitivity and SLO-1 function highlighted in the previous chapter indicates that it is the former. However, it seems

that SLO-1 does play a role in neurotransmitter release as it has that ability to rescue the lethargic phenotype of *unc-64* in the *unc-64*, *slo-1* double mutant. The *unc-64* lethargic phenotype is restored by expression of *slo-1*(+) in the neurons of the double mutant (Wang *et al*, 2001).

Expression of *slo-1*(+) in the body wall muscle of *slo-1*(*js379*) results in a slight but significant decrease in aldicarb sensitivity. This indicates that *slo-1* expression in the muscle influences aldicarb sensitivity. This is contrary to what is reported by Wang *et al* (2001) who suggest that the increased aldicarb sensitivity of *slo-1*(*js379*) is due to loss of *slo-1* in the neurons.

Worms pre-treated with emodepside have a reduced sensitivity to aldicarb. This supports the idea that emodepside acts to reduce transmitter release. The aldicarb sensitivity of *slo-1*(*js379*) cannot be influenced by emodepside, demonstrating that this effect is dependent on SLO-1. A summary of the changes in the sensitivity of worms to aldicarb and levamisole is shown in table 6.01.

| Change in aldicarb and levamisole sensitivities **compared to *N2*** | |
|---|---|
| **Condition** | **Change in aldicarb sensitivity** |
| *slo-1*(*js379*) | ↑ |
| *N2* on 100 nM emodepside | ↓ |
| | **Change in levamisole sensitivity** |
| *slo-1*(*js379*) | ↓ |
| *N2* on 100 nM emodepside | ↑ |

| Change in aldicarb sensitivities **compared to *slo-1*(*js379*)** | |
|---|---|
| **Condition** | **Change in aldicarb sensitivity** |
| *slo-1*(*js379*) on 100 nM emodepside | No change |
| *slo-1*(*js379*) + neuronal *slo-1*(+) | No change |
| *slo-1*(*js379*) + body wall muscle *slo-1*(+) | ↓ |

**Table 6.01. Factors affecting aldicarb and levamisole sensitivity. A)** Changes in aldicarb and levamisole sensitivity of *slo-1*(*js379*) and 100 nM emodepside treated *N2* compared to *N2* sensitivity. **B)** Changes in aldicarb sensitivity of *slo-1*(*js379*) on 100 nM emodepside, *slo-1*(*js379*) + neuronal *slo-1*(+) and *slo-1*(*js379*) + body wall muscle *slo-1*(+) compared to *slo-1*(*js379*) sensitivity.

Levamisole was used to investigate the effect of emodepside on the body wall muscle. Levamisole is a nicotinic receptor agonist and causes spastic paralysis of nematode body wall muscle (Aceves *et al* 1970). Attempts were made to use changes in levamisole sensitivity to make predictions about muscle cell excitability. *N2* animals pre-treated with emodepside have an increased sensitivity to levamisole. *slo-1*(*js379*) have a decreased sensitivity to levamisole. These results are consistent with each other in that loss of SLO-1 function in *slo-1*(*js379*) and the hypothesised increase in SLO-1 function in emodepside treated *N2* have opposite effects. The changes in levamisole sensitivity observed are however contrary to any predicted result. If SLO-1 in the body wall muscle has an important role in mediating emodepside's effects,

the hypothesised emodepside induced increase in SLO-1 function would be predicted to decrease cell excitability and therefore decrease levamisole sensitivity (Salkoff *et al* 2006, Orio *et al* 2002). Loss of function of SLO-1 would be predicted to result in increased cell excitability and therefore increase levamisole sensitivity. If SLO-1 in the body wall muscle does not have an important role in mediating emodepside's effects, it would be predicted that no change in levamisole sensitivity would be observed. There are a variety of possible explanations for effects opposite to those predicted being observed.

One possibility is that of adaptation. In *slo-1*(*js379*) an increase in cell excitability may result in a down regulation of nicotinic ACh receptors. This may result in a decrease in levamisole sensitivity. Similarly, treatment with emodepside may result in an up regulation of nicotinic ACh receptors. This may result in an increase in levamisole sensitivity. However, if this type of adaptation occurs, one would expect to see similar results in the aldicarb assay, which is not the case.

Robertson *et al* (1993) found levamisole was able to cause a block of nACh receptors at concentrations between 30 and 90 μM. If levamisole causes nACh receptor block, reducing cell excitability, it would be expected that emodepside and levamisole effects would be cumulative. However, the paralysis of *C. elegans* by emodepside and 100 μM levamisole do not resemble each other. Emodepside causes a flaccid paralysis in which the body of the worm loses its sinusoidal wave form, where as levamisole causes spastic paralysis in which the body of the worm shortens as the muscle becomes hyper-contracted.

The mechanism by which levamisole causes paralysis in *C. elegans* is likely to be more complex than a simple spastic paralysis through activation of nACh receptors on the body wall muscle. nACh receptor subunits are expressed on neurons and muscle of *C. elegans* (Flemming *et al* 1997, Gottschalk *et al* 2005, Gally *et al* 2004, Gottschalk and Schafer 2005, Culetto *et al* 2004). Levamisole would be expected to affect transmitter release by acting on neuronal nACh receptors. Endogenous cholinergic activity on neuronally expressed nicotinic ACh receptors has been shown to modulate release of inhibitory neurotransmitters in a variety of systems (Wang *et al* 2002, Takeda *et al* 2007). The effects of levamisole on neurotransmitter release are likely to contribute to the paralysis, as well as its direct effect on the body wall muscle.

The effect that emodepside has on cell excitability is unclear. Emodepside reduces *N2* sensitivity to aldicarb, suggesting it reduces ACh release and the excitability of cholinergic neurons. Alternatively, it may indicate that the response of the body wall muscle to ACh is reduced, i.e. muscle cell excitability is reduced. Emodepside increases *N2* sensitivity to levamisole, suggesting it increases body wall muscle cell excitability. However, this is not consistent with the observed emodepside induced flaccid paralysis in *C. elegans* and in *Ascaris suum* muscle strip (Willson *et al* 2003). It may be that this interpretation of the change in levamisole sensitivity is too simplistic, as previously discussed. Further investigation, using direct electrophysiological recording techniques, will be required to obtain a fuller understanding of emodepside's effects on cell excitability. Whatever the precise effect of emodepside on cell excitability, it is clear that the ability of *slo-1*(+) to rescue emodepside sensitivity in both neurons and body wall muscle of *slo-1*(*js379*) indicates emodepside acts through SLO-1 in both these tissues. Indeed, high level of resistance of *slo-1* null mutants and the fact that only *slo-1* mutants were recovered from the screens for emodepside resistance might suggest a direct action of emodepside on SLO-1. The following chapter attempts to address this.

# Chapter 7

# Electrophysiological analysis of emodepside's effects on SLO-1

## 7.1 Introduction

There is strong evidence for a key role of SLO-1 in emodepside's mode of action. The genetic evidence indicates that emodepside causes an activation of SLO-1 as loss of SLO-1 function mutations cause high level resistance. The physiological effects are consistent with an activation of SLO-1 in that the emodepside induced paralysis is flaccid. Emodepside treated worms have reduced aldicarb sensitivity, suggesting it either causes a reduction in ACh release or a reduction in the response of the muscle to ACh. Activation of SLO-1 in neurons or muscle would be expected to reduce cell excitability. Emodepside causes a calcium dependent relaxation of the *Ascaris suum* muscle strip preparation which may indicate activation of a BK channel (Willson *et al* 2003). The fact that *slo-1* gain-of-function mutants are not hypersensitive to emodepside suggests that it either directly activates SLO-1 or activates SLO-1 via a pathway. Only *slo-1* mutants were recovered from the screen for emodepside resistant strains. This indicates that the action of emodepside on SLO-1 is direct. However, if loss of function of components of a SLO-1 activation pathway resulted in a lethal phenotype they would not be recovered from the screen.

In order to test if emodepside activates SLO-1, and to see if this activation is through direct interaction with SLO-1, a heterologous expression system was used and whole cell currents were analysed. A variety of expression systems have been used for expression of BK channels from a range of species. The most commonly used systems are *Xenopus* oocytes and HEK293 cells. Berns *et al* (1972) showed that expression of exogenous mRNA in *Xenopus* oocytes was possible. Adelman *et al* (1992) expressed *slo* cDNA from *Drosophila melanogaster* by injection of RNA into X*enopus* oocytes. Functional analysis using patch clamp showed that the channel had a voltage and $Ca^{2+}$ dependence. Differences between splice variants was also observed. The mouse *slo* (*mSlo*) and human *slo* (*hSlo*) have also both been expressed in X*enopus* oocytes (McCobb *et al* 1995, Butler *et al* 1993) and are voltage and $Ca^{2+}$ dependent. They were also shown to be sensitive to the specific BK channel blocker iberiotoxin. The single channel conductance of both *mSlo* and *hSlo* are 272 and 282 pS respectively, whereas the *dSlo* is only 126 pS. *C. elegans slo-1* has also been expressed in *Xenopus* oocytes (Wang *et al* 2001) and is both voltage and $Ca^{2+}$ dependent. It has a single channel conductance of ~250 pS. The similarity in the biophysical properties of BK channels between species is not surprising as they have a very strong sequence similarity. Table 7.01 shows the amino acid

sequence identity of BK channels from *Haemonchus contortus*, *Drosophila melanogaster* and *Homo sapiens* compared with *C. elegans* SLO-1.

| Species | Sequence accession number | % identity |
|---|---|---|
| *Haemonchus contortus* | ABS45068.1 | 85.4 % |
| *Drosophila melanogaster* | NP_0010014655.1 | 61.3 % |
| *Homo sapiens* | NP_002238.2 | 50.8 % |

**Table 7.01. BK channel sequence identity.** Amino acid sequence identity of BK channels compared to *C. elegans* SLO-1. Global alignments were conducted using Readseq version 2.1.24. The following parameters were used: gap open/ext; -14/-4.

Mammalian cell cultures are also commonly used for transient or stable expression of BK channels. Strobaek *et al* (1996) stable expressed the *hSlo* α subunit in HEK293 cells. They showed that *hSlo* has similar biophysical properties when expressed in HEK293 cells or *Xenopus* oocytes. Its single channel conductance is ~250 pS when expressed in HEK293 cells, similar to in *Xenopus* oocytes. HEK293 cells have also been used to express invertebrate BK channels. Shumin *et al* (2001) expressed *dSlo* in HEK293, demonstrating the versatility of using HEK293 cells.

HEK293 cells have been used to express invertebrate BK channels (Shumin *et al* 2001) as well as other *C. elegans* genes (Mertens *et al* 2005). Mertens *et al* (2005) functionally expressed the *C. elegans* GPCR Y59H11AL.1 in order to determine the ligand for this orphan receptor. Due to previous successful expression of invertebrate BK channels and other *C. elegans* gene, HEK293 cells were chosen to express the *C. elegans slo-1* gene. Practical considerations also made mammalian cell culture the choice heterologous expression system.

A variety of compounds have been shown to be ligands for BK channels both blocking and activating the channel. Commonly used specific blockers of BK channels include iberiotoxin (Galvez *et al* 1990) and charybdotoxin (Miller *et al* 1985), which are components to scorpion venom. Non specific potassium channel blockers include 4-amino-pyridine (Sherratt *et al* 1980) and tetraethyl ammonium.

The human embryonic kidney cell line HEK293 was chosen for this (Graham *et al* 1977). HEK293 cell line has been used extensively for expression of recombinant proteins and is amenable to transfection and patch clamp analysis (Thomas and Smart 2005). HEK293 cells are able to generate functional mammalian and non-mammalian proteins and have been used for expression of *C. elegans* genes (Mertens *et al* 2005). HEK293 cells have also been used extensively for expression of BK channels form a variety of species, including *D. melanogaster* (Bian *et al* 2001). A range of compounds have been shown to have activating properties of BK channels from a variety of species. These include cannabinoid methanandamide, which was shown to increase the outward current in BK-α transfected HEK293 cells (Sade *et al* 2006). The compound NS11021 has been shown to activate BK channel currents in KCa1.1 transfected HEK293 cells using the whole-cell patch technique (Bentzen *et al* 2007).

## 7.2 Expression of *C. elegans slo-1* in HK293 cells

In order to express *C. elegans slo-1* in HEK293 cells the pIRES2-EGFP vector from BD biosciences Clontech was used. This vector has several benefits. It contains an internal ribosome entry site (IRES) that allows the gene of interest and EGFP to both be generated from the same transcript. This avoids the need to generate a *slo-1*GFP fusion which may affect the functioning of the channel. EGFP is a variant of WT GFP but has been optimised for higher fluorescence in mammalian cell culture (Cormack *et al* 1996). This system allows cells carrying *slo-1* pIRES2-EGFP to be easily identified. However, it does not provide any information on whether *slo-1* is translated or trafficked to the membrane in the way that a *slo-1 gfp* fusion would.

*slo-1* cDNAa was PCR amplified from pBK3.1 using primers designed to generate suitable restriction sites for ligating into the MCS of pIRES2-EGFP, as well as the Kozak sequence. The Kozak sequence is a 5' non-coding sequence directly upstream of the start codon that is required for efficient translation in eukaryotic cells (Kozak 1987).

Three rounds of PCR were used to progressively build up the 5' end to incorporate a Kozak sequence and a Nhe-1 restriction site. Five extra nucleotides were incorporated in front of the Nhe-1 site to ensure efficient digestion. Attempts to generate a restriction site at the 3' end were made using a variety of different primer designs. These however failed and primers in the *unc-54* terminator sequence were subsequently used. Figure 7.01 shows the 5' primers used to build up these sequences.

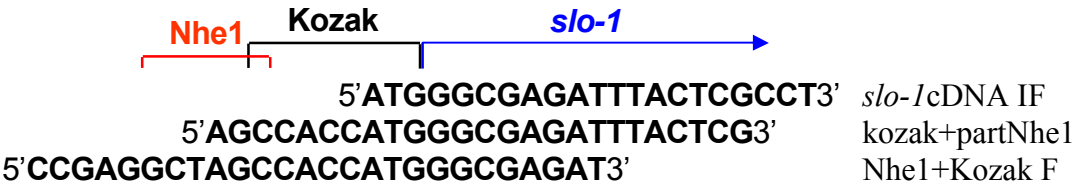


**Figure 7.01. Primer design for *slo-1* cDNAa amplification**. The Kozak sequence and Nhe-1 restriction site are incorporated onto 5' end of *C. elegans slo-1* cDNAa. These three primers were used in subsequent rounds with nested primers downstream of the *slo-1* stop codon.

The "Expand Long Template PCR System" was used to amplify *slo-1* cDNA. This is a mix of Taq DNA polymerase and Tgo DNA polymerase with proofreading activity. It has a 3 fold lower error rate than Taq DNA polymerase alone ($7.3 \times 10^{-6}$ errors per nucleotide per cycle). Enzymes with lower error rates were used (PfuUltra™ HF DNA polymerase) with little success, resulting in production of multiple fragments.

In order to reduce the error rate when using the "Expand Long Template PCR System", 10 cycle programmes were used for the first two rounds of PCR, followed by a 25 cycles for the final round, a total of 45 cycles. The probable number of errors for this process is ~1. Figure 7.02 A and B show optimisation rounds of PCR using primers *slo-1* cDNAa IF and *unc-54*-seq-R2 for the first round and kozak+partNhe1 and *unc-54* R3 for the second round. Figure 7.02 C shows the final PCR product, generated using primers Nhe1+Kozak F and *unc-54* R4. This PCR product was used in further enzymic reactions in preparation for ligation into pIRES2-EGFP.

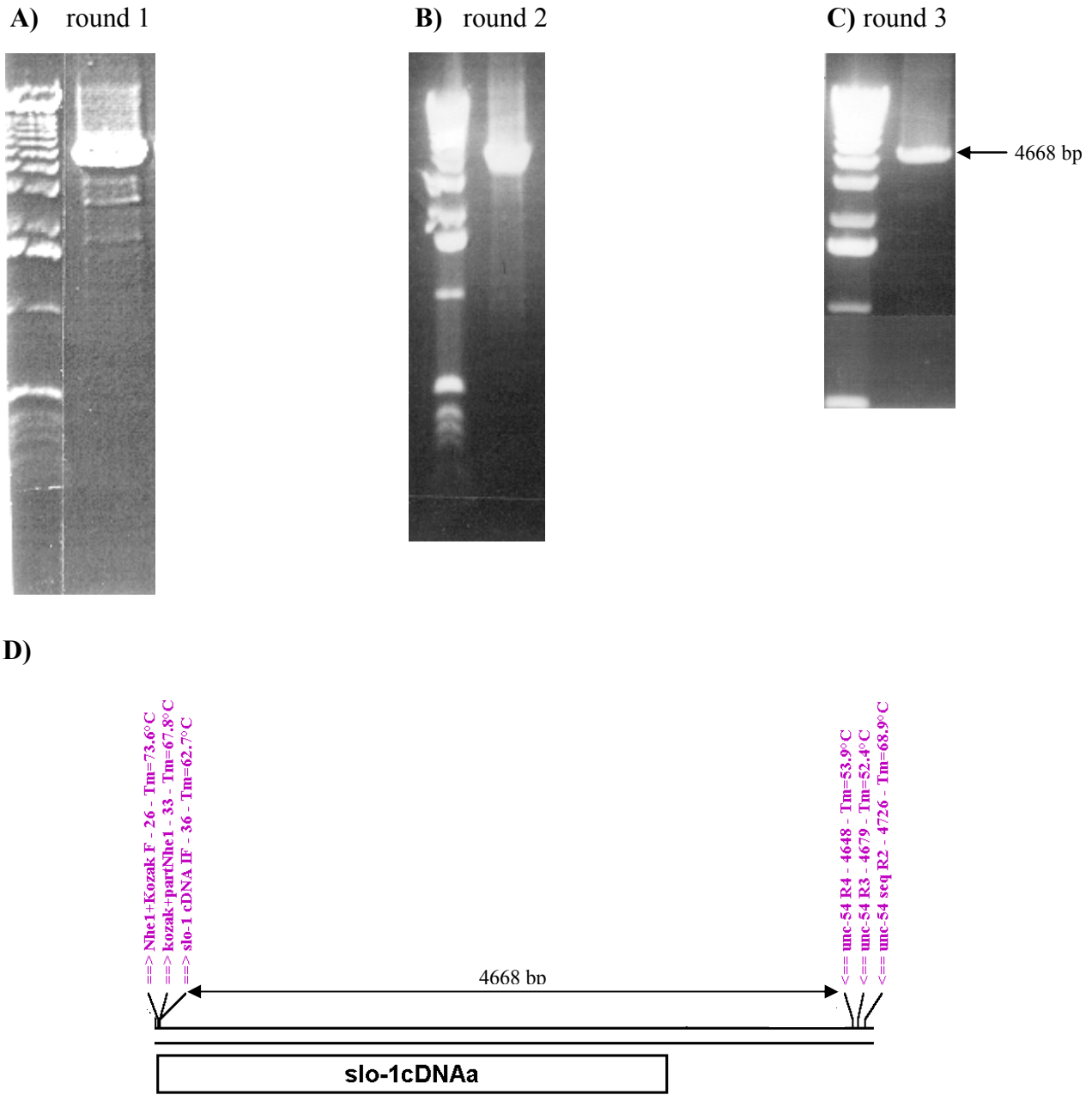


**Figure 7.02. Amplification of *slo-1* cDNAa by PCR.** PCR products from three consecutive rounds. **A)** Round one PCR using primers *slo-1*cDNA IF and *unc-54*-seq-R2, **B)** Round two PCR using primers kozak+partNhe1 and *unc-54* R3, **C)** Round cycle PCR using primers Nhe1+Kozak F and *unc-54* R4. **D)** Cartoon of PCR fragment containing *slo-1* cDNAa with annotated primer sites.

The final PCR product and the pIRES2-EGFP vector were initially cut with Nhe-1. Cutting the *slo*-1 cDNAa PCR product with Nhe1 produces fragments of 6 and 4668 bp (Figure 7.03 A), B), and C)). These digests were purified using QIAquick PCR

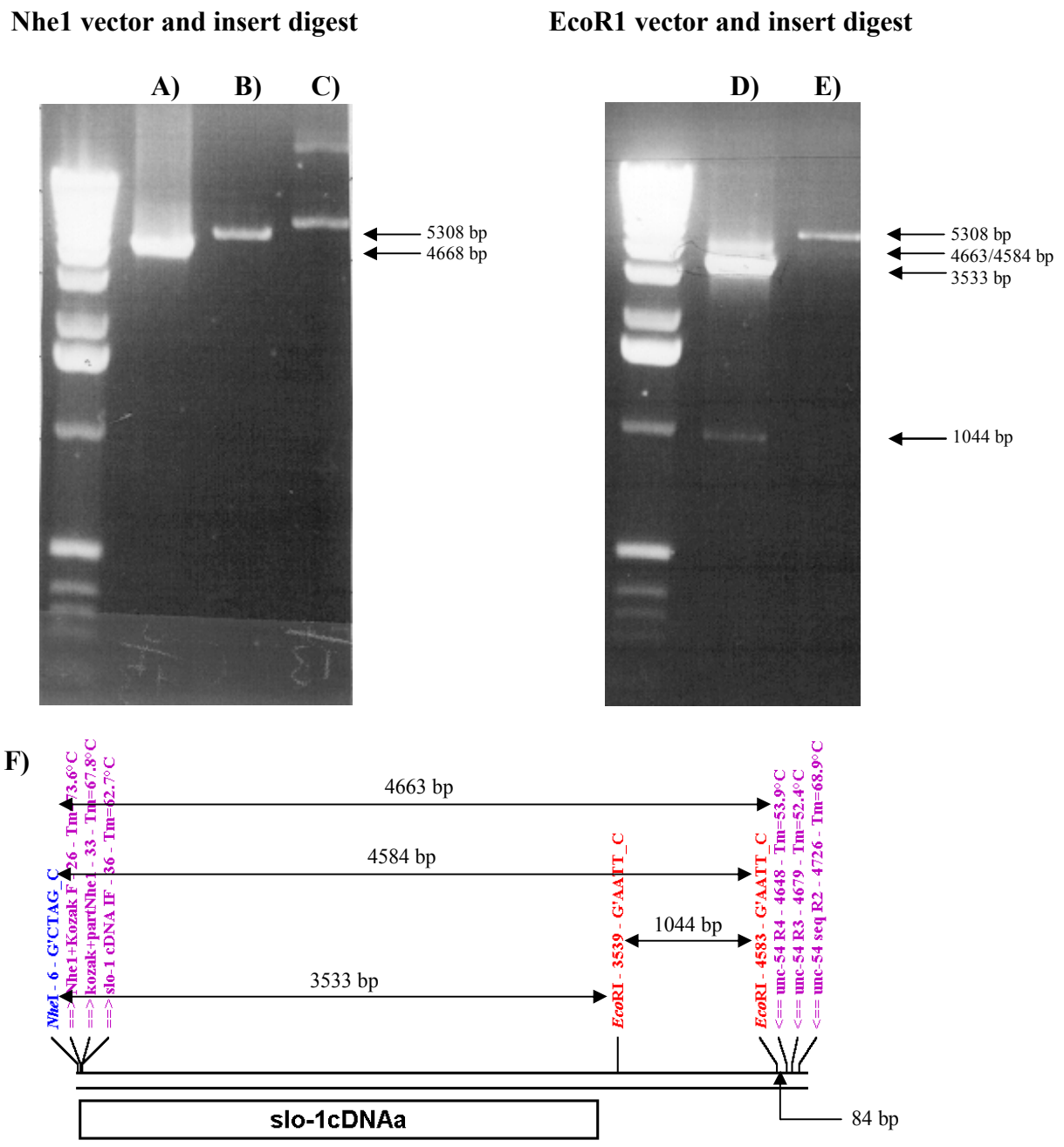


**Figure 7.03. *slo-1* cDNA insert and pIRES2-EGFP digest.** Gel electrophoresis of **A)** *slo-1* cDNA PCR fragment Nhe1 digest, **B)** pIRES2-EGFP Nhe1 digest, **C)** Uncut pIRES2-EGFP, **D)** *slo-1* cDNAa PCR fragment EcoR1 digest, **E)** pIRES2-EGFP EcoR1 digest. **F)** Cartoon of PCR fragment containing *slo-1* cDNAa with annotated primer and restriction enzyme sites.

Purification Kit. The *slo-1* cDNAa PCR product and the cut pIRES2-EGFP vector were then cut with EcoRI (Figure x **D)** and **E)**). The EcoRI digest of the *slo-1* cDNA PCR product removes the majority of the downstream sequence, leaving only 102 bp after the stop codon. EcoRI digest of *slo-1* cDNAa PCR product produces fragments of 3533, 1044 and 84 bp. It is the 3533 bp product that is required for ligation into pIRES2-EGFP.

Digested pIRES2-EGFP was treated with shrimp alkaline phosphatase to prevent re-ligation of the vector without the insert. The 3533 bp *slo-1* cDNAa PCR product was put into a ligation reaction in a 3 fold molar excess with pIRES2-EGFP, using T4 DNA Ligase. dh5α cells were transformed with the ligation product. Six colonies were isolated and cultured. Due to the presence of multiple fragments in the ligation reaction there was the potential to obtain vectors containing incorrect inserts. In order to identify colonies containing the correct sized inserts, analytical digests were conducted on extracted Plasmid DNA. Of the six extracts, five of these displayed the correct digestion pattern (7019 and 1781 bp) when cut with sal1 (Figure 7.04).

Due to the low proofreading activity of the "Expand Long Template PCR System" many of the *slo-1* cDNAa cloned into pIRES2-EGFP vector contained errors. The five *slo-1* cDNAa constructs were therefore sequenced. Table 7.02 shows the mutations generated in the PCR for the individual constructs. Only one had no mutations.

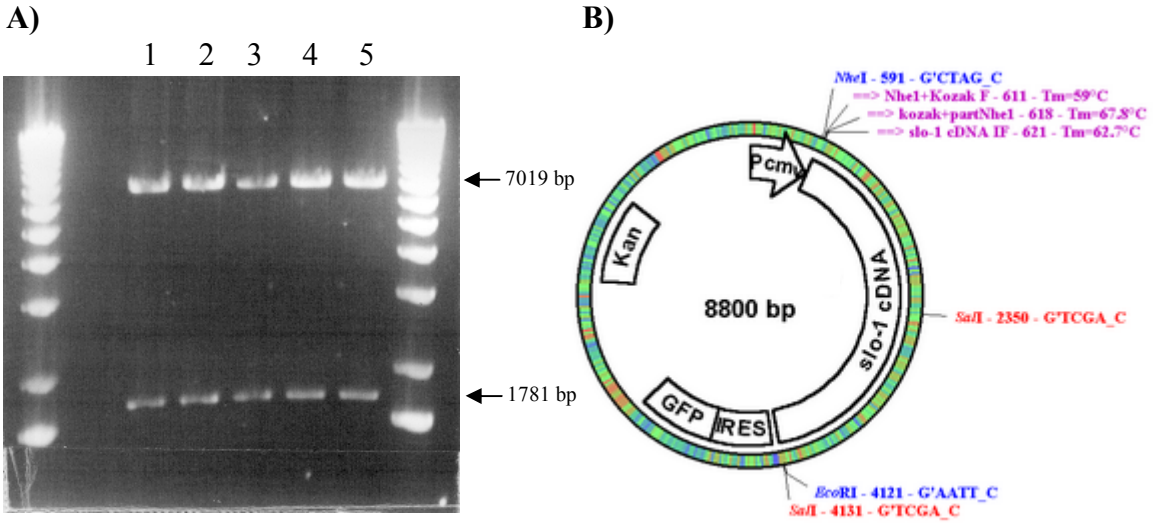


**Figure 7.04. Analytical digest of pIRES2-EGFP with *slo*-1 cDNA inserted. A)** Gel electrophoresis of a sal1 digest for five extracts of pIRES2-EGFP with *slo-1* inserted. **B)** Vector map for pIRES2-EGFP with *slo-1* cDNAa inserted. The sal1 restriction sites are highlighted in red.

| Construct | Errors | | | |
|---|---|---|---|---|
| **1** | | | | |
| **2** | A224G<br>Gln75Gln | T616C<br>Phe206Ser | C1504T<br>Pro502Leu | T3165C<br>Ser1056Pro |
| **3** | C593T<br>Ile198Ile | T1957C<br>Val653Ala | | |
| **4** | C973T<br>Thr325Met | C3245T<br>Tyr1082Tyr | | |
| **5** | C198T<br>Arg67Stop | A771G<br>Thr258Ala | A1909G<br>Lys637Arg | |

**Table 7.02. pIRES2-EGFP *slo-1* cDNAa errors.** pIRES2-EGFP *slo-1* vectors were sequenced. Nucleotide changes in *slo-1* cDNAa are shown. The resulting amino acid changes are shown. pIRES2-EGFP *slo-1* vector 1 is the only one without any errors.

## 7.3 Patch clamp analysis

Whole cell currents were recorded in HEK293 cells using patch clamp techniques. Single cells measuring between 20-30 μm were selected for patch clamp analysis. Figure 7.05 shows a typical example of the types of cells used. Initially recordings of endogenous HEK293 cell currents were made. HEK293 cells have been reported to have a variety of endogenous currents (Kurejova *et al* 2007, Zhu *et al* 1998, Jiang *et al* 2002) and it was therefore important to analyse these before looking at currents in HEK293 cells transiently transfected with BK channels.

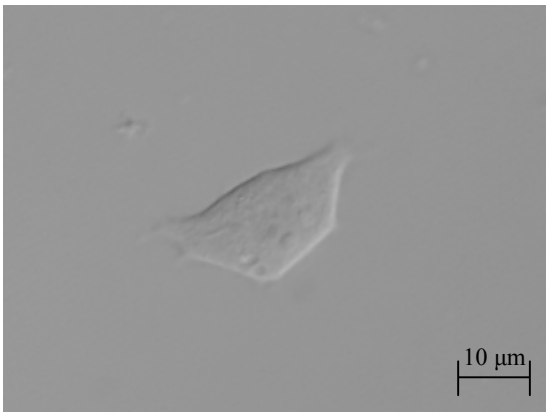


**Figure 7.05. Single HEK293 cell.** An example of a single HEK293 cell typically used for patch clamp recording. The smooth edges of the cell allow for tight seals to be formed between the cell membrane and the micro-pipette.

## 7.4 Endogenous currents in HEK293 cells

Recordings of endogenous currents were made using the whole cell patch clamp technique (Hamill *et al* 1981). Single cells were selected for patch clamp recordings A voltage step protocol was used to record currents, clamping at 10 mV intervals between -90 and +50 mV. Each voltage step lasted 100 ms before returning to a holding potential of -80 mV. Figure 7.06 shows currents typically seen when recoding in the whole cell configuration. Due to a high level of background noise steps have been separately displayed.

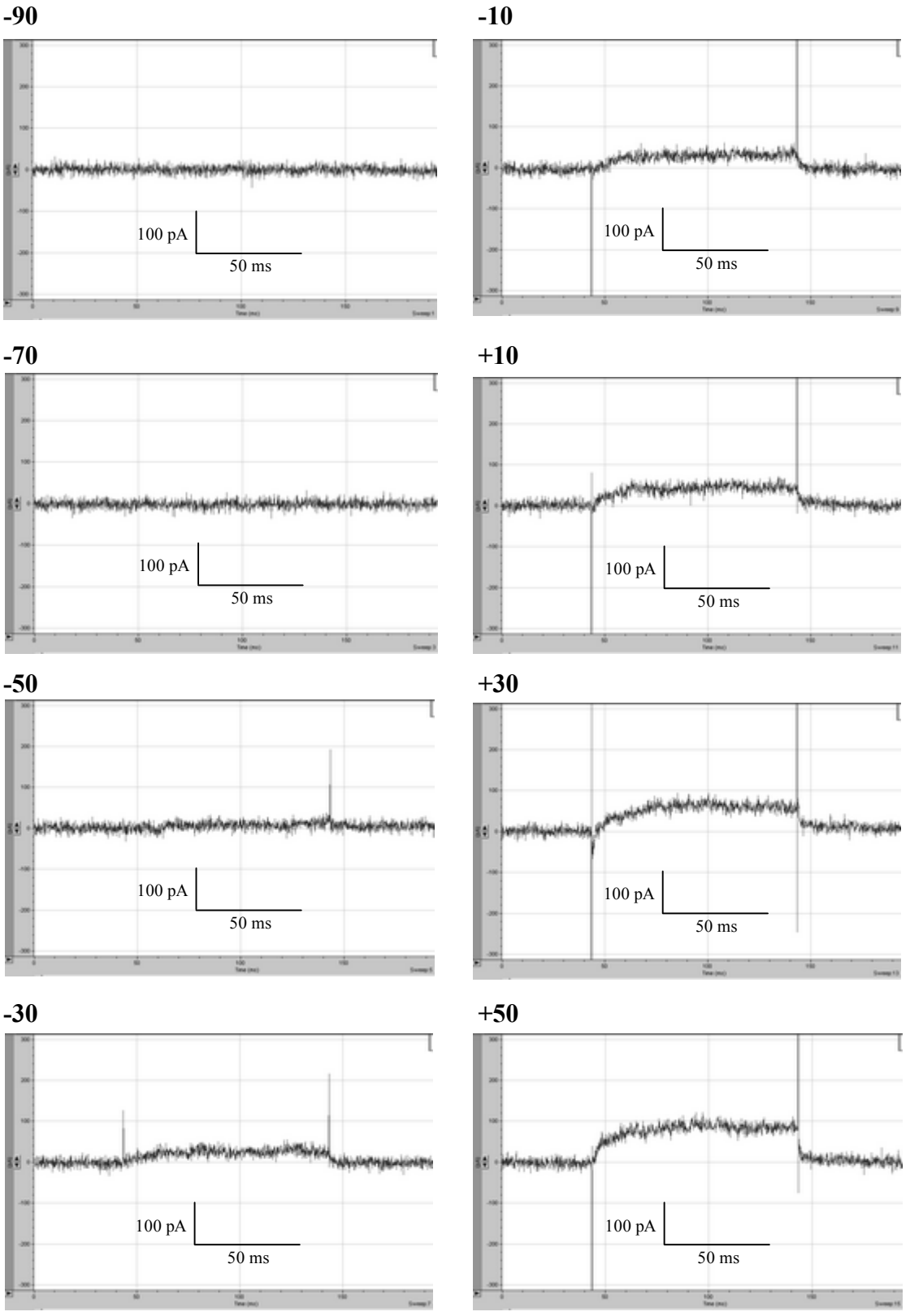


**Figure 7.06. HEK293 endogenous whole cell currents.** Endogenous whole cell outward currents typically observed in HEK293 cells. 100 ms voltage steps were applied, stepping from a holding potential of -80 mV, to between -90 mV and +50 mV. Leak subtraction applied.

The cells displayed outward currents, which most likely reflect an outward flow of potassium ions. The presence of endogenous potassium currents in HEK293 cells has been previously reported (Jiang *et al* 2002, Zhu *et al* 1998, Kurejova *et al* 2007 and Thomas and Smart 2004). Figure 7.07 shows the current voltage relationship for endogenous currents in HEK293. The average current at +50 mV is 66.4 ± 10.7 pA. The currents did not show inactivation during the 100 ms depolarising pulses.

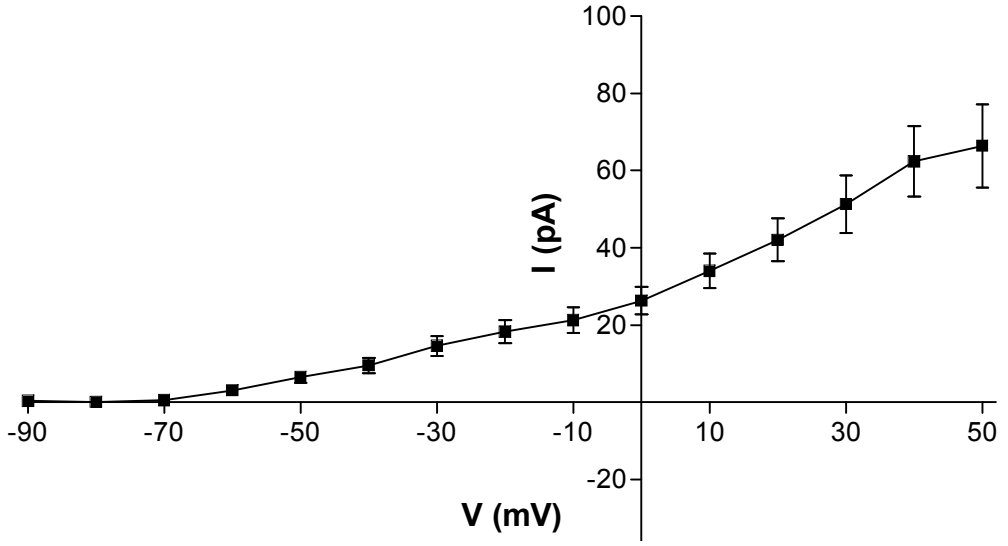


**Figure 7.07. IV relationship for whole cell currents from HEK293 cells.** 100 ms voltage steps were applied, stepping from a holding potential of -80 mV, to between -90 mV and +50 mV. For each point n=19 and is the mean ± the S.E. Mean. Leak subtraction applied.

## 7.5 Endogenous currents are 4-AP sensitive

The effect of 4-AP on the size of the whole cell currents was tested. 4-AP was added to the recording chamber to a final concentration of 10 mM. The voltage step protocol was run before and 2 minutes after the addition of 4-AP. In four out of four tests 4-AP caused a reduction in the amplitude of the outward current at voltage steps between –30 and + 50. However, the difference between the currents before and after 4-AP application at each voltage step was found not to be significantly different using a paired, two tailed t-test at each voltage step (Figure 7.08).

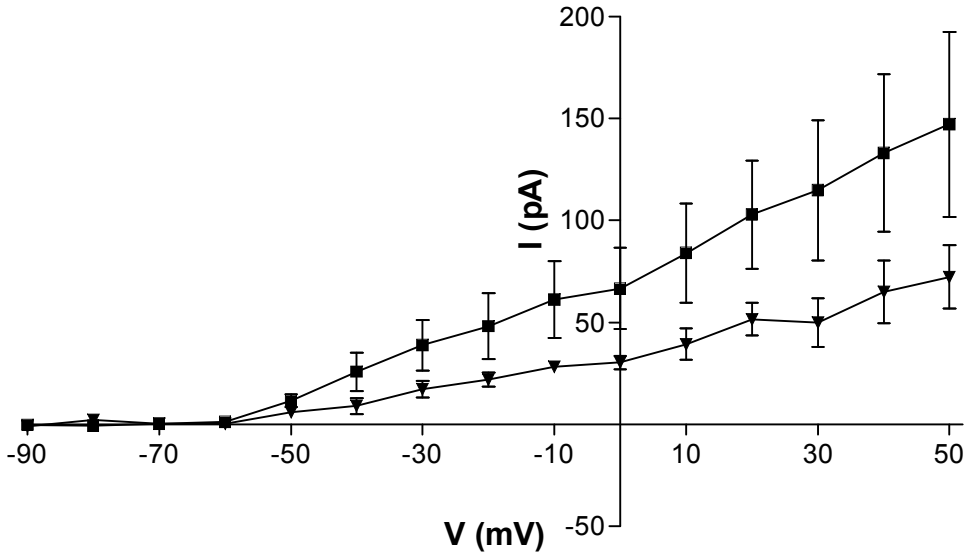


**Figure 7.08. IV relationship for whole cell currents from HEK293 cells +/- 4-AP.** 100 ms voltage steps were applied, stepping from a holding potential of -80 mV, to between -90 mV and +50 mV. HEK293 cells pre (■) and post (▼) 4-AP application. For each point n=4 and is the mean ± the S.E. Mean. Leak subtraction applied.

## 7.6 *C. elegans slo-1* transfected cells do not have large whole cell currents

HEK293 cells were transfected with pIRES2-EGFP *slo-1* using lipofectamine 2000 (Invitrogen). Cell were transfected when at approximately 20 % confluence. The transfection efficiency was estimated to be between 20 % and 50 %. Recordings were made using the whole cell patch clamp technique (Hamill *et al* 1981). Single cells expressing *gfp* were selected for patch clamp recordings. Cells strongly expressing *gfp* were not used as these were generally unhealthy. A voltage step protocol was used to record currents, clamping at 10 mV intervals between -90 and +50 mV. Each voltage step lasted 100 ms before returning to a holding potential of -80 mV. Figure 7.09 shows the voltage current relationship for un-transfected HEK293 cells and for HEK293 cells transfected with pIRES2-EGFP *slo-1*.

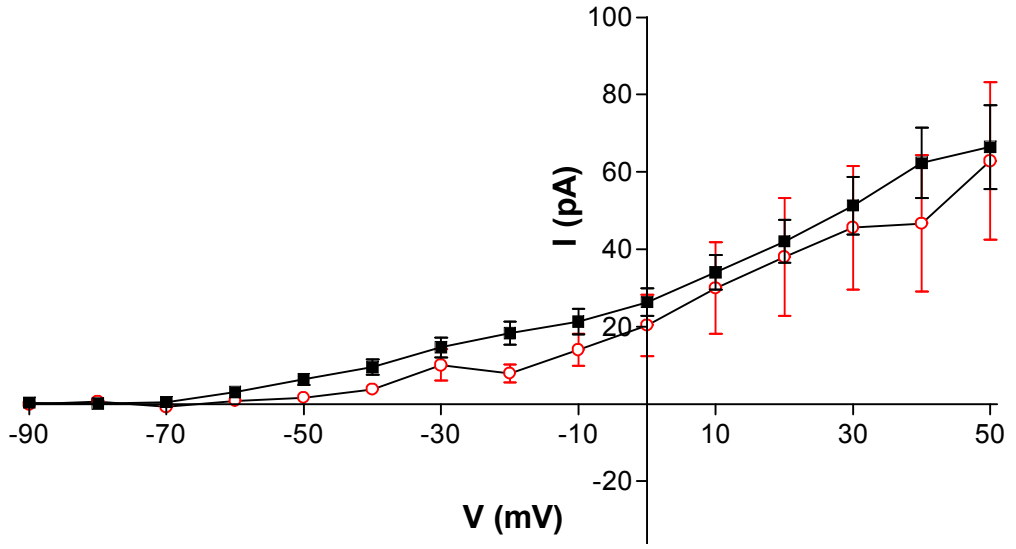


**Figure 7.09. IV relationship for whole cell currents from *C. elegans slo-1* transfected and non-transfected HEK293 cells.** 100 ms voltage steps were applied, stepping from a holding potential of -80 mV, to between -90 mV and +50 mV. Untransfected HEK293 cells (■) and *C. elegans slo-1* transfected HEK293 cells (○). For each point n≥6 and is the mean ± the S.E. Mean. Leak subtraction applied.

The current voltage relationships for both un-transfected cells and for cells transfected with pIRES2-EGFP *slo-1* was found not to be significantly different using a paired, two tailed t-test at each voltage step. This indicates that *slo-1* is not being functionally expressed. Expression of BK channel α subunits in HEK293 cells usually results in whole cell currents the nA range at potentials of +50 mV (Sade *et al* 2005).

## 7.7 *Homo sapiens kcnma1* transfected cells have large whole cell currents

HEK293 cells were co-transfected with pCMV4-XL6 *kcnma1* and pIRES2-EGFP as a marker at a ratio of 3:1. Recordings were made using the whole cell patch clamp technique (Hamill *et al* 1981). Single cells expressing *gfp* were selected for patch clamp recordings. A voltage step protocol was used to record currents, clamping at 10 mV intervals between -90 and +50 mV. Each voltage step lasted 100 ms before returning to a holding potential of -80 mV. Figure 7.10 shows the voltage current relationship for un-transfected HEK293 cells and for HEK293 cells transfected with pIRES2-EGFP *slo-1* and cells transfected with pCMV4-XL6 *kcnma1*.

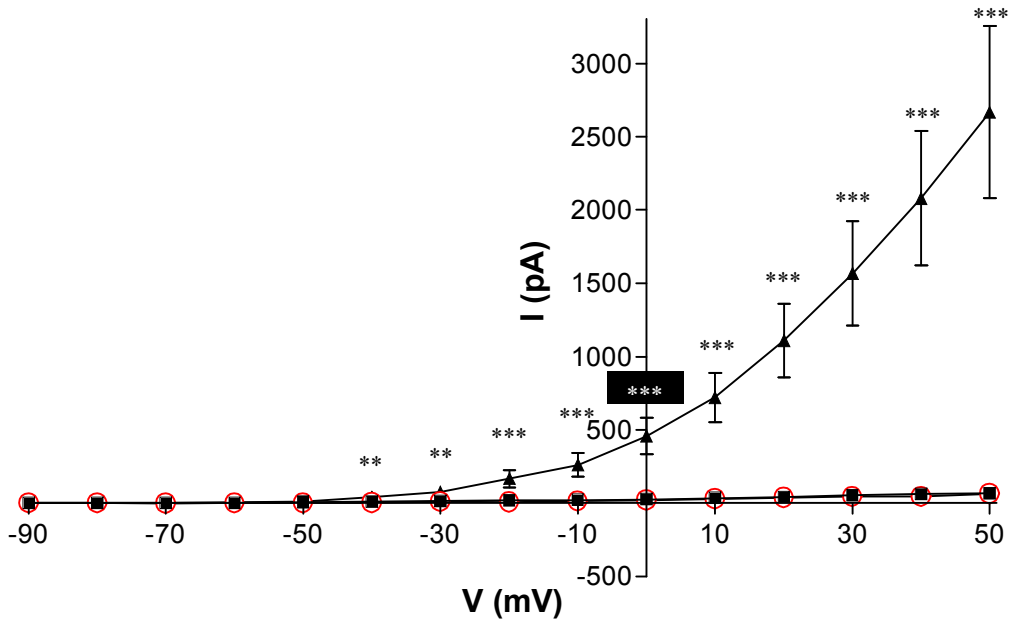


**Figure 7.10. IV relationship for whole cell currents from *H. sapiens kcnma1* transfected, *C. elegans slo-1* transfected and non-transfected HEK293 cells.** 100 ms voltage steps were applied, stepping from a holding potential of -80 mV, to between -90 mV and +50 mV. Untransfected HEK293 cells (■), *C. elegans slo-1* transfected HEK293 cells (○) and *H. sapiens kcnma1* transfected HEK293 cells (▲). For each point n≥6 and is the mean ± the S.E. Mean. Leak subtraction applied.

Figure 7.11 shows the currents typical seen in HEK293 cells transfected with *kcnma1*. A voltage step protocol was used to record currents, clamping at 10 mV intervals between -90 and +50 mV. Each voltage step lasted 100 ms before returning to a holding potential of -80 mV.

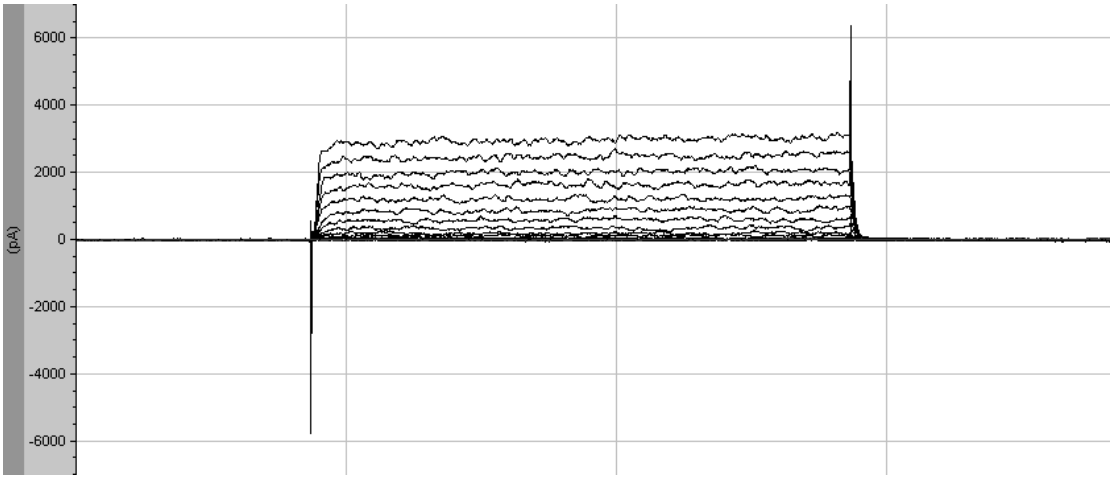


**Figure 7.11. *kcnma1* currents in transfected HEK293 cells.** Typical currents seen in HEK293 cells transfected with pCMV4-XL6 *kcnma1*. 100 ms 10 mV voltage steps were applied, stepping from a holding potential of -80 mV, to between -90 mV and +50 mV. Leak subtraction applied.

## 7.8 Discussion

Endogenous currents in HEK293 cells were successfully measured. These currents were found to be smaller than those reported in the literature. The average size of endogenous currents at + 50 mV was found to be 66 pA. Jiang *et al* (2002) observed outward currents in HEK293 cells under whole cell patch configuration. Using internal and external solutions similar to those used here, Jiang *et al* (2002) observed an average outward current of approximately 250 pA at + 50 mV. Yu *et al* (1998) observed an average outward current of approximately 350 pA at +50 mV. Variation in the size of endogenous currents observed in HEK293 cells has been reported (Kurejová *et al*, 2007). Over the course of two months, the size of whole cell currents was found to progressively decrease. This decrease is thought to reflect changes in the expression levels of ion channels.

The smaller size of currents observed here could result from a different level of ion channel expression in the batch of HEK293 cells used. The smaller outward currents observed make these cells more suitable for the analysis of BK channel currents. HEK293 cells expressing BK channel α subunits typically have currents in the nA range. The endogenous currents observed in these cells are in the pA range and would therefore be expected to have a minimal impact on whole cell currents observed in HEK293 cells expressing BK channels.

Due to difficulties encountered using the patch clamp technique, a thorough pharmacological analysis of whole cell currents could not conducted. Cells in the whole cell patch clamp configuration were found to be unstable. The mechanical forces on the cell that resulted from the application of pharmacological compounds frequently disrupted the seal between the cell and micro-pipette.

10 mM 4-AP was successfully applied to four cells in the whole cell patch configuration. In each case this resulted in a decrease of the outward current at potentials between –30 and + 50. The average size of the outward current was reduced from 147 pA to 72 pA at + 50 mV. Although the application of 4-AP did not result in a statistically significant decrease in the outward current, the trend suggests that the currents are 4-AP sensitive. This indicates the presence of endogenous potassium channels. A 51 % inhibition in the size of the average outward currents was observed with application of 10 mM 4-AP. This is similar to what is

reported in the literature. Jiang *et al* (2002) found a 40% inhibition of endogenous whole cell currents at + 50 mV using 5 mM 4-AP.

The aim of this chapter was to investigate the possibility of a direct action of emodepside on the SLO-1 channel. Unfortunately *slo-1* was not functionally expressed in the HEK293 cells. There are several possible reasons for this failure to express. HEK293 cells were maintained at 37$^{o}$C. However, *C. elegans* do not survive at such high temperatures. Lithgow *et al* (1995) reported that maintaining *N2* at 35$^{o}$C killed 100 % of worms within 500 minutes. In some cases it has been reported that by lowering the temperature after transfection, functional expression of *C. elegans* genes that was not possible at 37$^{o}$C can be achieved (Kubiak *et al* 2003). This has been shown to be the case for both *npr-1* and *npr-3* neuropeptide receptors. Lowering the temperature of *C. elegans slo-1* transfected HEK293 cells to 28$^{o}$C may result in functional expression. However, the lack of functional expression may result from differences in the post-translational modifications between *H. sapiens* and *C. elegans*.

Although an effect of emodepside on *C. elegans slo-1* currents could not be established, attempts to investigate its possible effects on *kcnma1* currents were made. There is 50.8 % amino acid sequence identity between *C. elegans slo-1* and *Homo sapiens kcnma1* BK channels. The high level of sequence identity suggests that if emodepside binds to *C. elegans* SLO-1 to elicit a response, there is a good chance this mechanism would exist in *kcnma1*.

*Kcnma1* was successfully expressed in HEK293 cells. The average whole cell current size at + 50 mV was 2668 pA. These currents were easily distinguishable from the endogenous currents, with the average size of currents in HEK cells expressing *kcnma1* being forty times larger. The size of the currents seen in HEK293 cells expressing *kcnma1* are comparable to those reported in the literature (Sade *et al* 2006; Fukao *et al* 2001).

However, due to difficulties with the patch clamp technique, pharmacological compounds could not be successfully applied to the preparation. Ideally, iberiotoxin would have been applied in order to confirm that the observed currents were due to the presence of BK channels. Of the two preparations to which emodepside was successfully applied, neither displayed changes in the amplitude of the outward current. The expectation is that emodepside activates SLO-1, which would be reflected as an increase in the size of the outward currents. The fact that this is not observed could be due to a lack of sensitivity of the

*kcnma1* channel to emodepside due to sequence differences compared to *slo-1*. Alternatively, the absence of components of a BK channel activation pathway may be responsible. However, due to the low n number, no solid conclusions can be drawn.

# Chapter 8

# Discussion

The development of resistance to currently used anthelmintics has led to the requirement for anthelmintics with novel mechanisms of action. Emodepside, a member of the cyclo-octadepsipeptide family of compounds, is one such compound. Its resistance breaking properties in a variety of parasitic nematodes initially indicated that emodepside has a novel mechanism of action (Harder & Samson-Himmelstjerna, 2002). The aim of this project has been to better define the mechanism of action of emodepside. Understanding emodepside's mechanism of action may be beneficial for future drug design and may inform possible future applications for emodepside. It may also provide insight into biological mechanisms within *C. elegans* and therefore of parasitic nematodes. The identification of novel targets may prove useful for the development of future drugs. These may be new anthelmintics or alternatively compounds for treatment of other diseases. Potential applications not previously considered may be identified for emodepside. The usefulness of *C. elegans* as a parasitic model (Geary and Thompson 2001) can only be judged on a case by case basis. This project has shown that with regard to emodepside, *C. elegans* provides a representative model for its effects in parasitic nematodes.

This study started with the hypothesis that emodepside activates neuronal latrophilin receptors resulting in the release of neurotransmitters and paralysis of the muscle. The evidence for the involvement of the latrophilin receptors comes from studies that demonstrated binding of a PF1022A-keyhole limpet haemocyanin (KLH) conjugate to the *Haemonchus contortus* latrophilin receptor HC110R. Emodepside was shown to antagonize the LTX-induced influx of calcium in HEK293 cells expressing HC110R although it could not induce calcium influx itself. Studies in *C. elegans* also indicated that the latrophilin receptors play a role in emodepside's mode of action. RNAi was used to knock down *lat-1*. This resulted in a decrease in sensitivity of emodepside's effects on the pharynx and on locomotion (Willson *et al* 2005, Amliwala 2005). RNAi knock down of *lat-2* resulted in a decrease in sensitivity to emodepside's effects on locomotion (Amliwala 2005).

However, the current study demonstrates that neither LAT-1 nor LAT-2 have a role in emodepside's effects on locomotion. The *lat-1*(*ok1465*) and *lat-2*(*tm463*) alleles both contain large deletions that are predicted to result in loss-of-function of the receptor. Regions putatively involved in emodepside binding are disrupted. Neither of these alleles displayed any reduction in sensitivity to emodepside's effects on locomotion. The *lat-1*(*ok1465*) allele was however found to have reduced sensitivity to emodepside's effects on the pharynx (Bull

2007). The reduction in sensitivity of the pharynx of *lat-1*(*ok1465*) was similar to that observed in animals with RNAi knock down of *lat-1*.

Plate assays were used to assess the effect of emodepside on the locomotion of *lat-1*(*ok1465*) and *lat-2*(*tm463*) as opposed to the thrashing assay which was used to investigate the effect of RNAi knock down of *lat-1* and *lat-2* (Willson *et al* 2004, Amliwala 2005). However, it is unlikely that this prevented any difference in emodepside sensitivity being detected. Several strains carrying loss-of-function mutations in components of the latrophilin-mediated vesicle release pathway were found to have reduced sensitivity to emodepside when assessed using the plate assay (Amliwala 2005). Knock out of the emodepside receptor would be expected to result in resistance at least as strong as knock out of down stream elements. The lack of resistance observed in *lat-1*(*ok1465*) and *lat-2*(*tm463*) led to the hypothesis of functional redundancy between *lat-1* and *lat-2* with regard to emodepside's mode of action. However, the lack of resistance to emodepside of the *lat-2 lat-1* double mutant rules out this possibility. This also indicates that previous results obtained with RNAi are not specific to effects on either *lat-1* or *lat-2* genes. There is however a role for the LAT-1 receptor in emodepside's effects on pharyngeal pumping. *lat-1*(*ok1465*) was found to result in a similar level of resistance to emodepside as knock down of *lat*-1 by RNAi in the EPG assay. *lat-2* has been found not to influence the sensitivity of the pharynx to emodepside in the EPG assay. The decrease in sensitivity of *lat-1*(*ok1465*) to emodepside's effects on the pharynx rather than complete resistance indicates there must be another mechanism by which emodepside has its effects.

The BK channel SLO-1 is key to emodepside's mode of action. Concentrations of emodepside of up to 10 μM failed to inhibit the locomotion of *slo-1*(*js379*). *slo-1*(*js379*) contains an early stop codon in the S4 transmembrane domain. This mutation is predicted to cause a loss of function of SLO-1. SLO-1 loss-of-function therefore results in high level resistance to emodepside. Restoration of emodepside sensitivity can be achieved through expression of *slo-1*(+) in either body wall muscle or neurons. This confirms that it is SLO-1 loss-of-function that results in emodepside resistance, rather than a mutation in the background of the *slo-1*(*js379*) strain *NM1968*. The genetic evidence suggests that emodepside activates SLO-1.

All of the emodepside resistant mutants generated through random mutagenesis are alleles of *slo-1*. This has been demonstrated through the use of complementation tests. This, coupled with the high level of resistance observed in *slo-1* loss-of-function mutants, indicates that SLO-1 is the main modulator of emodepside's effects and is currently the best candidate for an emodepside receptor. Although no other genes involved in emodepside's mode of action were identified in the mutagenesis screens, the possibility that emodepside binds to a receptor upstream of SLO-1 remains.

Mutations in *slo-1* have been identified in four emodepside resistant strains. *pd24* and *pd23* contain mutations that result in early stop codons in the RCK1 domain. Mutations in *pd17* are in the RCK1 (A524V) and RCK2 (A870V) domains. In *pd19* there is a mutation in the RCK1 domain (G432R). The fact that these mutation are clustered in the RCK domains is interesting and may indicate that emodepside acts in this region.

The relationship between SLO-1 function and emodepside sensitivity was investigated using reversal frequency and aldicarb sensitivity as read outs for SLO-1 activity. *slo-1* loss-of-function mutants have an increased reversal frequency compared to N2. In general, there was a strong correlation between reversal frequency and emodepside resistance, indicating that the level of SLO-1 function directly relates to the level of emodepside resistance. The exception to this is *pd21*, which has an intermediate level of emodepside resistance but has a reversal frequency not significantly different from N2. This may indicate that the mutation in *pd21* that confers emodepside resistance does not interfere with SLO-1 function. The identification of this mutation would be very useful as it may help to determine a site of interaction, possible an emodepside binding site, on SLO-1. This study brings into question the use of aldicarb sensitivity as a read-out of SLO-1 function. Aldicarb sensitivity does not correlate well with emodepside resistance. Although some predicted SLO-1 loss-of-function mutants are hypersensitive to aldicarb, other are not. This indicates that it is mutations present in the background of some strains that causes aldicarb hypersensitivity, rather than loss of SLO-1 function itself. Attempts were made to rescue the aldicarb hypersensitivity of *slo-1*(*js379*) by expressing *slo-1*(+) in either neurons or muscle. Expression of *slo-1*(+) in the muscle partially rescues the aldicarb hypersensitivity of *slo-1*(*js379*). *slo-1*(*ky389*) and *slo-1*(*ky399*) gain-of-function mutants have been shown to have reduced aldicarb sensitivity compared to N2 (Davies *et al* 2003). These results demonstrate that SLO-1 has the ability to influence aldicarb

sensitivity. However, whether or not the decrease in aldicarb sensitivity observed in *slo-1*(*js379*) when *slo-1*(+) is expressed in the muscle is genuine rescue remains unanswered.

The SLO-1 gain-of-function mutants *slo-1*(*ky399*) and *slo-1*(*ky389*) have proved valuable in understanding the involvement of SLO-1 in emodepside's mechanism of action. In loss of SLO-1 function mutants, emodepside resistance could be due to an indirect opposition of emodepside's effects or due to loss of SLO-1 activation by emodepside. If resistance results from the former, the effect of a gain of SLO-1 function mutation and emodepside would be cumulative. The effect of SLO-1 gain-of-function mutation and emodepside are not cumulative, suggesting that emodepside acts directly through SLO-1.

The evidence discussed suggests that emodepside activates SLO-1, resulting in inhibition of locomotion. In chapter six the result of SLO-1 activation by emodepside and the tissues in which this activation occurs was considered. *slo-1* is endogenously expressed in both neurons and body wall muscle (Wang *et al* 2001). By expressing *slo-1*(+) in either body wall muscle or neurons of *slo-1*(*js379*) emodepside sensitivity could be restored. Emodepside can therefore activate SLO-1 in either neurons or muscle, both of which result in the inhibition of locomotion. Emodepside treated *slo-1*(*js379*) expressing *slo-1*(+) in the body wall muscle results in an inhibition of locomotion that most closely resembles N2. Emodepside treated *slo-1*(*js379*) expressing *slo-1*(+) in the neuron results in an inhibition of locomotion that is characterized by coiling. There are several possible explanations for the coiling phenotype observed when expressing *slo-1* in the neurons. The fact that *slo-1* expression is not driven by the endogenous promoter is likely to influence this. Neuronal expression of *slo-1*(+) in *slo-1*(*js379*) is driven by the pan-neuronal *snb-1* promoter. This may result in expression in neurons that do not normally express *slo-1*. Another factor that might result in the coiling phenotype is the fact that only one splice variant of *slo-1*(+) was expressed. Three splice variants have been identified (Wang *et al* 2001). It may be that the splice variants are differentially expressed in different tissues and that non-endogenous expression results in the coiling phenotype observed. The coiling phenotype is not a result of a lack of expression in the body wall muscle as it is still observed when *slo-1*(+) is co-expressed in the neurons and body wall muscle of *slo-1*(*js379*). The coiling phenotype is likely to result from one or more of the above mentioned possibilities.

As *slo-1* is normally expressed in body wall muscle and neurons and as *slo-1*(+) can restore emodepside sensitivity to *slo-1*(*js379*) when expressed in both tissues, it seems likely that the inhibition of locomotion by emodepside in N2 results from an action in both tissues. The fact that the inhibition of locomotion in *slo-1*(*js379*) expressing *slo-1*(+) in muscle more closely resembles that in N2 may suggest that SLO-1 in the muscle plays a more prominent role in locomotion inhibition.

The pharynxes of *slo-1*(*js379*) are highly resistant to the effects of emodepside (Bull 2007). Interestingly, expression of *slo-1*(+) in the neurons completely restores emodepside sensitivity. Expression of *slo-1*(+) in the pharyngeal muscle of *slo-1*(*js379*) does not restore emodepside sensitivity. This suggests that emodepside's effects on the pharynx are purely neuronal. This may also indicate that additional proteins that are not expressed in the pharynx are required for emodepside's effects, as SLO-1 alone is not sufficient to restore sensitivity.

Attempts were made to determine the relative role of emodepside's effects on neurotransmitter release and on muscle cell excitability using the compounds aldicarb and levamisole. The sensitivity of emodepside treated N2 and *slo-1*(*js379*) to aldicarb was assessed to investigate the effect emodepside has on ACh release. N2 worms treated with a sub-paralysing concentration of emodepside were found to have a decreased sensitivity to aldicarb. The sensitivity of *slo-1*(*js379*) treated with a sub-paralysing concentration of emodepside was found to be unaltered. This suggests that emodepside causes a reduction in ACh release (Miller *et al* 1996) and that this is dependent on SLO-1. However, this decrease in aldicarb sensitivity could reflect a post-synaptic effect of emodepside. To investigate whether this is a post-synaptic effect, the nicotinic agonist levamisole was used. If emodepside acts post synaptically to reduce muscle cell excitability, it would be predicted that *N2* worms treated with a sub-paralysing concentration of emodepside would have decreased sensitivity to levamisole. *slo-1*(*js379*), which are thought to have increased muscle cell excitability (Carre-Pierrat *et al* 2006), would be predicted to by hypersensitive to levamisole. In fact the opposite was observed. Pre-treatment of *N2* with emodepside resulted in hypersensitivity to levamisole. *slo-1*(*js379*) were found to have reduced sensitivity to levamisole. This suggests that emodepside acts to increase muscle cell excitability via activation of SLO-1. However, this interpretation is not consistent with the observed flaccid paralysis in *C. elegans* and the reduction in tension in *Ascaris suum* muscle strip caused by emodepside (Willson 2003). Electrophysiological recording from *C. elegans* neuromuscular

junction muscle would be useful in order to clarify what emodepside's effect on muscle cell excitability are (Richmond 2006). These pharmacological and expression studies overall indicate that SLO-1 mediates emodepside's effects in both neurons and body wall muscles. The evidence presented in this thesis suggests that a mechanism of action of emodepside involving activation of SLO-1 in neurons and body wall muscle exists. The activation of SLO-1 leads to a reduction in ACh release, presumably through a decrease in excitability in cholinergic neurons. It may be that emodepside's effect of reducing neurotransmitter release in cholinergic neurons is common to all types of neurons. Further investigation is required in order to determine what effect emodepside has on muscle cell excitability. Whether or not activation of SLO-1 is through a direct interaction with emodepside or is down stream on a pathway activated by emodepside remains to be determined.

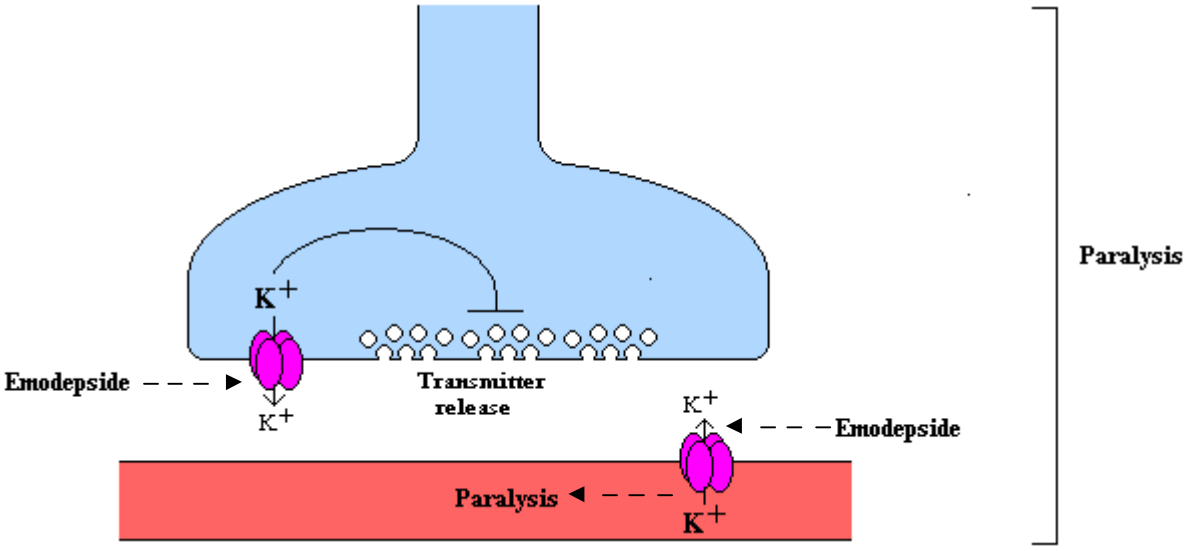


**Figure 8.01. Proposed mechanism of action for emodepside.**

However, such a mechanism is at odds with previous findings by Willson *et al* (2004) and Amliwala (2005) which suggest that emodepside acts to increase neurotransmitter release. Mutations in components of the latrophilin vesicle release pathway were found to result in a decrease in emodepside sensitivity, supporting the idea that emodepside causes neurotransmitter release. The $G\alpha_q$ *egl-3* reduction-of-function mutants were found to have reduced emodepside sensitivity in both EPG and locomotion assays. $G\alpha_q$ *egl-30* gain-of-function have increased emodepside sensitivity in both EPG and locomotion assays. PLCβ *egl-8* reduction-of-function mutants were found to have a decreased sensitivity to emodepside

in both EPG and locomotion assays. These mutants showed modest changes in sensitivity to emodepside. A similar decrease in sensitivity to emodepside's effects on locomotion was observed in *lat-2*(*ok301*) *VC158*. After out-crossing, *lat-2*(*ok301*) *XA3726* had an emodepside sensitivity similar to that of *N2*. This decreased emodepside sensitivity in *lat-2*(*ok301*) *VC158* resulted from unidentified background mutation(s). The resistance conferred by these unidentified background mutation(s) indicates that mutants with reduced levels of emodepside sensitivity may be relatively easy to generate. Caution should therefore be taken when interpreting such results. Multiple reduction-of-function alleles were used to investigate the role of PLCβ *egl-8* and $G\alpha_q$ *egl-30*, strengthening the evidence for an involvement of these genes in emodepside's mode of action. However, rescue of the reduced sensitivity to emodepside in these strains would be useful to determine whether these genes have an important role in emodepside's mode of action. Either way, it seems clear that this pathway plays a relatively minor role in emodepside's mechanism of action, with regard to locomotion. The role of this pathway in emodepside's effects on the pharynx, which was the focus of the paper by Willson *et al* (2004), may well be more prominent, although there is a clear involvement of SLO-1.

Whether or not emodepside acts directly on SLO-1 to open the channel remains to be answered. Unfortunately, attempts to address this by conducting patch clamp recordings from HEK293 cell expressing *C. elegans slo-1* were unsuccessful. Based on the evidence presented in this thesis it would be predicted that emodepside would activate SLO-1, resulting in an opening of the channel and the flow of potassium ions. However, patch clamp recordings from the terminal bulb of *slo-1*(*js379*) expressing *slo-1*(+) in the pharyngeal muscle show that emodepside blocks SLO-1 (Bull 2007). The fact that BK currents are produced when *slo-1* is expressed in the pharyngeal muscles but are blocked by emodepside rather than activated suggests that its mechanism may be altered in this system. This altered mechanism may result from post translational modification of SLO-1 specific to the pharyngeal muscle or the presence of a SLO-1 regulatory protein specific to the pharyngeal muscle. *Xenopus* oocytes have been successfully used to express *C. elegans slo-1* (Wang *et al* 2001) and may provide a cleaner system to investigate the action of emodepside on SLO-1 currents.

The relevance of this mechanism in parasitic nematodes has recently been confirmed by using *C. elegans* as an exogenous expression system for parasitic nematode SLO-1 channels. The *Ancylostoma caninum slo-1* and *Coperia oncophora slo-1* were expressed in *slo-1*(*js379*)

using both *snb-1* promoter and the native *C. elegans slo-1* promoter (3.5 kb sequence upstream of the start codon). Expression of both *slo-1* channels using the *snb-1* promoter resulted in a partial rescue. Expression of both BK channels using the native *C. elegans slo-1* promoter resulted in a complete rescue of emodepside sensitivity. These animals strongly resembled N2 animals on emodepside (Personal communication with Nina Krüger). This process highlights the strength of using *C. elegans* as a model for parasitic nematodes. Similar techniques have recently been used to determine the mechanism of action of the novel amino-acetonitrile class of anthelmintic compounds (Kaminsky *et al* 2008)

One concern about emodepside is the relative ease at which resistant *C. elegans* could be obtained. With many anthelmintics, screens for resistant *C. elegans* results in the generation of mutants with partial resistance. This is often due to the presence of multiple targets for anthelmintic compounds. For example, there are multiple nicotinic receptor subunits on which levamisole acts (Fleming *et al* 1997). Multiple mutations may therefore be required before resistance emerges. In comparison, there is only one SLO-1 subunit in *C. elegans* in which mutations are required to cause high level resistance. If the situation is the same in parasitic species then the potential for resistance to develop will be increased. Additionally, *slo-1* loss-of-function in *C. elegans* results in a relatively mild phenotype. If *slo-1* loss-of-function in parasitic nematodes results in similarly mild phenotype, the potential for resistance to develop would increase. However, it should be remembered that the environment in which *slo-1* loss-of-function *C. elegans* are observed is highly controlled and seemingly mild phenotypes may be unsustainable in the wild. Parasitic nematodes may well be unable to maintain a *slo-1* loss-of-function.

Several key questions over emodepside's mechanism remain to be answered. 1) Does emodepside increase the open probability of SLO-1 channels. 2) If emodepside functions in this way, does emodepside bind directly to SLO-1 in order to achieve this? The majority of the evidence indicates that this is the mechanism by which emodepside causes paralysis, however, this has not been shown directly. Investigating the effect of emodepside on *C. elegans* SLO-1 currents in *Xenopus* oocytes can hopefully be used to answer the question of whether or not emodepside increases the open probability of SLO-1. If it proves that emodepside can increase the open probability of SLO-1 in this system then it would also indicate that SLO-1 is the receptor for emodepside. Radio-labelled emodepside could be used in binding studies in order to determine if emodepside binds to SLO-1. If SLO-1 is found to

be the emodepside receptor it may be possible to characterize the binding site through the use of site-directed mutagenesis and analysis of SLO-1 currents in *Xenopus* oocytes.

# Appendix 1

**Primers for detecting deletions in and sequencing latrophilin receptors**

| | |
|---|---|
| *ok301* in left | TGGAAAAATCGGAAAAATC |
| *ok301* in right | CCTCGCGTCTCACAATCAT |
| *ok301* out left | TTTTGTTATGGAACTCCGG |
| *ok301* out right | CTGGAAACTCGTCTCTTCC |
| *ok301* in del left | AACGACATCGCCGTGTTCGA |
| | |
| *tm463* in left | CGTAGGGCTTACCTTTTAGA |
| *tm463* in right | CGAGACGGACTAAGTATTAG |
| *tm463* out left | GGCAGACGTTTTTGTGACTA |
| *tm463* out right | AACGGAATGAATGCGCAACC |
| *tm463* in del left | TAACCTCACCTCCAGACGCA |
| *tm463* seq | CAGAAAGTTGATAACTTCCG |
| | |
| *ok1465* out left | CTTTTCTATCTTGCCGCCTG |
| *ok1465* out right | CTCCTAGCAAACTCGCCAAC |
| *ok1465* in left | GAAGTGGACATCTCGGGAAA |
| *ok1465* in right | AACATCGTGACGACATGGAA |
| *ok1465* in del reverse | GTGAAGTAGCACATTGAGTC |
| *ok1465* seq | ATTATGCAATAATTGCAAG |

**Primers for sequencing of *slo-1* cDNA**

| | |
|---|---|
| *slo-1* cDNA 0 | ATGGGCGAGATTTACTCGCCT |
| *slo-1* cDNA 1 | GGACTGGGCTGGCGAGCTGAT |
| *slo-1* cDNA 2 | ACATTCTACAGTACCTCAACA |
| *slo-1* cDNA 3 | AAGCACATAGTGGTCTGTGGC |
| *slo-1* cDNA 4 | GGCCTACCTTCTAAATATCCC |
| *slo-1* cDNA 5 | TCATCCAGCCTCAAACTCAAG |
| *slo-1* cDNA 6 | AATTCGATGAGTATTCCGCCA |
| *slo-1* cDNA 7 | GCTATCTCGAGCAGATTTACG |
| *slo-1* cDNA 8 | TCGCCATTTCAGTGTTGGATT |
| *slo-1* cDNA 9 | AGGATTAAAAATACTGATTAC |

**Primers for confirmation of mutations in genomic DNA sequence**

| | |
|---|---|
| e66 confirm seq | CCGCAAAGCGTCGTACAATAG |
| e66 confirm seq OF | TCCAGGATTCCGTTTCCTCCG |
| e66 confirm seq IF | CTACAGTACCTCAACATCCTG |
| e66 confirm seq OR | CGCTAGGTTCCTAAAATCATG |
| e66 confirm seq IR | GCCGTTTCCAGCCCGATTTCG |
| | |
| e42 confirm seq | CGCATAACTCAGTCAGTTTTG |
| e42 confirm seq IF | CATATCACCTACGATTCGGTG |
| e42 confirm seq IR | TAATCTAGTGGCTATGGGTGG |
| e42 confirm seq OR | TAATCTAGTGGCTATGGGTGG |

| | |
|---|---|
| e76/13a confirm seq | GTCCCATGATGTCCCATGTGC |
| e76/13a confirm seq OF | TGCCTGGTCCTTGCCAACAAG |
| e76/13a confirm seq IF | ACAAGTACAGTACCAATCCGG |
| e76/13a confirm seq OR | GCCTGAAACGGCCTACTTTCG |
| e76/13a confirm seq IR | TCACTAAGAAGAGCAAGTCCG |
| | |
| e13b confirm seq | CACCAAGCTCCGTAATCATCG |
| e13b confirm seq OF | GAACCAAGTTACAAGGATTTG |
| e13b confirm seq IF | ACCCAAGGTTCCAAAATAGTG |
| e13b confirm seq OR | ATGGCGAAGGCAGTTCCGCAG |
| e13b confirm seq IR | GGTCGAGGAATTGCACATTTG |
| | |
| *pd24* confirm seq (*slo-1* gap 9 seq 3) | GACAAGGTGAATCGAACAAG |
| *pd24* confirm seq (*slo-1* gap 9) IF | TGTGGGCCGAAAATCTTTCC |
| *pd24* confirm seq (*slo-1* gap 9) OF | ATTAGGCCGAAAGTAGGCCG |
| *pd24* confirm seq (*slo-1* gap 9) OR | TCCTTCGGGCCTTTTTCAGC |
| *pd24* confirm seq (*slo-1* gap 9) IR | CCAAAATCGGCCTGAAAACG |

**Primers for amplification and sequencing individual *slo-1* exons**

| | |
|---|---|
| *slo-1* gap 1 OF | GACAGATATGTCTAGGCACG |
| *slo-1* gap 1 IF | GCCTAACTGGTCCATTATG |
| *slo-1* gap 1 OR | TTCAACCGCGACGCGACCGC |
| *slo-1* gap 1 IR | GTCAATTGAAAGCTGGCAAC |
| *slo-1* gap 1 seq | TTCATTTATTCGTCGGGAGG |
| *slo-1* gap 2 IF | AGCCACAAACTCAAAGTATC |
| *slo-1* gap 2 OF | TTATTTTGAAGCTAGCGACG |
| *slo-1* gap 2 IR | AGCTGCATCGCTAGAGAATC |
| *slo-1* gap 2 OR | TGCGGTCCCGAATACTTCTG |
| *slo-1* gap 2 seq | AATTCCGACCGCGACGCGAC |
| *slo-1* gap 3 OF | TCAAATTGAAGCTGAAAACG |
| *slo-1* gap 3 IF | AGAACCGAGTGAGTTTGATG |
| *slo-1* gap 3 IR | CCAGGTCGATTTGTTGCGAG |
| *slo-1* gap 3 OR | TCGGACGCGGCGATGAACTG |
| *slo-1* gap 3 seq | TGTAGCCTACACCTGTTGAG |
| *slo-1* gap 4 OF | AATTGGTCTCAGAATGTCCC |
| *slo-1* gap 4 IF | TGTTCCCACAGTGTCGCCAG |
| *slo-1* gap 4 seq | ATGCCTGAATTTTGTGTCTG |
| *slo-1* gap 5 OF | CATATTGCCAATATGGACTG |
| *slo-1* gap 5 IF | CAAGTTTCGTCTATTCTACC |
| *slo-1* gap 5 IR | AAAGGCGTCTAAGGGTGTGG |
| *slo-1* gap5 OR | TTCTCTACCAAAACTACCAG |
| *slo-1* gap 5 seq | GGAAATTTGACGGAGAATCC |
| *slo-1* gap 6 OF | TCAAAACTCACATTTTCCCG |
| *slo-1* gap 6 IF | CCTCGTATCACTCGACACAC |
| *slo-1* gap 6 IR | CCAGTGGAACATTCCAGTAC |
| *slo-1* gap 6 OR | GTTGAGTACGGTCATAGCGG |
| *slo-1* gap 6 seq | CAGTCATCACCGCTTCCAGC |
| *slo-1* gap 7 OF | GCCACTTTCAAGCCCGAAGG |
| *slo-1* gap 7 IF | CCGTTTCGGGCCGTATTCAG |

| | |
|---|---|
| *slo-1* gap 7 seq | ACCTAGCCAATATGAGTGTC |
| *slo-1* gap 7 IR | TATTGGTCCTTCGGAGTCGG |
| *slo-1* gap 7 OR | ATTCAGGTCCACACGATACC |
| *slo-1* gap 8 IF | CCCATATCGGCTATATTTGG |
| *slo-1* gap 8 OF | CGAACTCCTGATGTTTTAAG |
| *slo-1* gap 8 seq 1 | CTTAAAATCGCACGGATAAC |
| *slo-1* gap 8 seq 2 | GATGTACCCAAGTGTCCCCG |
| *slo-1* gap 8 IR | AAGTCGCATAACTCAGTCAG |
| *slo-1* gap 8 OR | TATGGGTGTCAAATTTACGG |
| *slo-1* gap 9 IF | TGTGGGCCGAAAATCTTTCC |
| *slo-1* gap 9 OF | ATTAGGCCGAAAGTAGGCCG |
| *slo-1* gap 9 seq 1 | GTGTTCGCATTGTCTATGTC |
| *slo-1* gap 9 seq 2 | AAATTGTCCGTTTCAGTCCG |
| *slo-1* gap 9 seq 3 | GACAAGGTGAATCGAACAAG |
| *slo-1* gap 9 IR | CCAAAATCGGCCTGAAAACG |
| *slo-1* gap 9 OR | TCCTTCGGGCCTTTTTCAGC |

**Primers for generation of *slo-1* insert for insertion into pIRES2-EGFP**

| | |
|---|---|
| *slo-1* cDNA 0 | ATGGGCGAGATTTACTCGCCT |
| Kozak + part Nhe1 F | AGCCACCATGGGCGAGATTTACTCG |
| Nhe1 + Kozak F | CCGAGGCTAGCCACCATGGGCGAGAT |
| *unc-54* R2 | GTCAGAGGCACGGGCGCG |
| *unc-54* R3 | TACTCGTTAGTTAGTAGAACTC |
| *unc-54* R4 | AACTTACTCTGATGACAGCGGC |

# Appendix 2

| **Genotype** | **Allele** | **Strain** |
|---|---|---|
| Wild type | | *N2* |
| Wild type | | *CB4856* |
| *lat-1 / mIn1* | *ok1465* | *VC965* |
| *lat-1 / lat-1* | *ok1465* | *XA3750* (selected from *VC965*) |
| *lat-2 / lat-2* | *ok301* | *VC158* |
| *lat-2 / lat-2* | *ok301* | *XA3726* (*VC158* out crossed 5X) |
| *lat-2 / lat-2* | *tm463* | *TM463* |
| *lat-2 / lat-2* | *tm463* | *XA3727* (*TM463* out crossed 5X) |
| *lat-2 lat-1 / mIn1* | *tm463 ok1465* | *XA3744* |
| *lat-1 lat-2 / lat-1 lat-2* | *tm463 ok1465* | *XA3749* (selected from *XA3744*) |
| *slo-1* | *js379* | *NM1968* |
| *slo-1* | *ky399* | *CX3940* |
| *slo-1* | *ky399* | *XA3751* (*CX3940* out crossed 1X) |
| *slo-1* | *ky389* | *CX3933* |
| *slo-1* | *pd17* | *XA3745* |
| *slo-1* | *pd19* | *XA3746* |
| *slo-1* | *pd21* | |
| *slo-1* | *pd23* | *XA3747* |
| *slo-1* | *pd24* | *XA3748* |
| *slo-1* | *pd46* | |
| *slo-1* | *pd47* | |
| *dpy-20* | *e1282* | *CB1282* |

# Appendix 3

| Construct name | Description / Use |
|---|---|
| pPD118.33 | Used as a transfection marker when generating transgenic *C. elegans*. Contains *gfp* driven by the *myo-2* promoter. |
| pBK3.1 | Used for expression of *C. elegans slo-1*(+) in neurons. Contains *C. elegans slo-1* cDNAa driven by the *snb-1* promoter. |
| pBK4.1 | Used for expression of *C. elegans slo-1*(+) in body wall muscle. Contains *C. elegans slo-1* cDNAa driven by the *myo-3* promoter |
| pIRES2-EGFP | Used for expressing *C. elegans slo-1* in HEK293 cells. Expression in eukaryotic cells is driven using the CMV promoter. GFP and the insert (*slo-1*) are translated independently due to the presence of the internal ribosomal entry site (IRES). |
| pCMV4-XL6 | Used for expressing *kcnma1* in HEK293 cells. Expression in eukaryotic cells is driven using the CMV promoter. |

# Appendix 4

## Variability in *lat-2*(*tm463*) *XA3727* thrashing assays

**1)**

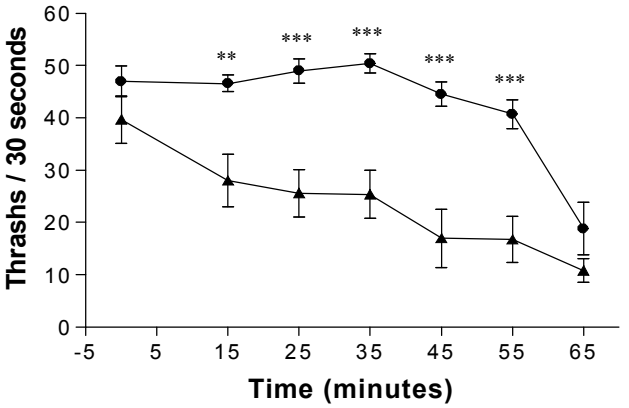


**2)**

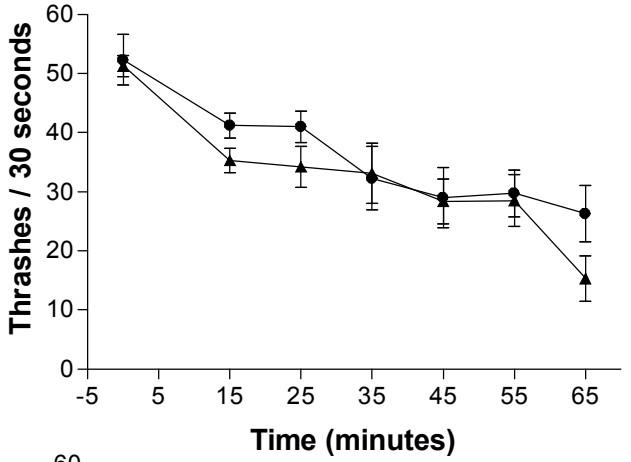


**3)**

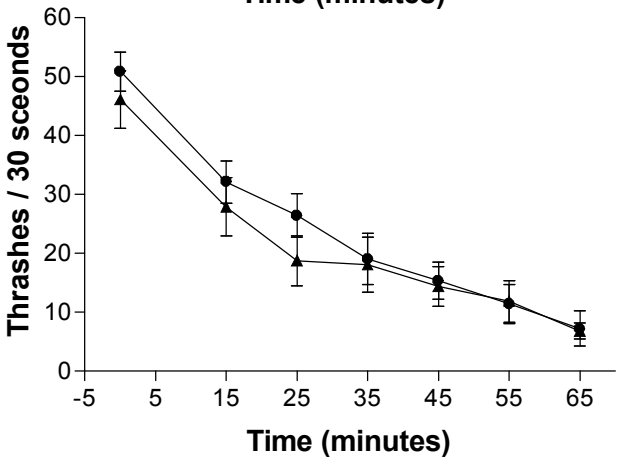


**Figure A. *lat-2*(*tm465*) *XA3727* thrashing assay.** Effect of 10 μM emodepside on N2 (▲) and *lat-2*(*tm463*) (●) *C. elegans* thrashing behaviour over the course of 65 minutes. Graphs 1, 2 and 3 show data collected in three independent assays. Each point in an average of 10 ± the S. E. Mean. ** indicates $P<0.01$ and *** indicates $P<0.001$ compared to WT.

**Effect of out crossing on *lat-2*(*ok301*) emodepside sensitivity in body bends assay**

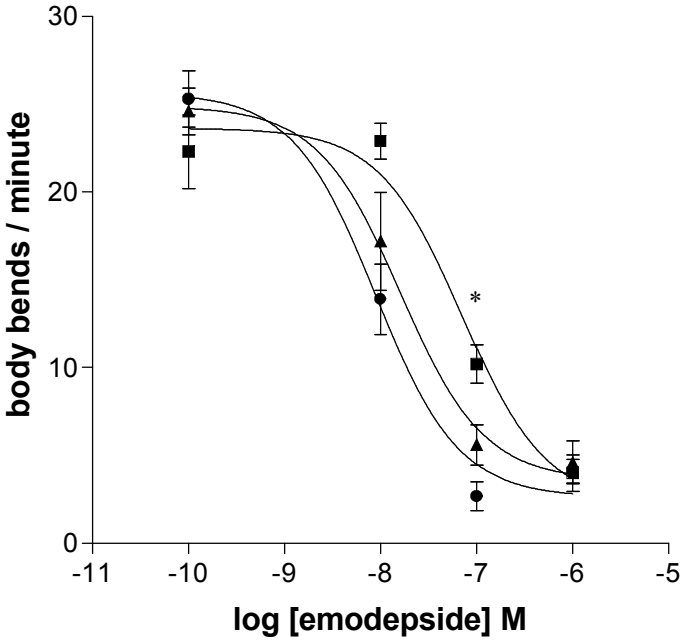


**Figure B. *lat-2*(*ok301*) out crossing increases emodepside sensitivity.** Dose response curve for emodepside on *lat-2*(*ok301*) *XA3726* (●), *lat-2*(*ok301*) *VC158* (■) and WT (▲). Each point is the mean ± S.E.Mean of 10 determinants. * indicates $P<0.05$ compared to WT.

**Example of tracking *lat-2*(*ok301*) deletion during out crossing using PCR.**

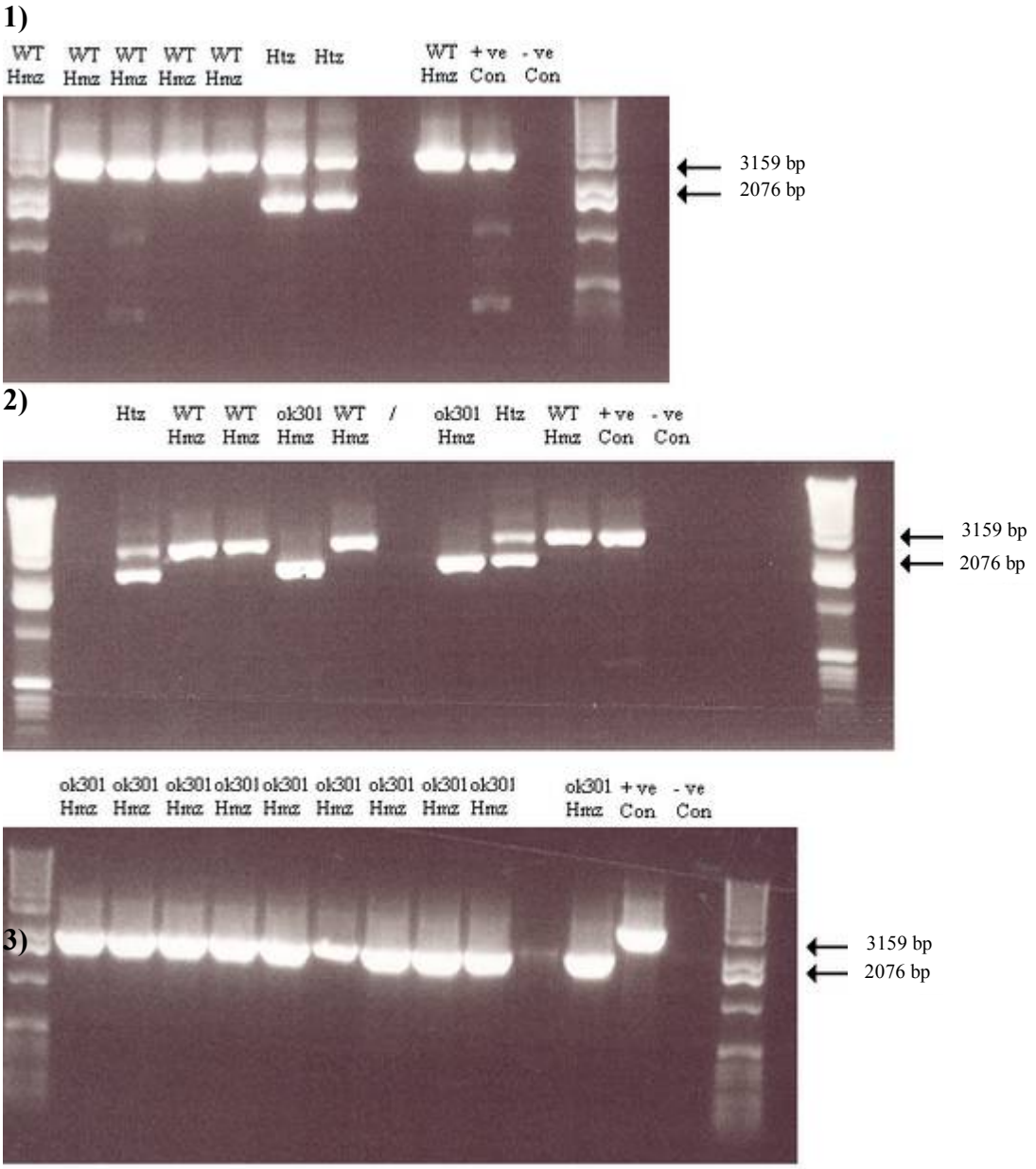


**Figure C. Tracking *lat-2*(*ok301*) deletion during out crossing.** Shows **1)** the genotype of progeny from a WT hermaphrodite X *ok301* homozygous male cross, **2)** the genotype of progeny from a *ok301* heterozygous hermaphrodite self cross, **3)** the genotype of progeny from a *ok301* homozygous hermaphrodite self cross.

**Identification of possible *slo-1* splice variant**

Amplification of *slo*-1 cDNA revealed the presence of a fragment of ~1600 bp (figure 4.12). Sequencing of these cDNA was hindered by the presence of more than one sequence. Double sequence was present in a region not identified as encoding one of the three alternate splice variants, a, b and c (Wang *et al* 2001). By reading through the double sequence, a region between exons 2 and 3 (of the identified splice variants) was found to be encoded in the *slo-1* cDNA of *pd17*, *pd19*, *pd21*, *pd23* and *pd24*. The sequence of this region between exon 2 and 3 is shown in figure D. This sequence follows into exon 14, missing out exons 3 to 13. The sum of exons 1 and 2, the shown in figure D and exons 14 to 20 is 1630 bp. This corresponds to the size of the PCR fragments observed in figure 4.12. This may represent an alternate splice variant for *slo-1*.

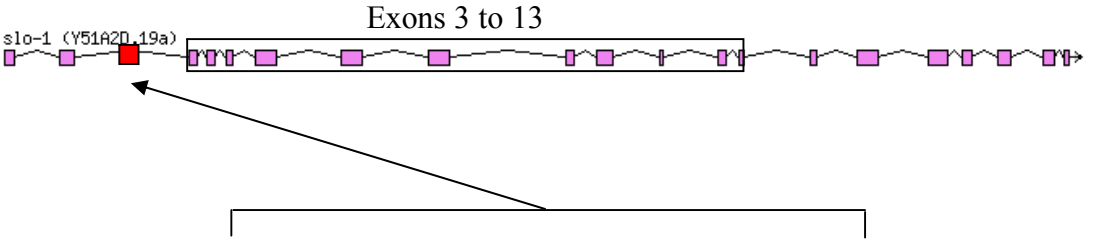


**gattctctagcgatgcagctttacagaagtattcgggaccgcagg**

**Figure D. Possible alternate *slo-1* spice variant.** The sequence between exon 2 and 3 in splice variant a is shown above in the gene model.

However, the intron exon boundaries for this putative exon lack some of the conserved consensus sequence. The intron sequence at the 5' end of the putative exon ends in AG, which is conserved. The intron sequence at the 3' end of the putative exon begins in GC, whereas the conserved sequence is GT. Using a translate tool (www.expasy.ch) revealed that the proposed exons reads into exon 14 out of frame.

# Reference list


Amliwala K. (2005). Molecular and genetic determinants of the inhibitory action of emodepside on *C. elegans* muscle. PhD thesis

Amliwala K, Bull K, Willson J, Harder A, Holden-Dye L, & Walker RJ. (2004). Emodepside, a cyclo-octadepsipeptide anthelmintic with a novel mode of action. *Drugs of the Future* **29**, 1015-1024.

Aceves J., Erlij D. and Martínez-Marañón R. The mechanism of the paralysing action of tetramisole on *Ascaris* somatic muscle (1970). *British Journal of Pharmacology* **38**, 602-607.

Adelman J.P., Shen K.Z., Kavanaugh M.P., Warren R.A., Wu Y.N., Lagrutta A., Bond C.T. and North R.A. (1992). Calcium-activated potassium channels expressed from cloned complementary DNAs. *Neuron*. **9**, 209-216.

Ahring P.K., Strøbaek D., Christophersen P., Olesen S.P. and Johansen T.E. (1997). Stable expression of the human large-conductance Ca2+-activated K+ channel alpha- and beta-subunits in HEK293 cells. *FEBS* **415**, 67-70.

Albertson D.G. and Thomson J.N. (1976). The pharynx of Caenorhabditis elegans. *Philos. Trans. R. Soc. Lond. B. Biol. Sci*. **275**, 299-325.

Alfonso A., Grundahl K., Duerr J.S., Han H.-P., and Ran, J.B. (1993). The *Caenorhabditis elegans unc-17* gene: a putative vesicular acetylcholine transporter. *Science*. **261**, 617–619.

Alkema M.J., Hunter-Ensor M., Ringstad N. and Horvitz H.R. (2005). Tyramine Functions Independently of Octopamine in the *Caenorhabditis elegans* Nervous System. *Neuron*. **46**, 247–260.

Anderson P. (1995). Mutagenesis. *Methods. Cel.l Biol*. **48**, 31-58.

Angstadt J.D. and Stretton A. O. (1989). Slow active potentials in ventral inhibitory motor neurons of the nematode Ascaris. *J. Comp. Physiol*. **166**, 165-177.

Arena J.P., Liu K.K., Paress P.S., Schaeffer J.M. and Cully D.F. (1992). Expression of a glutamate-activated chloride current in Xenopus oocytes injected with Caenorhabditis elegans RNA: evidence for modulation by avermectin. *Brain. Res. Mol. Brain. Res*. 15, 339-348.

Atkinson N.S., Robertson G.A. and Ganetzky B. (1991). A component of calcium-activated potassium channels encoded by the Drosophila slo locus. *Science* **253**, 551-555.

Avery L. (1993). Motor neuron M3 controls pharyngeal muscle relaxation timing in *Caenorhabditis elegans*. *J. Exp. Biol*. ***175***, 283–297.

Bakker N., Vervelde L., Kanobana K., Knox D.P., Cornelissen A.W., de Vries E. and Yatsuda A.P. (2004). Vaccination against the nematode Haemonchus contortus with a thiol-binding fraction from the excretory/secretory products (ES). *Vaccine*. **22**, 618-628.

Bamber B.A., Beg A.A., Twyman R.E. and Jorgensen E.M. J Neurosci. (1999). The Caenorhabditis elegans unc-49 locus encodes multiple subunits of a heteromultimeric GABA receptor. *J. Neurosci*. **19**, 5348-5359.

Bao L., Rapin A., M. Holmstrand E.C. and Cox D.H. (2002). Elimination of the $BK_{Ca}$ Channel's High-Affinity $Ca^{2+}$ Sensitivity. *Journal of General Physiology*. **120**, 173-189.

Bastiani C., and Mendel J. (2006). Heterotrimeric G proteins in *C. elegans*. Wormbook

Beg A.A. and Jorgensen E.M. (2003). EXP-1 is an excitatory GABA-gated cation channel. *Nat. Neurosci*. **6**, 1145-1152.

Benatar, M. (2000). Neurological potassium channelopathies. *QJM*. **93**, 787-797.

Bentzen B.H., Nardi A., Calloe K., Madsen L.S., Olesen S.P. and Grunnet M. (2007). The small molecule NS11021 is a potent and specific activator of Ca2+-activated big-conductance K+ channels. *Mol. Pharmacol*. **72**, 1033-1044.

Berns A.J., Van Kraaikamp M., Bloemendal H. and Lane C.D. (1972). Calf crystallin synthesis in frog cells: the translation of lens-cell 14S RNA in oocytes. *Proc. Natl. Acad. Sci. USA*. **69**, 1606-1609.

Bian S., Favre I. and Moczydlowski E. (2001). Ca2+-binding activity of a COOH-terminal fragment of the Drosophila BK channel involved in Ca2+-dependent activation. *Proc. Natl. Acad. Sc. USA*. **98**, 4776-4781.

Bittner M. A. (2000). Alpha-latrotoxin and its receptors CIRL (latrophilin) and neurexin 1 alpha mediate effects on secretion through multiple mechanisms. *Biochimie*. **82**, 447-452.

Blaxter M.L., De Ley P., Garey J.R., Liu L.X., Scheldeman P., Vierstraete A., Vanfleteren J.R., Mackey L.Y., Dorris M., Frisse L.M., Vida J.T. and Thomas W.K. (1998). A molecular evolutionary framework for the phylum Nematoda. *Nature*. **392**, 71-75.

Brenner S. (1974). The genetics of *Caenorhabditis elegans*. *Genetics*. **77**, 71-94.

Brockie, P.J., Madsen, D.M., Zheng, Y., Mellem, J., and Maricq, A.V. (2001). Differential expression of glutamate receptor subunits in the nervous system of *C. elegans* and their regulation by the homeodomain protein UNC-42. *J. Neurosci*. **21**, 1510–1522

Brundage L., Avery L., Katz A., Kim U.J., Mendel J.E., Sternberg P.W., and Simon M.I. (1996). Mutations in a C. elegans $G_q$alpha Gene Disrupt Movement, Egg Laying, and Viability. *Neuron*. **16**, 999-1009.

Bull K., Cook A., Hopper N.A., Harder A., Holden-Dye L., Walker R.J. (2007). Effects of the novel anthelmintic emodepside on the locomotion, egg-laying behaviour and development of *Caenorhabditis elegans*. *Int. J. Parasitol*. **37**, 627-636.

Burglin T.R.(1998). Caenorhabditis elegans as a model for parasitic nematodes. *Int. J. Parasitol*. **28**, 395-411.

Butler A., Tsunoda S., McCobb D.P., Wei A. and Salkoff L. (1993). mSlo, a complex mouse gene encoding "maxi" calcium-activated potassium channels. *Science*. **261**, 221-224.

Carre-Pierrat M., Grisoni K., Gieseler K., Mariol M.C., Martin E., Jospin M., Allard B.and Ségalat L. (2006). The SLO-1 BK channel of *Caenorhabditis elegans* is critical for muscle function and is involved in dystrophin-dependent muscle dystrophy. *J. Mol. Biol*. **358**, 387-395.

Chalfie M, Sulston JE, White JG, Southgate E, Thomson JN, Brenner S. (1985). The neural circuit for touch sensitivity in *Caenorhabditis elegans*. *J. Neurosci*. **5,** 956-964.

Chase D.L., and Koelle M.R. Biogenic amine neurotransmitters in *C. elegans.* (2007). Wormbook.

Chen W., Terada M. and Cheng J.T. (1996). Characterization of subtypes of gamma-aminobutyric acid receptors in an Ascaris muscle preparation by binding assay and binding of PF1022A, a new anthelmintic, on the receptors. *Parasitol. Res.* **82**, 97-101

Chen L., Krause M., Sepanski M. and Fire A. (1994). The *Caenorhabditis elegans* MYOD homologue HLH-1 is essential for proper muscle function and complete morphogenesis. *Development*. **120**, 1631-1641.

Chiang J.T., Steciuk M., Shtonda B. and Avery L. (2006). Evolution of pharyngeal behaviours and neuronal functions in free-living soil nematodes. *J. Exp. Biol*. **209**, 1859-1873

Chiba C.M., Rankin C.H. (1990). A developmental analysis of spontaneous and reflexive reversals in the nematode *Caenorhabditis elegans*. *J. Neurobiol*. **21**, 543-554.

Cook A., Franks C.J. and Holden-Dye L. (2006). Electrophysiological recordings from the pharynx. *Wormbook*.

Cormack B.P., Valdivia R.H. and Falkow S. (1996). FACS-optimized mutants of the green fluorescent protein (GFP) *Gene*. **173**, 33-38

Corwin R.M. (1997). Economics of gastrointestinal parasitism of cattle. *Vet. Parasitol*. **72**,451-457.

Culetto, E., Baylis, H.A., Richmond, J.E., Jones, A.K., Fleming, J.T., Squire, M.D., Lewis, J.A., and Sattelle, D.B. (2004). The *Caenorhabditis elegans unc-63* gene encodes a levamisole-sensitive nicotinic acetylcholine receptor β subunit. *J. Biol. Chem*. **279**, 42476–42483

Crowder C. M. (2004). Ethanol targets: a BK channel cocktail in *C. elegans*. *Trends Neurosci.* **27**, 579-582.

Cully D.F., Vassilatis D.K., Liu K.K, Paress P.S., Van der Ploeg L.H., Schaeffer J.M. and Arena J.P. (1994). Cloning of an avermectin-sensitive glutamate-gated chloride channel from *Caenorhabditis elegans*. *Nature*. **371**, 707-711.

Davies A.G., Pierce-Shimomura J.T., Kim H., VanHoven M.K., Thiele T.R., Bonci A., Bargmann C. I. and McIntire S.L. (2003). A central role of the BK potassium channel in behavioral responses to ethanol in *C. elegans*. *Cell* **115**, 655-666.

Davletov1 B.A., Meunier F.A., Ashton A.C., Matsushita H., Hirst W.D., Lelianova V.G., Wilkin G.P., Dolly J.O. and Ushkaryov Y.A. (1998). Vesicle exocytosis stimulated by a-latrotoxin is mediated by latrophilin and requires both external and stored Ca2F. *EMBO*. **17**, 3909–3920.

Dent J.A., Smith M.M., Vassilatis D.K. and Avery L. (2000). The genetics of ivermectin resistance in *Caenorhabditis elegans*. *Proc. Natl. Acad. Sci. USA*. **97**, 2674-2679

Dillon J., Hopper N.A., Holden-Dye L. and O'Connor V. (2006). Molecular characterization of the metabotropic glutamate receptor family in *Caenorhabditis elegans. Biochem. Soc. Trans*. **34**, 942-948.

Doyle D.A., Morais Cabral J., Pfuetzner R.A., Kuo A., Gulbis J.M., Cohen S.L., Chait B.T. and MacKinnon R. (1998). The structure of the potassium channel: molecular basis of K+ conduction and selectivity. *Science*. **280**, 69-77.

Dryer S.E. (1994). $Na^+$-activated $K^+$ channels: a new family of large-conductance ion channels. *Trends. Neurosci*. **17**, 155-60

Edgley M.L. and Riddle D.L. (2001). LG II balancer chromosomes in *Caenorhabditis elegans*: mT1(II;III) and the mIn1 set of dominantly and recessively marked inversions. *Mol. Genet. Genomics*. **266**, 385-395.

Elkins T., Ganetzky B. and Wu C.F. (1986). A Drosophila mutation that eliminates a calcium-dependent potassium current. *Proc. Natl. Acad. Sci. USA*. **83**, 8415-8419.

Esposito G., Di Schiavi E., Bergamasco C. and Bazzicalupo P. (2007). Efficient and cell specific knock-down of gene function in targeted *C. elegans* neurons. *Gene*. **395**, 170-176.

Fisher M. (2003). Toxocara cati: an underestimated zoonotic agent. *Trends Parasitol*. **19**, 167-170.

Fleming J.T., Squire M.D., Barnes T.M., Tornoe C., Matsuda K., Ahnn J., Fire A., Sulston J.E., Barnard E.A., Sattelle D.B. and Lewis J.A. (1997). *Caenorhabditis elegans* levamisole resistance genes *lev-1*, *unc-29*, and *unc-38* encode functional nicotinic acetylcholine receptor subunits. *J. Neurosci*. **17**, 5843-5857.

Foord S. M., Jupe S., Holbrook J. (2002). Bioinformatics and type II G-protein-coupled receptors. *Biochem. Soc. Trans*. **30**, 473-479.

Frontali N., Ceccarelli B., Gorio A., Mauro A., Siekevitz P., Tzeng M.C. and Hurlbut W.P. (1976). Purification from black widow spider venom of a protein factor causing the depletion of synaptic vesicles at neuromuscular junctions. *J. Cell. Biol.*. 68, 462-479.

Gally C., Eimer S., Richmond J.E. and Bessereau J.L. (2004). A transmembrane protein required for acetylcholine receptor clustering in *Caenorhabditis elegans*. *Nature*. **431**, 578-582.

Galvez A., Gimenez-Gallego G., Reuben J.P., Roy-Contancin L., Feigenbaum P., Kaczorowski G.J., Garcia M.L. (1990). Purification and characterization of a unique, potent, peptidyl probe for the high conductance calcium-activated potassium channel from venom of the scorpion *Buthus tamulus*. *J. Biol. Chem.* **265**, 11083-11090.

Gami M.S. and Wolkow C.A. (2006). Studies of *Caenorhabditis elegans* DAF-2/insulin signaling reveal targets for pharmacological manipulation of lifespan. *Aging Cell.* **5**, 31-37.

Garthwaite D., Thomas M.R., Dawson A. and Stoddart H. (2003). Arable crops in Great Britain 2002. *Pesticides usage survey report*. **187**.

GeBner G., Meder S., Rink T. and Boheim G. (1996). Ionophore and Anthelmintic Activity of PF1022A, a Cyclooctadepsipeptide, Are Not Related. *Pestic. Sci.* **48**, 399-407.

Gray J.M., Hill J.J., Bargmann C.I. (2005). A circuit for navigation in *Caenorhabditis elegans*. *Proc. Natl. Acad. Sci. USA*. **102**, 3184-3191

Gottschalk A., Almedom R.B., Schedletzky T., Anderson S.D., Yates J.R. and Schafer W.R.(2005). Identification and characterization of novel nicotinic receptor-associated proteins in *Caenorhabditis elegans*. *EMBO J*. **24**, 2566-2578

Hamill O.P., Marty A., Neher E., Sakmann B. and Sigworth F.J. (1981). Improved patch-clamp techniques for high-resolution current recording from cells and cell-free membrane patches. *Pflugers Arch*. **391**, 85-100.

Harder A. and Samson-Himmelstjerna G. (2002). Cyclooctadepsipeptides, a new class of anthelmintically active compounds. *Parasitol. Res.* **88**, 481-488

Harmar A. J. (2001). Family-B G-protein-coupled receptors. *Genome. Biol*. **2**, 12.

Hawasli A.H., Saifee O., Liu C., Nonet M.L., Crowder C.M. (2004). Resistance to volatile anesthetics by mutations enhancing excitatory neurotransmitter release in *Caenorhabditis elegans*. *Genetics*. **168**, 831-843.

Hensley S.H., Yang X.L. and Wu S.M. (1993). Relative contribution of rod and cone inputs to bipolar cells and ganglion cells in the tiger salamander retina. *J. Neurophysiol*. **69**, 2086-2098.

Hirsh D., Oppenheim D. and Klass M. (1976). Development of the reproductive system of *Caenorhabditis elegans*. *Developmental Biology*. **49**, 200-219.

Hoekstra R., Visser A., Wiley L.J., Weiss A.S., Sangster N.C. and Roos M.H. (1997). Characterization of an acetylcholine receptor gene of *Haemonchus contortus* in relation to levamisole resistance. *Mol. Biochem. Parasitol*. **84**, 179-187.

Holden-Dye L., Krogsgaard-Larsen P., Nielsen L., and Walker R.J. (1989). GABA receptors on the somatic muscle cells of the parasitic nematode, Ascaris suum: stereoselectivity indicates similarity to a GABAA-type agonist recognition site. *Br. J. Pharmacol.* **98**, 841-850.

Holden-Dye L. and Walker R.J. (1990). Avermectin and avermectin derivatives are antagonists at the 4-aminobutyric acid (GABA) receptor on the somatic muscle cells of *Ascaris*; is this the site of anthelmintic action? *Parasitology*. **101**, 265-271.

Horn R. and Patlak J. (1980). Single channel currents from excised patches of muscle membrane. *Proc. Natl. Acad. Sci. USA*. **77**, 6930-6934.

Hurley H.J., Newton A.C., Parker P.J., Blumberg P.M. and Nishizuka Y. (1997). Calcium activation of $BK_{Ca}$ potassium channels lacking the calcium bowl and RCK domains. *Protein Science*. **6**, 477-480

Husson S.J., Clynen E., Baggerman G., Janssen T., and Schoofs L. (2006). Defective processing of neuropeptide precursors in *Caenorhabditis elegans* lacking proprotein convertase 2 (KPC-2/EGL-3): mutant analysis by mass spectrometry. *J. Neurochem*. **98**, 1999-2012.

Isaac R.E., MacGregor D. and Coates D. (1996). Metabolism and inactivation of neurotransmitters in nematodes. *Parasitology*. **113**, S157-S173.

Jacob T.C. and Kaplan J.M. (2003). The EGL-21 carboxypeptidase E facilitates acetylcholine release at *Caenorhabditis elegans* neuromuscular junctions. *J. Neurosci*. **23**, 2122-2130.

Le Jambre L.F., Gill J.H., Lenane I.J. and Baker P. (2000). Inheritance of avermectin resistance in *Haemonchus contortus*. *Int. J. Parasitol*. **30**, 105-111.

Lim H., arh B. J., Choi H. S., Park C S., Eom S. H. and Ahnn J. (1999). Identification and characterisation of a putative *C. elegans* potassium channel gene (Ce-slo-2) distantly related to $Ca^{2+}$-activated $K^{+}$ channels. *Gene*. **240**, 35-43.

Liu J. and Misler S. (1998). alpha-Latrotoxin alters spontaneous and depolarization-evoked quantal release from rat adrenal chromaffin cells: evidence for multiple modes of action. *J. Neurosci*. **18**, 6113-6125.

Jiang B., Sun X., Cao K. and Wang R. (2002). Endogenous Kv channels in human embryonic kidney (HEK-293) cells. *Mol. Cell. Biochem*. **238**, 69-79.

Johnson C.D., Rand J.B. Herman R.K. Stern, B.D. and Russell R.L. (1988). The acetylcholinesterase genes of *C. elegans*: identification of a third gene (*ace-3*) and mosaic mapping of a synthetic lethal phenotype. *Neuron*. **1**, 165–173.

Johnson C.D. and Stretton A.O. (1985). Localization of choline acetyltransferase within identified motoneurons of the nematode *Ascaris*. *J. Neurosci*. **5**, 1984-1992.

Jorgensen E.M. GABA. (2005). *Wormbook*.

Kameyama M., Kakei M., Sato R., Shibasaki T., Matsuda H. and Irisawa H. (1984). Intracellular Na+ activates a K+ channel in mammalian cardiac cells. *Nature.* **309**, 354-356.

Kaminsky R., Ducray P., Jung M., Clover R., Rufener L., Bouvier J., Weber S.S., Wenger A., Wieland-Berghausen S., Goebel T., Gauvry N., Pautrat F., Skripsky T., Froelich O., Komoin-Oka C., Westlund B., Sluder A. and Maser P. (2008). A new class of anthelmintics effective against drug-resistant nematodes. *Nature*. **452**, 176-180.

Karbowski J., Schindelman G., Cronin C.J., Seah A. and Sternberg P.W. (2008). Systems level circuit model of *C. elegans* undulatory locomotion: mathematical modeling and molecular genetics. *J Comput Neurosci*. **24**, 253-276.

Kass J,. Jacob T.C, Kim P. and Kaplan J.M. (2001). The EGL-3 proprotein convertase regulates mechanosensory responses of *Caenorhabditis elegans*. *J. Neurosci*. **21**, 9265-9272.

Kerry B., Barker A. and Evans K. (2003). Investigation of potato cyst nematode control. Nematode Interactions Unit, Plant-Pathogens Interactions Division, Rothamsted Research. Commissioned by DEFRA under contract no. HH3111TPO.

Kimble J. and Hirsh D. (1979). The postembryonic cell lineages of the hermaphrodite and male gonads in *Caenorhabditis elegans*. *Developmental Biology*. **70**, 396-417.

Knaus H.G., Eberhart A., Koch R.O.A., Munujos P., Schmalhofer W.A., Warmke J.W., Kaczorowski G.J. and Garcia M.L. (1995). Characterization of tissue-expressed alpha subunits of the high conductance Ca(2+)-activated K+ channel. *J. Biol. Chem*. **270**, 22434-22439.

Knox D.P. and Smith W.D. (2001). Vaccination against gastrointestinal nematode parasites of ruminants using gut-expressed antigens. *Vet. Parasitol*. **100**, 21-32.

Köhler P. (2001). The biochemical basis of anthelmintic action and resistance. *Int. J. Parasitol*. **31**, 336-345.

Kozak M. (1987). An analysis of 5'-noncoding sequences from 699 vertebrate messenger RNAs. *Nucleic Acids Res*. **15**, 8125-8148.

Kubiak T.M., Larsen M.J., Zantello M.R., Bowman J.W., Nulf S.C. and Lowery D.E. (2003). Functional annotation of the putative orphan *Caenorhabditis elegans* G-protein-coupled receptor C10C6.2 as a FLP15 peptide receptor. *J. Biol. Chem*. **278**, 42115-42120.

Kubiak T.M., Larsen M.J., Nulf S.C., Zantello M.R., Burton K.J., Bowman J.W., Modric T. and Lowery D.E. (2003). Differential activation of "social" and "solitary" variants of the *Caenorhabditis elegans* G protein-coupled receptor NPR-1 by its cognate ligand AF9. *J. Biol. Chem*. **278**, 33724-33729.

Kurejová M., Uhrík B., Sulová Z., Sedláková B., Križanová O. and Lacinová L. Changes in ultrastructure and endogenous ionic channels activity during culture of HEK 293 cell line. *Eur. J. Pharmacol*. **567**, 10-18.

Kwa, M.S.G., Veenstra, J.G., Dijk, M.V. and Roos, M.H.. (1995). β-Tubulin genes from the parasitic nematode *Haemonchus contortus* modulate drug resistance in *Caenorhabditis elegans*. *J. Mol. Biol.* **246**, 500–510.

Kwa, M.S.G., Veenstra, J.G. and Roos, M.H., 1994. Benzimidazole resistance in *Haemonchus contortus* is correlated with a conserved mutation at amino acid 200 in β-tubulin isotype 1. *Mol. Biochem. Parasitol*. **63**, 299–303.

Lacey E. (1988). The role of the cytoskeletal protein, tubulin, in the mode of action and mechanism of drug resistance to benzimidazoles. *Int. J. Parasitol.* **18**, 885–936.

Lackner M.R., Nurrish S.J. and Kaplan J.M. (1999). Facilitation of Synaptic Transmission by EGL-30 $G_q\alpha$ and EGL-8 PLCβ: DAG Binding to UNC-13 Is Required to Stimulate Acetylcholine Release. *Neuron*. **24,** 335-346.

Larsson H.P., Baker O.S., Dhillon D.S. and Isacoff E.Y. Transmembrane movement of the shaker K+ channel S4. *Neuron*. **16**, 387-397.

Levinson JN.and El-Husseini A. (2007). A crystal-clear interaction: relating neuroligin/neurexin complex structure to function at the synapse. *Neuron*. **56**, 937-939.

Lewis J.A., Wu C., Berg H., Levine J.H. (1980). The genetics of levamisole resistance in the nematode *Caenorhabditis elegans*. *Genetics*. **95**, 905-928.

Li C. (2005). The ever-expanding neuropeptide gene families in the nematode *Caenorhabditis elegans*. *Parasitology*. **131**, S109-127.

Lichtinghagen R., Stocker M., Wittka R., Boheim G., Stühmer W., Ferrus A. and Pongs O. (1990). Molecular basis of altered excitability in Shaker mutants of *Drosophila melanogaster*. *EMBO J*. **9**, 4399-4407.

Lim H. H., Park B. J., Choi H. S., Park C. S., Eom H. S. and Ahnn J. (1999). Identification and characterisation of a putative *C. elegans* potassium channel gene (*Ce-slo-2*) distantly related to $Ca^{2+}$-activated $K^+$ channels. *Gene*. **240**, 35-43.

Lints R. and Emmons S.W. (1999). Patterning of dopaminergic neurotransmitter identity among *Caenorhabditis elegans* ray sensory neurons by a TGFbeta family signaling pathway and a Hox gene. *Development*. **126**, 5819–5831.

Lithgow G.J., White T.M., Melov S. and Johnson T.E. (1995) Thermotolerance and extended life-span conferred by single-gene mutations and induced by thermal stress. *Proc. Natl. Acad. Sci. USA*. **92**, 7540-7544.

Liu L., Wan Q., Lin X., Zhu H., Volynski K., Ushkaryov Y. and Xu, T. (2005). α-Latrotoxin modulates the secretory machinery via receptor mediated activation of protein kinase C. *Traffic*. **6**, 759-765.

Liu T., Kim K., Li C. and Barr M.M. (2007). FMRFamide-like neuropeptides and mechanosensory touch receptor neurons regulate male sexual turning behavior in *Caenorhabditis elegans*. *J. Neurosci*. **27**, 7174-7182.

MacKinnon R. and Yellen G. (1990). Mutations affecting TEA blockade and ion permeation in voltage-activated K+ channels. *Science*. **250**, 276-279.

Mahoney T.R., Luo S and Nonet M.L. (2006). Analysis of synaptic transmission in *Caenorhabditis elegans* using an aldicarb-sensitivity assay. *Nat. Protoc*.**1**, 1772-1777.

Martin R.J. and Robertson A.P. (2007). Mode of action of levamisole and pyrantel, anthelmintic resistance, E153 and Q57. *Parasitology*. **134**, 1093-1104.

Martin R.J. (1985). Gamma-Aminobutyric acid- and piperazine-activated single-channel currents from *Ascaris suum* body muscle. *Br. J. Pharmacol*. **84**, 445-461.

Martin R.J. (1982). Electrophysiological effects of piperazine and diethylcarbamazine on *Ascaris suum* somatic muscle. *Br. J. Pharmacol*. **77**, 255-265.

Martin RJ, Robertson AP, Bjorn H. (1997). Target sites of anthelmintics. *Parasitology*. **114**, S111-124.

Marrion N.V. and Tavalin S.J. (1998). Selective activation of Ca2+-activated K+ channels by co-localized Ca2+ channels in hippocampal neurons. *Nature*. **395**, 900-905.

McIntire S.L., Jorgensen E., Kaplan J. and Horvitz H.R. (1993). The GABAergic nervous system of *Caenorhabditis elegans*. *Nature*. **364**, 337-341.

Mee C.J., Tomlinson S.R., Perestenko P.V., Pomerai D., Duce I.R., Usherwood P.N.R. and Bell D.R. (2004). latrophilin is required for toxicity of black widow spider venom in *Caenorhabditis elegans*. *J. Biochem.* **378**, 185-191.

Meera P., Wallner M., Song M.and Toro L. (1997). Large conductance voltage- and calcium-dependent K+ channel, a distinct member of voltage-dependent ion channels with seven N-terminal transmembrane segments (S0-S6), an extracellular N terminus, and an intracellular (S9-S10) C terminus. *Proc. Natl. Acad. Sci. USA*. **94,** 14066-14071.

Mello C.C., Kramer J.M., Stinchcomb D. and Ambros V. Efficient gene transfer in *C. elegans*: extrachromosomal maintenance and integration of transforming sequences. *EMBO J.* **10**, 3959-3970.

Mertens I., Clinckspoor I., Janssen T., Nachman R. and Schoofs L. (2006). FMRFamide related peptide ligands activate the *Caenorhabditis elegans* orphan GPCR Y59H11AL.1. *Peptides*. **27**, 1291-1296.

Miller K.G., Alfonso A., Nguyen M., Crowell J.A., Johnson C.D. and Rand J.B. (1996). A genetic selection for *Caenorhabditis elegans* synaptic transmission mutants. *Proc. Natl. Acad. Sci. USA*. **93**, 12593-12598.

Miller K.G., Emerson M.D. and Rand J.B. (1999). $G_o$alpha and diacylglycerol kinase negatively regulate the $G_q$alpha pathway in *C. elegans*. *Neuron*. **24**, 323-333.

Nishida M., Cadene M., Chait B.T. and MacKinnon R. Crystal structure of a Kir3.1-prokaryotic Kir channel chimera. (2007). *EMBO*. **26**, 4005-4015.

Nonet M.L., Saifee O., Zhao H., Rand J.B., Wei L. (1998). Synaptic transmission deficits in *Caenorhabditis elegans* synaptobrevin mutants. *J. Neurosci*. **18**, 70-80.

Nurrish S., Ségalat L. and Kaplan J.M. (1999). Serotonin inhibition of synaptic transmission: Galpha(0) decreases the abundance of UNC-13 at release sites. *Neuron*. **24**, 231-242.

Orio P., Rojas P., Ferreira G. and Latorre R. (2002). New disguises for an old channel: MaxiK channel beta-subunits. *News. Physiol. Sci*. **17**, 156-161.

Orlova E.V., Rahman M.A., Gowen B., Volynski K.E., Ashton A.C., Manser C., van Heel M. and Ushkaryov Y.A. (2000). Structure of alpha-latrotoxin oligomers reveals that divalent cation-dependent tetramers form membrane pores. *Nat. Struct. Biol*. **7**, 48-53

Papaioaanou S., Holden-Dye L. and Walker R.J. (2008). The actions of *Caenorhabditis elegans* neuropeptide-like peptides (NLPs) on body wall muscle of *Ascaris suum* and pharyngeal muscle of *C. elegans*. *Acta. Biol. Hung.* **59** (Suppl.), 189-197.

Papaioannou S., Marsden D., Franks C.J., Walker R.J. and Holden-Dye L. (2005). Role of a FMRFamide-like family of neuropeptides in the pharyngeal nervous system of *Caenorhabditis elegans*. *J. Neurobiol*. **65**, 304-319.

Papazian D.M., Timpe L.C., Jan Y.N. and Jan L.Y. (1991). Alteration of voltage-dependence of Shaker potassium channel by mutations in the S4 sequence. *Nature*. **349**, 305-310.

Pemberton D.J., Franks C.J., Walker R.J. and Holden-Dye L. (2001). Characterization of glutamate-gated chloride channels in the pharynx of wild-type and mutant *Caenorhabditis elegans* delineates the role of the subunit GluCl-alpha2 in the function of the native receptor. *Mol. Pharmacol*. **59**, 1037-1043.

Piskorowski R. and Aldrich R.W. (2002). Calcium activation of $BK_{Ca}$ potassium channels lacking the calcium bowl and RCK domains. *Nature.* **420**, 499-502.

Rand J.B. (2007). Acetylcholine. *Wormbook*.

Raizen D.M. and Avery L. (1994). Electrical activity and behavior in the pharynx of *Caenorhabditis elegans*. *Neuron*. **12**, 483-495.

Redman C.A., Robertson A., Fallon P.G., Modha J., Kusel J.R., Doenhoff M.J. and Martin R.J. (1996). Praziquantel: an urgent and exciting challenge. *Parasitol. Today*. **12**, 14-20.

Rhee J., Betz A., Pyott S., Reim K., Varoqueaux F., Augustin I., Hesse D., Sudhof T.C., Takahashi M., Rosenmund C. and Brose N. (2002). β Phorbol Ester- and Diacylglycerol-Induced augmentation of Transmitter Release Is Mediated by Munc13s and Not by PKCs. *Cell*. **108**, 121-133.

Richmond J.E. (2006). Electrophysiological recordings from the neuromuscular junction of *C. elegans*. *Wormbook*.

Richmond J.E. and Jorgensen E.M. (1999). One GABA and two acetylcholine receptors function at the *C. elegans* neuromuscular junction. *Nat. Neurosci*. **2**, 791–797.

Robertson S.J. and Martin R.J. (1993). Levamisole-activated single-channel currents from muscle of the nematode parasite *Ascaris suum*. *Br. J. Pharmacol*. **108**, 170-178.

Sade H., Muraki K., Ohya S., Hatano N. and Imaizumi Y. (2006). Activation of large-conductance, Ca2+ activated K+ channels by cannabinoids. *Am. J. Physiol. Cell. Physiol*. **290**, 77-86.

Saeger B., Schmitt-Wrede H.P., Dehnhardt M., Benten W.P., Krucken J., Harder A., Samson-Himmelstjerna G., Wiegand,H. and Wunderlich F. (2001). Latrophilin-like receptor from the parasitic nematode *Haemonchus contortus* as target for the anthelmintic depsipeptide PF1022A. *FASEB J.* **15**, 1332-1334.

Saifee O., Wei L. and Nonet M.L. (1998). The *Caenorhabditis elegans* unc-64 locus encodes a syntaxin that interacts genetically with synaptobrevin. *Mol. Biol. Cell*. **9**, 1235-1252.

Salkoff L., Butler A., Ferreira G., Santi C. and Wei A. (2006). High-conductance potassium channels of the SLO family. *Nat. Rev. Neurosci*. **7**, 921-931.

Samson-Himmelstjerna G., Harder A., Schnieder T., Kalbe J. and Mencke N. (2000). In vivo activities of the ne anthelmintic depsipeptide PF1022A. *Parisitol. res*. **86**, 194-199

Sangster N.C., Prichard R.K. and Lacey E. (1985). Tubulin and benzimidazole-resistance in *Trichostrongylus colubriformis* (Nematoda). *J. Parasitol*. **71**, 645-651.

Sangster N.C., Riley F.L. and Wiley L.J. (1998). Binding of [3H]m-aminolevamisole to receptors in levamisole-susceptible and -resistant *Haemonchus contortus*. *Int. J. Parasitol*. **28**, 707-717.

Santi C.M., Yuan A., Fawcett G., Wang Z.W., Butler A., Nonet M.L., Wei A., Rojas P. and Salkoff L. (2003). Dissection of $K^+$ currents in *Caenorhabditis elegans* muscle cells by genetics and RNA interference. *Proc. Natl. Acad. Sci. USA.* **100**, 14391-14396.

Sasaki T., Takagi M., Yaguchi T., Miyadoh S., Okada T. and Koyama M. (1992). A new anthelmintic cyclodepsipeptide, PF1022A. *J. Antibiot.* (*Tokyo*) **45**, 692-697.

Schreiber M. and Salkoff L. (1997). A novel calcium-sensing domain in the BK channel. *Biophys. J.* **73,** 1355-1363.

Schreiber M., Yuan A. and Salkoff L. (1999). Transplantable sites confer calcium sensitivity to BK channels. *Nat. Neurosci.* **2**, 416-421.

Schubert R., Noack T. and Serebryako V.N. (1999). protein kinase C reduces the $K_{ca}$ current of rat tail artery smooth muscle cells. *Am. J. Phys*. **276**, C648-C658.

Sherratt R.M., Bostock H. and Sears T.A. (1980). Effects of 4-aminopyridine on normal and demyelinated mammalian nerve fibres. *Nature*. **283**, 570-572.

Sigworth F.J. and Neher E. (1980). Single Na+ channel currents observed in cultured rat muscle cells. *Nature*. **287**, 447-449.

Stinchcomb D.T., Shaw J.E., Carr S.H. and Hirsh D. (1985). Extrachromosomal DNA transformation of *Caenorhabditis elegans*. *Mol. Cell. Biol*. **5**, 3484-3496.

Stretton A.O., Fishpool R.M., Southgate E., Donmoyer J.E., Walrond J.P., Moses J.E. and Kass I.S. (1978). Structure and physiological activity of the motoneurons of the nematode *Ascaris*. *Proc. Natl. Acad. Sci. USA*. **75**, 3493-3497.

Strøbaek D., Christophersen P., Holm N.R., Moldt P., Ahring P.K., Johansen T.E. and Olesen SP. Modulation of the Ca(2+)-dependent K+ channel, hslo, by the substituted diphenylurea NS 1608, paxilline and internal Ca2+. *Neuropharmacology*. **35**, 903-914.

Sulston J.E. and Hodgkin J. (1988). The nematode *Caenorhabditis elegans*. *Cold spring harbour laboratory press*. 594-595.

Sulston J.E. and Horvitz H.R. (1977). Post-embryonic cell lineages of the nematode, *Caenorhabditis elegans*. *Dev. Biol*. **56**, 110-156.

Sze J.Y., Victor M., Loer C., Shi Y. and Ruvkun G. (2000). Food and metabolic signalling defects in a *Caenorhabditis elegans* serotonin-synthesis mutant. *Nature*. **403**, 560–564.

Takeda D., Nakatsuka T., Gu J.G. and Yoshida M. (2007). The activation of nicotinic acetylcholine receptors enhances the inhibitory synaptic transmission in the deep dorsal horn neurons of the adult rat spinal cord. *Mol. Pain*. **3**, 26

Terada M (1992). Neuropharmacological Mechanism of Action of PF1022A, and Antinematode Anthelmintic with a New Structure of Cyclic Depsipeptide, on *Angiostrongylus cantonesis* and Isotated Frog Rectus. *Jpn. J. Parasitol*. **41**, 108-117.

The *C. elegans* sequencing consortium. (1998). Genome sequence of the nematode *C. elegans*: A platform for investigating biology. *Science*. **282**, 2012-2018.

Thomas P., Smart T.G. (2005). HEK293 cell line: a vehicle for the expression of recombinant proteins. *J. Pharmacol. Toxicol. Methods*. **51**, 187-200.

Touroutine D., Fox R.M., Von Stetina S.E., Burdina A., Miller D.M. and Richmond J.E. (2005). *acr-16* encodes an essential subunit of the levamisole-resistant nicotinic receptor at the *Caenorhabditis elegans* neuromuscular junction. *J. Biol. Chem*. **280**, 27013–27021.

Townes-Anderson E., MacLeish P.R. and Raviola E. (1985). Rod cells dissociated from mature salamander retina: ultrastructure and uptake of horseradish peroxidase. *J. Cell. Biol*. **100**, 175-88.

Trailovic S.M., Verma S., Clark C.L., Robertson A.P. and Martin R.J. (2008). Effects of the muscarinic agonist, 5-methylfurmethiodide, on contraction and electrophysiology of *Ascaris suum* muscle. *Int. J. Parasitol*. **38**, 945-957.

Troemel E.R., Sagasti A. and Bargmann C.I. (1999). Lateral signaling mediated by axon contact and calcium entry regulates asymmetric odorant receptor expression in C. elegans. *Cell*. **99**, 387-398.

Van Den Bossche H. and De Nollin S. (1973). Effects of mebendazole on the absorption of low molecular weight nutrients by *Ascaris suum*. *Int. J. Parasitol*. **3**, 401-407.

Vergara C., Latorre R., Marrion N.V. and Adelman J.P. (1998). Calcium-activated potassium channels. *Curr. Opin. Neurobiol*. **8**, 321-329.

Waggoner L.E., Hardaker L.A., Golik S. and Schafer W.R. (2000). Effect of a neuropeptide gene on behavioral states in *Caenorhabditis elegans* egg-laying. *Genetics*. **154**, 1181-1192.

Walker R.J., Colquhoun L. and Holden-Dye L. (1992). Pharmacological profiles of the GABA and acetylcholine receptors from the nematode, *Ascaris suum*. *Acta. Biol. Hung*. **43**, 59-68.

Waller P. J. and Chandrawathani P.. (2005).*Haemonchus contortus:* Parasite problem No. 1 from tropics – Polar Circle. Problems and prospects for control based on epidemiology. *Tropical biomedicine*. **22**: 131-137.

Wang J., Wang X., Irnaten M., Venkatesan P., Evans C., Baxi S. and Mendelowitz D. (2003). Endogenous acetylcholine and nicotine activation enhances GABAergic and glycinergic inputs to cardiac vagal neurons. *J. Neurophysiol*. **89**, 2473-2481.

Wang Z.W., Saifee O., Nonet M.L. and Salkoff L. (2001). SLO-1 potassium channels control quantal content of neurotransmitter release at the *C. elegans* neuromuscular junction. *Neuron*. **32**, 867-881.

Warbington L., Hillman T., Adams C. and Stern M. (1996). Reduced transmitter release conferred by mutations in the slowpoke-encoded Ca2(+)-activated K+ channel gene of *Drosophila*. *Invert. Neurosci*. **2**, 51-60.

Walthall W.W., Li L., Plunkett J.A. and Hsu C.Y. (1993). Changing synaptic specificities in the nervous system of Caenorhabditis elegans: differentiation of the DD motoneurons. *J Neurobiol*. **24**, 1589-1599.

Wei A., Jegla T. and Salkoff L. (1996). Eight potassium channel families revealed by the *C. elegans* genome project. *Neuropharmacology*. **35**, 805-829.

White J.G., Southgate E., Thomson J.N. and Brenner S. (1986). The structure of the nervous system of the nematode *Caenorhabditis elegans*. *Phil. Trans. Royal. Soc. London. Series B, Biol. Scien*. **314**, 1-340.

White J.G. (1988). The nematode *C. elegans*. The anatomy. *Cold Spring Harbor Laboratory Press USA*.

Wicks S.R., Yeh R.T., Gish W.R., Waterston R.H. and Plasterk R.H.A. (2001) Rapid gene mapping in *Caenorhabditis elegans* using a high density polymorphism map. *Genetics*. **28**, 160-164.

Williams J.C. (1997). Anthelmintic treatment strategies: current status and future. *Veterinary Parasitology*. **72**, 461-477.

Willson J., Amliwala K., Davis A., Cook A., Cuttle M.F., Kriek N., Hopper N.A., O'Connor V., Harder A., Walker R.J. and Holden-Dye L. (2004). Latrotoxin receptor signaling engages the UNC-13-dependent vesicle-priming pathway in *C. elegans*. *Curr. Biol*. **14**, 1374-1379.

Willson J., Amliwala K., Harder A., Holden-Dye L. and Walker R.J. (2003) The effect of the anthelmintic emodepside at the neuromuscular junction of the parasitic nematode *Ascaris suum*. *Parasitology*. **126**, 79-86.

Wood W.B., Hecht R., Carr S., Vanderslice R., Wolf N. and Hirsh D. (1980). Parental effects and phenotypic characterisation of mutations that affect early development in *Caenorhabditis elegans*. *Dev. Biol*. **74**, 446-469.

World health report. (2000). World Health Organization.

Wu S.M. (1985). Synaptic transmission from rods to bipolar cells in the tiger salamander retina. *Proc. Natl. Acad. Sci. USA*. **82**, 3944-3947.

Xia X.M., Zeng X. and Lingle C.J. (2002). Multiple regulatory sites in large-conductance calcium-activated potassium channels. *Nature*. **418**, 880-884.

Xu W.J. and Slaughter M.M. Large-Conductance Calcium-Activated Potassium Channels Facilitate Transmitter Release in Salamander Rod Synapses. *J. Neurosci*. **25**, 7660-7668.

Yu S.P. and Kerchner G.A. (1998). Endogenous Voltage-Gated Potassium Channels in Human Embryonic Kidney (HEK293) cells. *J. Neurosci Res*. **52**, 612-617.

Zajac A**.**M. (2006). Gastrointestinal nematodes of small ruminants: life cycle, anthelmintics, and diagnosis. *Vet Clin North Am Food Anim Pract*. **22**, 529-541

Zhao H. and Nonet M.L. (2001). A conserved mechanism of synaptogyrin localization. *Mol. Biol. Cell*. **12**, 2275-2289.

Zhao B., Khare P., Feldman L. and Dent J.A. (2003). Reversal frequency in *Caenorhabditis elegans* represents an integrated response to the state of the animal and its environment. *J. Neurosci*. **23**, 5319-5328.

Zeng X., Sun M., Liu L., Chen F., Wei L. and Xie W. Neurexin-1 is required for synapse formation and larvae associative learning in *Drosophila*. *FEBS*. **581**, 2509-2516.

Zheng Y., Brockie P.J., Mellem J.E., Madsen D.M. and Maricq A.V. (1999). Neuronal control of locomotion in *C. elegans* is modified by a dominant mutation in the GLR-1 ionotropic glutamate receptor. *Neuron*. **24**, 347-361.

Zhou Y. and MacKinnon R. (2003). The occupancy of ions in the K+ selectivity filter: charge balance and coupling of ion binding to a protein conformational change underlie high conduction rates. *J. Mol. Biol*. **333**, 965-975.

Zhu G., Zhang Y., Xu H. and Jiang C. (1998). Identification of endogenous outward currents in the human embryonic kidney (HEK 293) cell line. *J Neurosci Methods*. **81**. 73-83.